NASA Technical Memorandum 81878

Effect of Wing Location and Strakes on Stability and Control Characteristics of a Monoplanar Circular Missile With Low-Profile Tail Fins at Supersonic Speeds

A. B. Blair, Jr.

DECEMBER 1980

NASA

NASA Technical Memorandum 81878

Effect of Wing Location and Strakes on Stability and Control Characteristics of a Monoplanar Circular Missile With Low-Profile Tail Fins at Supersonic Speeds

A. B. Blair, Jr.
Langley Research Center
Hampton, Virginia

National Aeronautics
and Space Administration

**Scientific and Technical
Information Branch**

1980

SUMMARY

An experimental wind-tunnel investigation has been conducted at Mach numbers from 1.70 to 2.86 to extend the aerodynamic data base for wing-tail effects on stability and control characteristics of monoplanar circular missiles. The results are summarized to show the effects of tail-fin dihedral angle, wing location, and nose-body strakes.

The results indicate that an increase in tail-fin dihedral angle produces positive increments in directional stability that allow greater trimmed-lift-coefficient values (maneuver potential). An increase in wing-tail gap for the Mach number range reduces the aerodynamic-center travel and produces reductions in directional stability at the lower angles of attack. A change in wing height (vertical location) strongly influences the angle of attack at which pitch-up and the most directional stability occur. The addition of strakes to the baseline configuration increases directional stability, which allows a significant increase in stable-trimmed maneuver capability. The tail fins of the baseline configuration are effective in producing roll and yaw control accompanied by favorable yaw and roll, respectively.

INTRODUCTION

The National Aeronautics and Space Administration is currently conducting aerodynamic studies of various monoplanar missile configurations to provide insight into the potential for improving conformal carriage, performance, and maneuverability of future air-launched missiles. It is suggested in reference 1 that for some advanced medium-range missile weapon systems, the monoplanar missile concept with low-profile tails is a natural shape for efficient supersonic conformal carriage on supersonic-cruise-type aircraft. One desirable feature of this concept is a balance between good longitudinal and good directional aerodynamic stability and control characteristics. Two monoplanar missile configurations, each with circular bodies and low-profile tails, have been investigated and their aerodynamic characteristics are reported in reference 2.

The present experimental wind-tunnel investigation was conducted in an effort to extend the aerodynamic data base of reference 2 and to evolve a circular conformal-carriage missile candidate with better overall aerodynamics. The baseline model configuration had a circular body, centerline aft wing, and low-profile tail fins with dihedral angles of 30°. Limited comparisons are made with data from configurations in reference 2, which were identical to the present baseline except for having tail-fin dihedral angles of 22.5° and 45.0°.

The tests were conducted in the Langley Unitary Plan Wind Tunnel at Mach numbers from 1.70 to 2.86. The nominal angle-of-attack range was -3° to 26° and the nominal angle-of-sideslip range was about -4° to 6°. The test Reynolds

number was 6.6×10^6 per meter (2.0×10^6 per foot). The results are summarized to show the effects of tail-fin dihedral angle, of longitudinal and vertical wing location, and of nose-body strakes on the longitudinal, lateral, and directional aerodynamic stability and control characteristics of a monoplanar circular missile configuration. The four tail fins were deflected to obtain pitch, yaw, and roll control.

SYMBOLS

The aerodynamic-coefficient data are referred to the body-axis system except for lift and drag which are referred to the stability-axis system. The moment center was located 51.51 cm (20.28 in.) aft of the model nose (60.0 percent of the body length) unless otherwise noted.

Values are given in both SI and U.S. Customary Units. The measurements and calculations were made in U.S. Customary Units. Factors relating the two systems are given in reference 3.

b	wing span, 24.486 cm (9.640 in.)
C_A	axial-force coefficient, Axial force/qS
$C_{A,b}$	base axial-force coefficient, Base axial force/qS
C_D	drag coefficient, Drag/qS
$C_{D,b}$	base drag coefficient, $C_{A,b} \cos \alpha$
$C_{D,o}$	drag coefficient at $\alpha = 0^o$, Drag/qS
C_L	lift coefficient, Lift/qS
$C_{L,trim}$	trimmed-lift coefficient
C_{L_α}	slope of lift curve measured at $\alpha = 0^o$, per degree
C_l	rolling-moment coefficient, Rolling moment/qSb
C_{l_β}	effective-dihedral parameter, $\left(\frac{\Delta C_l}{\Delta \beta}\right)_{\beta=0^o,3^o}$
C_m	pitching-moment coefficient, Pitching moment/qS^l
$C_{m_{C_L}}$	longitudinal-stability parameter, $\partial C_m / \partial C_L$
C_{m_δ}	pitch-control effectiveness of four tail fins at $\alpha = 0^o$, per degree of deflection for tail-fin deflections of 0^o and -10^o
C_N	normal-force coefficient, Normal force/qS

C_n yawing-moment coefficient, Yawing moment/qSb

C_{n_β} directional-stability parameter, $\left(\frac{\Delta C_n}{\Delta \beta}\right)_{\beta=0^o,3^o}$

C_Y side-force coefficient, Side force/qS

C_{Y_β} side-force parameter, $\left(\frac{\Delta C_Y}{\Delta \beta}\right)_{\beta=0^o,3^o}$

L/D lift-drag ratio

l reference body length, 85.852 cm (33.800 in.)

l_s strake length (see fig. 1(c))

M Mach number

q free-stream dynamic pressure, kPa (lbf/ft^2)

S wing planform area including body centerline intercepts, 0.064933 m^2 (0.698965 ft^2)

x_{ac}/l aerodynamic-center location as fraction of model length, measured from nose apex

x_{cg}/l center-of-gravity location as fraction of model length, measured from nose apex

α angle of attack, deg

β angle of sideslip, deg

Γ_{tail} dihedral angle of tail fins, deg

δ_{pitch} pitch-control deflection of four tail fins (negative with leading edge down), deg

δ_{roll} differential deflections for roll control, individual tail fins deflected the indicated amount (positive to provide a clockwise rotation as viewed from rear), deg

δ_{yaw} yaw-control deflection of four tail fins (negative with leading edge left as viewed from rear), deg

Model-configuration nomenclature:

Aft baseline longitudinal location of model centerline wing

Mid centerline aft wing moved forward one body diameter

Fwd	centerline aft wing moved forward two body diameters
High	centerline aft wing moved up 0.375 body diameters
Centerline	baseline vertical location of model aft wing
Low	centerline aft wing moved down 0.375 body diameters
W_S	width of strake (see fig. 1(c))

Model components:

S_1	nose strake
S_2	nose-body strake
S_3	body strake

Subscripts:

a	narrow
b	wide
max	maximum
trim	trimmed conditions ($C_m = 0$)

The baseline model configuration of the present investigation has a centerline aft wing and tail fins with dihedral angles of 30.0°.

APPARATUS AND TESTS

Wind Tunnel

The investigation was conducted in the low Mach number test section of the Langley Unitary Plan Wind Tunnel, which is a variable-pressure, continuous-flow facility. The test section is approximately 2.13 m (7.00 ft) long and 1.22 m (4.00 ft) square. The asymmetric sliding-block nozzle leading to the test section permits a continuous variation in free-stream Mach number from about 1.5 to 2.9. (See ref. 4.)

Model

Dimensional details of the model are shown in figure 1, and photographs of the model are shown in figure 2. The model was a monoplanar, low-profile-tail configuration that consisted of a cylindrical body with a pointed tangent-ogive nose, delta wings, and four trapezoidal tail fins. The body had a fineness ratio of 13. The wings and tail fins had slab airfoil cross sections with beveled leading and trailing edges. For the present investigation the baseline-

model configuration had a centerline aft wing with tail fins in planes inclined 30.0° to the horizontal; the data were intended to complement the results reported in reference 2, which were obtained on configurations having tail-fin dihedral angles of 22.5° and 45.0°.

The present wind-tunnel model was constructed so that the wings could have three centerline longitudinal locations that enabled the effect of the wing-tail gap to be investigated. (See fig. 1(a).) In addition, the model was tested with only the aft wing in three vertical locations. By moving the centerline aft wing up or down 0.375 body diameters, high-, centerline-, and low-aft-wing configurations were obtained. Several centerline nose and body strakes that had variations in length and width were also tested with the centerline-aft-wing configuration. (See fig. 1(c).) For the baseline-model configuration the four tail fins were used to provide pitch, yaw, and roll control.

Test Conditions

Tests were performed at the tunnel conditions shown in the following table:

Mach number	Stagnation temperature		Stagnation pressure (absolute)		Reynolds number	
	K	°F	kPa	lbf/ft^2	per meter	per foot
1.70	339	150	56.4	1178	6.6×10^6	2.0×10^6
2.16	↓	↓	68.5	1430	↓	↓
2.36			75.7	1580		
2.86	↓	↓	98.4	2056	↓	↓

The dewpoint temperature measured at stagnation pressure was maintained below 239 K (-30°F) to assure negligible condensation effects. All tests were performed with boundary-layer transition strips on the body 3.05 cm (1.20 in.) aft of the nose and 1.02 cm (0.40 in.) aft of the leading edges measured streamwise on both sides of the wing and tail-fin surfaces. The transition strips were approximately 0.157 cm wide (0.062 in.) and were composed of No. 50 sand grains sprinkled in acrylic plastic. (See ref. 5.)

Measurements

Aerodynamic forces and moments on the model were measured by means of a six-component electrical strain-gage balance which was housed within the model.

The balance was attached to a sting which, in turn, was rigidly fastened to the model support system. Balance-chamber pressure, or base pressure, was measured by means of a single static-pressure orifice located in the vicinity of the balance.

Corrections

The angles of attack and sideslip were corrected for deflection of the balance and sting due to aerodynamic loads. Also, angles of attack were corrected for tunnel-flow misalignment. The drag and axial-force coefficient data were adjusted to free-stream static pressure acting over the model base. Typical measured values of base axial-force and drag coefficients are presented in figure 3.

PRESENTATION OF RESULTS

The results are presented in the following figures:

RESULTS AND DISCUSSION

Longitudinal Aerodynamic Characteristics

The effects of wing longitudinal location on the pitch characteristics of the centerline-wing configurations are presented in figure 4. Data are also presented for a constant level of static stability at each Mach number to better assess the effects of wing-tail gap on pitching-moment linearity. At $M = 1.70$ for a fixed static margin of $C_{m_{C_L}} = -0.14$, the forward-wing configuration exhibits the most pitch-up, which coincides with a small loss of lift coefficient over the angle-of-attack range of 4° to 10°. The pitch-up is probably

due to wing-tail interference, which results in temporary loss of tail lift. This interference occurs as the tail fins move through the wing-downwash flow field and through the low-energy-wake flow field behind the wing. In general, for constant-static-margin comparisons, all the configurations exhibit some degree of pitch-up, with the forward-wing configuration having the most restoring moments at the higher angles of attack.

At angles of attack above 12°, the nonlinear contribution to overall lift for the complete configurations is primarily due to wing-vortex lift that is characteristic of highly swept and sharp-leading-edge wings.

The effects of pitch control on longitudinal aerodynamic characteristics of the centerline-aft-, mid-, and forward-wing configurations are presented in figures 5, 6, and 7. The tail fins of all three configurations are effective in producing pitch control throughout the angle-of-attack and Mach number ranges.

The effects of wing vertical location on the longitudinal aerodynamic characteristics of the aft-wing configurations are shown in figure 8. The angle of attack at which pitch-up occurs is strongly related to the wing vertical location. The low-wing configuration exhibits the largest pitch-up tendency at about $\alpha = 12°$. The magnitude of pitch-up is reduced with increases in Mach number. In general, the angle of attack at which the pitch-up occurs progressively increases as the wing location is lowered. The aforementioned wing-tail interference contributes to the pitch-up as the tail fins move through the wing-downwash flow field. Additional tests are needed to resolve the question of whether the upper or lower pair of tail fins is the primary contributor to the pitch-up tendency.

The effects of pitch control on the longitudinal aerodynamic characteristics of the high- and low-aft-wing configurations are presented in figures 9 and 10. The tail fins of both configurations are effective in producing pitch control throughout the angle-of-attack and Mach number ranges.

It is suggested in reference 2 that the addition of nose-body strakes might provide more directional stability at the higher angles of attack. In addition, a reduction in static margin would result in higher trim-lift coefficients and lower trim drag. For these reasons, nose-body strakes were tested on the baseline configuration.

The effects of strake length and width on longitudinal aerodynamic characteristics of the centerline-aft-wing configuration are shown in figures 11 and 12. Figure 11 shows that with increases in strake length and width, correspondingly small increases in lift coefficient are obtained at the higher angles of attack. In addition, there are the expected reductions in stability level with progressive increases in pitch-up at lower angles of attack ($\alpha \approx 6°$ to $10°$) that decrease at the higher Mach numbers. The body-strake (fig. 12) characteristics indicate similar trends but to a lesser degree.

Figure 13 presents the effects of nose-body strake ($S_{2,b}$) on pitch-control characteristics of the centerline-aft-wing (baseline) configuration with $\delta_{pitch} = -20°$. The data indicate that the strake configuration has the

potential for higher $C_{L,trim}$ and lower $C_{D,trim}$. However, the pitch-up tendencies are similar to the trends shown in figures 11 and 12.

A summary of the longitudinal aerodynamic characteristics including the effects of tail-fin dihedral angle and wing longitudinal and vertical locations is presented in figure 14. This figure shows the usual decrease of $-C_{m_\delta}$, C_{L_α}, and $C_{D,o}$ with increase in Mach number. In figure 14(a), the $\Gamma_{tail} = 30.0^\circ$ configuration has slightly more $-C_{m_\delta}$, C_{L_α}, and $(L/D)_{max}$ at the lower Mach numbers than the other tail-fin configurations. Figure 14(b) shows that wing longitudinal position has little effect on the longitudinal aerodynamic characteristics with the obvious exception of aerodynamic center location x_{ac}/l. The forward-wing configurations have the least variation in aerodynamic-center location with Mach number. Figure 14(c) indicates the centerline-aft-wing configuration has greater $-C_{m_\delta}$, C_{L_α}, and $(L/D)_{max}$ for the test Mach numbers. The high-aft-wing configuration has the lowest $(L/D)_{max}$.

Lateral and Directional Aerodynamic Characteristics

The lateral and directional aerodynamic characteristics in sideslip at several angles of attack for the baseline configuration are presented in figure 15. These data are shown primarily to indicate the linearity of the coefficients with sideslip angles, since the rolling-moment, yawing-moment, and side-force coefficients were obtained from incremental results of tests made over the angle-of-attack range at $\beta = 0^\circ$ and 3°. The results were generally linear to $\beta = 3^\circ$ and indicate the comparative results shown for the lateral and directional parameters are valid. These data trends are typical for the other configurations as well.

The effects of pitch control on lateral and directional parameters of the centerline-, high-, and low-aft-wing configurations are presented in figures 16, 17, and 18. In general, pitch-control deflections increased the directional-stability parameter C_{n_β} at the higher angles of attack and decreased the positive effective-dihedral parameter $-C_{l_\beta}$ at the lower angles of attack for the centerline- and high-aft-wing configurations. (See figs. 16 and 17.) The low-aft-wing configuration (fig. 18) has a decrease in directional-stability parameter and positive effective-dihedral parameter with increases in angle of attack and Mach number.

The effects of wing longitudinal location and tail fins on lateral and directional parameters of the centerline-wing configurations at zero control deflection are presented in figure 19. For a constant static margin there is a reduction in C_{n_β} at the lower angles of attack with increases in wing-tail gap for the entire Mach number range. At $M = 1.70$ this reduction coincides with pitch-up and loss of lift coefficient ($\alpha \approx 4^\circ$ to 10°) as shown in

figure 4(a). In general there is an increase in positive effective-dihedral parameter $-C_{l_\beta}$ at higher angles of attack with increases in wing-tail gap for the Mach number range.

The effects of wing vertical location and tail fins on lateral and directional parameters of the aft-wing configurations at zero control deflection are shown in figure 20. For the complete configurations, the centerline-aft-wing exhibits the most positive C_{n_β} at the lower angles of attack. At intermediate angles (up to about 18°), the low-wing configuration produces the greatest directional stability. For the higher angles of attack ($\alpha > 18°$), the high-wing configuration has the most C_{n_β}.

The effects of strake length and width on lateral and directional parameters of the centerline-aft-wing configuration with zero control deflection are presented in figures 21 and 22. In figure 21, both the nose and nose-body strakes increase C_{n_β} at angles of attack above 4° for the range of Mach numbers. Increasing the strake width generally produces positive increments in C_{n_β}, and the wide nose strake $S_{1,b}$ provides the most positive C_{n_β} at the higher angles of attack (fig. 21). In general, there are increases in positive effective-dihedral parameter $-C_{l_\beta}$ with increases in strake length and width for intermediate angles of attack. The body strake $S_{3,b}$ is not very effective in generating positive increments of C_{n_β} especially at the higher angles of attack for which negative increments are produced (fig. 22).

Figure 23 presents the effects of the wide nose-body strake $S_{2,b}$ on lateral and directional parameters of the centerline-aft-wing configuration with $\delta_{pitch} = -20°$. For the selected moment center, the addition of the strake provides a positive increment of C_{n_β} such that with the induced positive increment of C_{n_β} from the pitch control (fig. 16), the configuration becomes directionally stable for the entire angle-of-attack and Mach number ranges. The strake also increases the positive effective dihedral parameter.

A summary of the lateral and directional aerodynamic parameters including the effects of tail-fin dihedral angle, wing locations, and strakes is given in figure 24. All the configurations have the expected decrease in directional stability with increased Mach number. For the selected moment center (0.60ℓ), the cruciform-tail configuration ($\Gamma_{tail} = 45.0°$, fig. 24(a)) shows directional stability throughout the Mach number range, whereas the $\Gamma_{tail} = 22.5°$ configuration is unstable beyond $M = 2.12$. The baseline configuration ($\Gamma_{tail} = 30.0°$) becomes directionally unstable beyond $M = 2.60$. Moving the wing forward increases C_{n_β} at the higher Mach numbers (fig 24. (b)). In figure 24(c) the centerline aft wing has the highest C_{n_β} at the lower Mach numbers. Figure 24(d) presents strake effects only at angles of attack of 10°

and 20° since strakes were not effective at very low angles of attack. For $\alpha = 10^{\circ}$, the configuration with the wide nose-body strake $S_{2,b}$ has the largest directional stability and positive effective dihedral parameter $-C_{l_\beta}$. For $\alpha = 20^{\circ}$, the configuration with the wide nose strake $S_{1,b}$ has the greatest directional stability at the lower Mach numbers.

The roll and yaw control characteristics of the centerline-aft-wing configuration are presented in figures 25 and 26. The baseline configuration is effective in providing both roll and yaw control throughout the angle-of-attack and Mach number ranges. The roll and yaw control are accompanied by favorable yaw and roll, respectively, at the higher angles of attack.

A summary of tail-fin dihedral effect on roll and yaw control effectiveness of the centerline-aft-wing configuration is presented in figure 27. This figure shows the usual decrease in roll and yaw control effectiveness with increased Mach number. The cruciform-tail configuration ($\Gamma_{tail} = 45.0^{\circ}$) produces the most yaw and roll control, whereas the extreme low-profile tail ($\Gamma_{tail} = 22.5^{\circ}$) produces the least.

Longitudinal and Directional Stability Parameters

The balance between good longitudinal and good directional aerodynamic stability and control characteristics is an important consideration when evaluating monoplanar missile configurations. Therefore, when making aerodynamic stability and control comparisons, one must be cognizant of the directional-stability parameter of each configuration in addition to its respective trimmed-lift coefficient. In the following discussion, figures are presented that show variations of trimmed-lift coefficient with center-of-gravity location for the various model configurations. Included are $C_{n_\beta} = 0$ boundary curves that indicate the rearward center-of-gravity limit for the condition of static directional stability.

The variation of $C_{L,trim}$ with center-of-gravity location that includes effects of tail-fin dihedral angle, wing vertical location, and nose-body strake is presented in figure 28 for a pitch-control deflection of -20°. In figure 28(a) the extreme low-profile-tail configuration ($\Gamma_{tail} = 22.5^{\circ}$) is severely limited in $C_{L,trim}$ (manuever potential) due to directional instability, especially at the higher Mach numbers. For the $C_{L,trim}$ values shown the $\Gamma_{tail} = 30.0^{\circ}$ configuration is limited in maneuver potential to some degree, whereas the cruciform-tail configuration ($\Gamma_{tail} = 45.0^{\circ}$) is unlimited. In figure 28(b) the high-aft-wing configuration for the $C_{n_\beta} = 0$ boundary conditions can obtain the highest $C_{L,trim}$ values at the most rearward center-of-gravity locations. For the centerline-aft-wing configurations of figure 28(c), the strake-off configuration has stable maximum $C_{L,trim}$ values that range from about 0.25 to 0.45 at the lowest Mach number. The addition of the strake increases these stable values above the range of the test variables ($C_{L,trim} > 0.60$).

CONCLUSIONS

An experimental wind-tunnel investigation has been conducted at Mach numbers from 1.70 to 2.86 to extend the aerodynamic data base for wing-tail effects on stability and control characteristics of monoplanar circular missiles. The results are summarized to show the effects of tail-fin dihedral angle, wing location, and nose-body strakes. The results of the investigation are as follows:

1. An increase in tail-fin dihedral angle produces positive increments in directional stability that allow greater $C_{L,trim}$ values (maneuver potential) to be obtained.

2. An increase in wing-tail gap for the Mach number range reduces the aerodynamic-center travel and produces reductions in directional stability at the lower angles of attack.

3. A change in wing height (vertical location) strongly influences the angle of attack at which pitch-up and the most directional stability occur.

4. The addition of strakes to the baseline configuration increases directional stability which allows a significant increase in stable-trimmed maneuver capability.

5. The tail fins of the baseline configuration are effective in producing roll and yaw control that are accompanied by favorable yaw and roll, respectively.

Langley Research Center
National Aeronautics and Space Administration
Hampton, VA 23665
September 29, 1980

REFERENCES

1. Sawyer, Wallace C.; Jackson, Charlie M., Jr.; and Blair, A. B., Jr.: Aerodynamic Technologies for the Next Generation of Missiles. Paper presented at the AIAA/ADPA Tactical Missile Conference (Gaithersburg, Maryland), Apr. 27-28, 1977.

2. Blair, A. B., Jr.: Stability and Control Characteristics of a Monoplanar Missile Configuration With Two Low-Profile Tail Arrangements at Mach Numbers From 1.70 to 2.86. NASA TM X-3533, 1977.

3. Standard for Metric Practice. E 380-79, American Soc. Testing & Mater., c.1980.

4. Schaefer, William T., Jr.: Characteristics of Major Active Wind Tunnels at the Langley Research Center. NASA TM X-1130, 1965.

5. Stallings, Robert L., Jr.; and Lamb, Milton: Effects of Roughness Size on the Position of Boundary-Layer Transition and on the Aerodynamic Characteristics of a 55° Swept Delta Wing at Supersonic Speeds. NASA TP-1027, 1977.

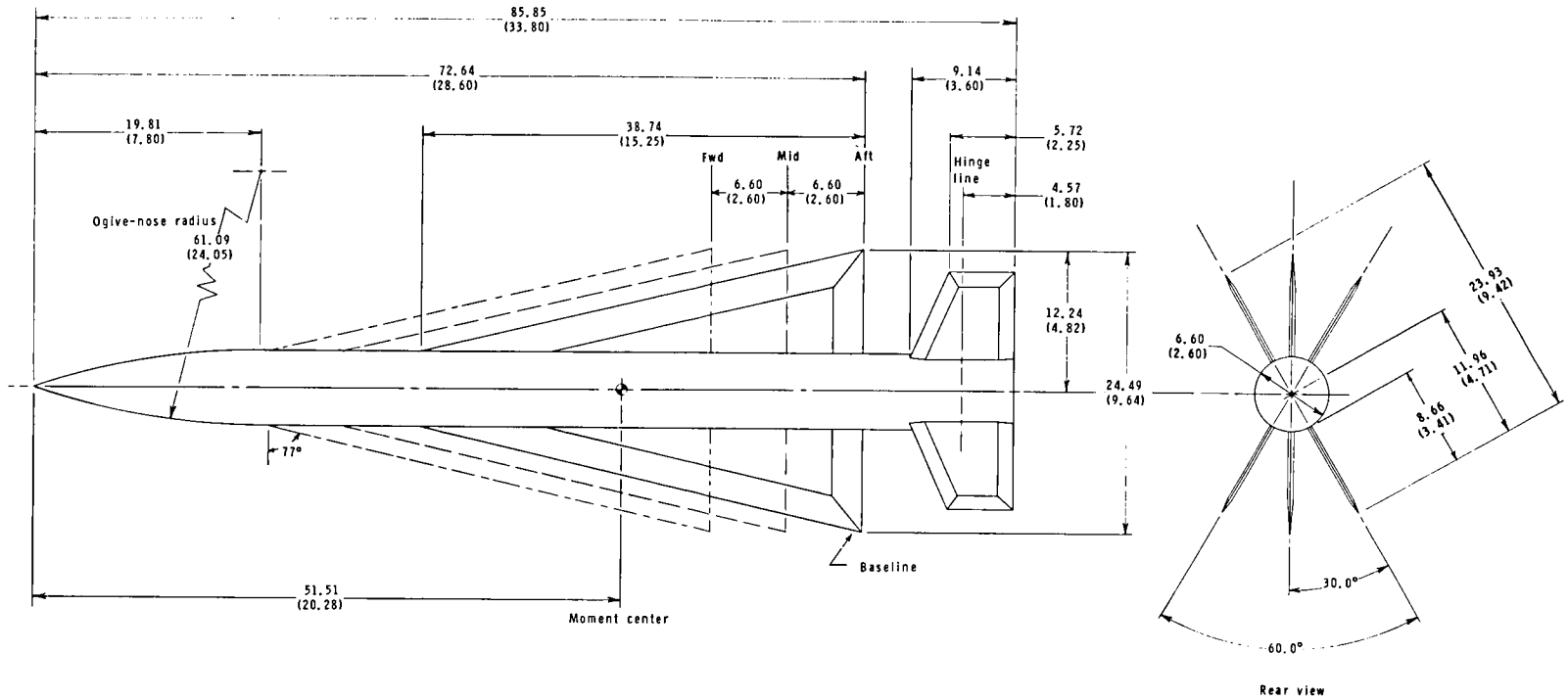

(a) Centerline wing configurations.

Figure 1.- Model details. All dimensions are in centimeters (inches) unless otherwise indicated.

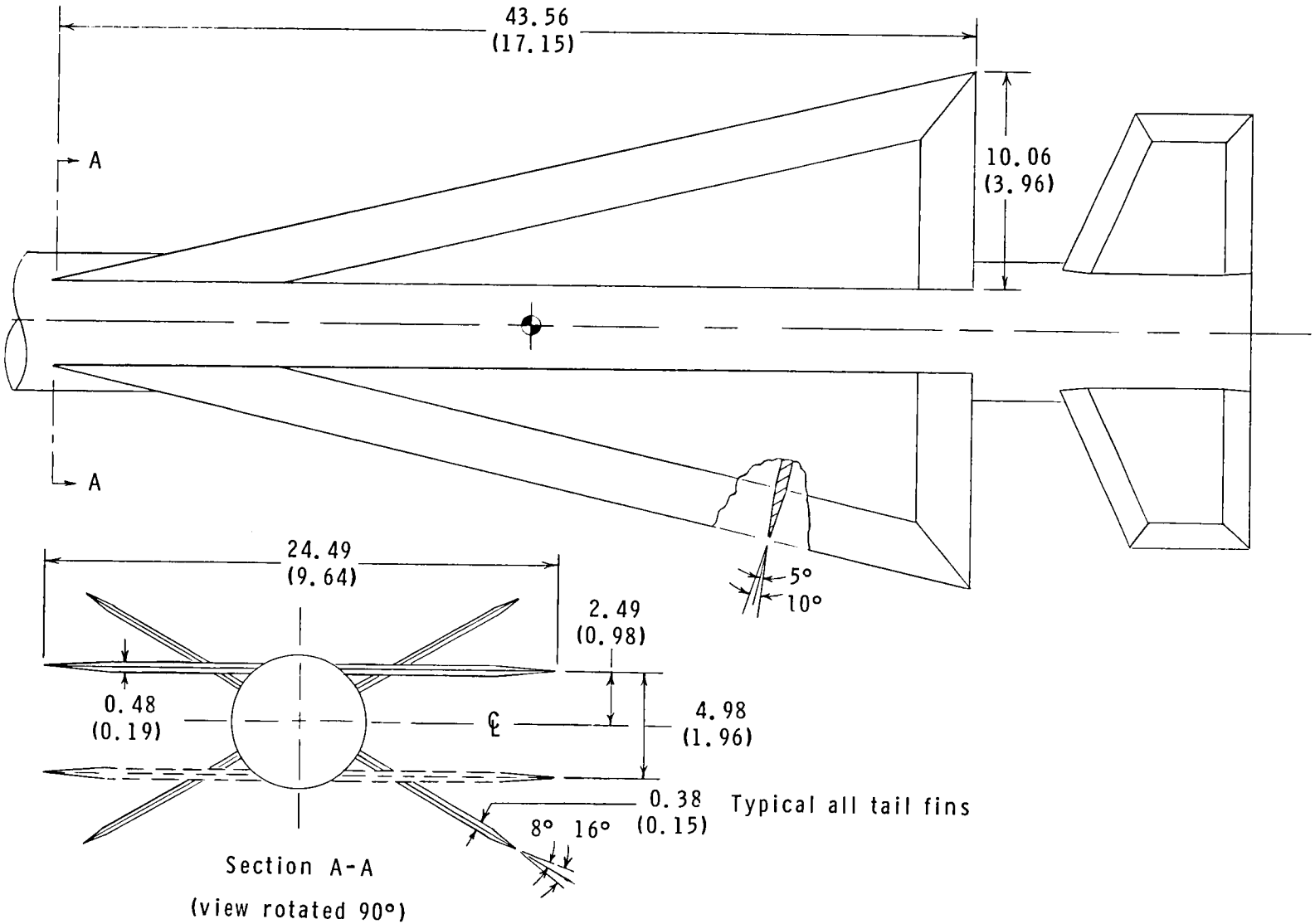

(b) High- and low-aft-wing configurations.

Figure 1.- Continued.

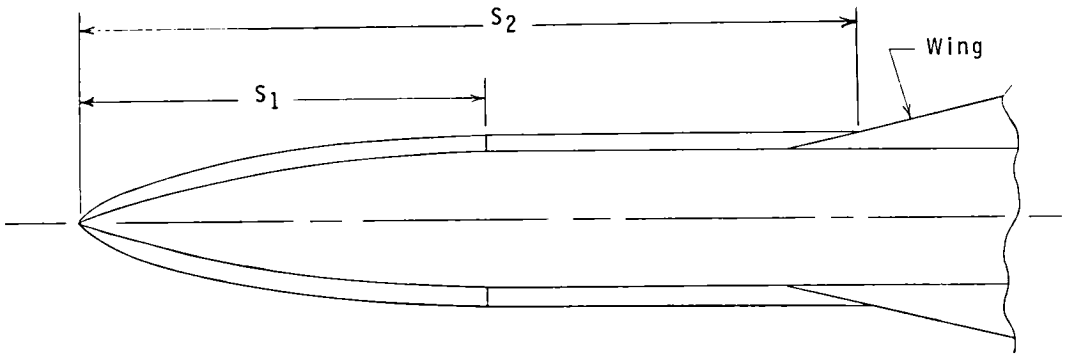

Nose and nose-body strakes

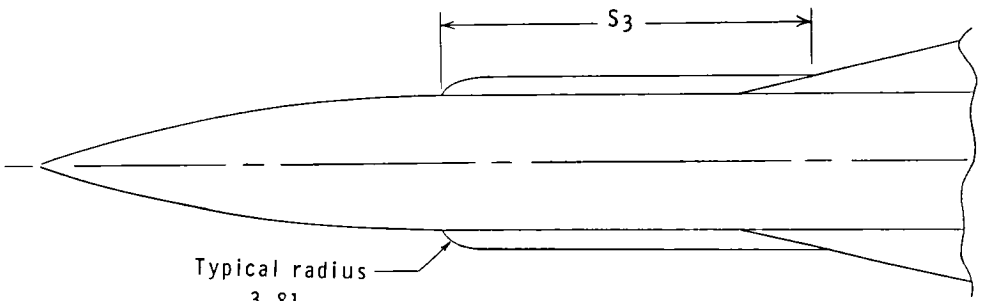

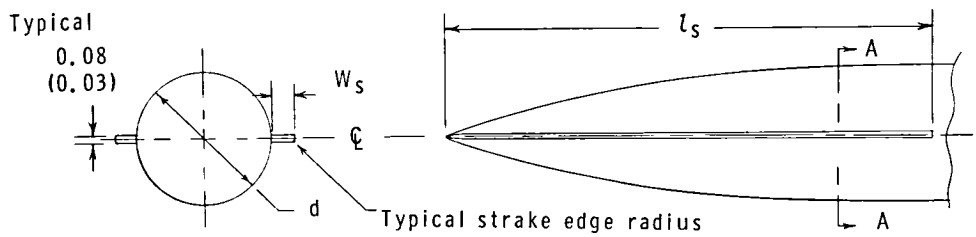

Strake	ℓ_s/d	W_s/d
$S_{1,a}$	3.00	0.05
$S_{1,b}$	3.00	.10
$S_{2,a}$	5.32	.05
$S_{2,b}$	5.53	.10
$S_{3,a}$	2.32	.05
$S_{3,b}$	2.53	.10

(c) Strakes.

Figure 1.- Concluded.

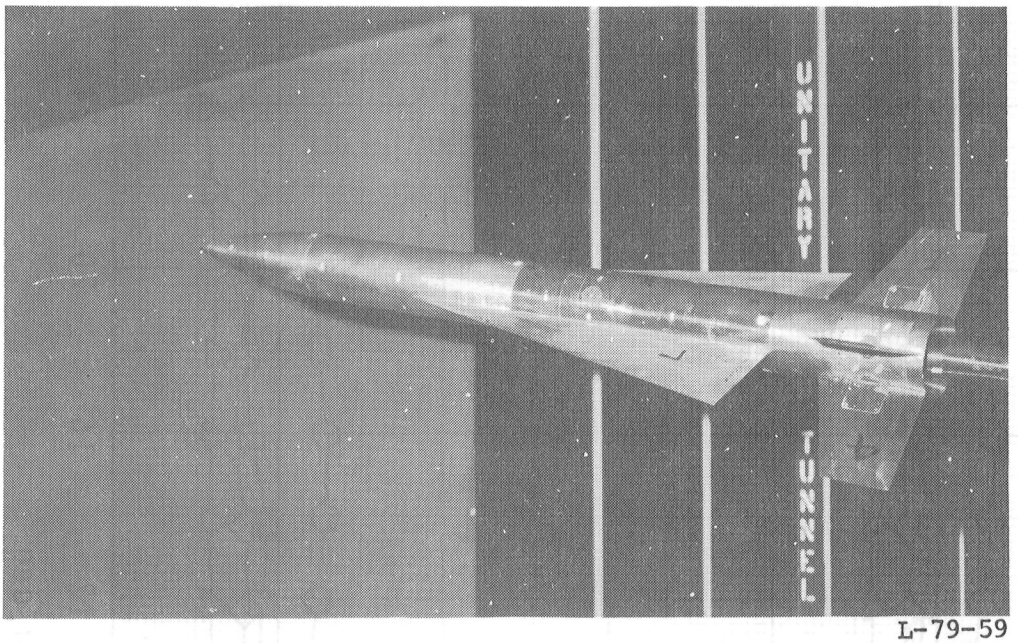

L-79-59

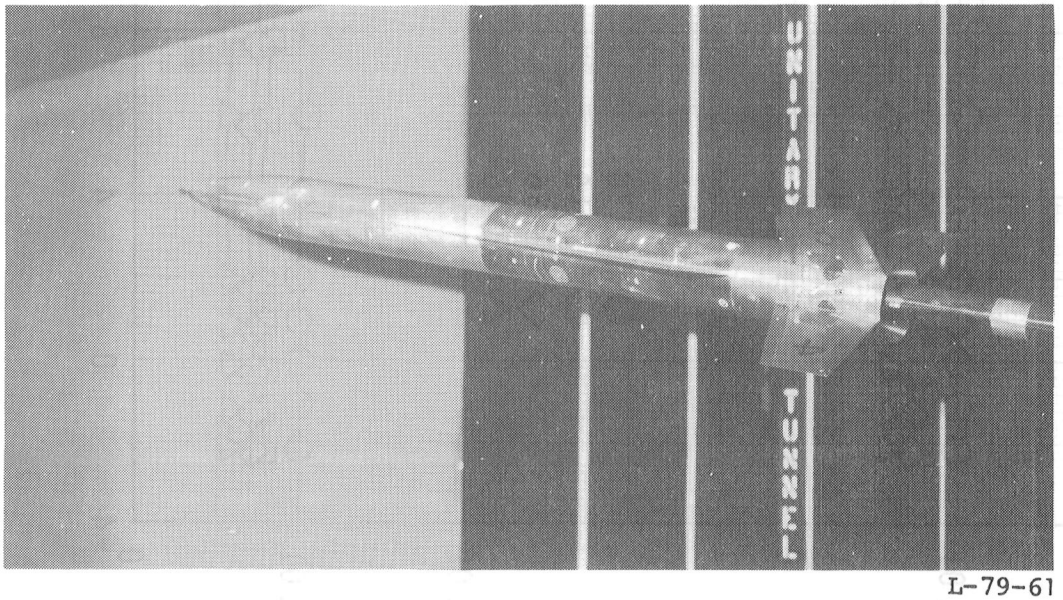

L-79-61

Figure 2.- Photographs of baseline-model configuration.

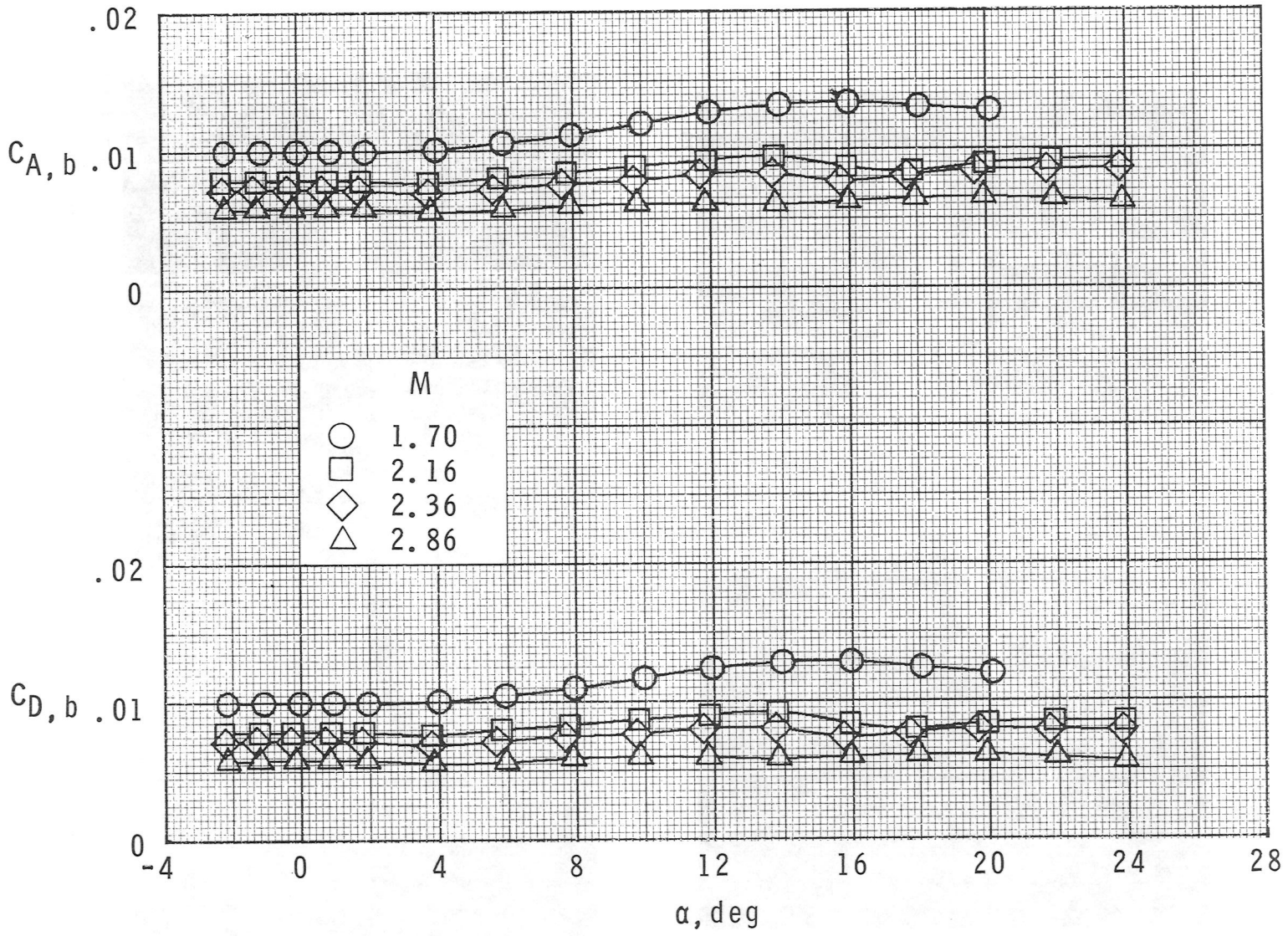

Figure 3.- Typical variation of measured base axial-force coefficient and base drag coefficient with angle of attack.

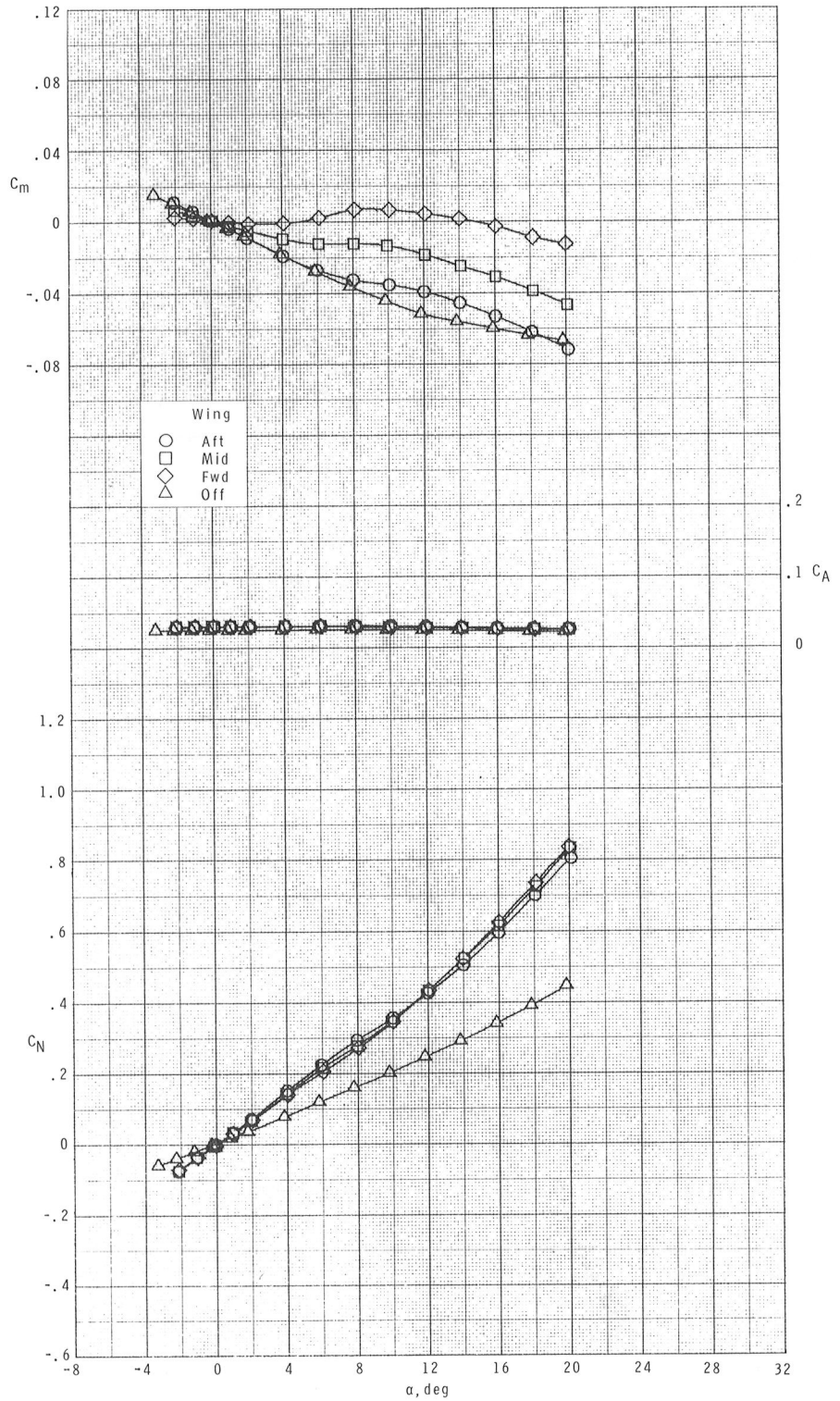

(a) M = 1.70.

Figure 4.- Effects of wing longitudinal location on longitudinal aerodynamic characteristics of the centerline-wing configurations.

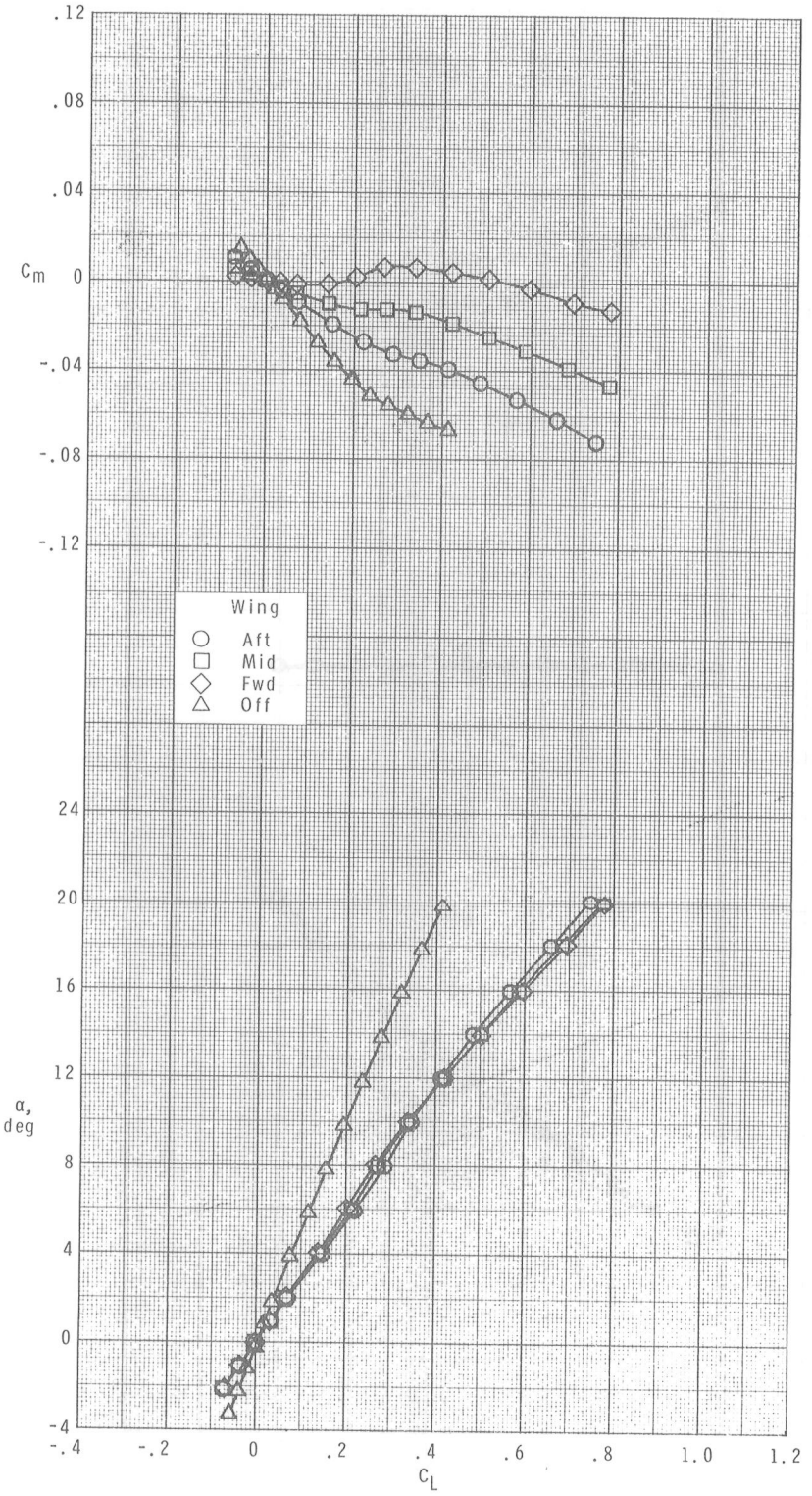

(a) Continued.

Figure 4.- Continued.

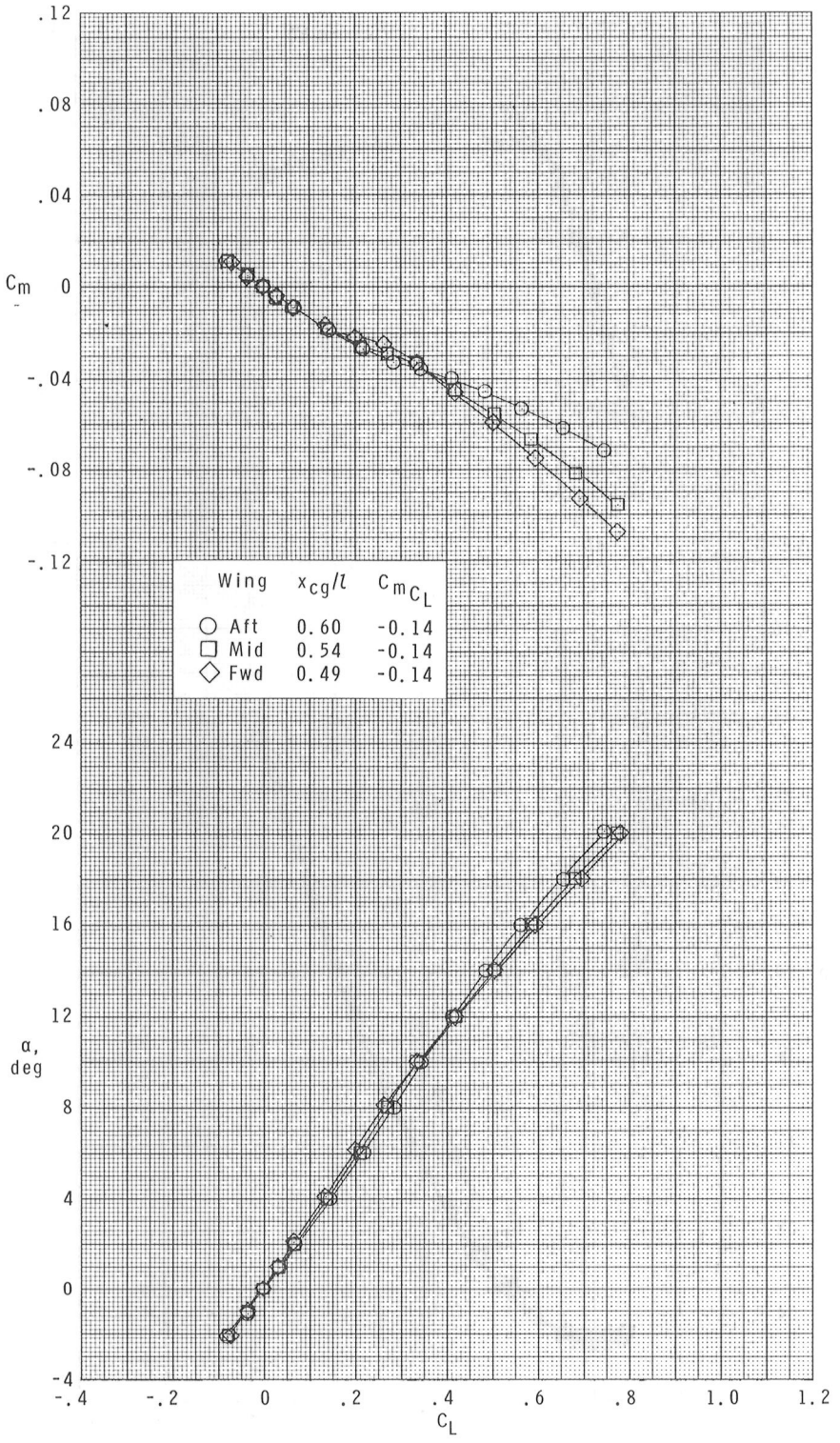

(a) Continued.

Figure 4.- Continued.

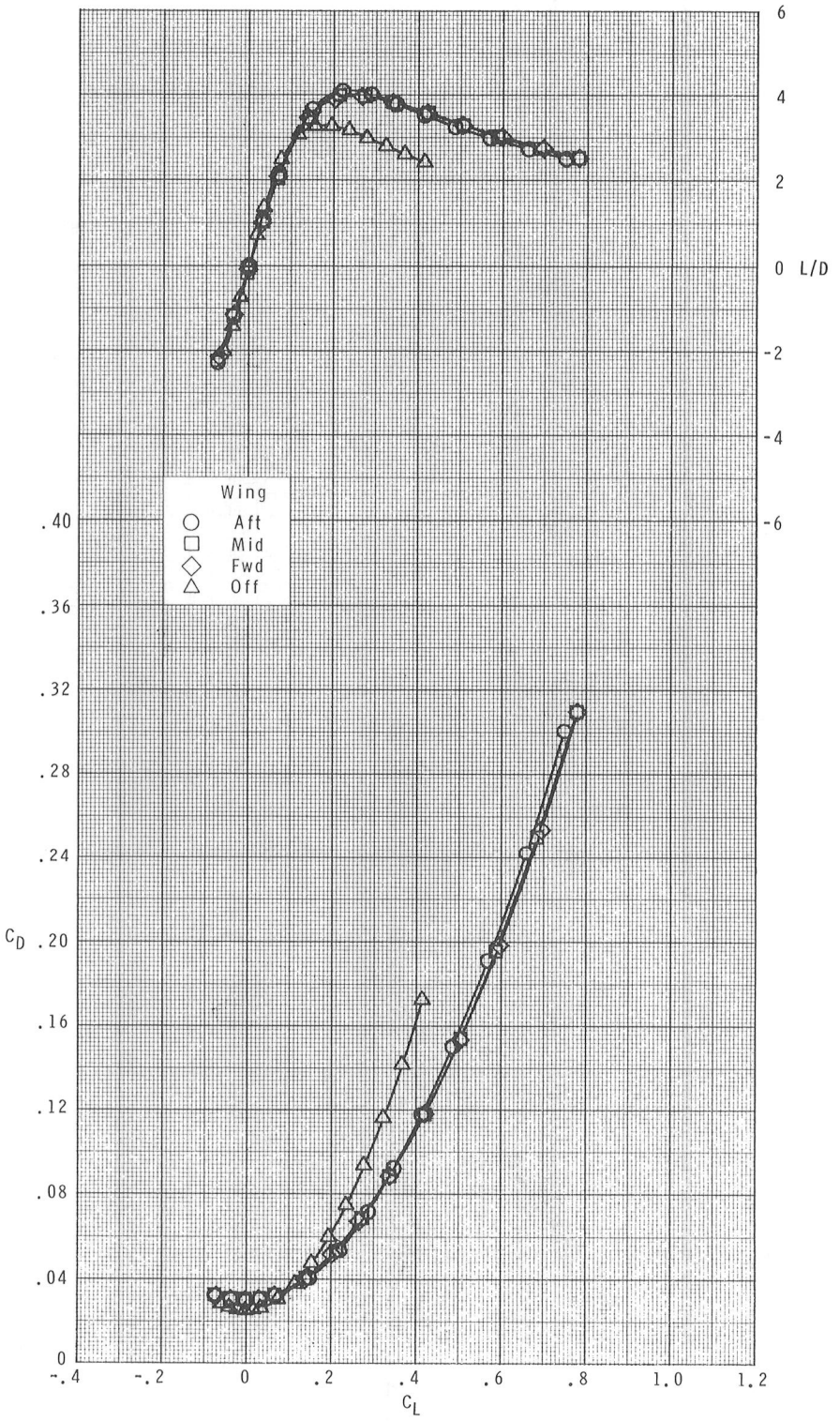

(a) Concluded.

Figure 4.- Continued.

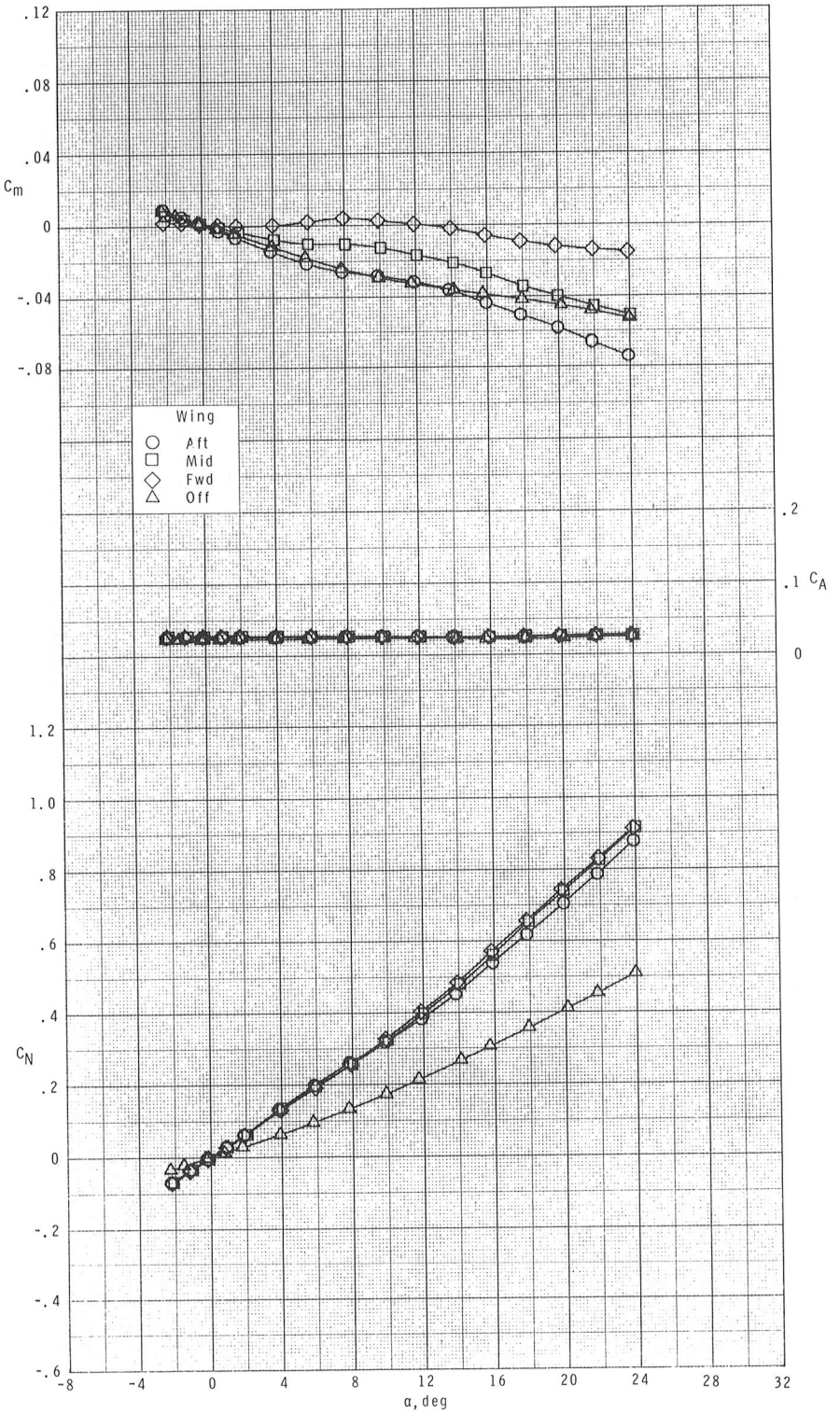

(b) M = 2.16.

Figure 4.- Continued.

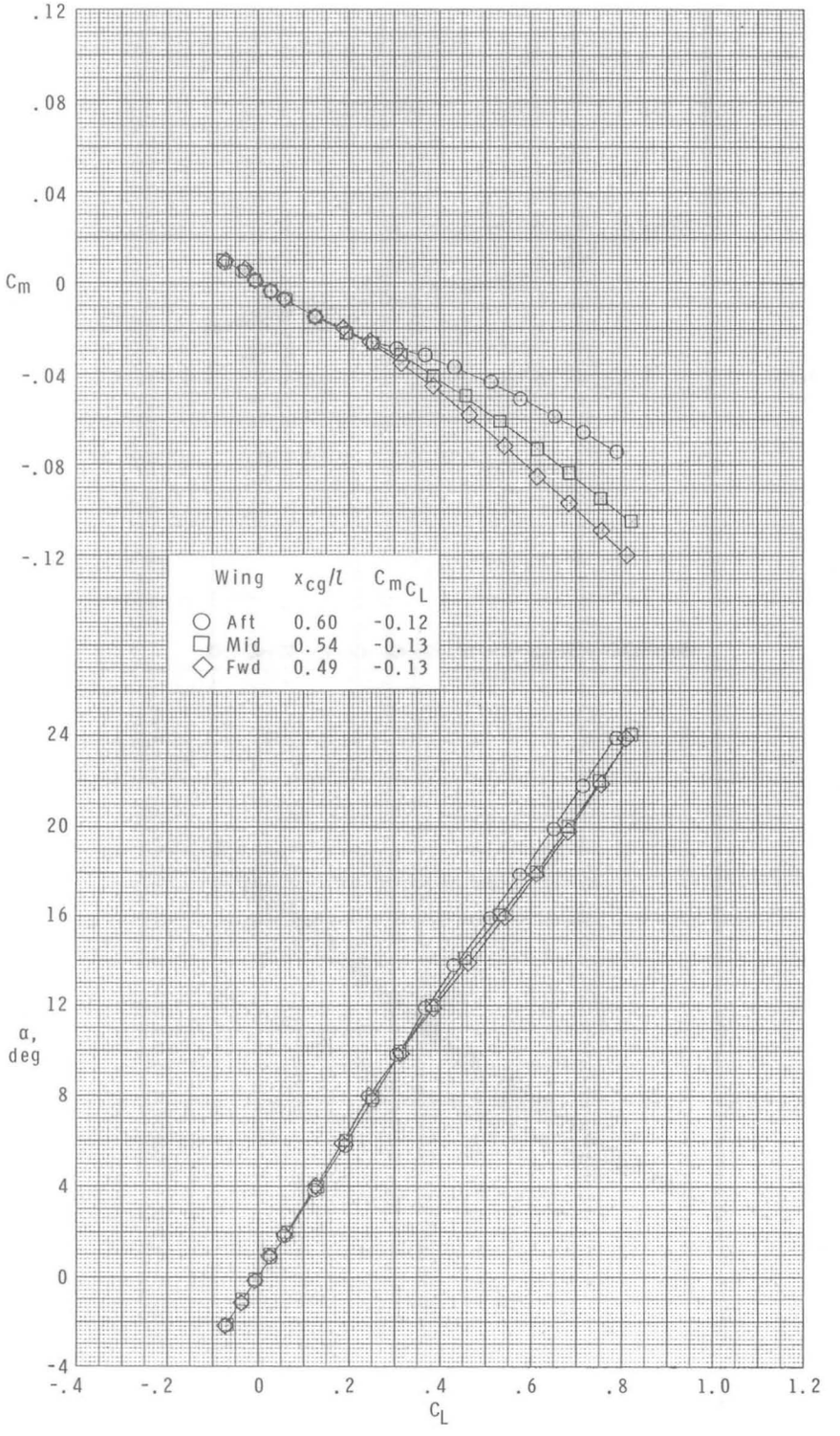

(b) Continued.

Figure 4.- Continued.

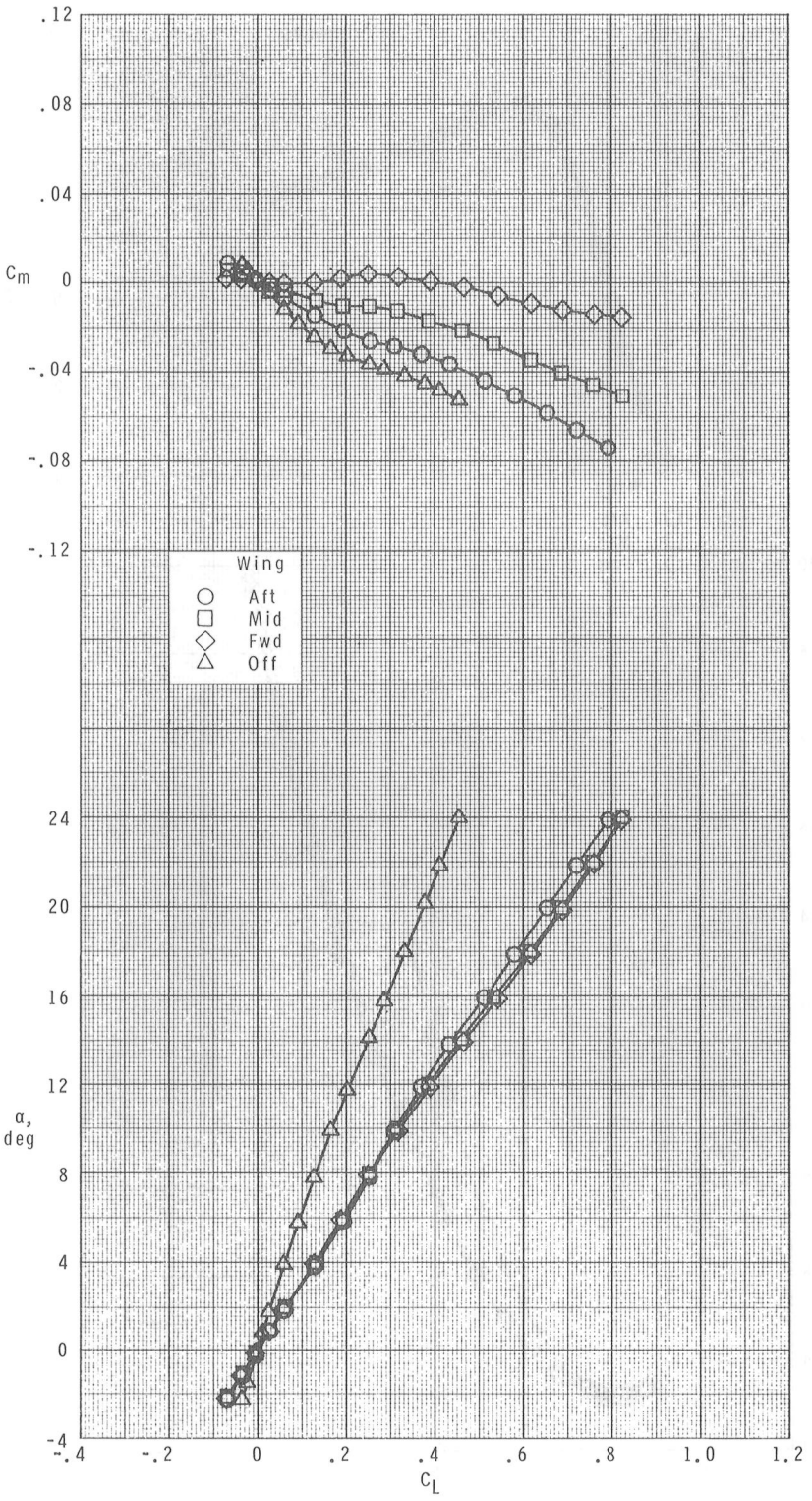

(b) Continued.

Figure 4.- Continued.

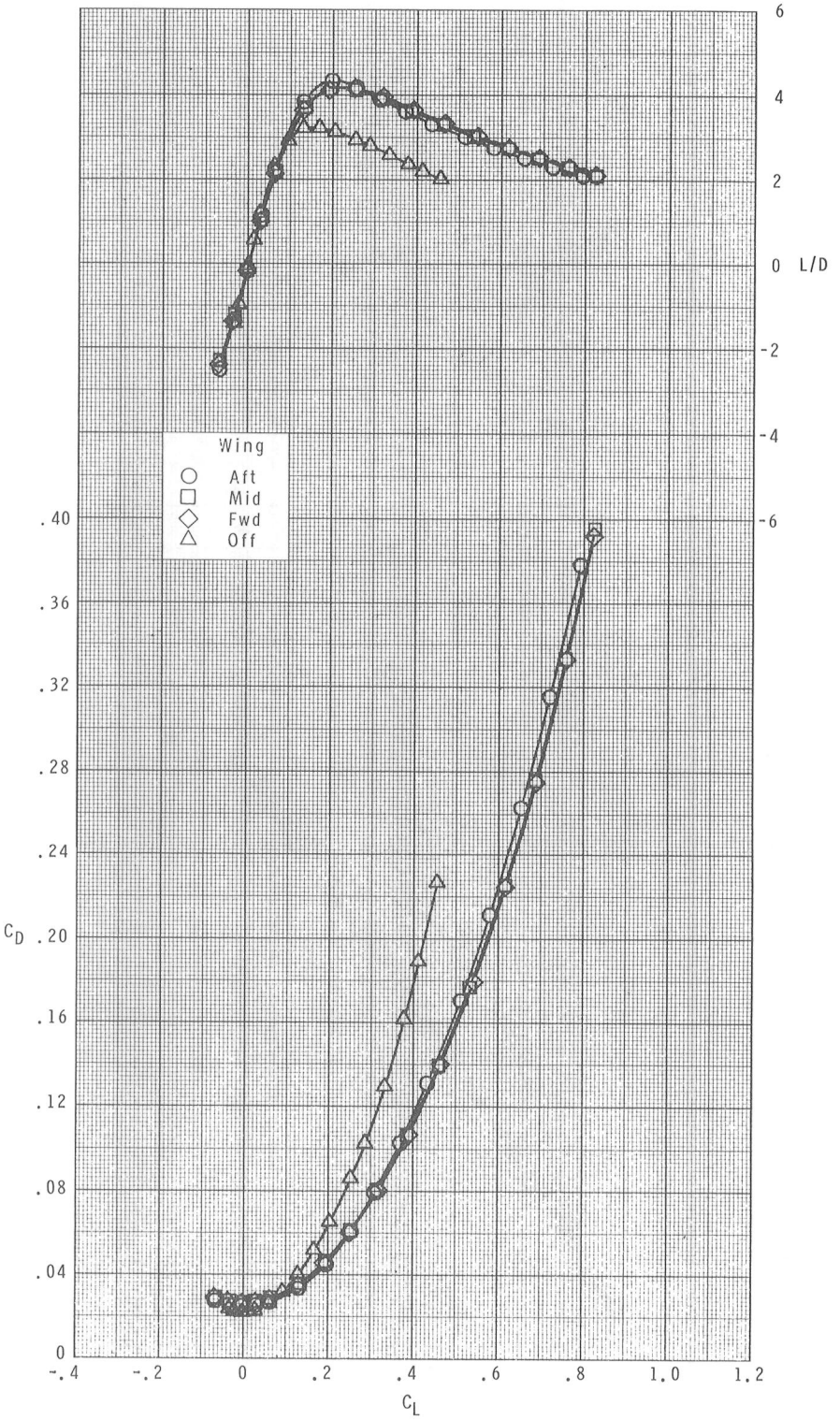

(b) Concluded.

Figure 4.- Continued.

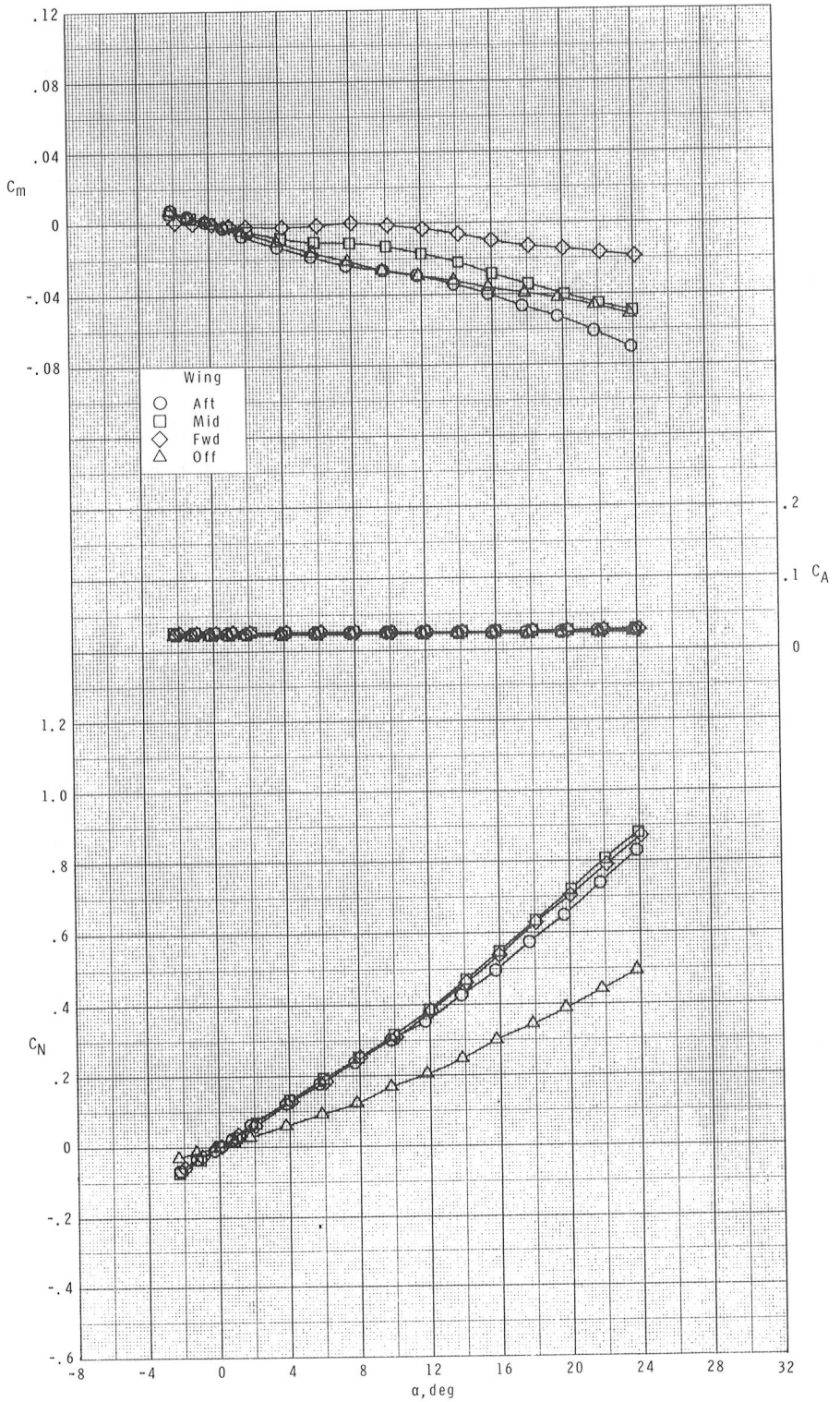

(c) M = 2.36.

Figure 4.- Continued.

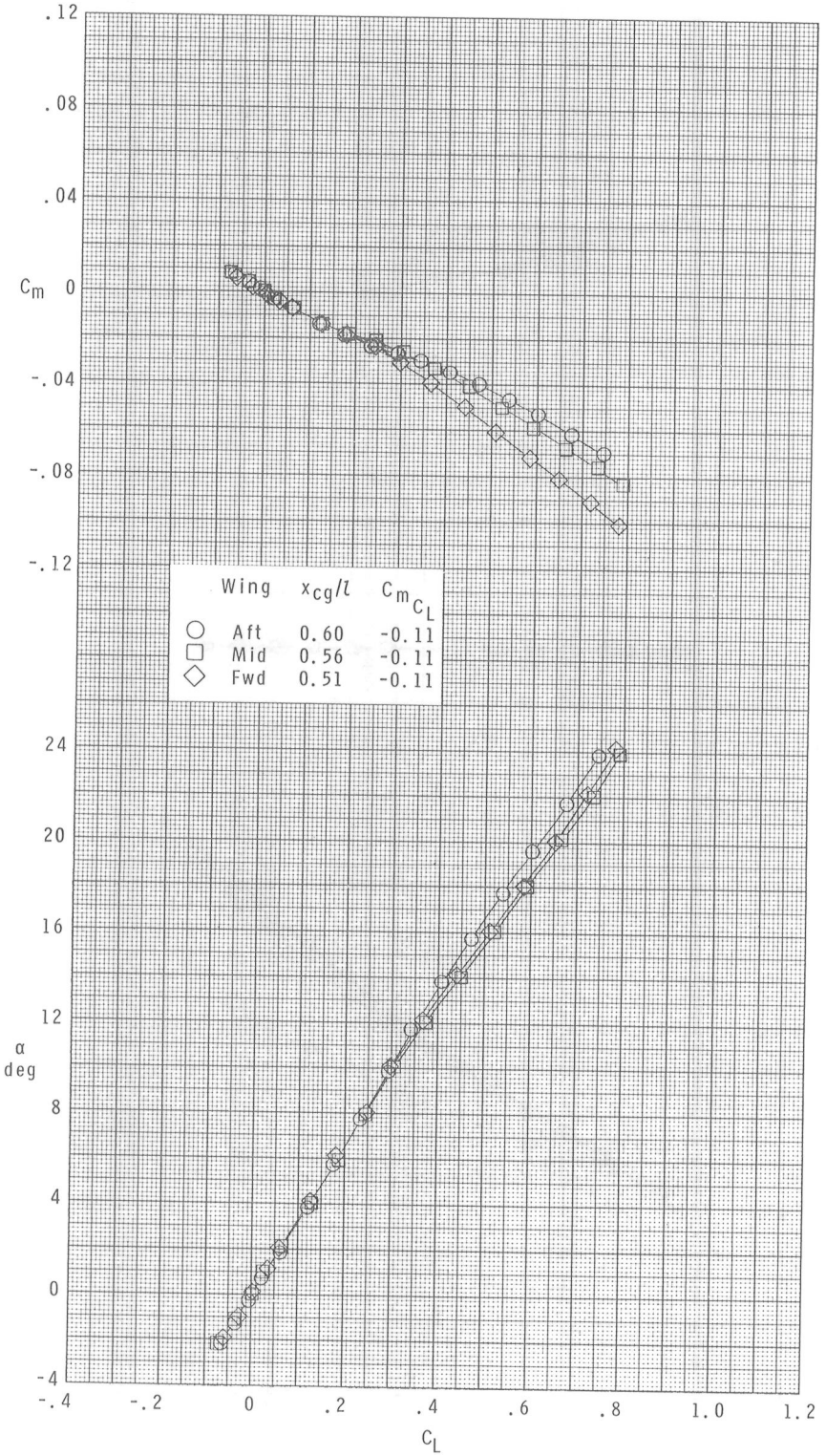

(c) Continued.

Figure 4.- Continued.

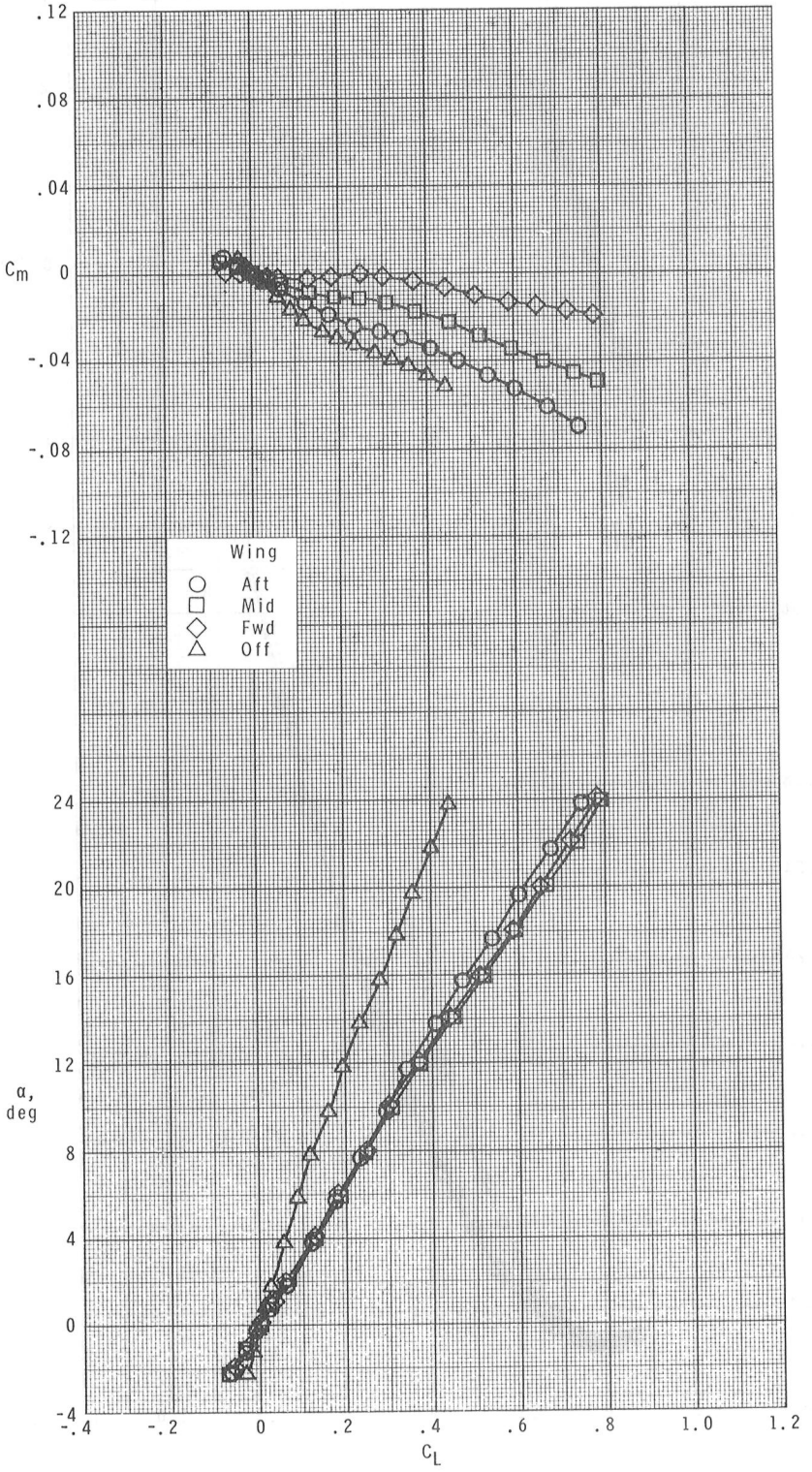

(c) Continued.

Figure 4.- Continued.

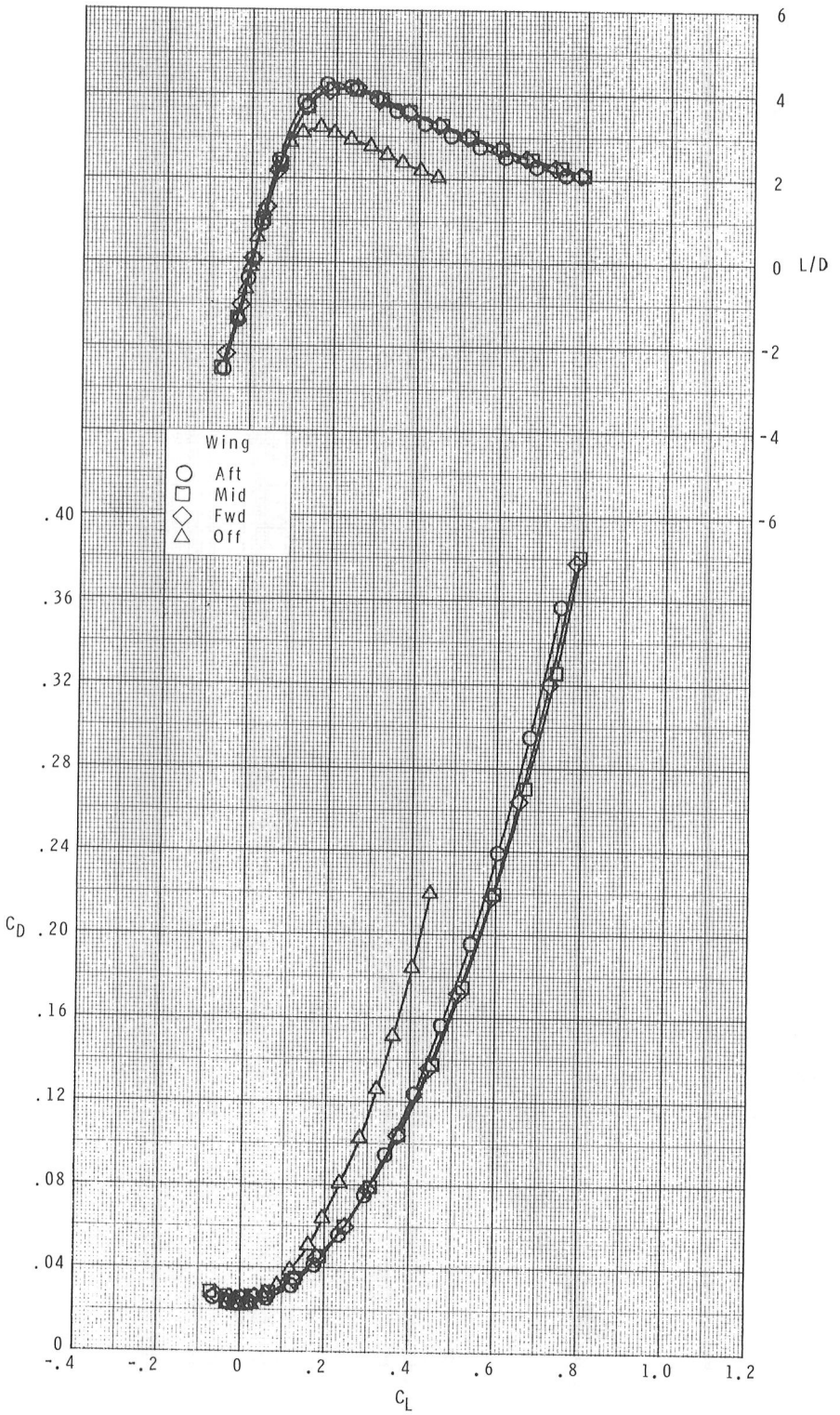

(c) Concluded.

Figure 4.- Continued.

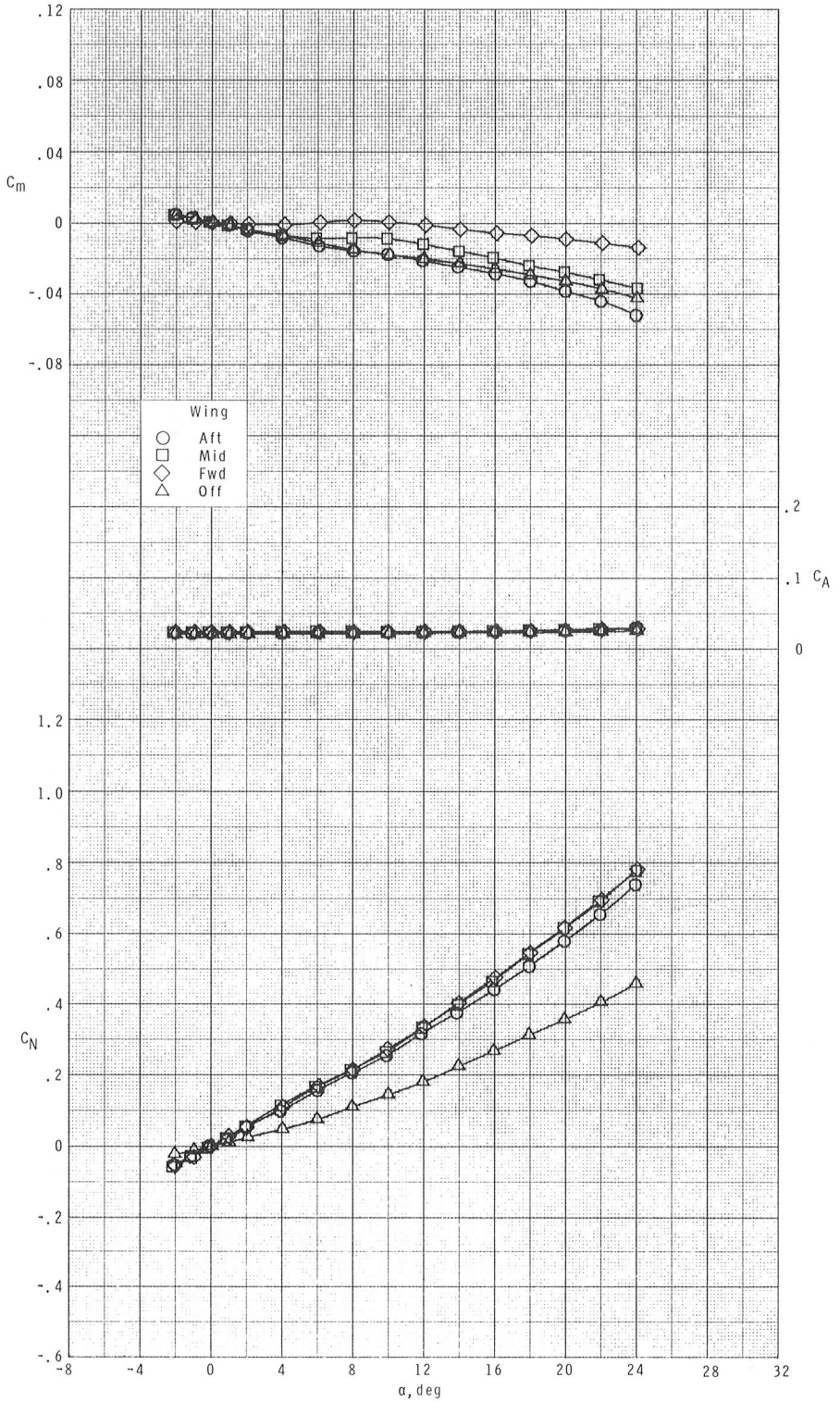

(d) M = 2.86.

Figure 4.- Continued.

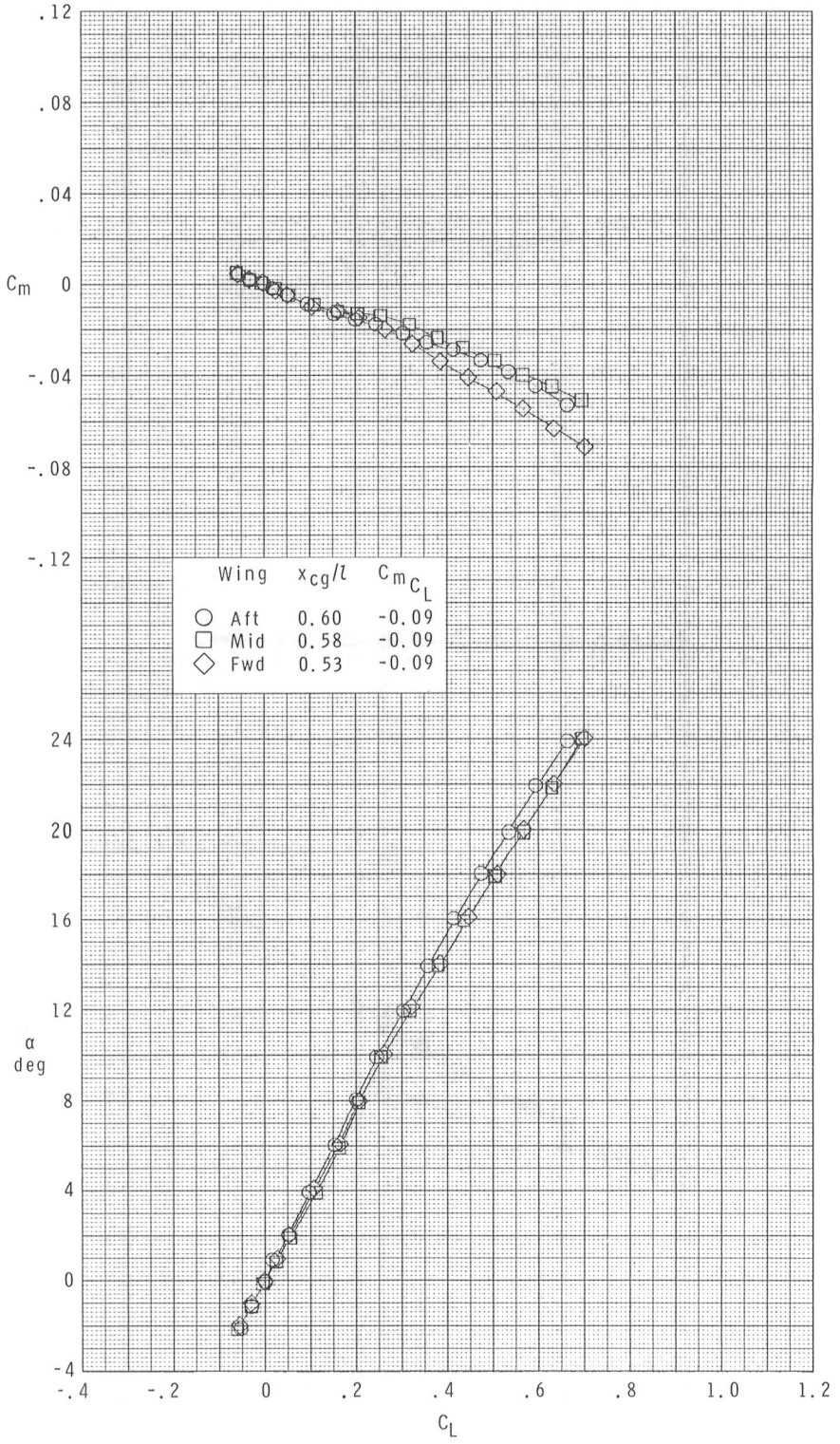

(d) Continued.

Figure 4.- Continued.

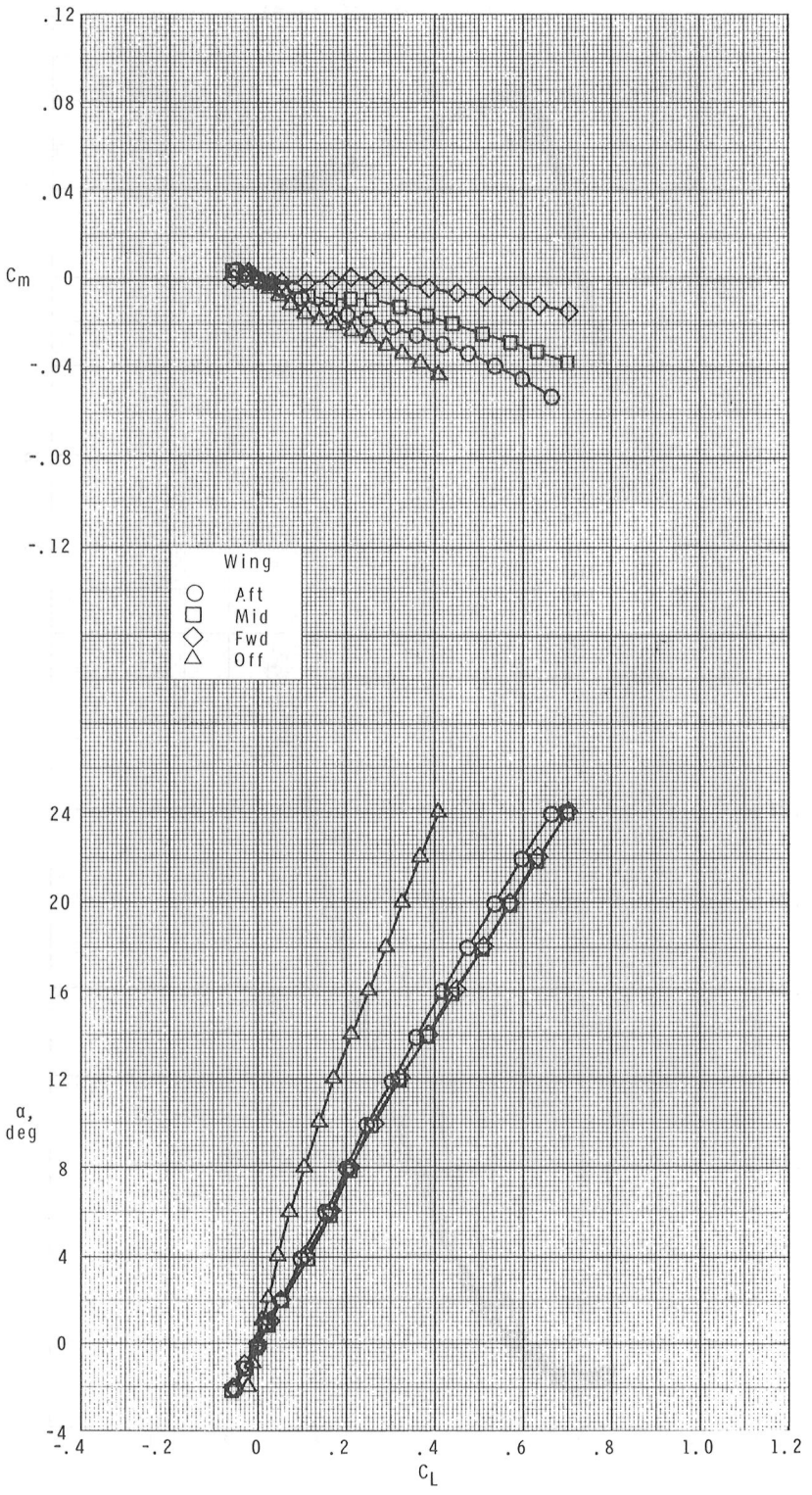

(d) Continued.

Figure 4.- Continued.

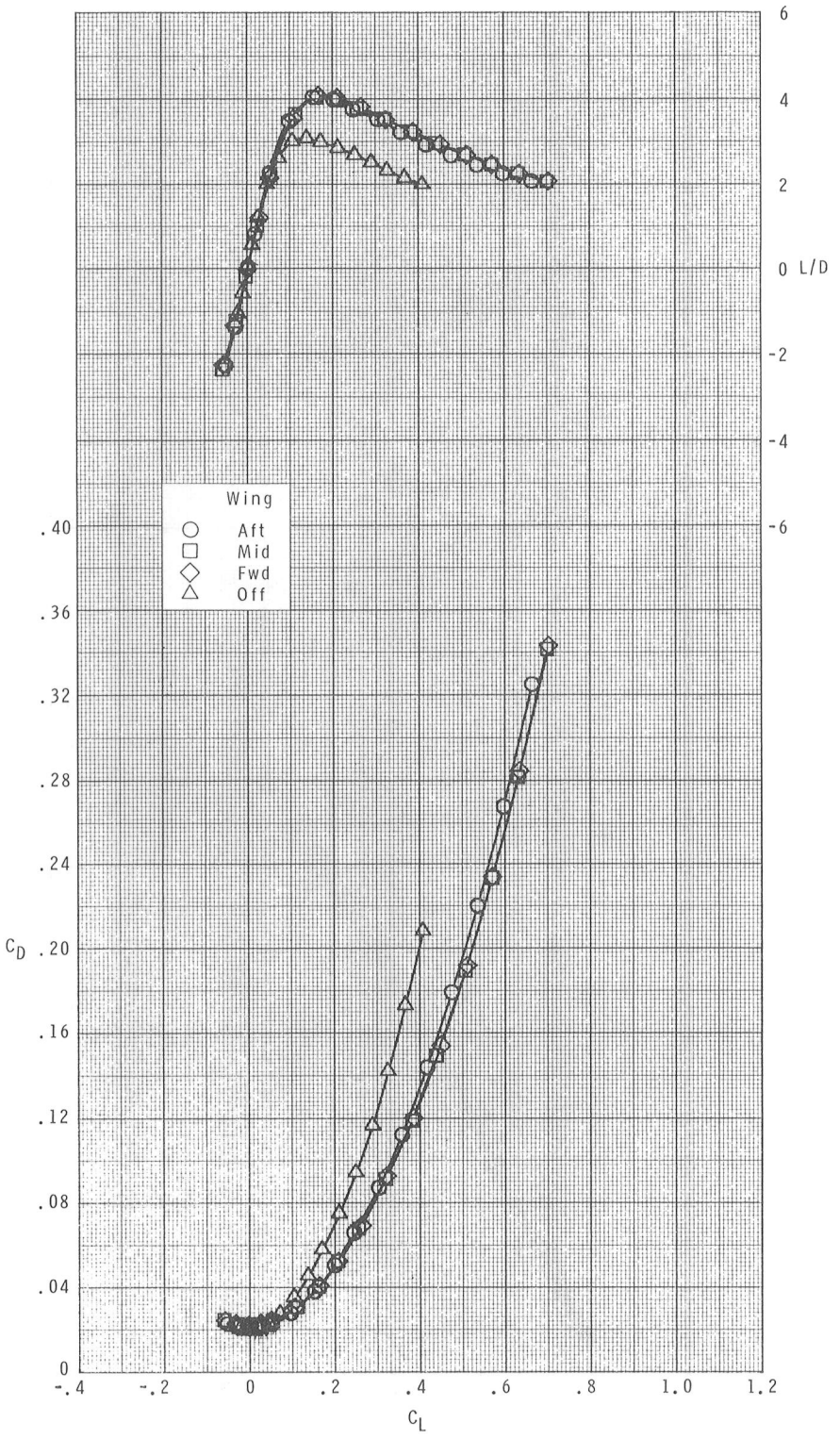

(d) Concluded.

Figure 4.- Concluded.

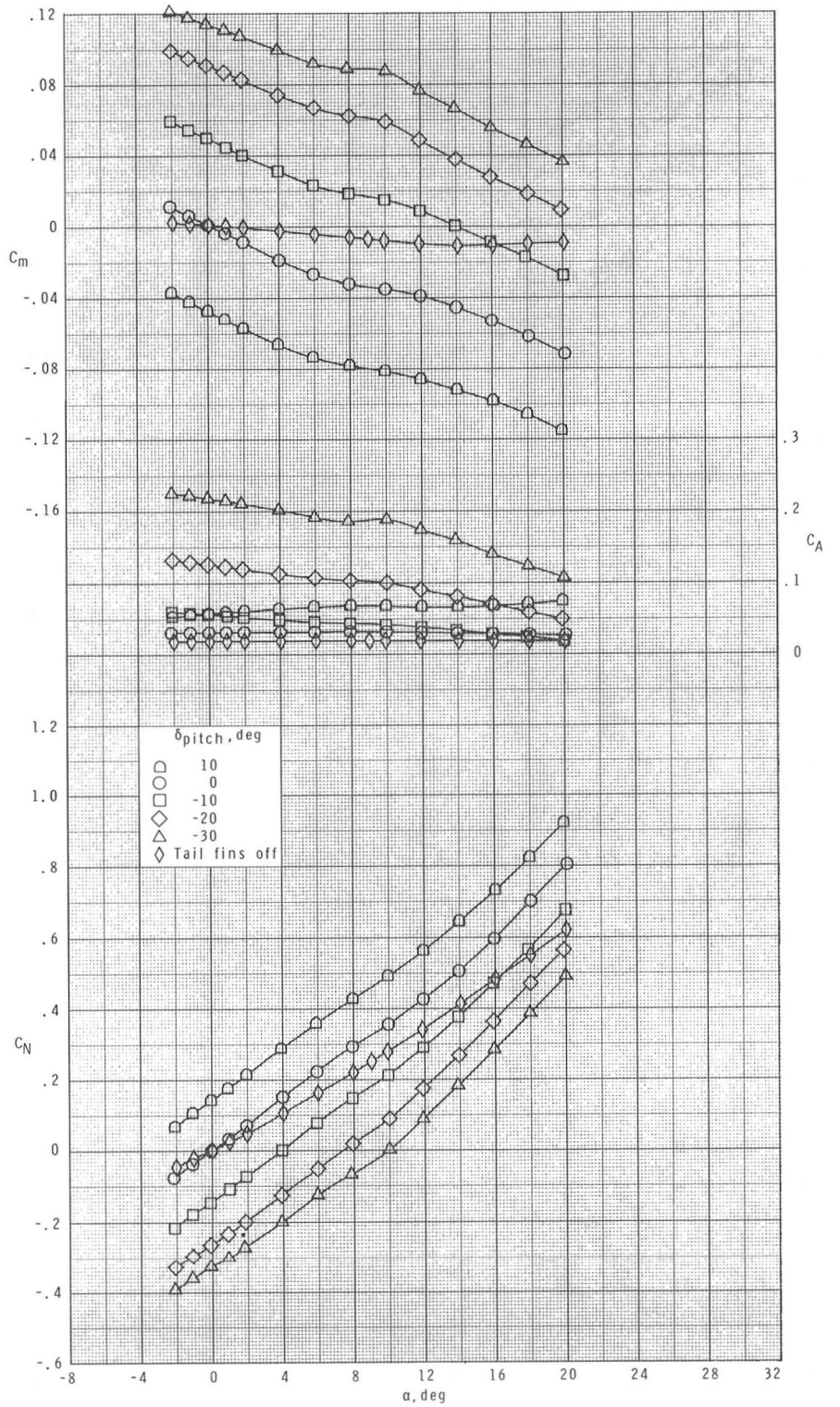

(a) M = 1.70.

Figure 5.- Effects of pitch control on longitudinal aerodynamic characteristics of the centerline-aft-wing configuration.

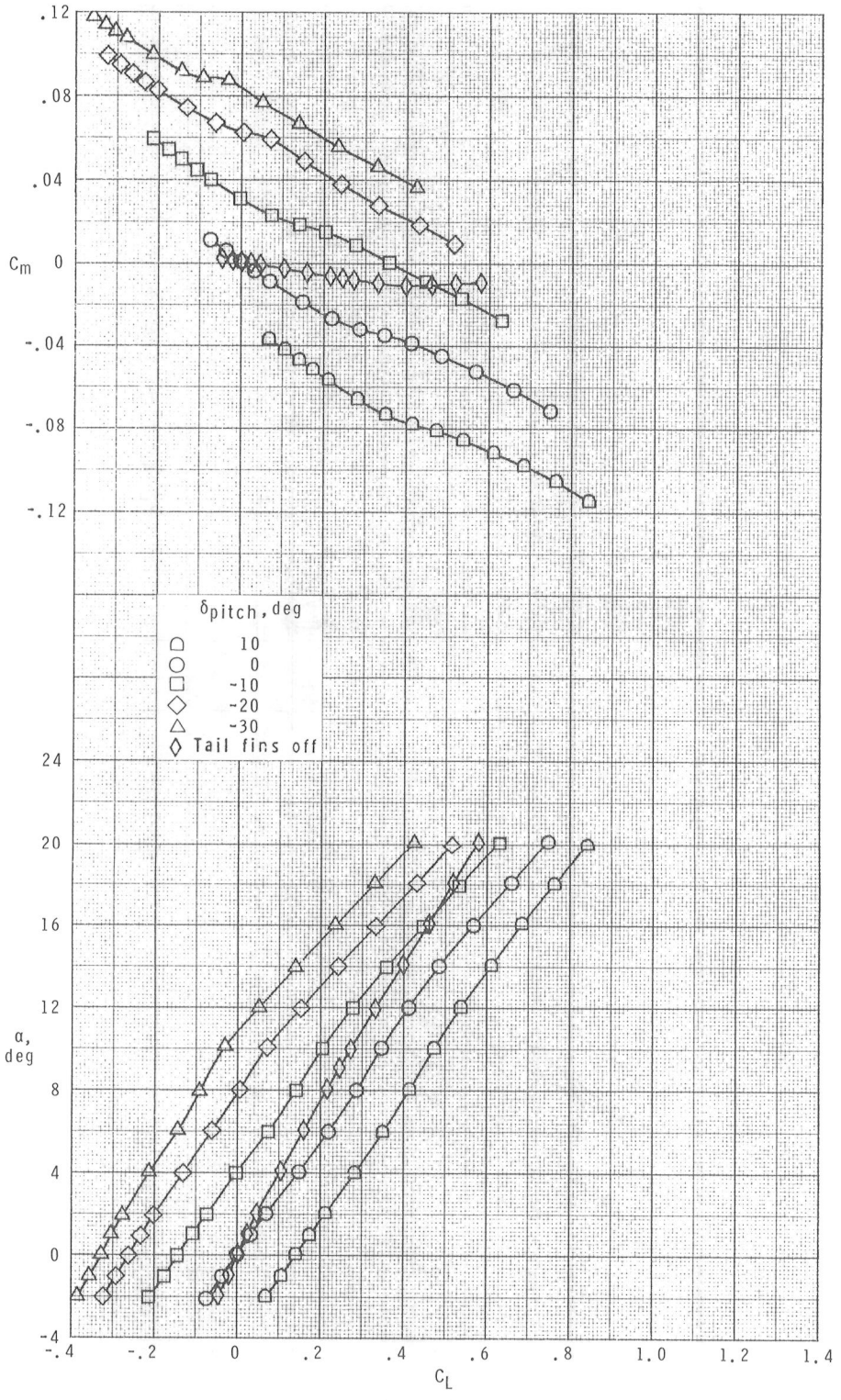

(a) Continued.

Figure 5.- Continued.

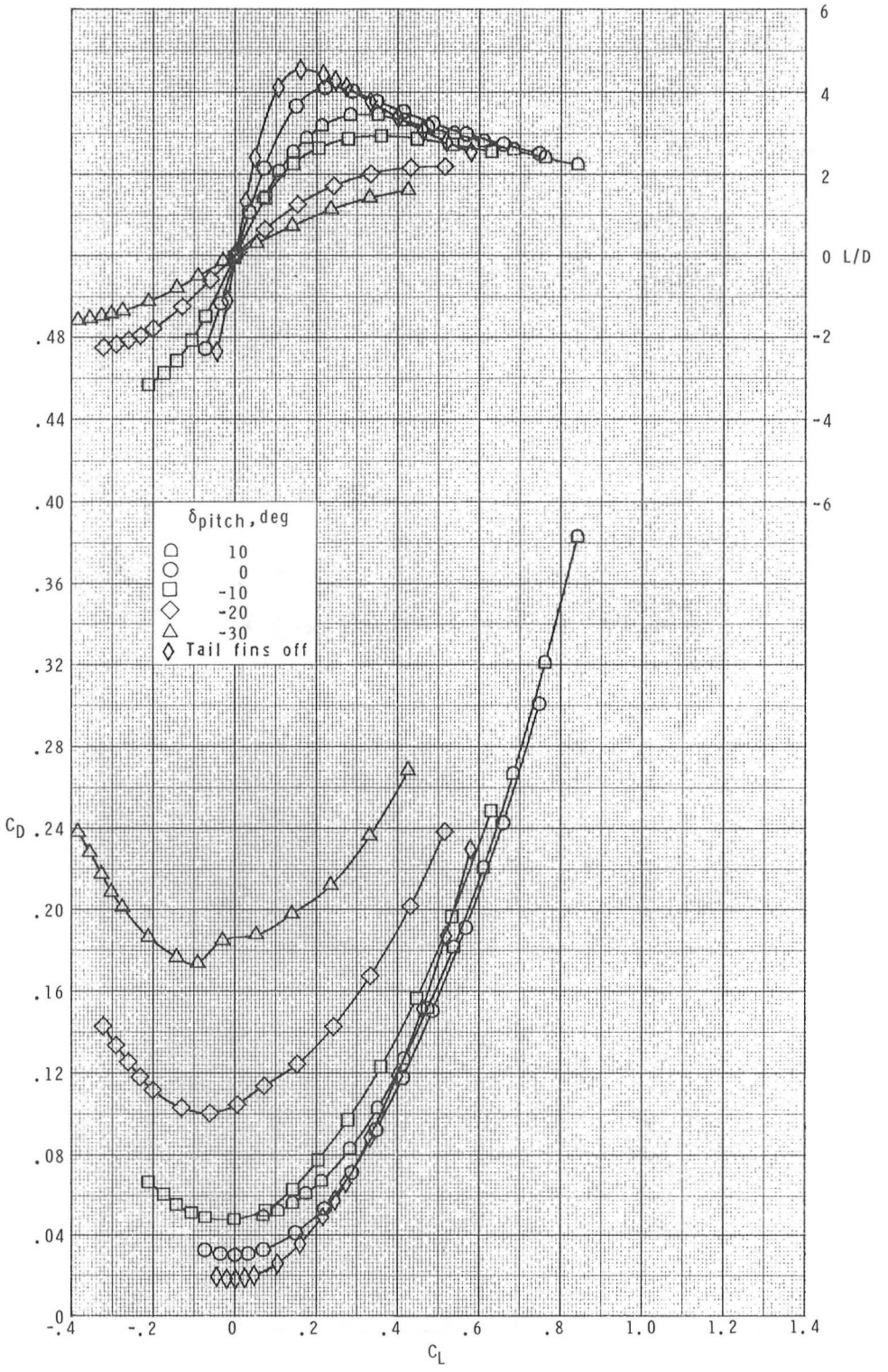

(a) Concluded.

Figure 5.- Continued.

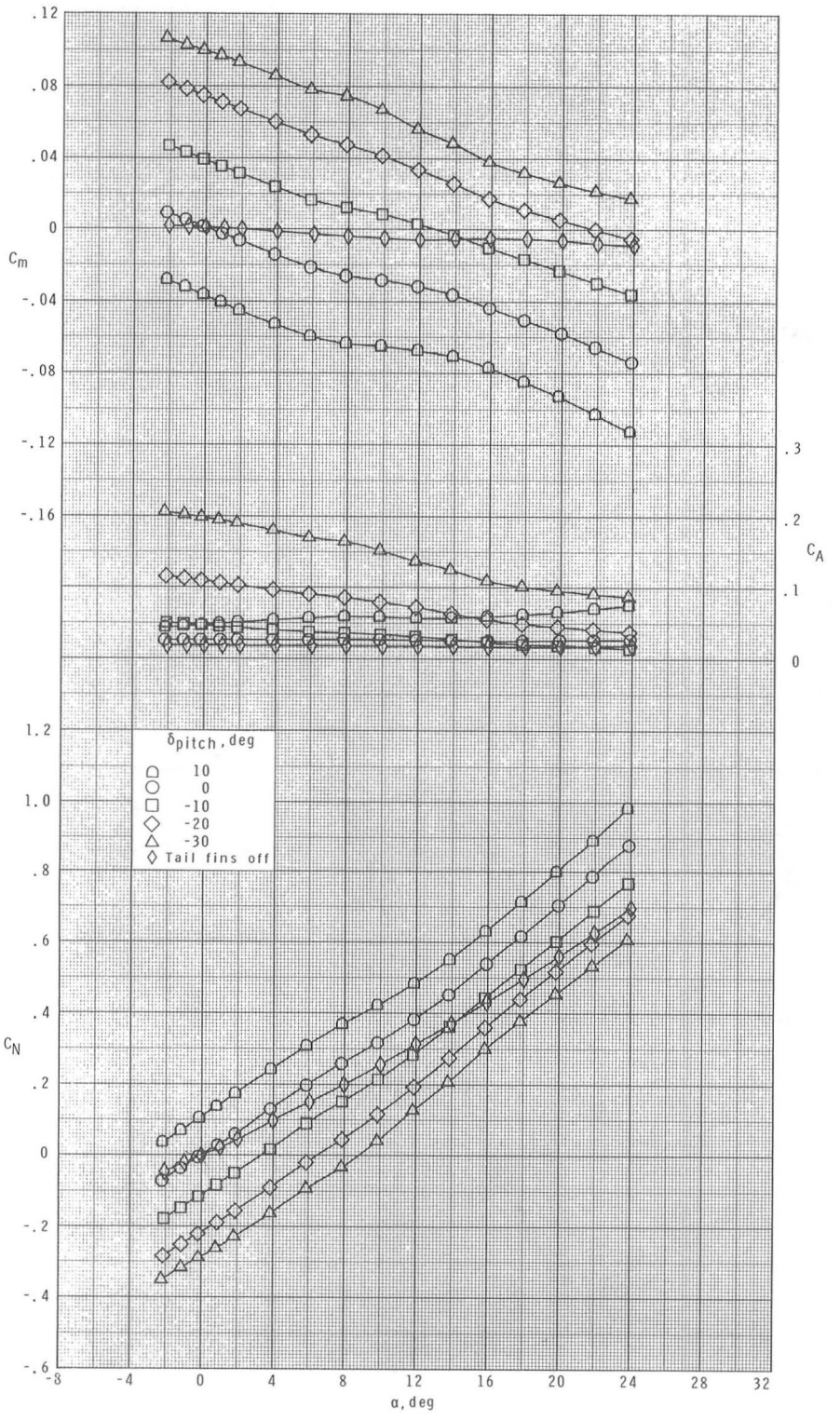

(b) M = 2.16.

Figure 5.- Continued.

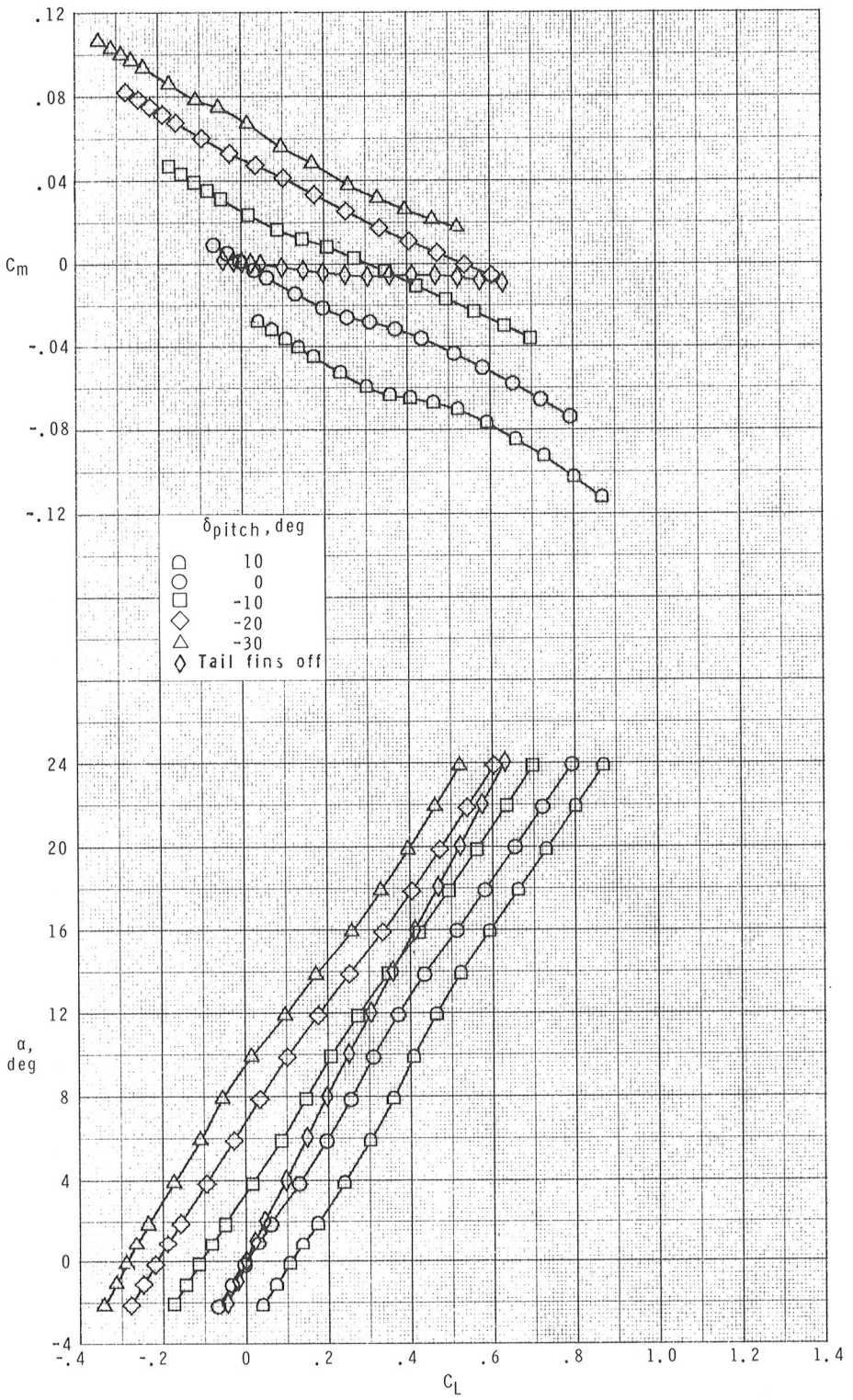

(b) Continued.

Figure 5.- Continued.

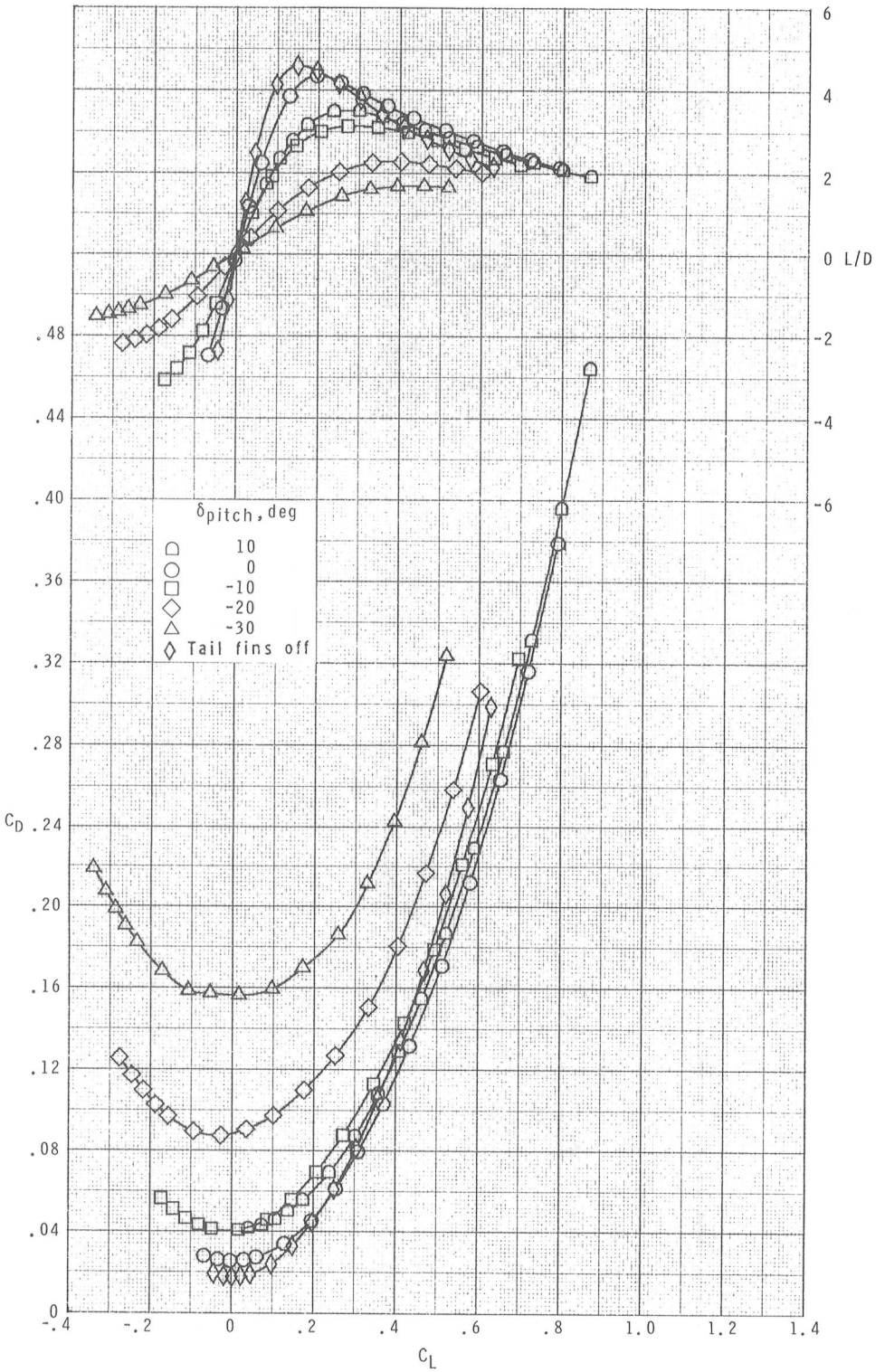

(b) Concluded.

Figure 5.- Continued.

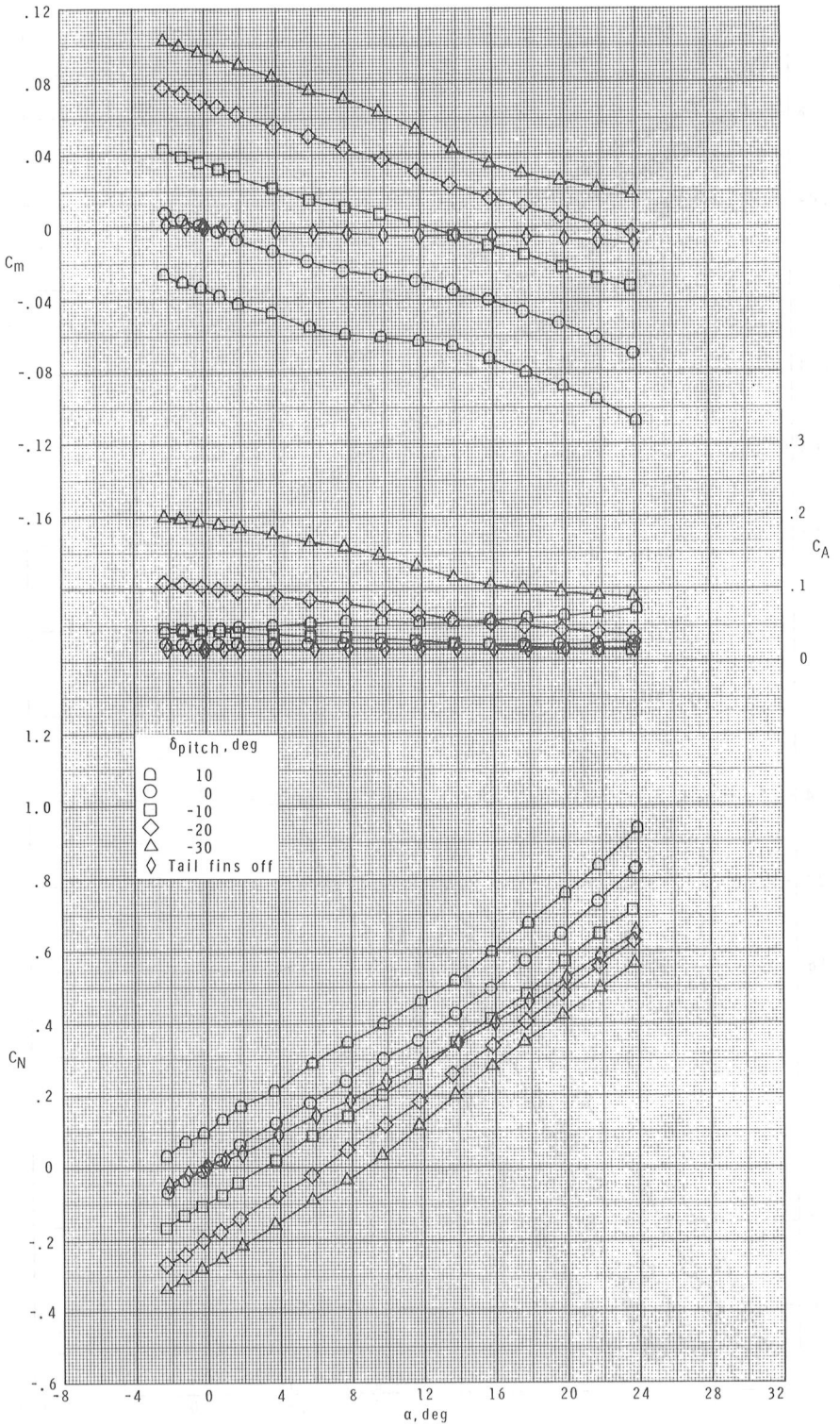

(c) M = 2.36.

Figure 5.- Continued.

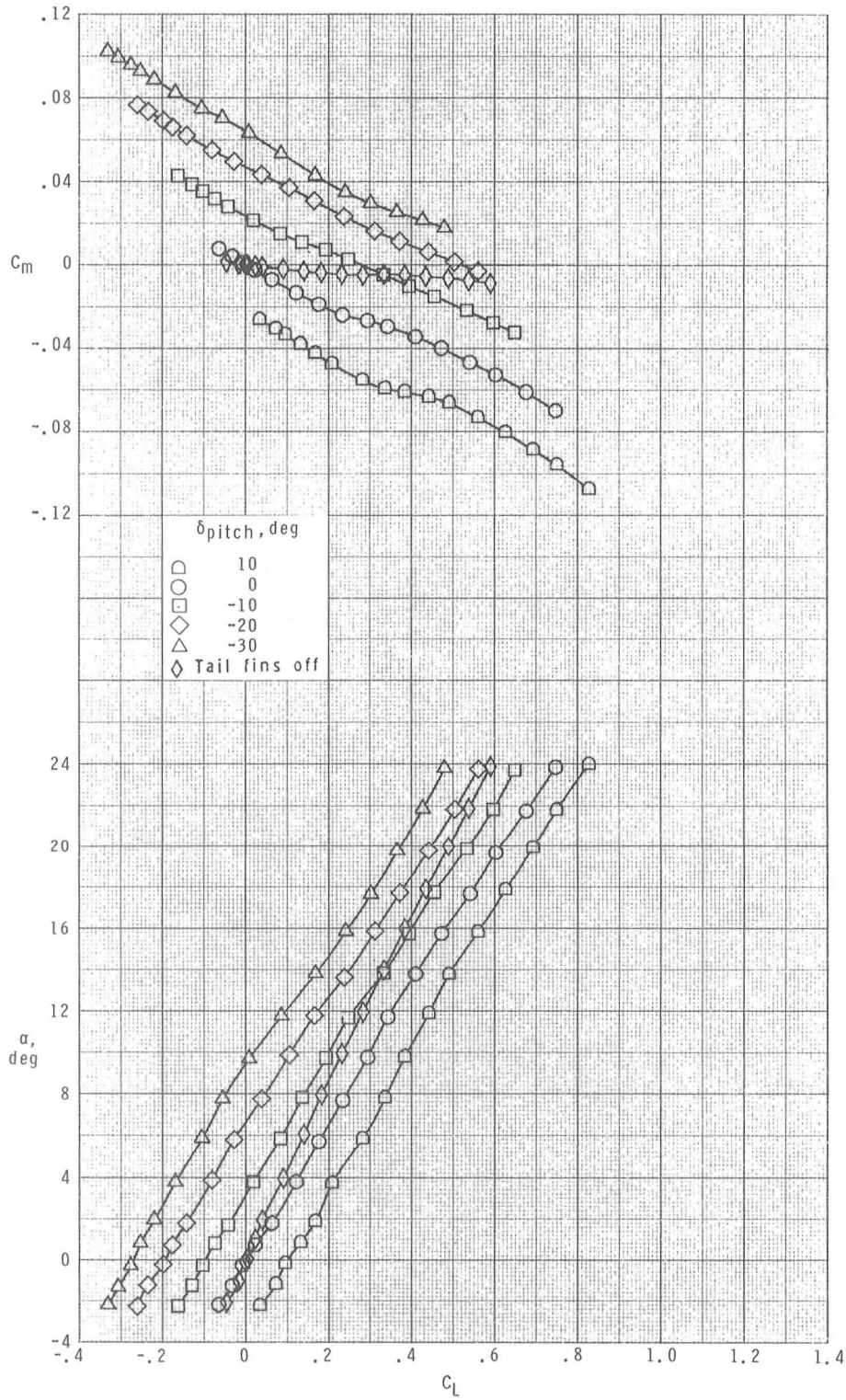

(c) Continued.

Figure 5.- Continued.

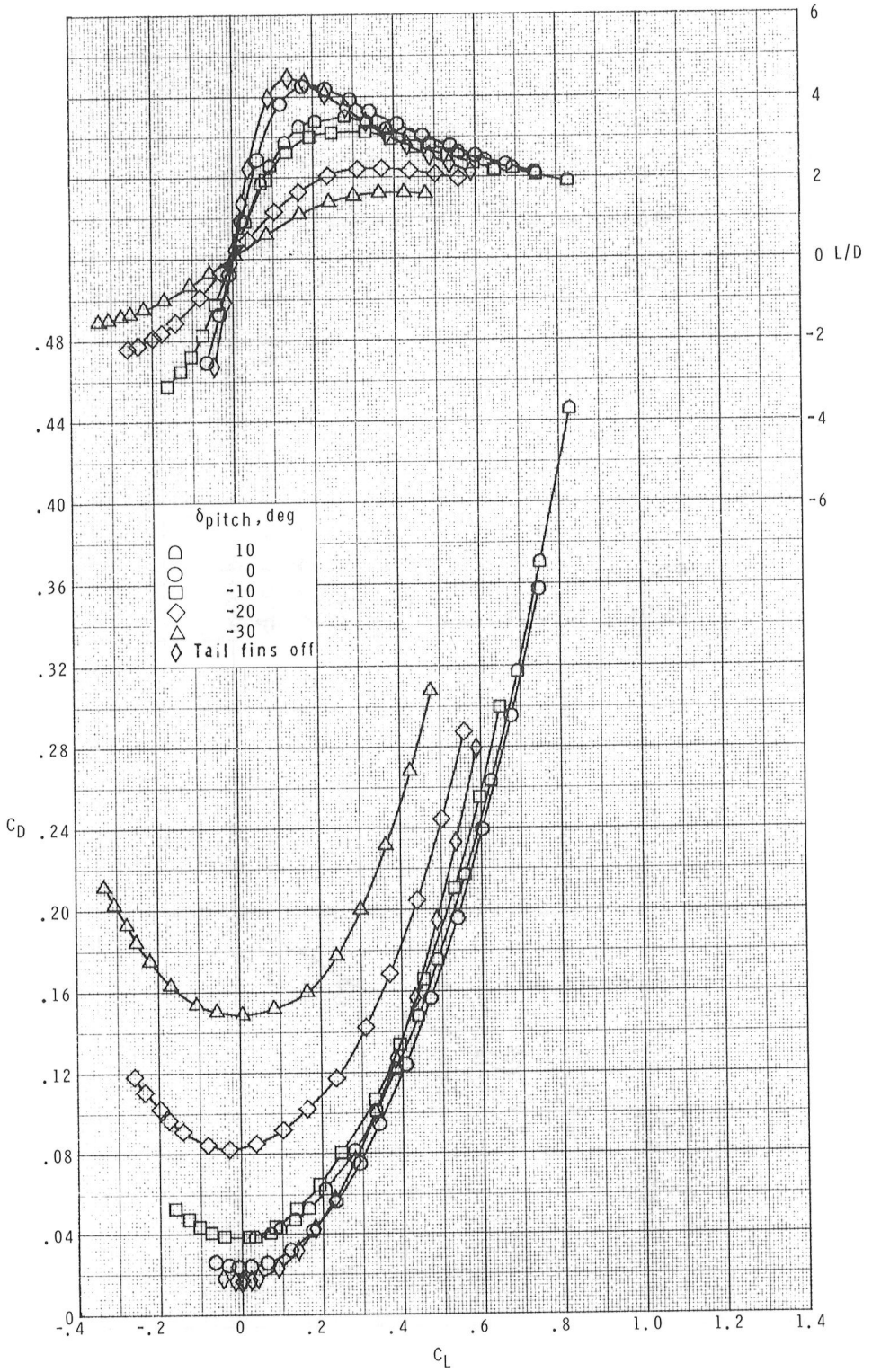

(c) Concluded.

Figure 5.- Continued.

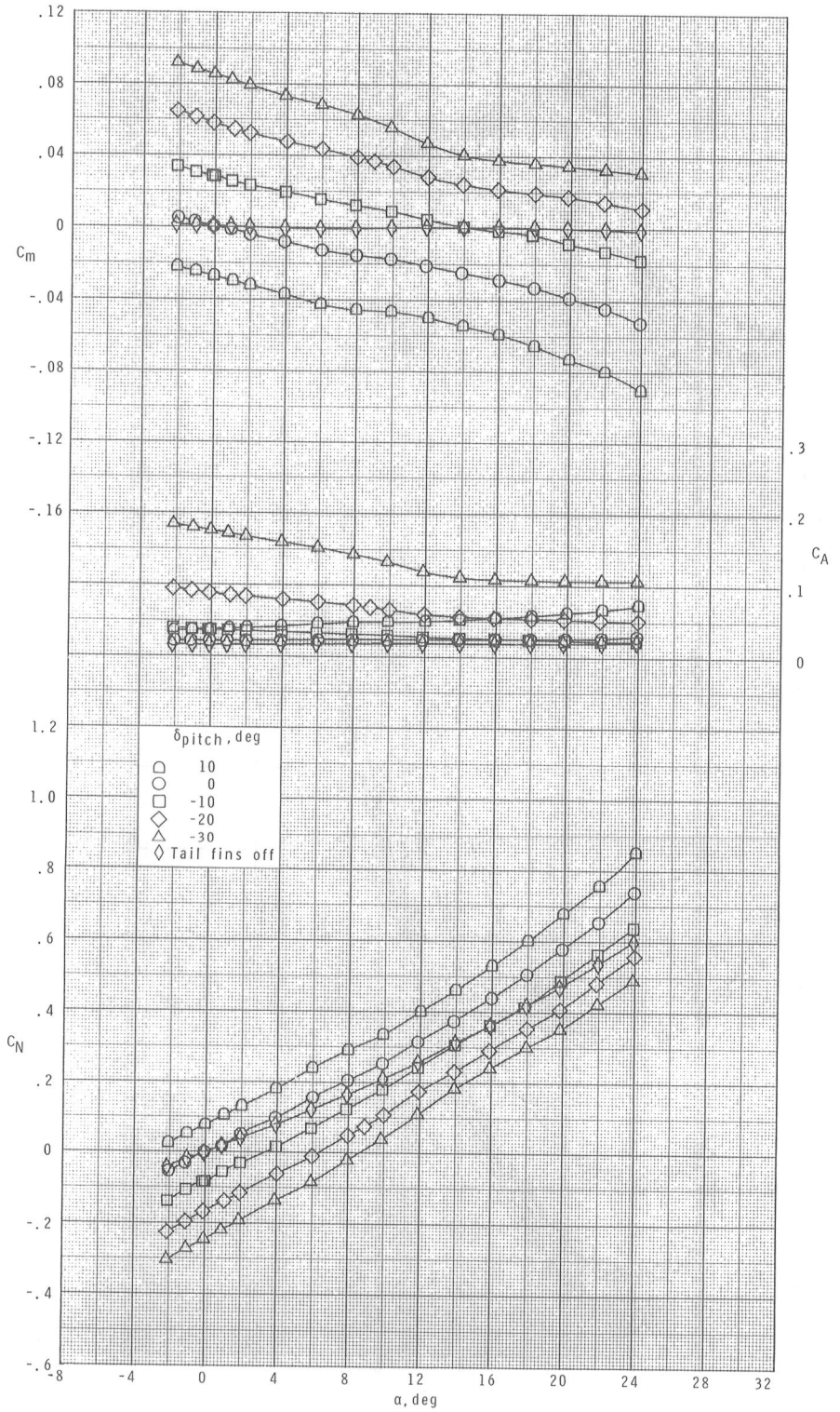

(d) M = 2.86

Figure 5.- Continued.

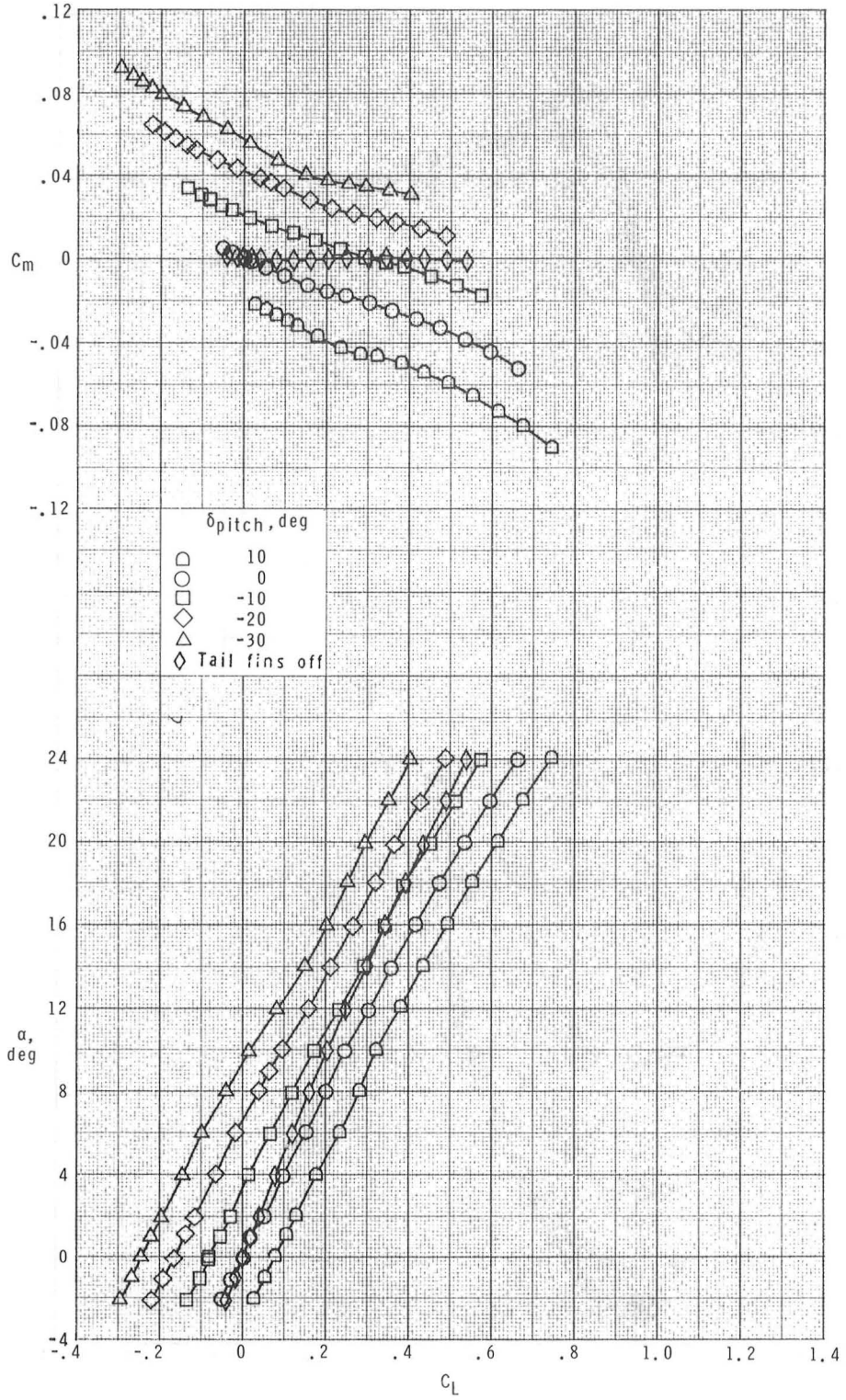

(d) Continued.

Figure 5.- Continued.

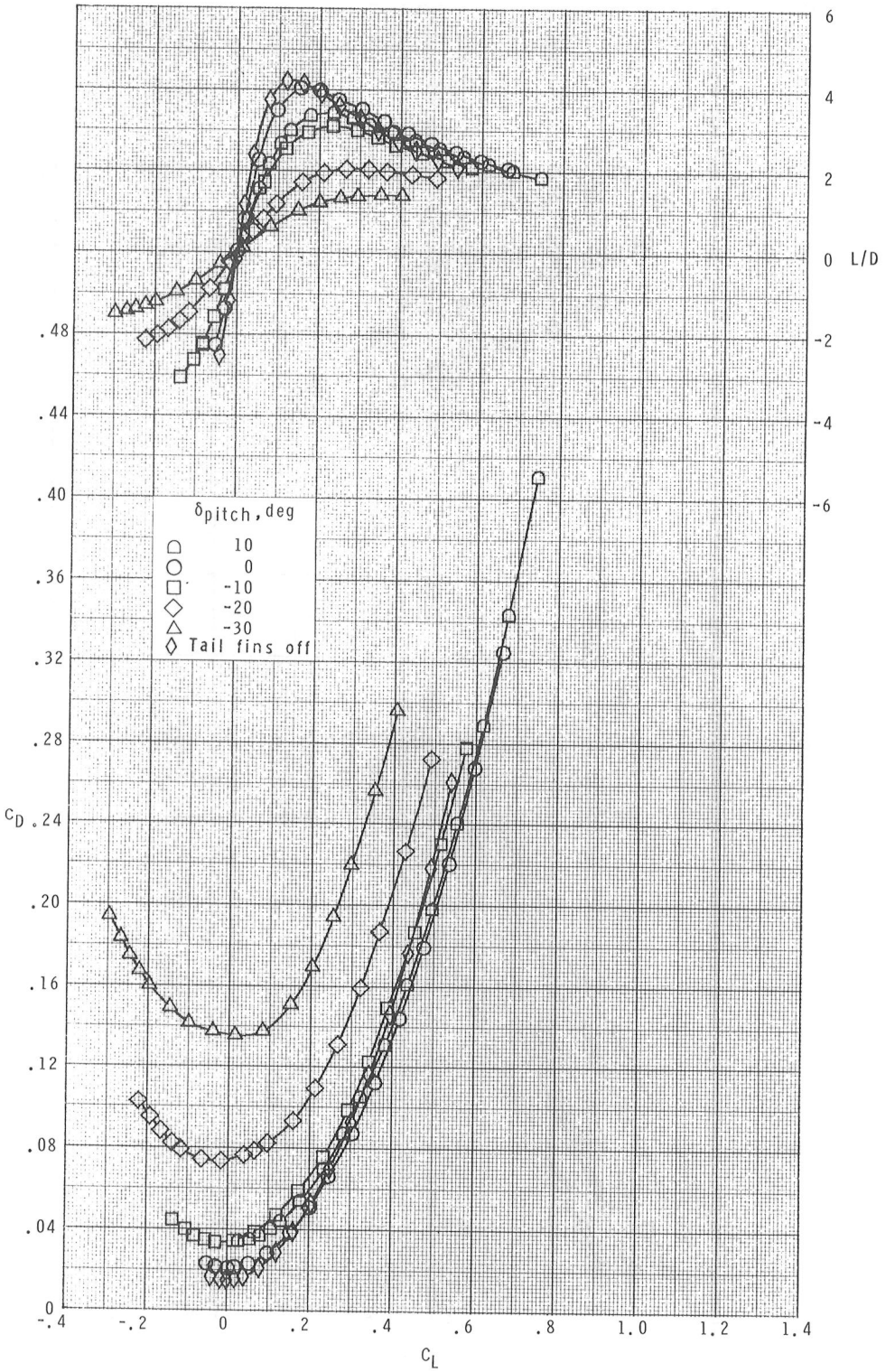

(d) Concluded.

Figure 5.- Concluded.

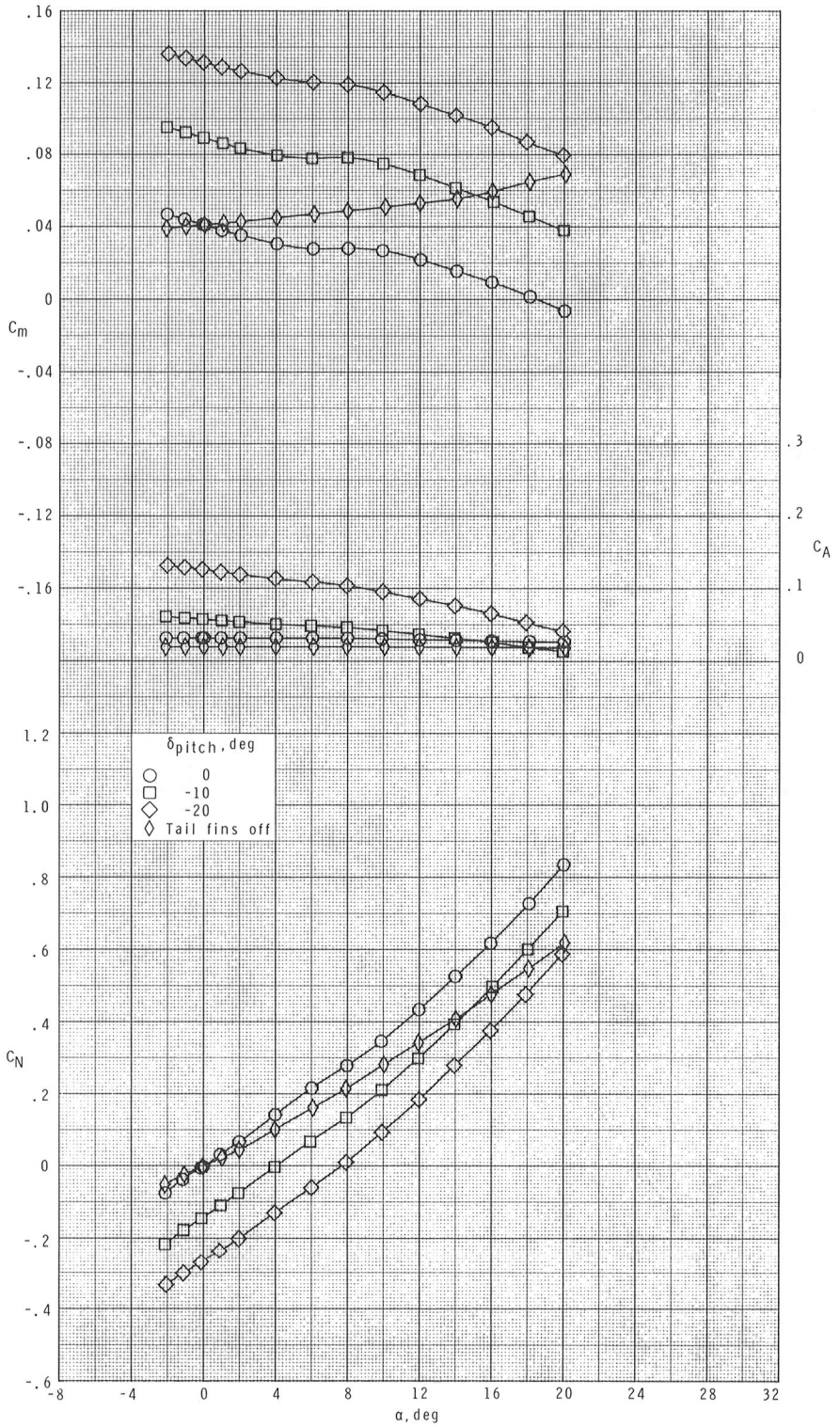

(a) M = 1.70.

Figure 6.- Effects of pitch control on longitudinal aerodynamic characteristics of the centerline-mid-wing configuration.

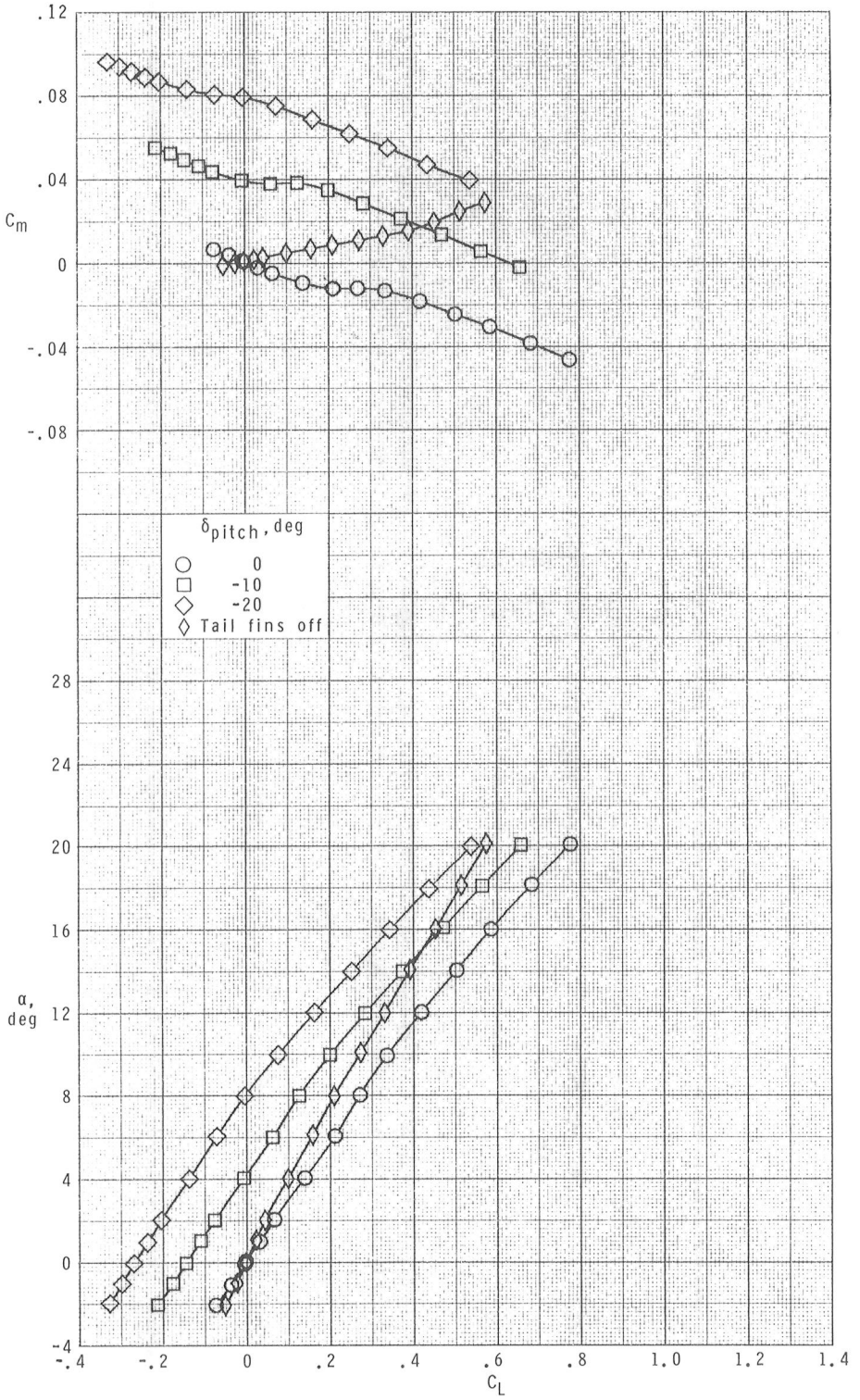

(a) Continued.

Figure 6.- Continued.

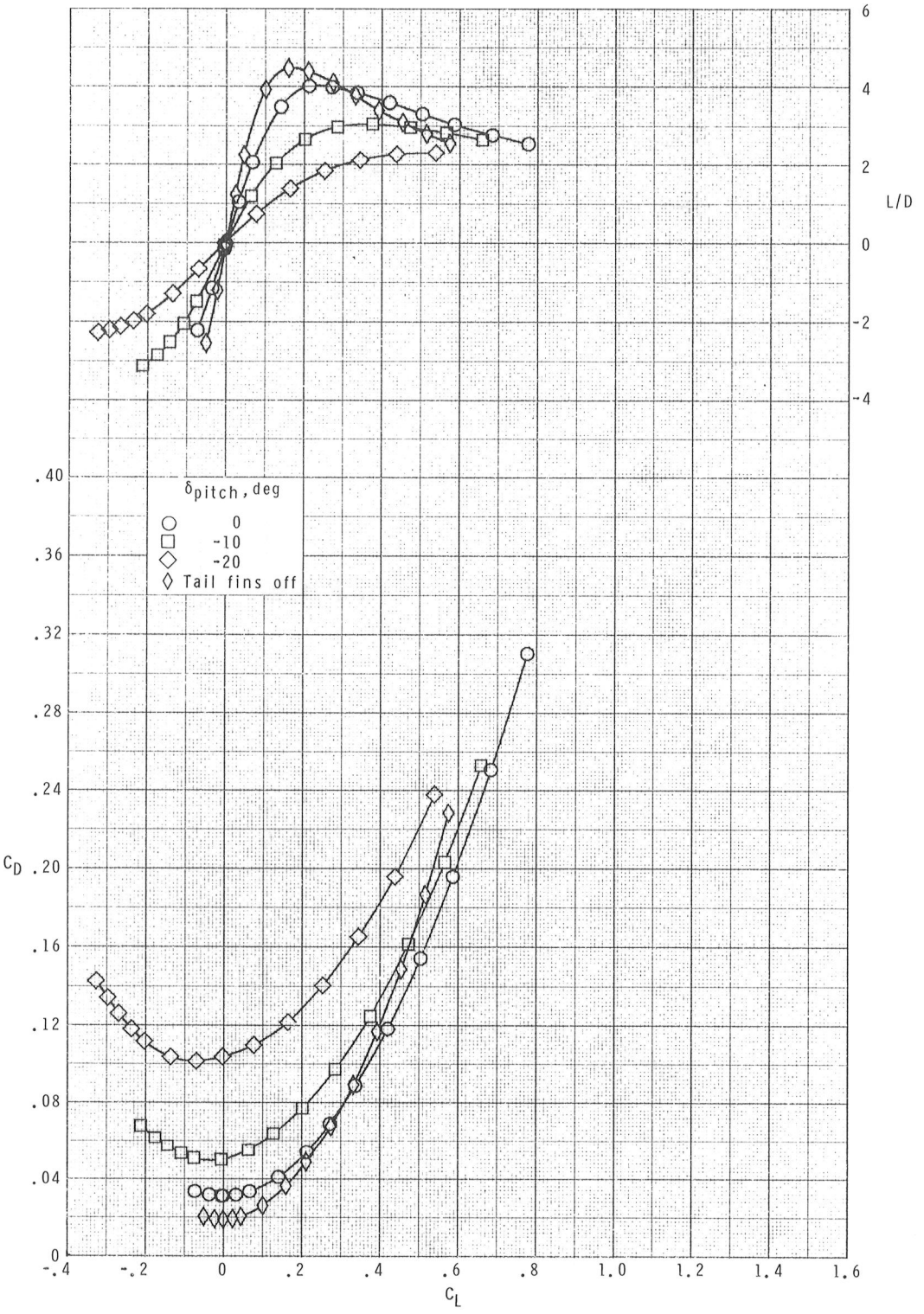

(a) Concluded.

Figure 6.- Continued.

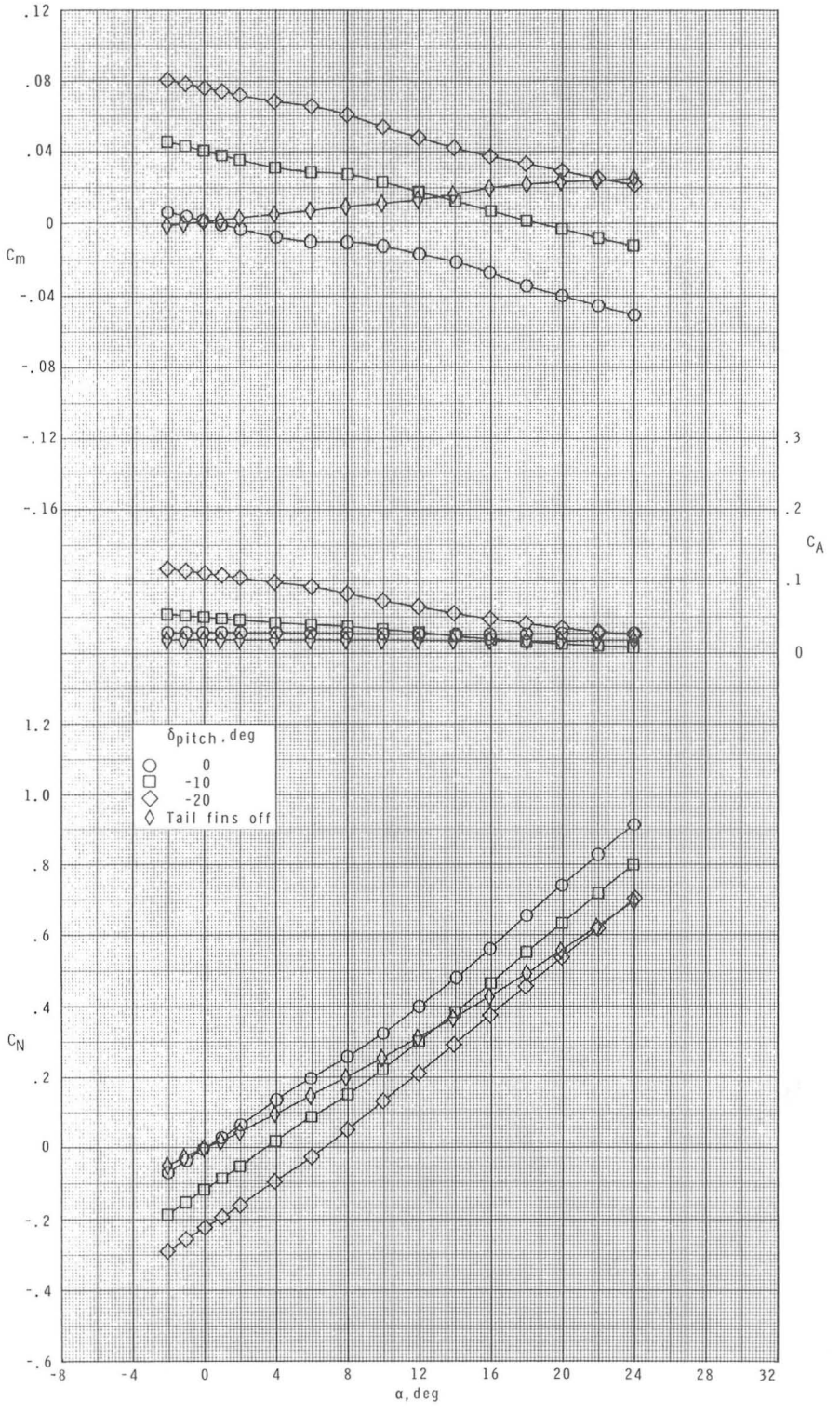

(b) M = 2.16

Figure 6.- Continued.

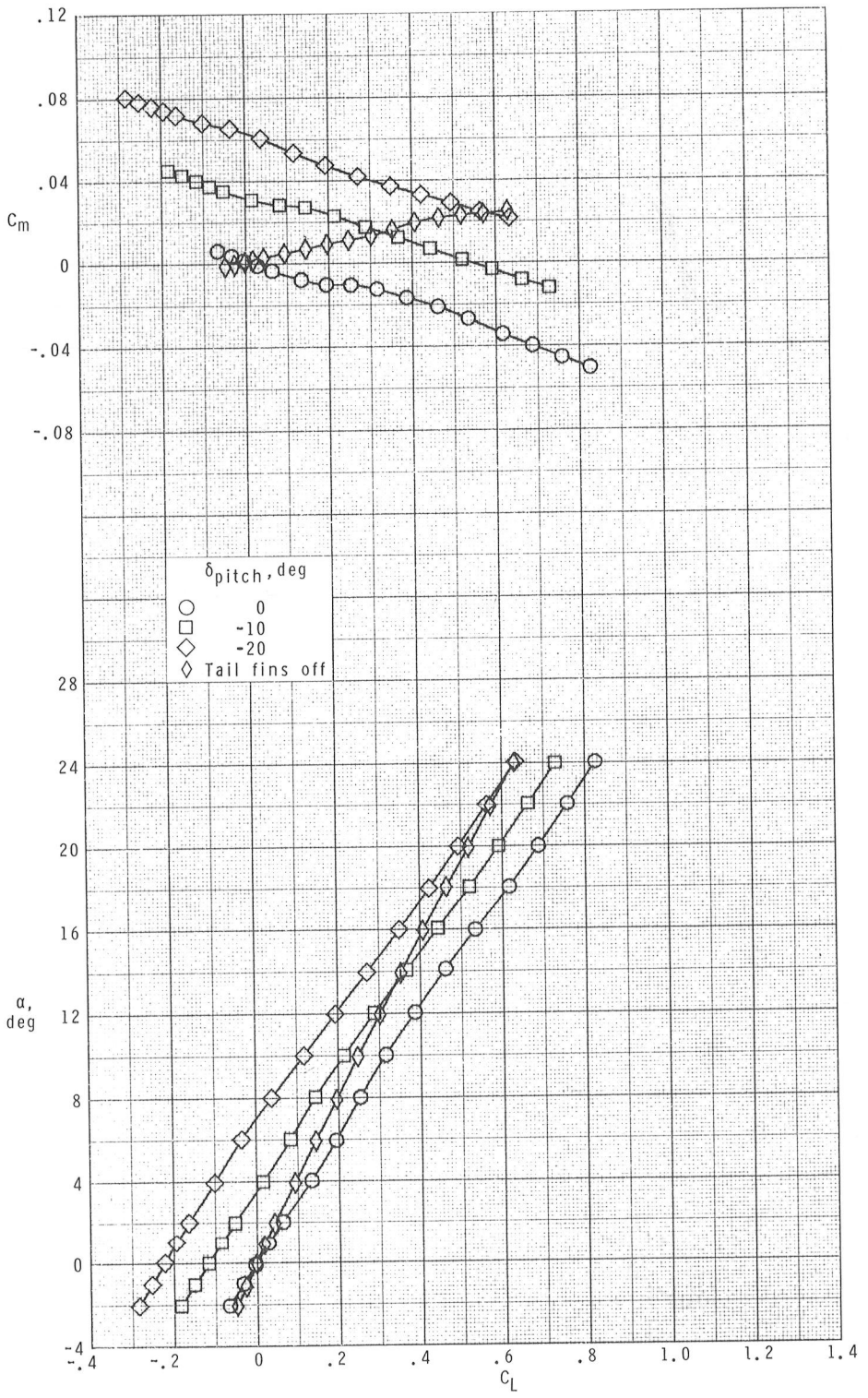

(b) Continued.

Figure 6.- Continued.

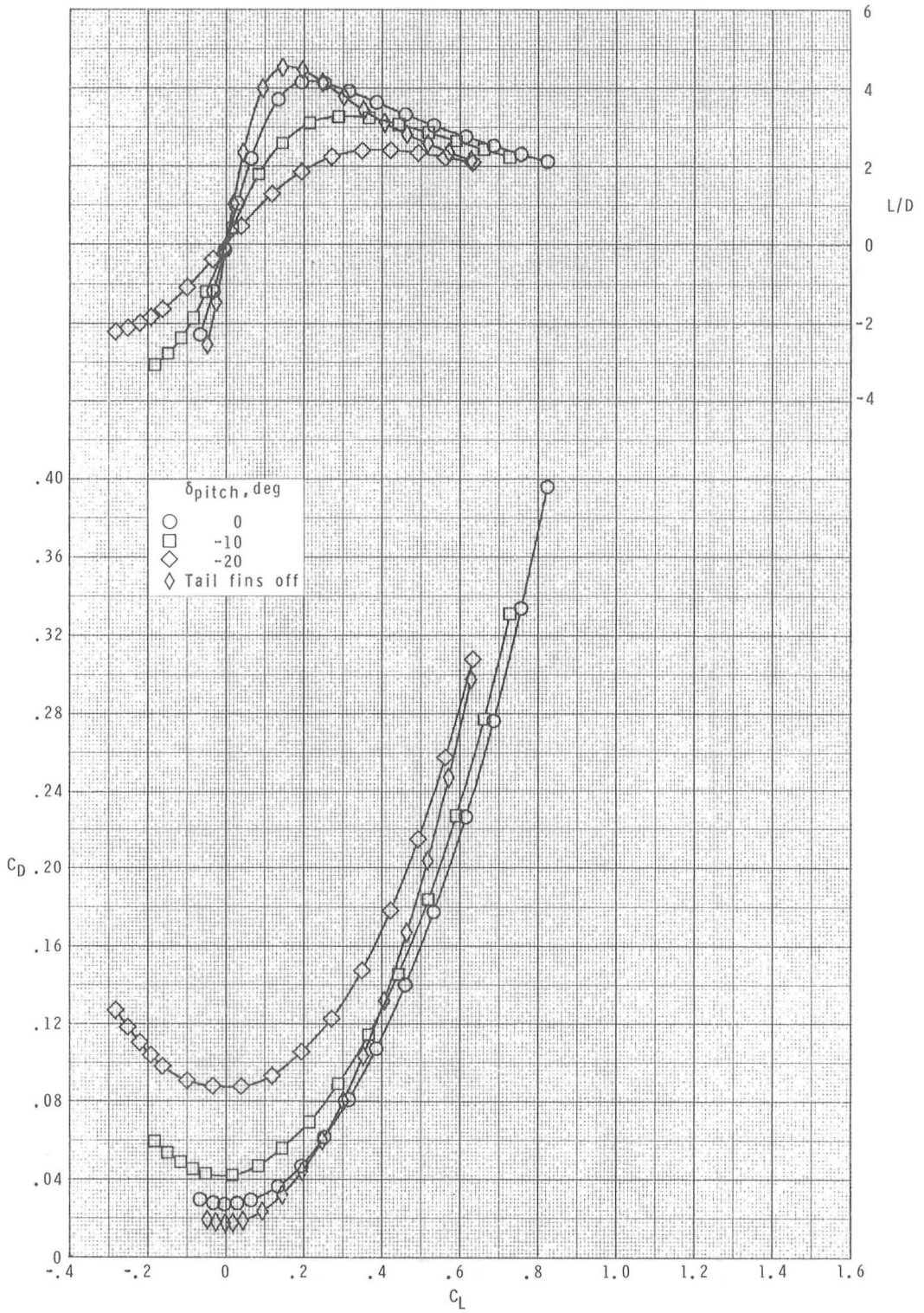

(b) Concluded.

Figure 6.- Continued.

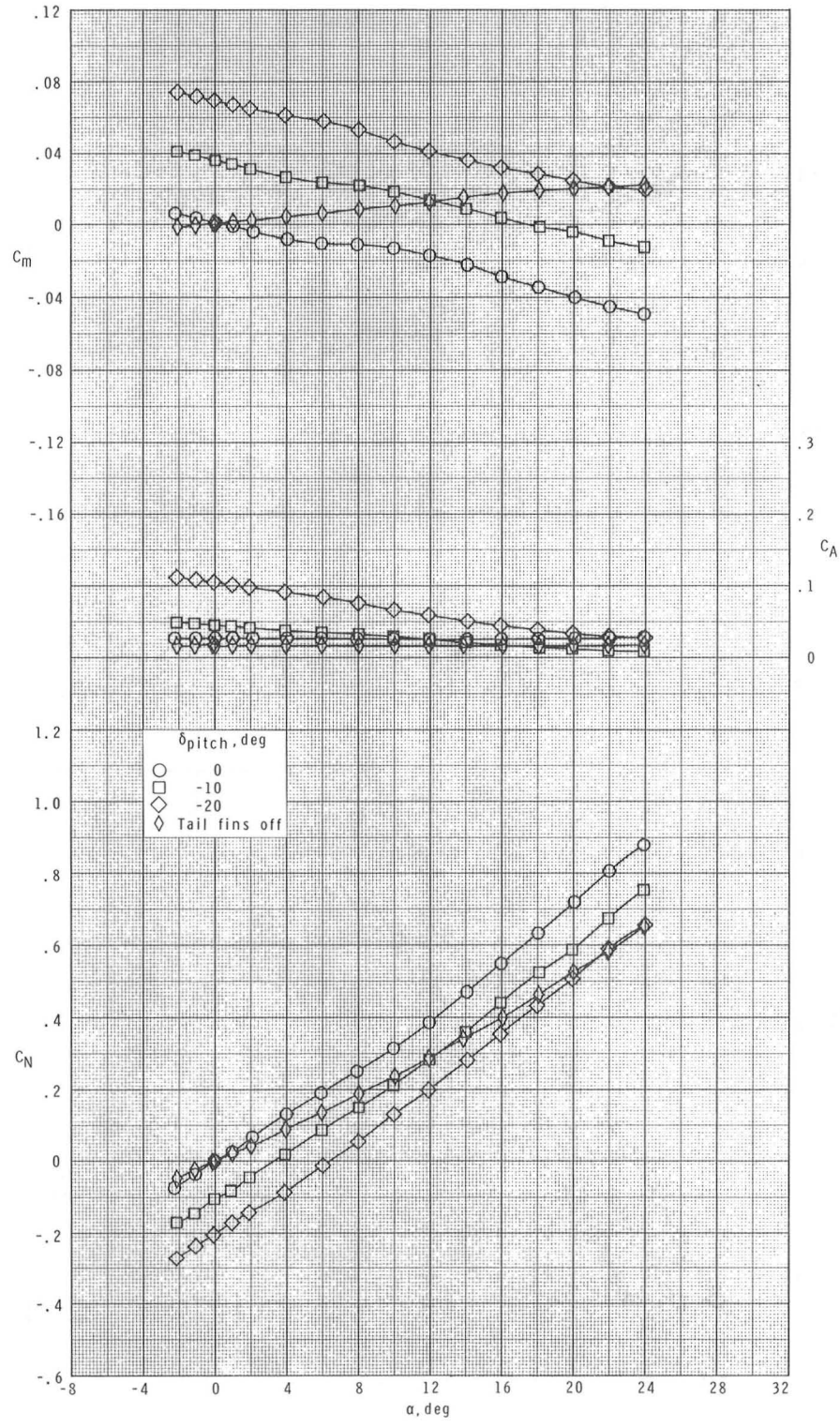

(c) M = 2.36.

Figure 6.- Continued.

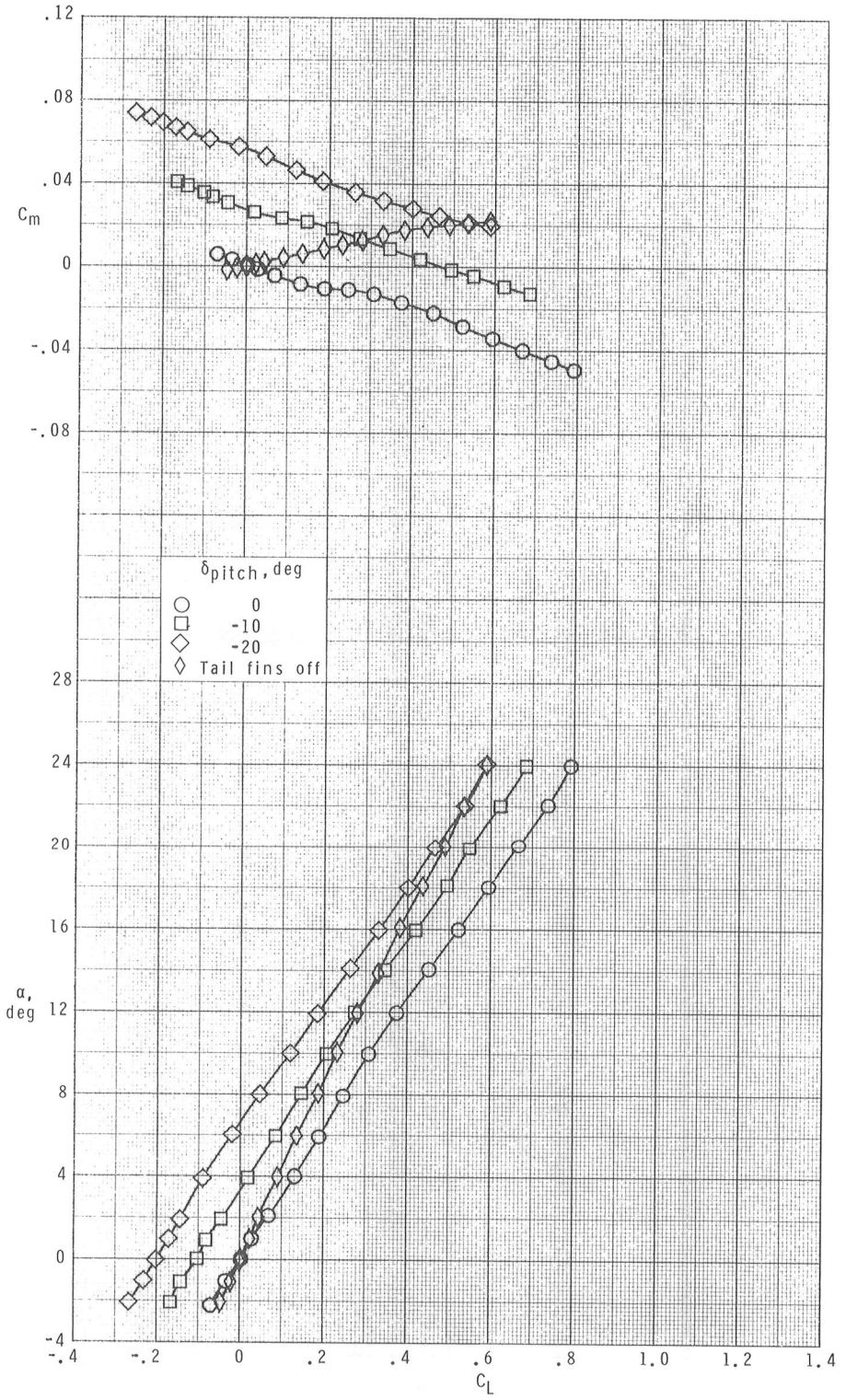

(c) Continued.

Figure 6.- Continued.

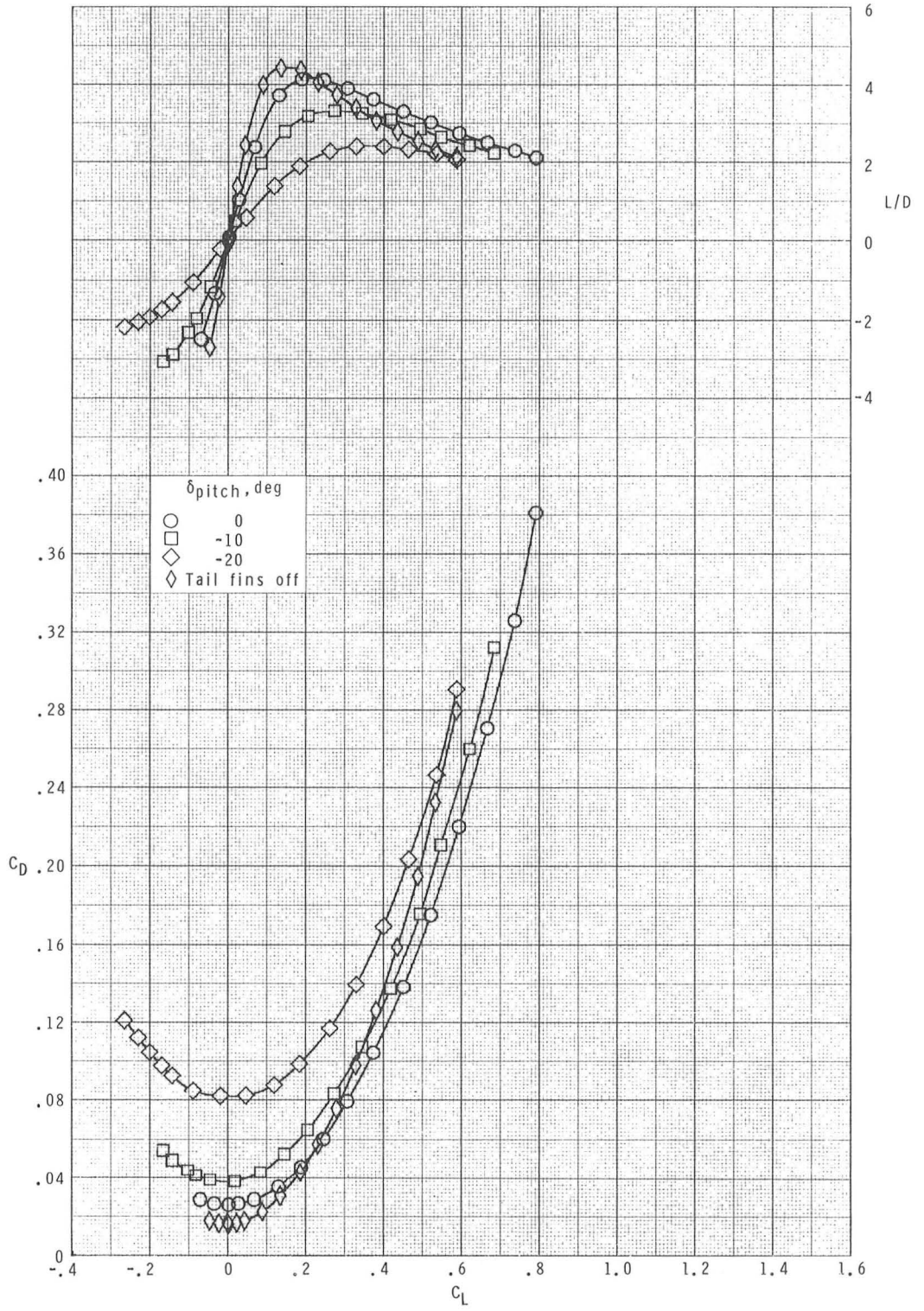

(c) Concluded.

Figure 6.- Continued.

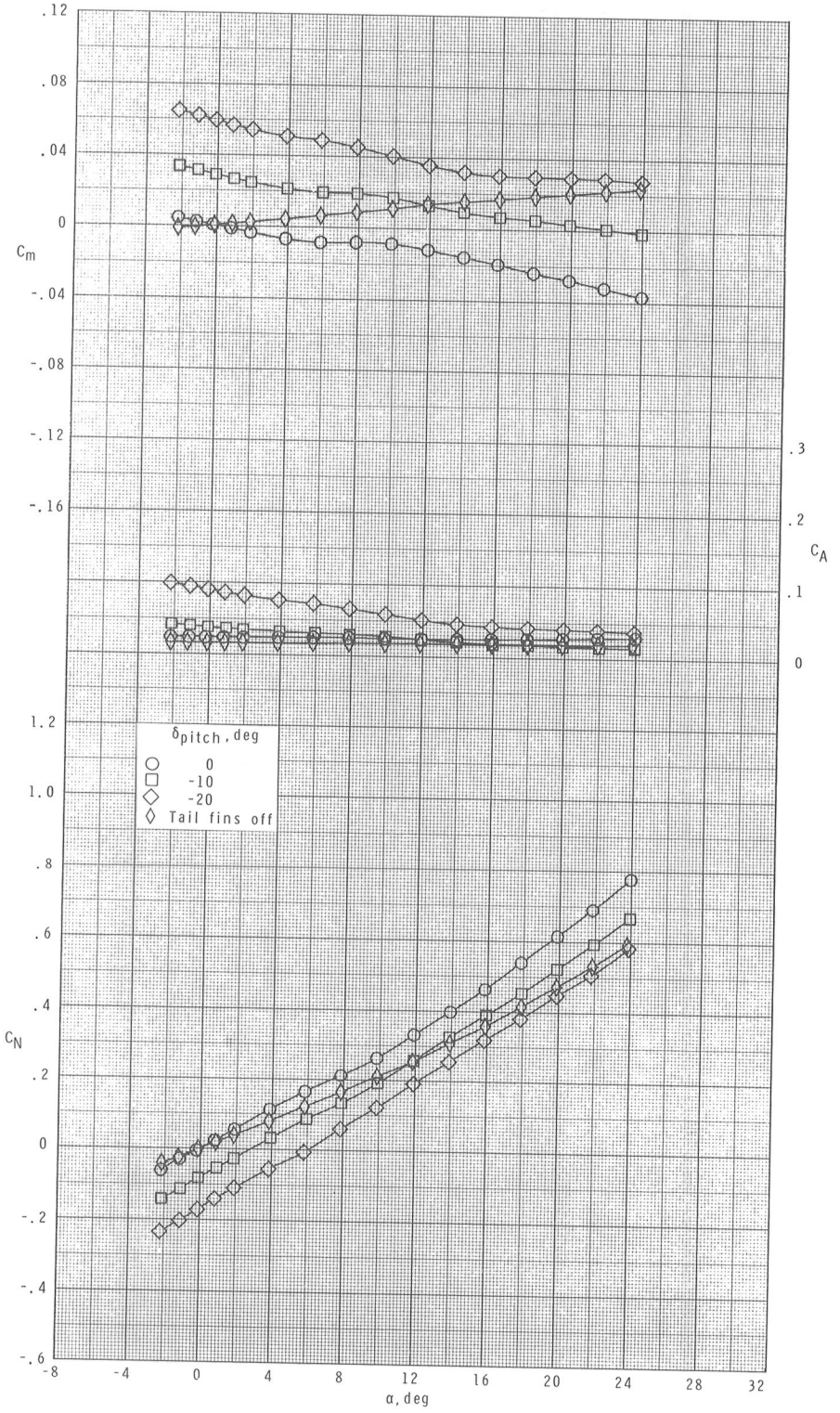

(d) M = 2.86.

Figure 6.- Continued.

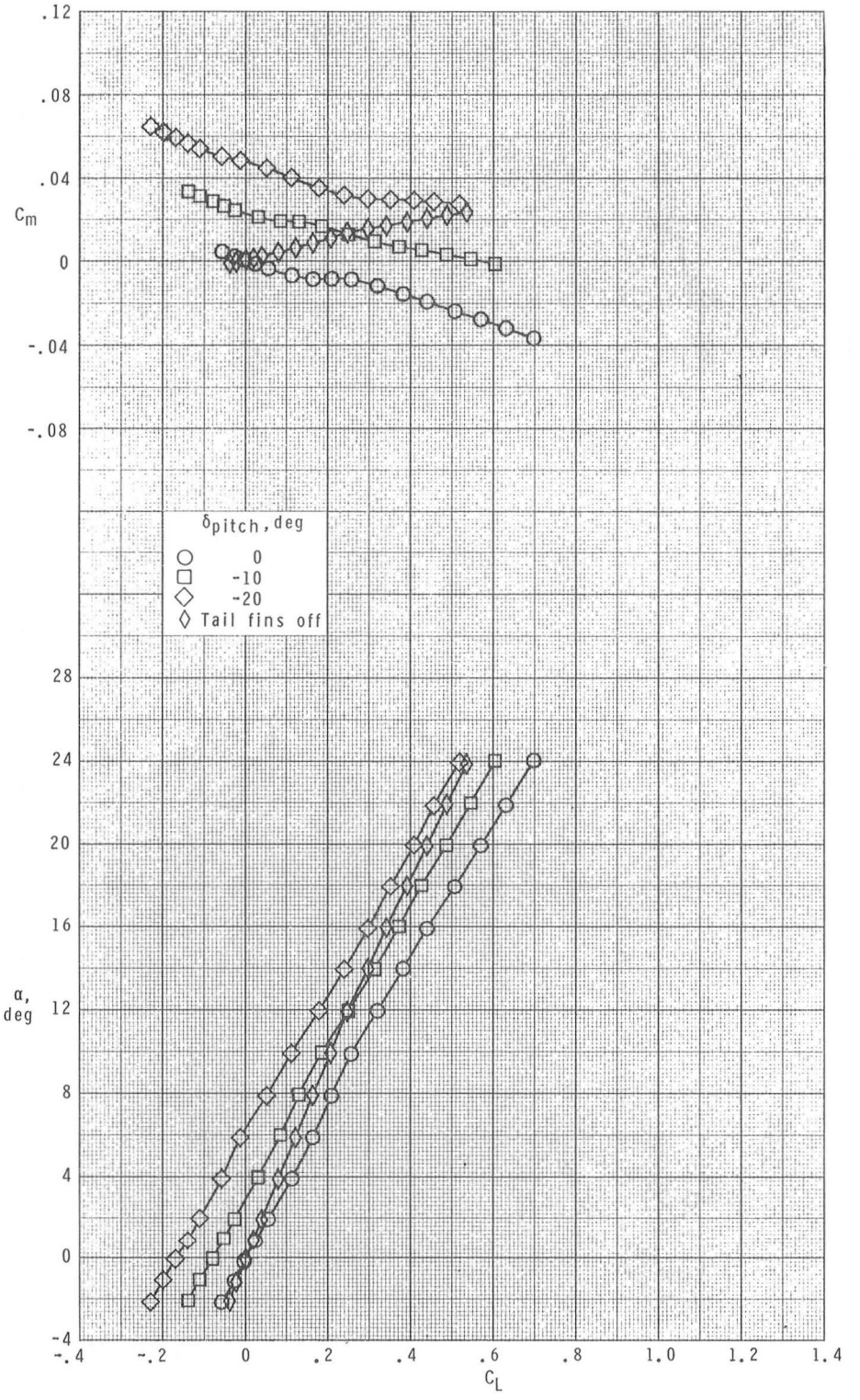

(d) Continued.

Figure 6.- Continued.

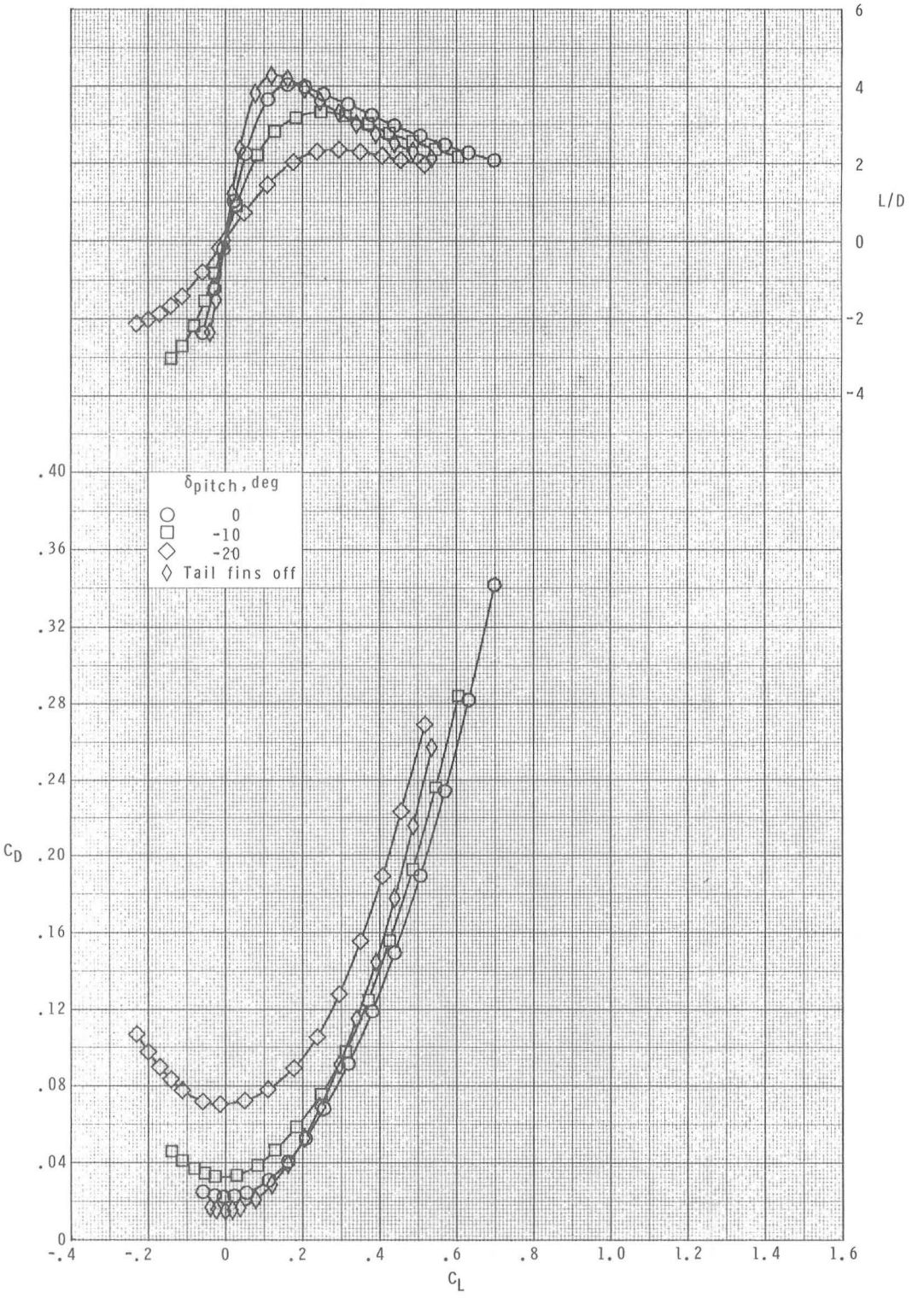

(d) Concluded.

Figure 6.- Concluded.

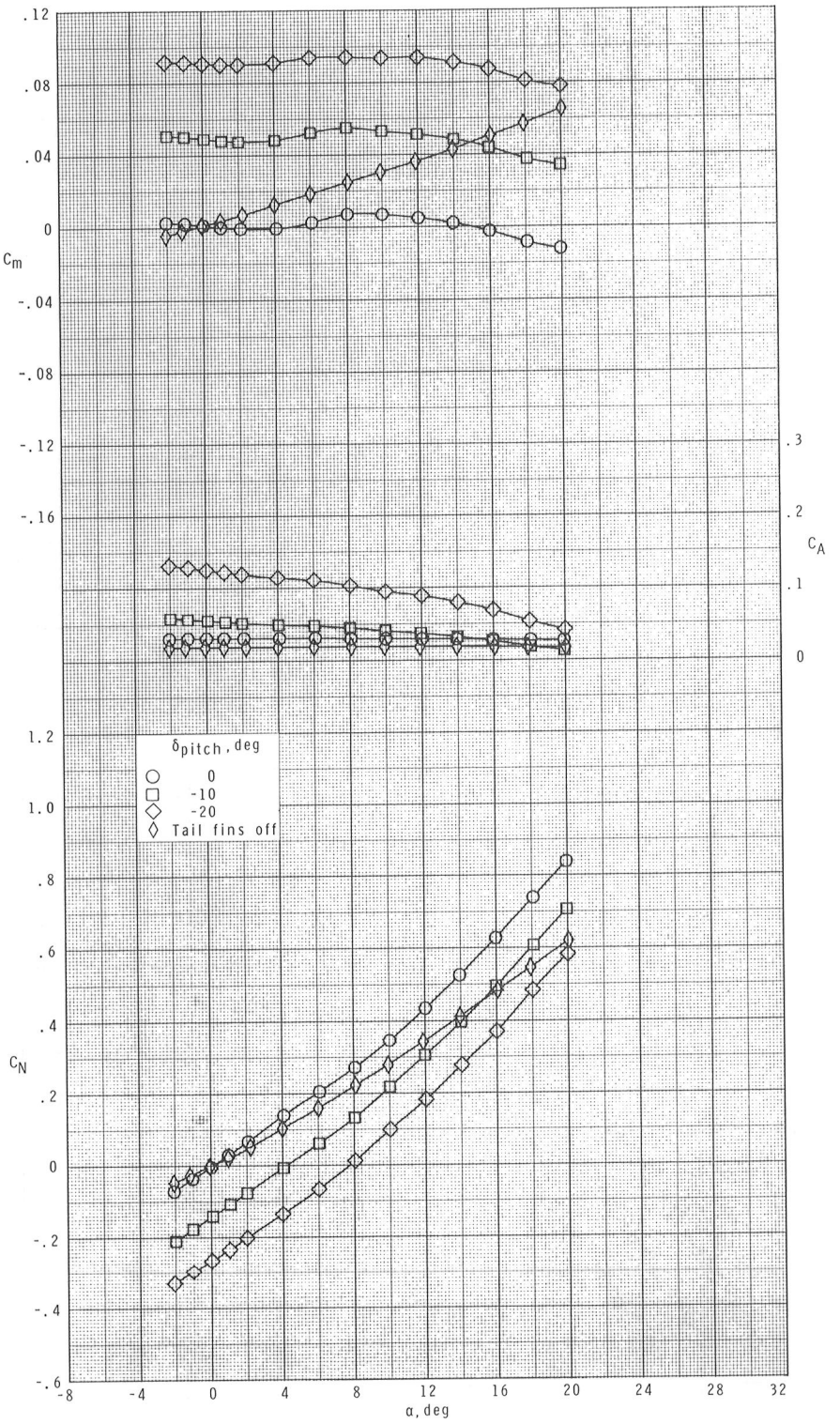

(a) M = 1.70.

Figure 7.- Effects of pitch control on longitudinal aerodynamic characteristics of the centerline-forward-wing configuration.

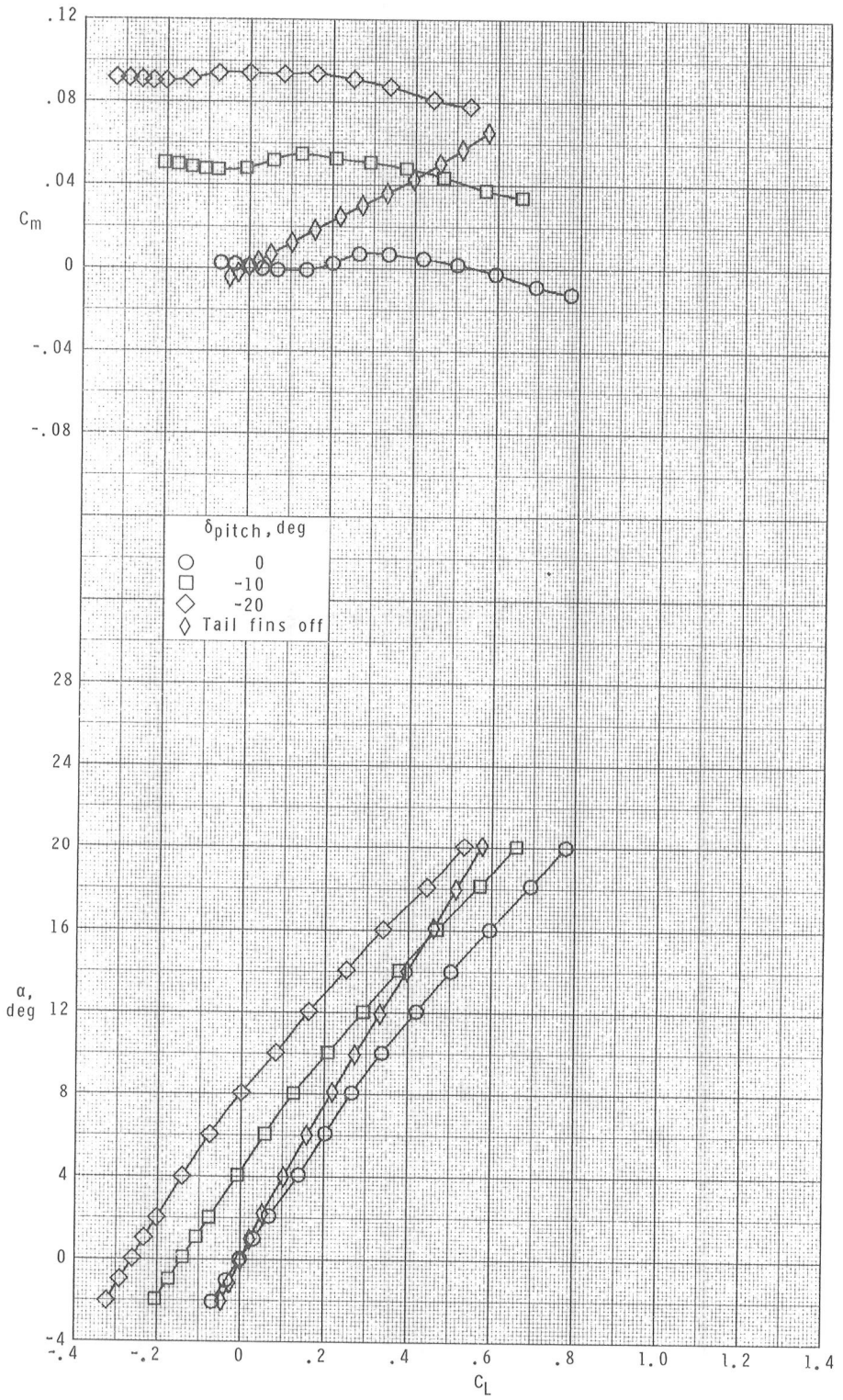

(a) Continued.

Figure 7.- Continued.

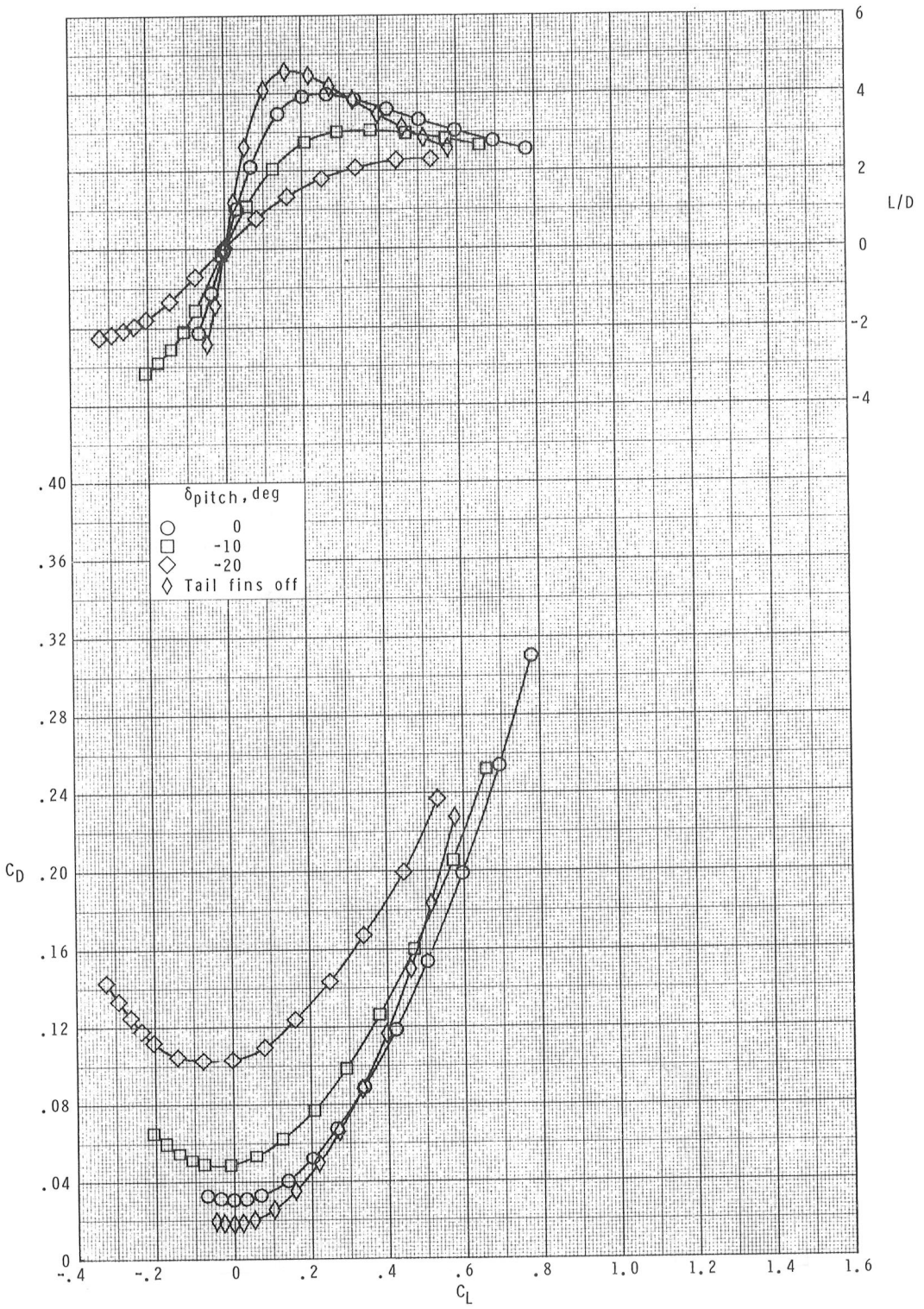

(a) Concluded.

Figure 7.- Continued.

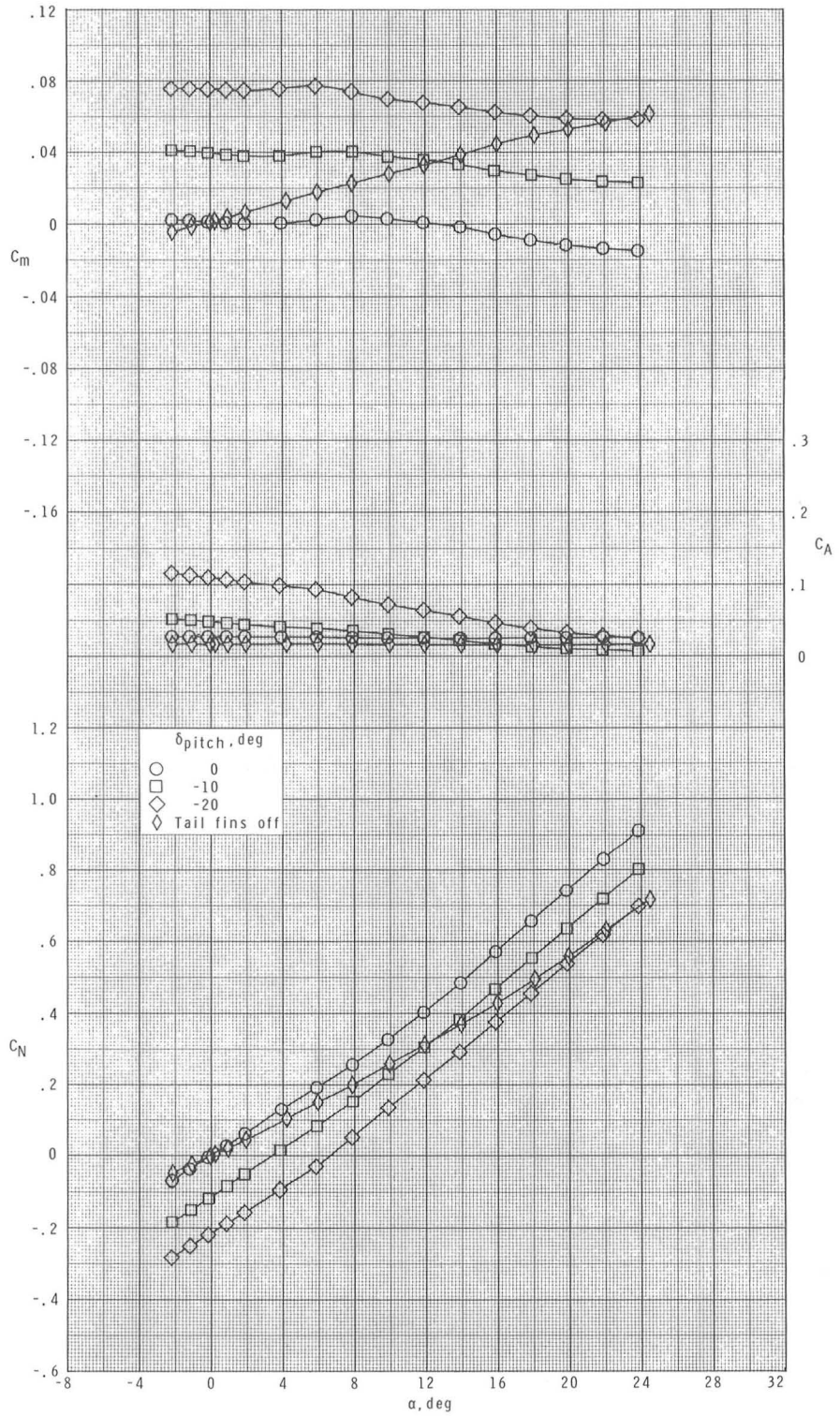

(b) M = 2.16.

Figure 7.- Continued.

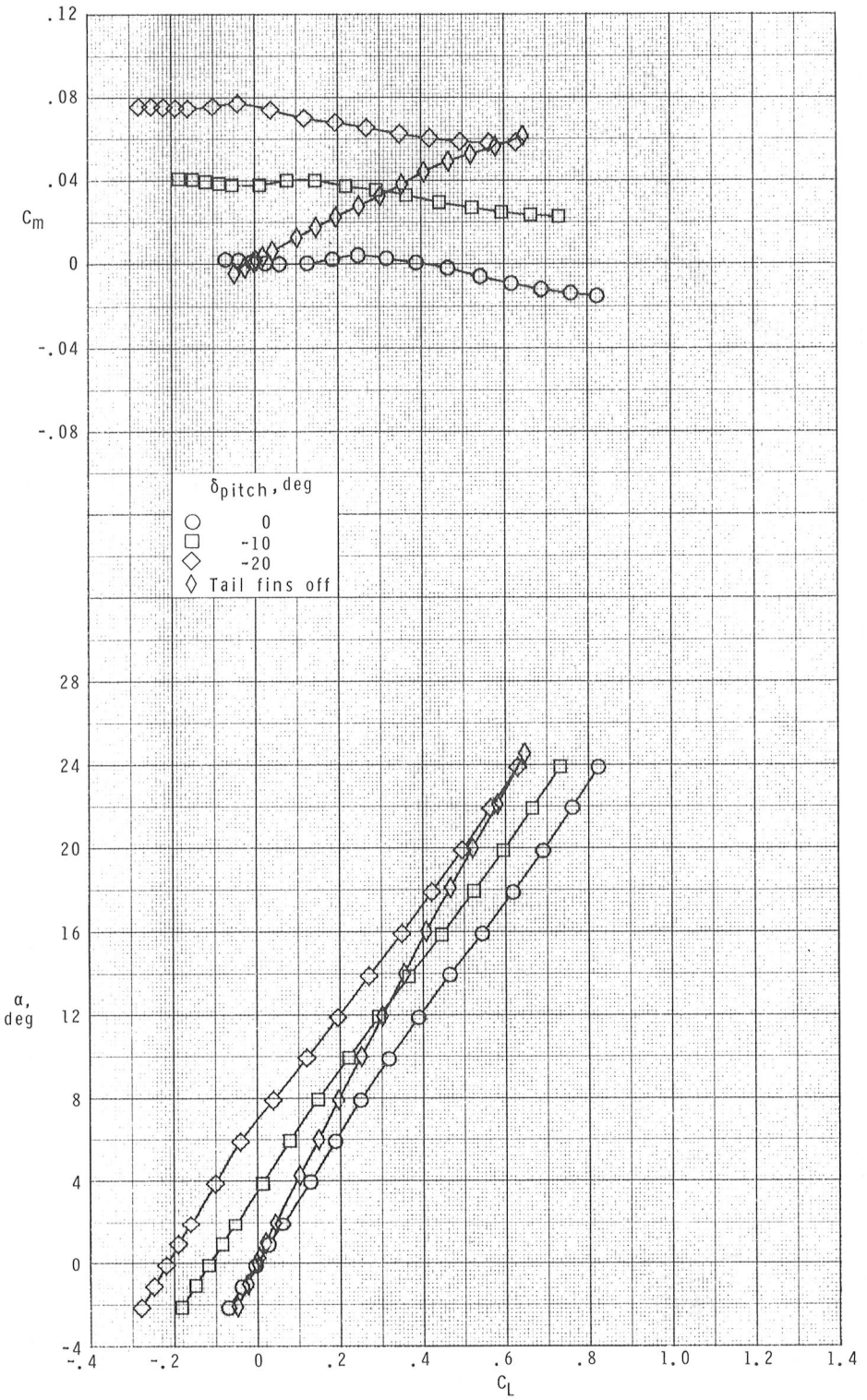

(b) Continued.

Figure 7.- Continued.

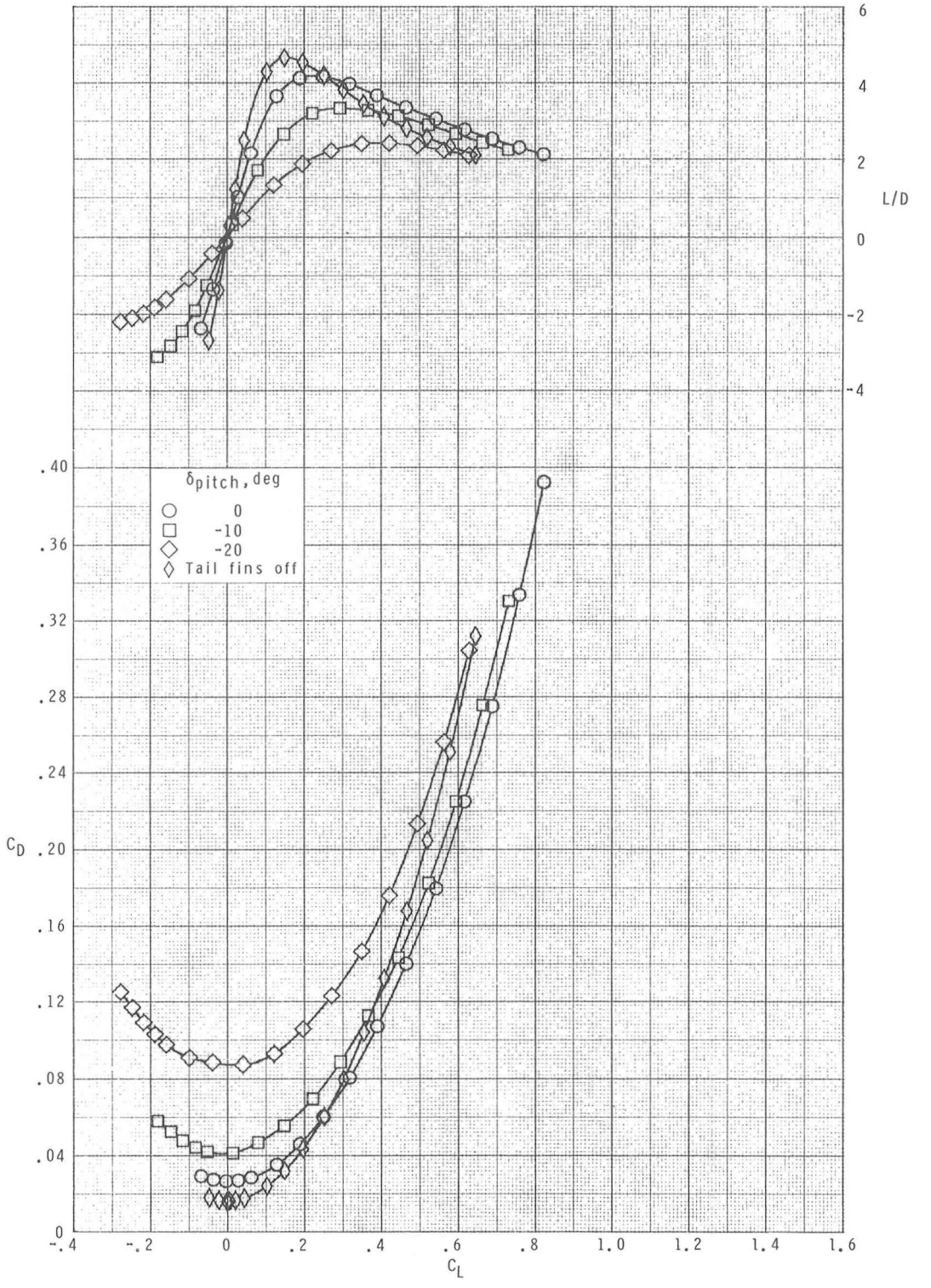

(b) Concluded.

Figure 7.- Continued.

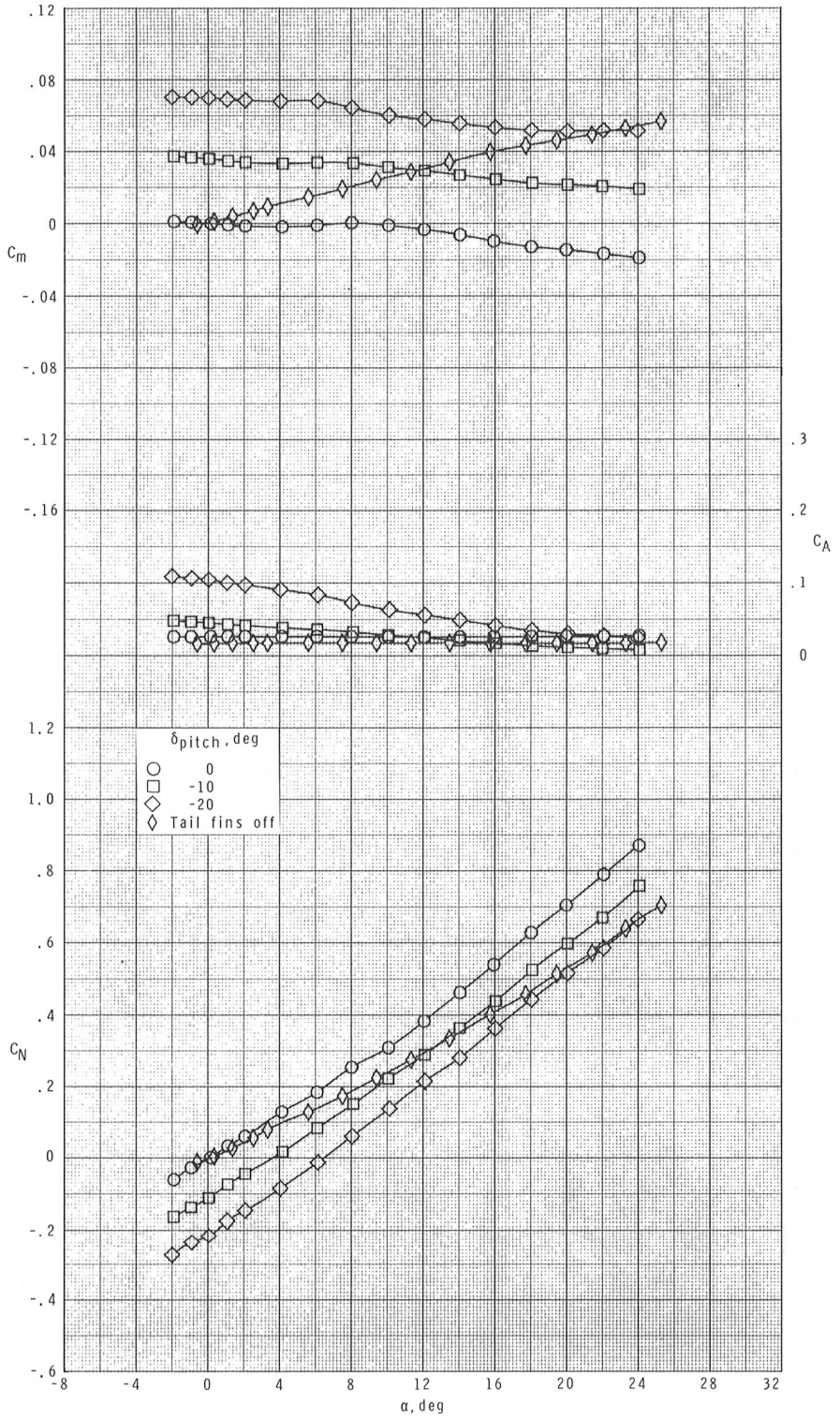

(c) M = 2.36.

Figure 7.- Continued.

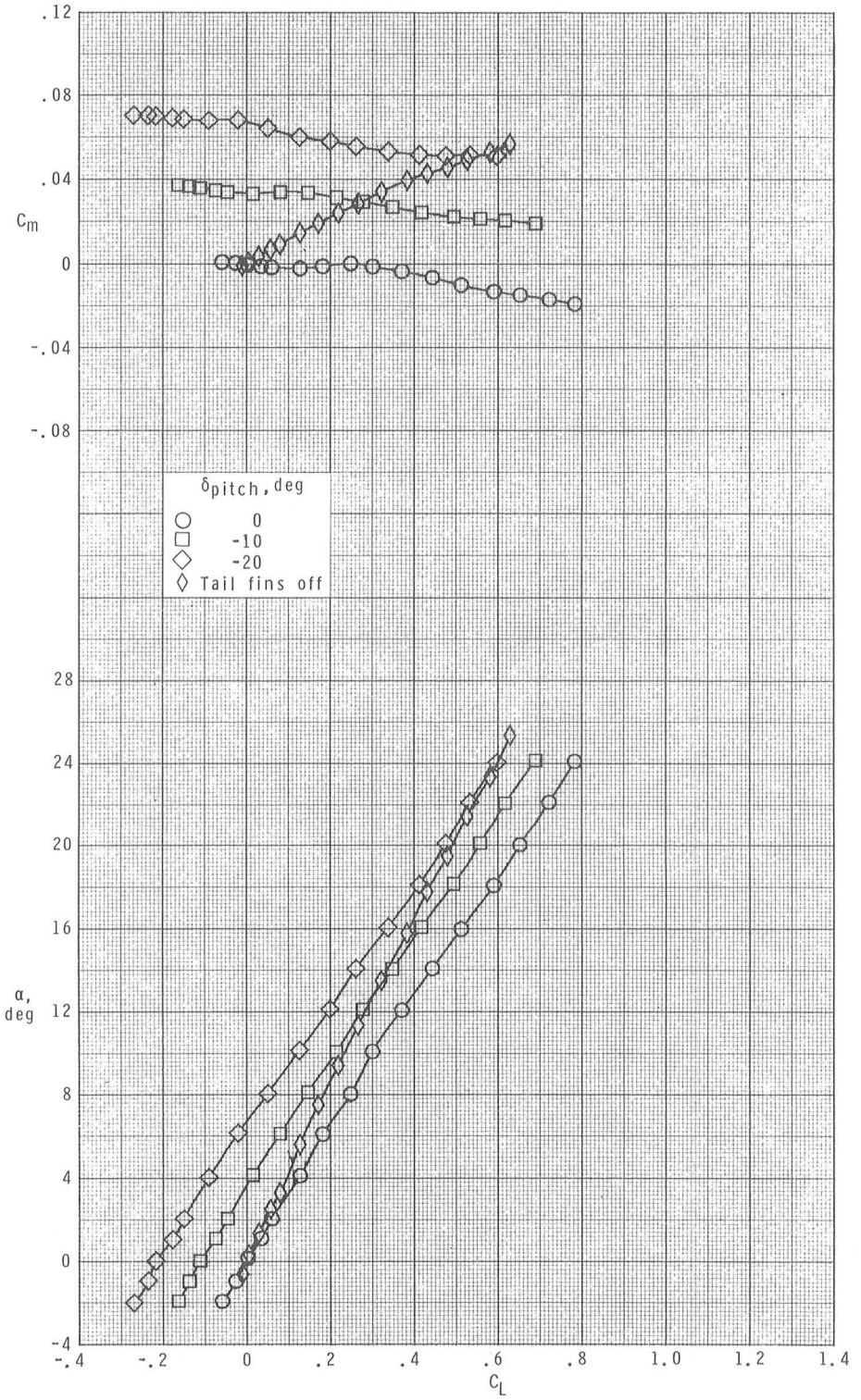

(c) Continued.

Figure 7.- Continued.

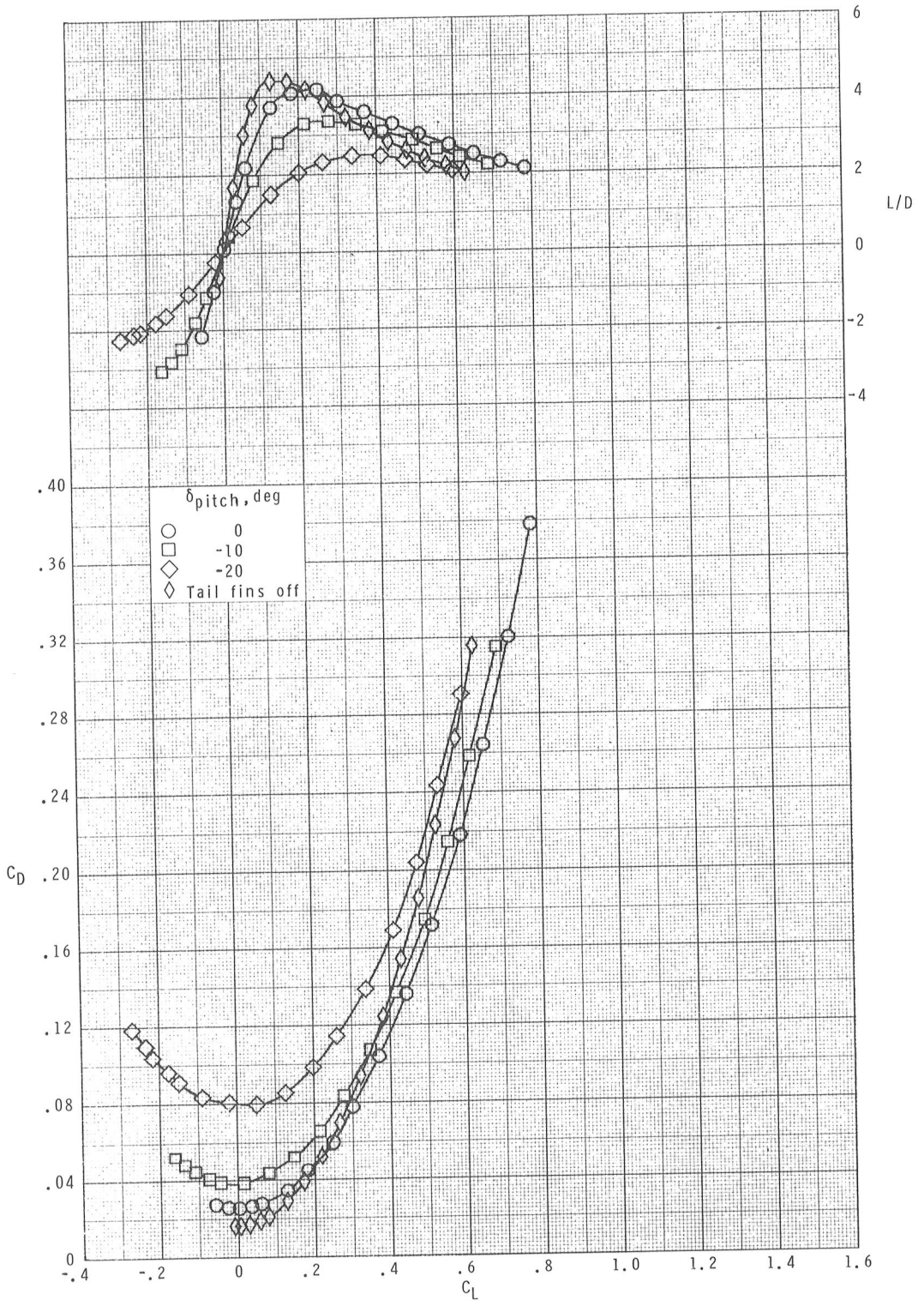

(c) Concluded.

Figure 7.- Continued.

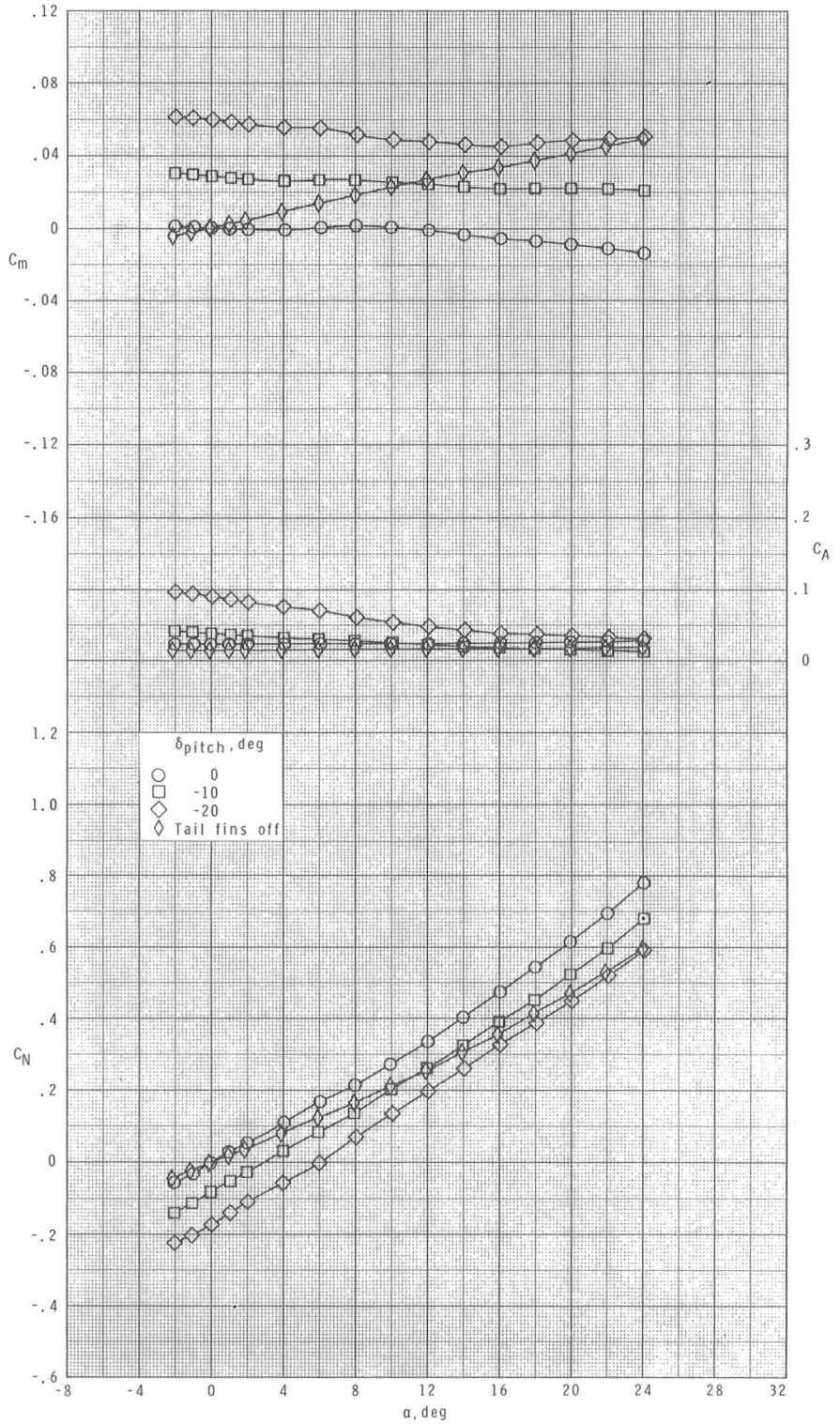

(d) M = 2.86.

Figure 7.- Continued.

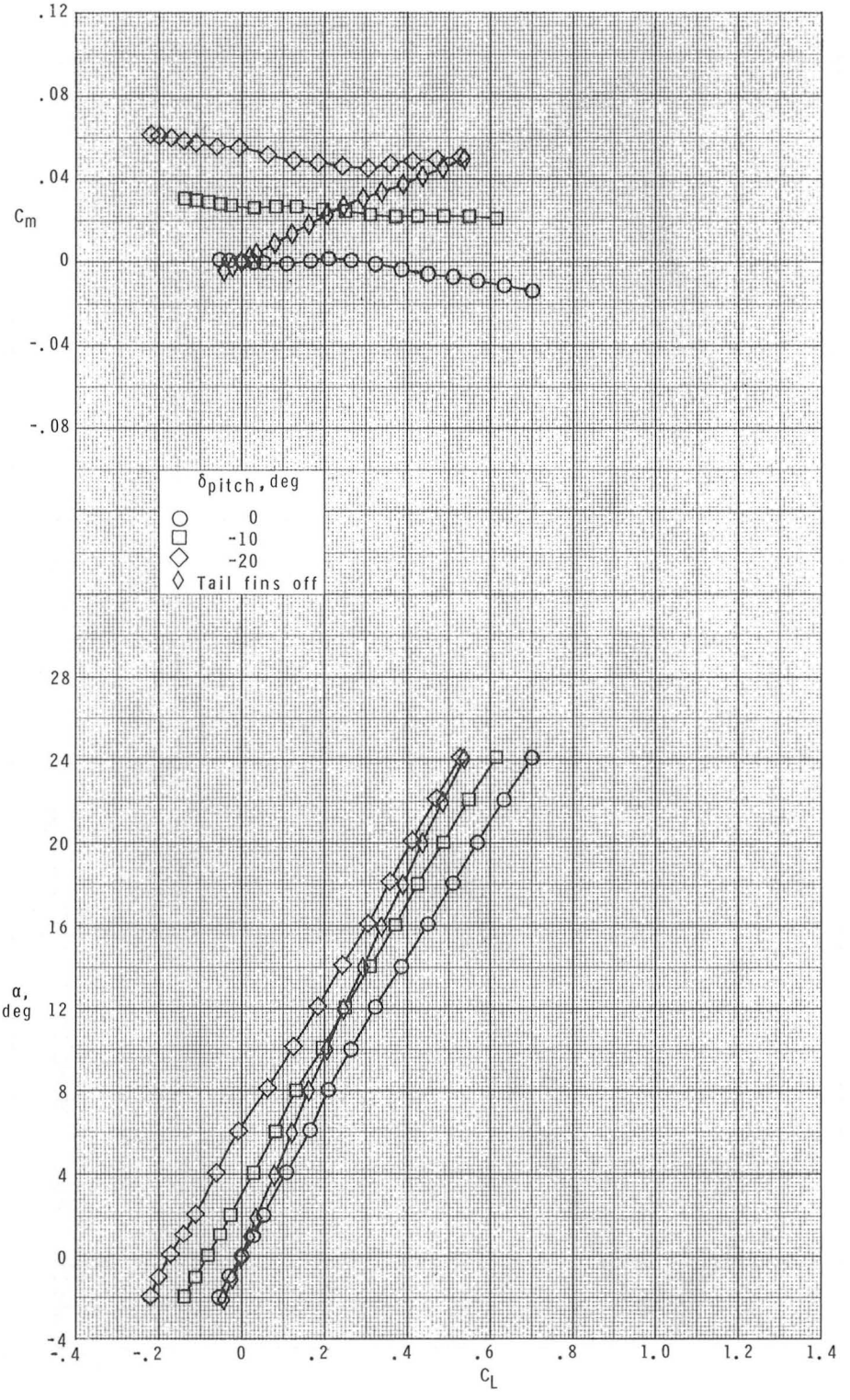

(d) Continued.

Figure 7.- Continued.

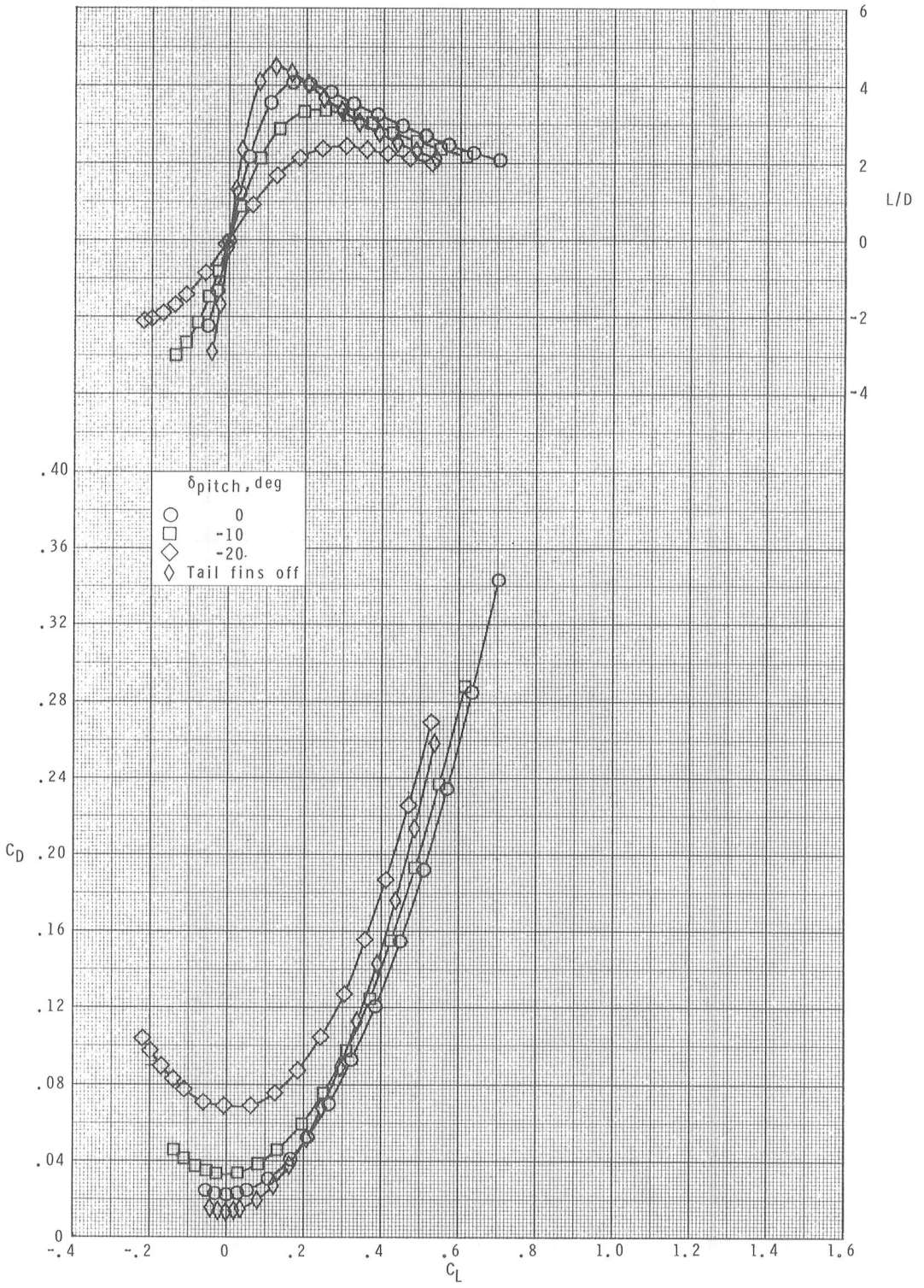

(d) Concluded.

Figure 7.- Concluded.

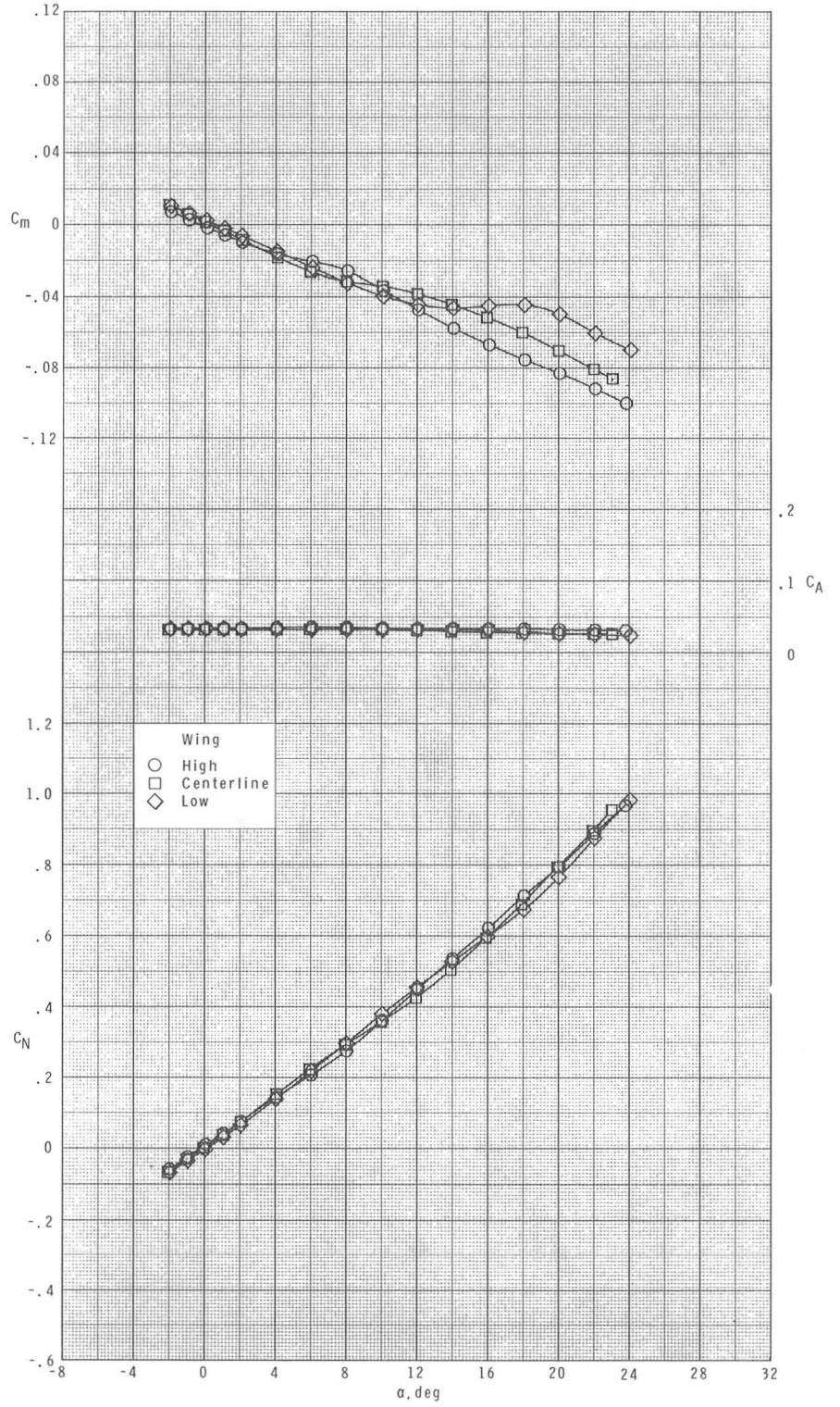

(a) M = 1.70.

Figure 8.- Effects of wing vertical location on longitudinal aerodynamic characteristics of the aft-wing configurations.

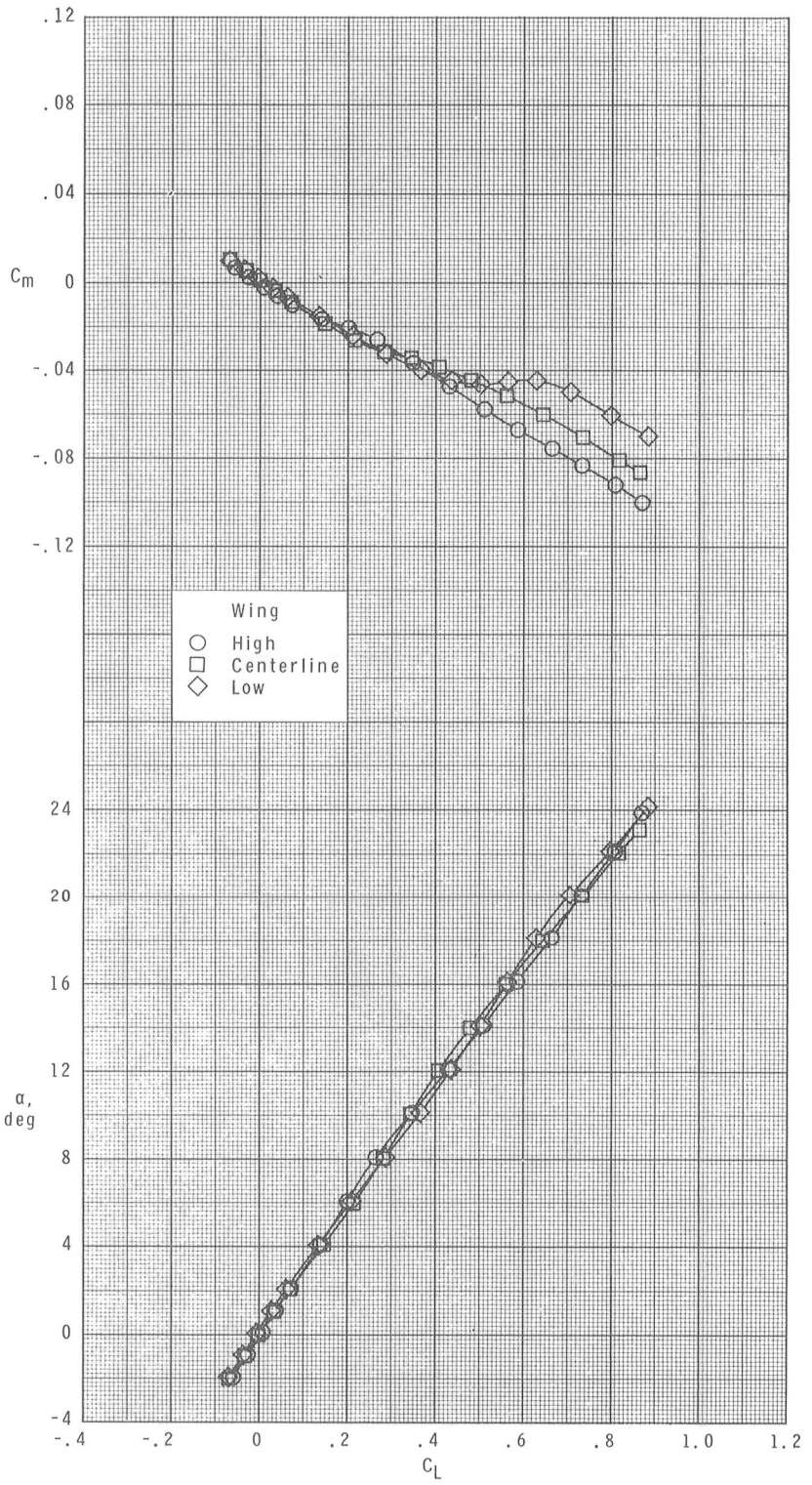

(a) Continued.

Figure 8.- Continued.

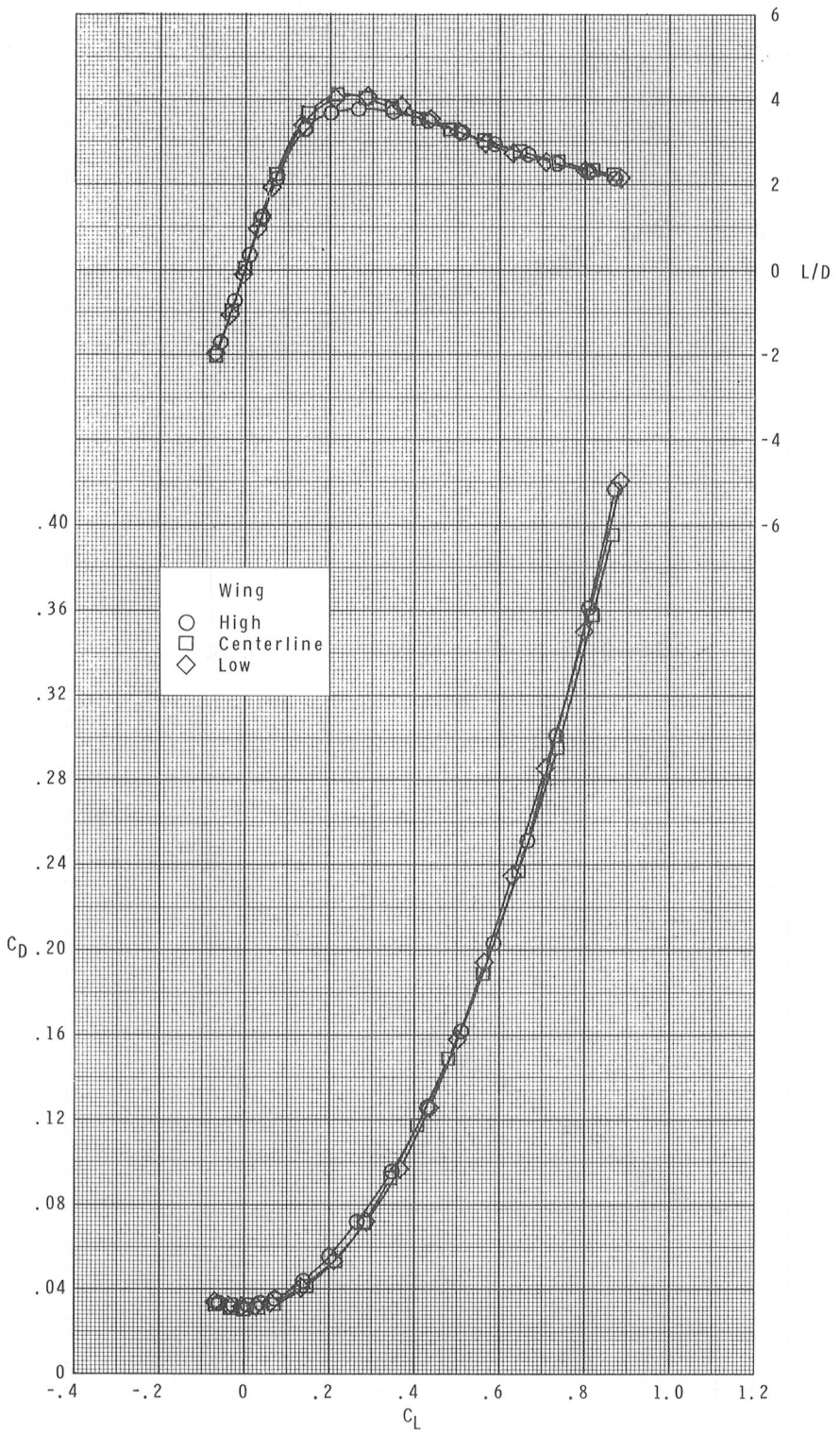

(a) Concluded.

Figure 8.- Continued.

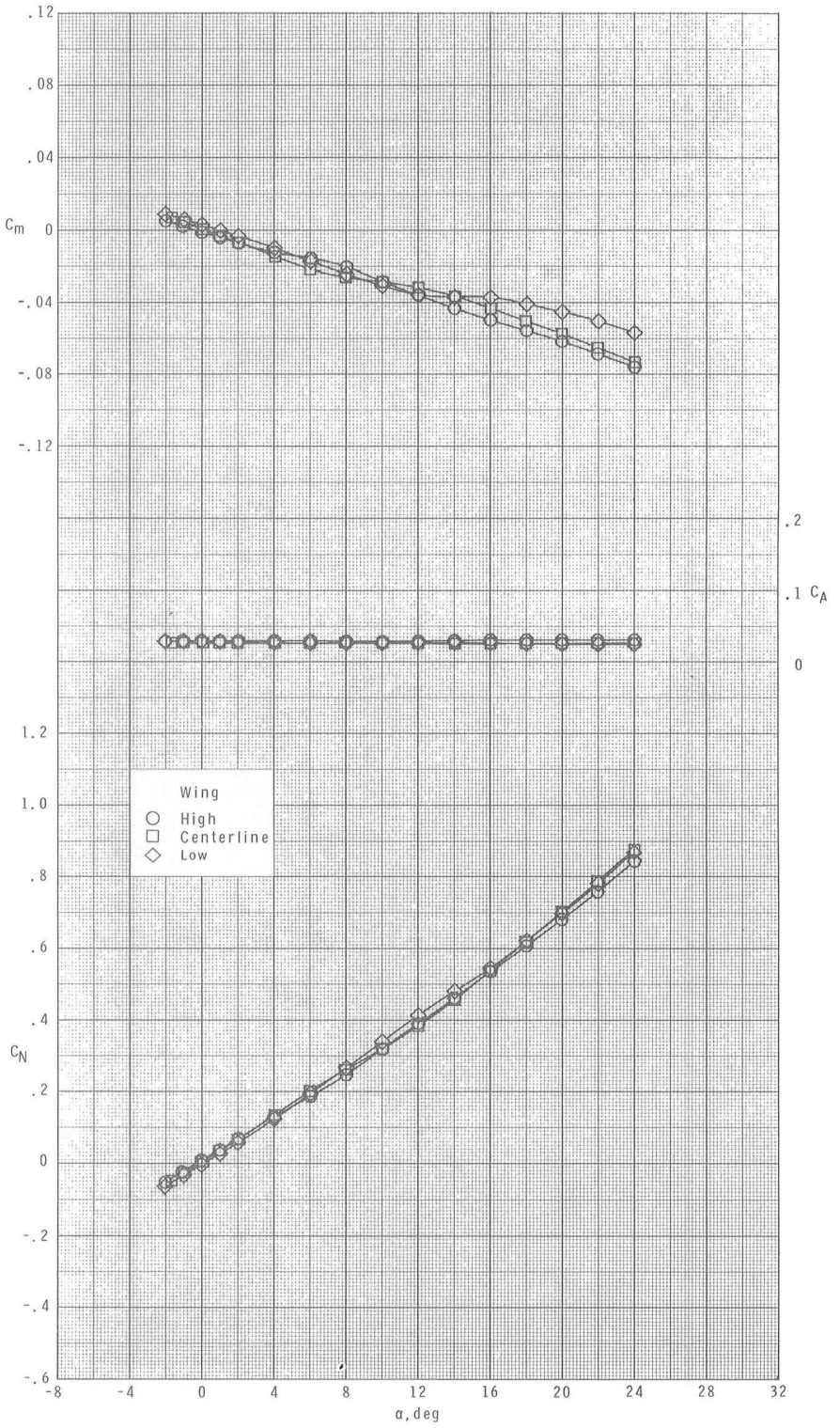

(b) M = 2.16.

Figure 8.- Continued.

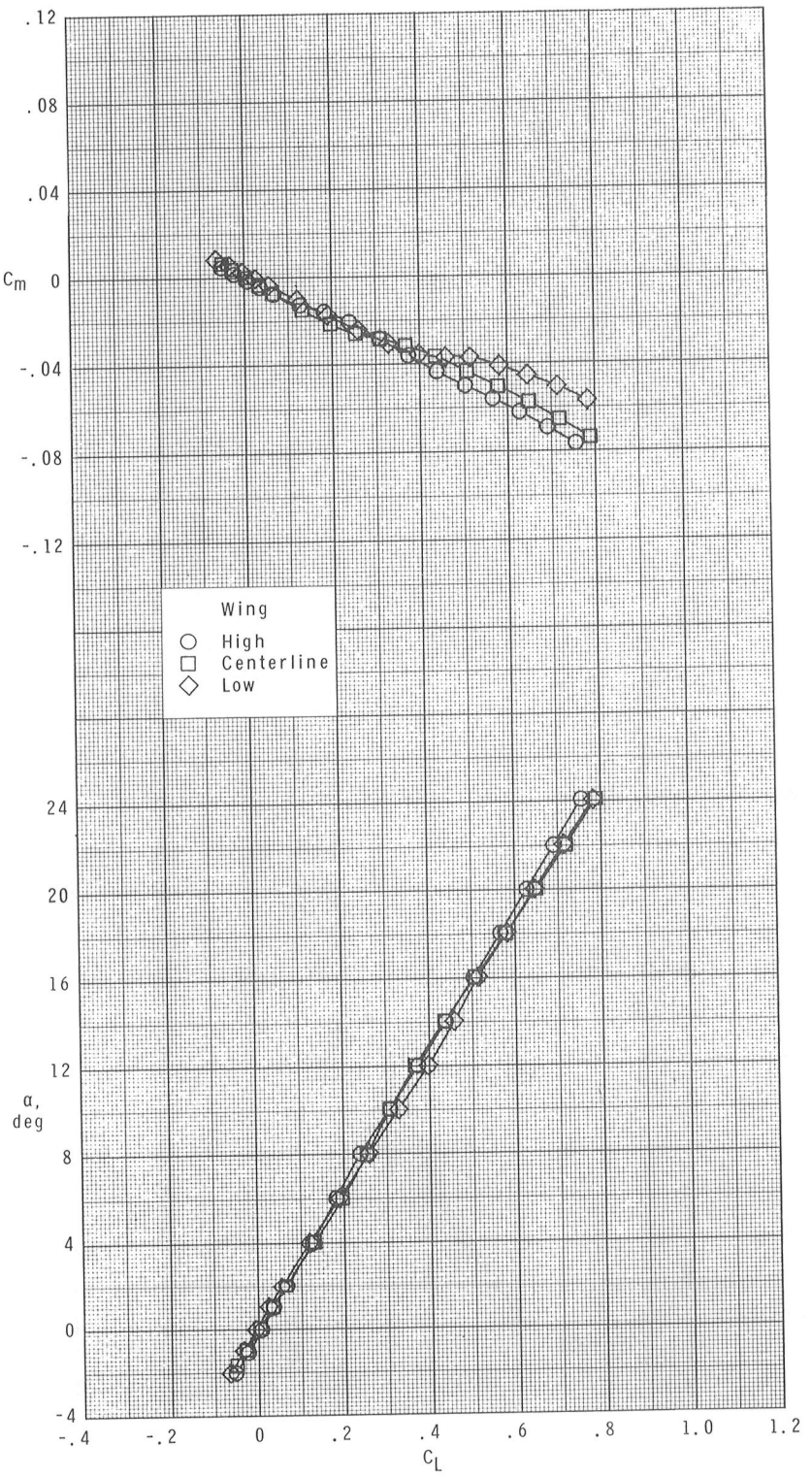

(b) Continued.

Figure 8.- Continued.

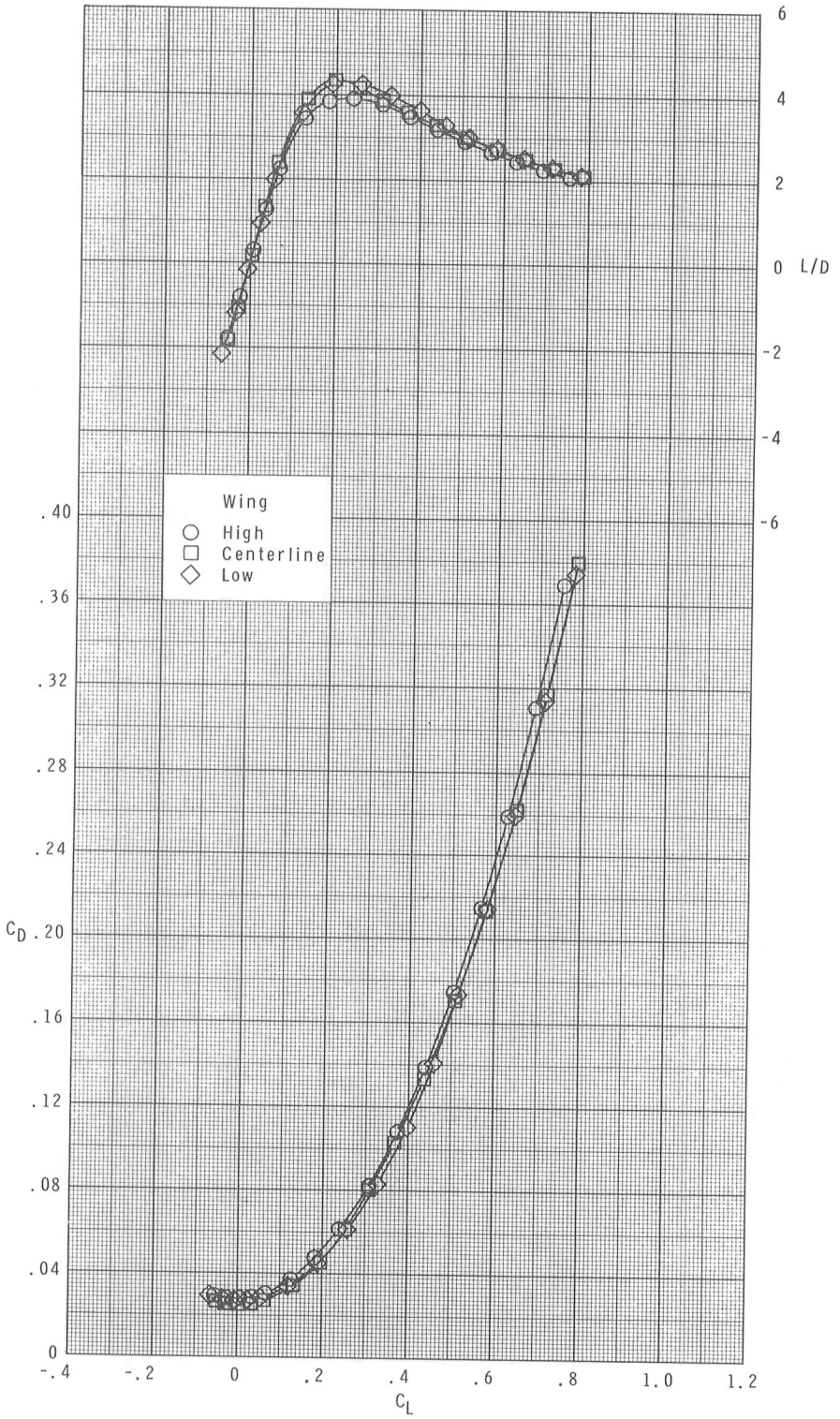

(b) Concluded.

Figure 8.- Continued.

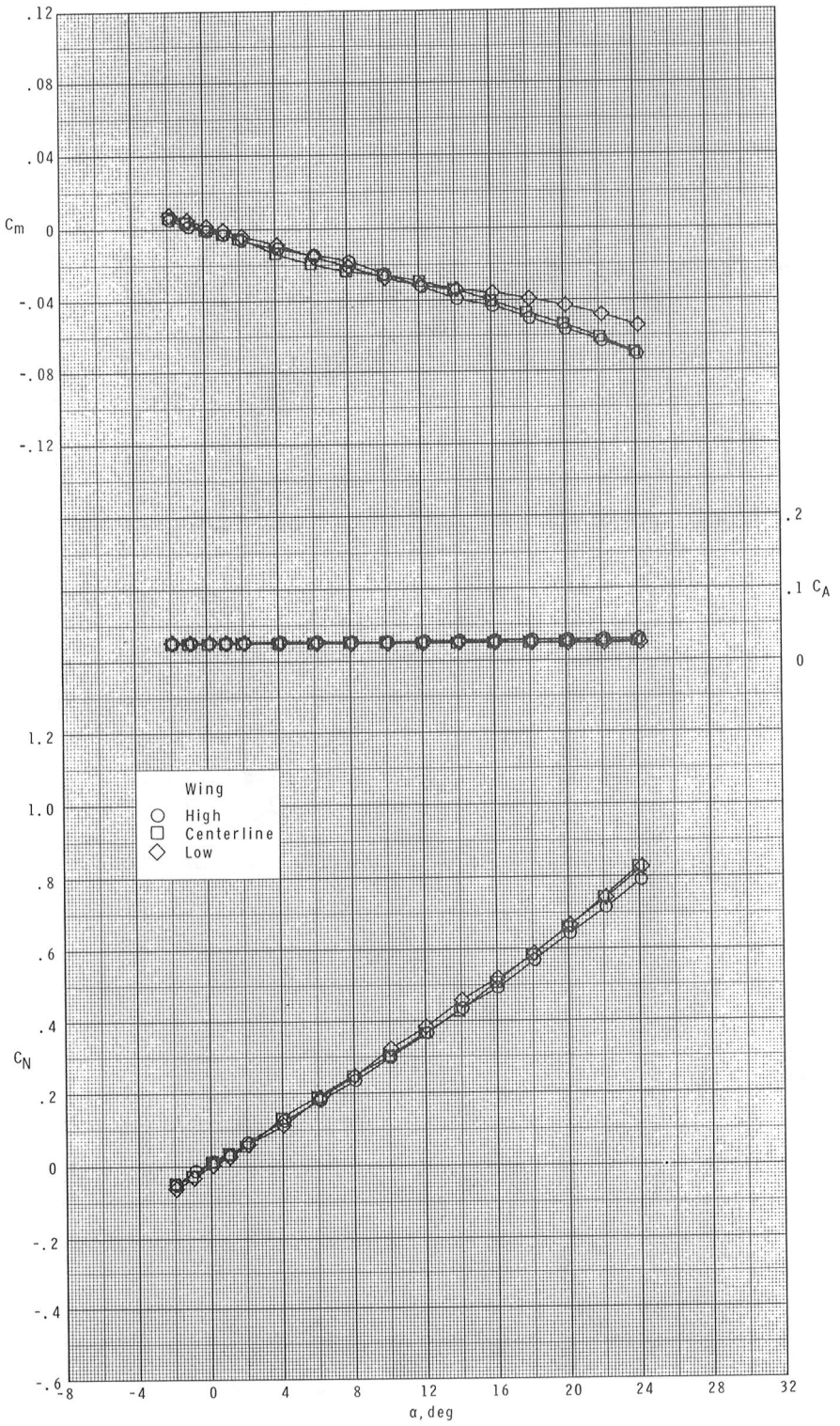

(c) M = 2.36.

Figure 8.- Continued.

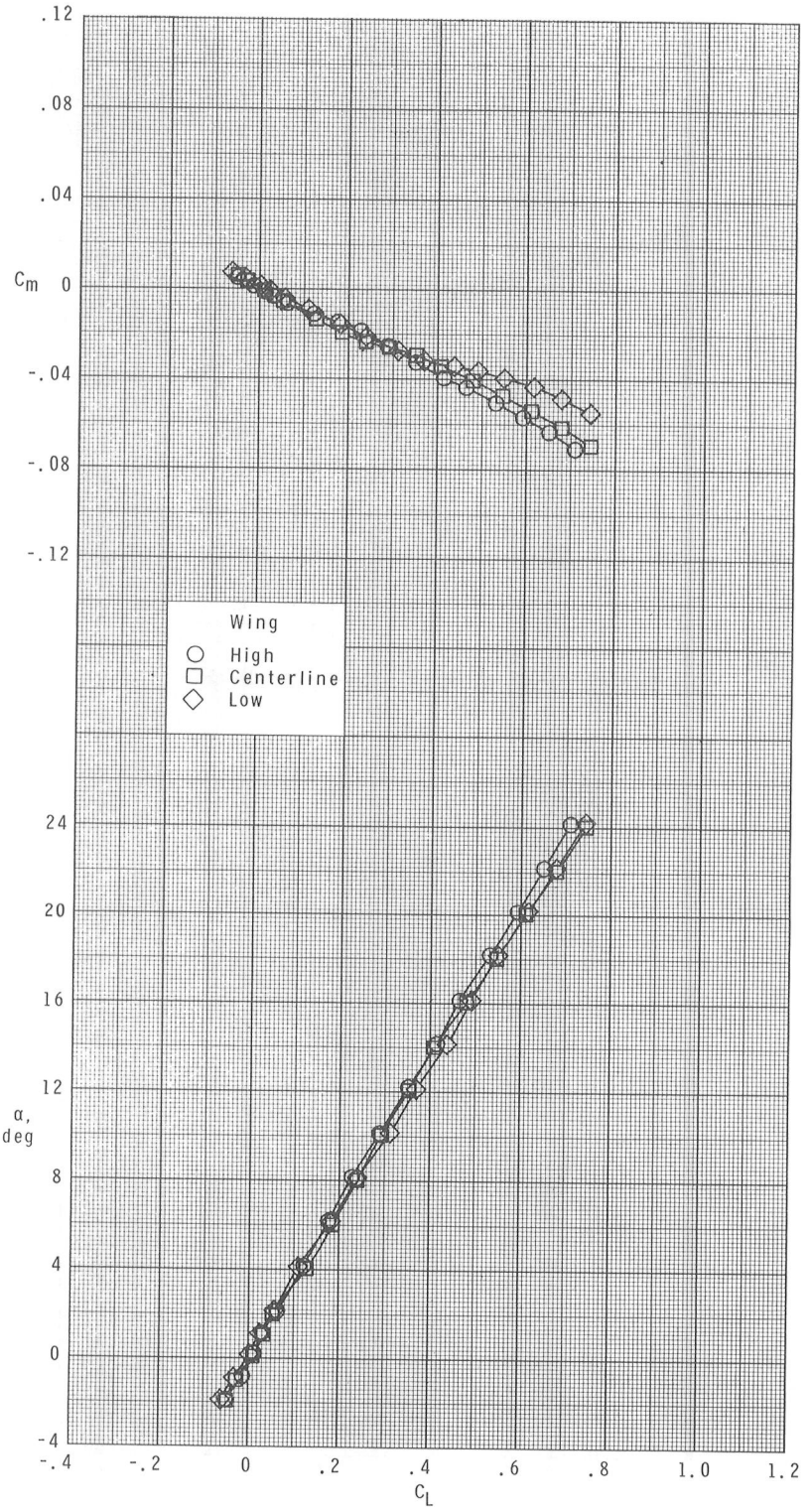

(c) Continued.

Figure 8.- Continued.

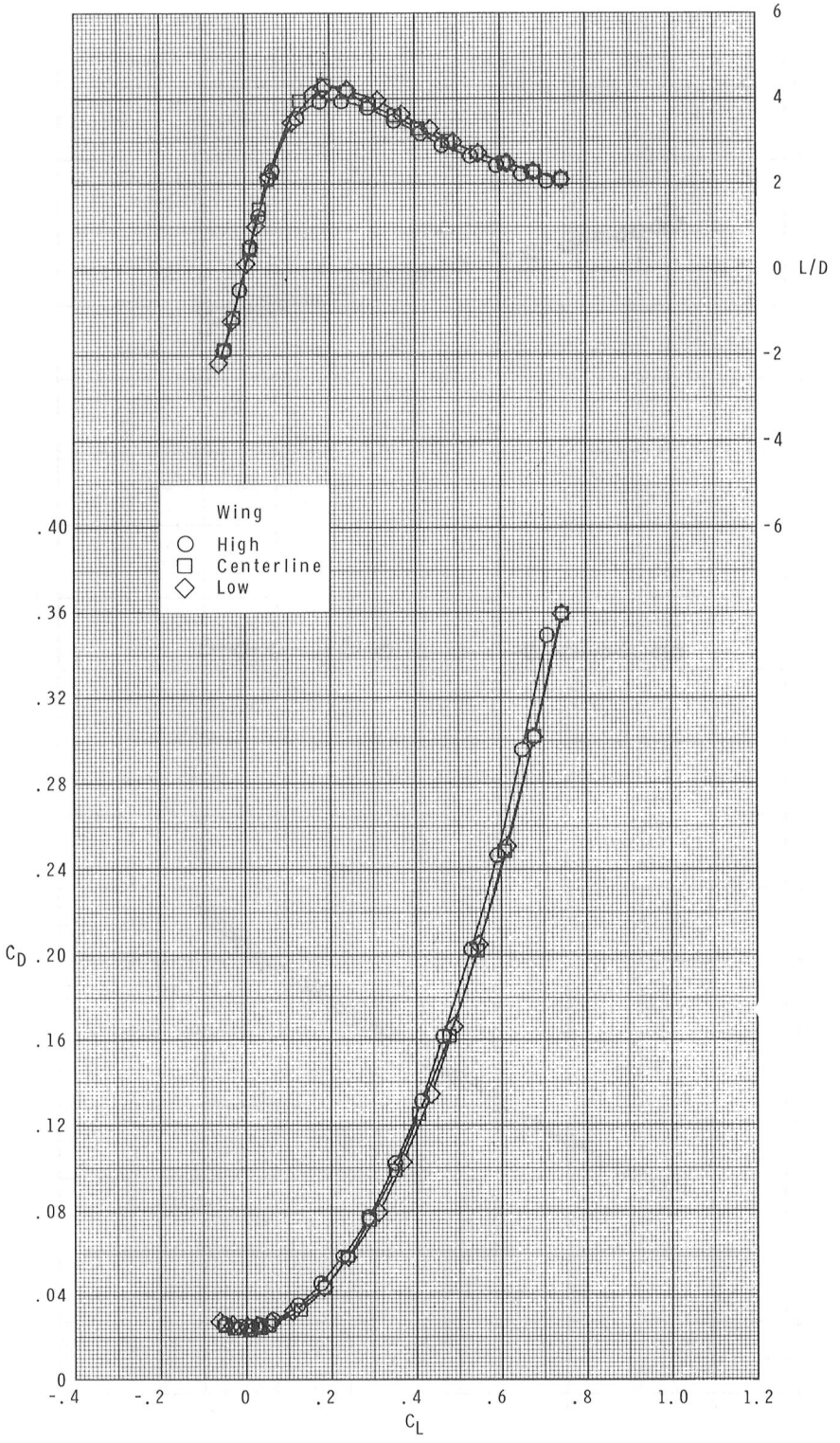

(c) Concluded.

Figure 8.- Continued.

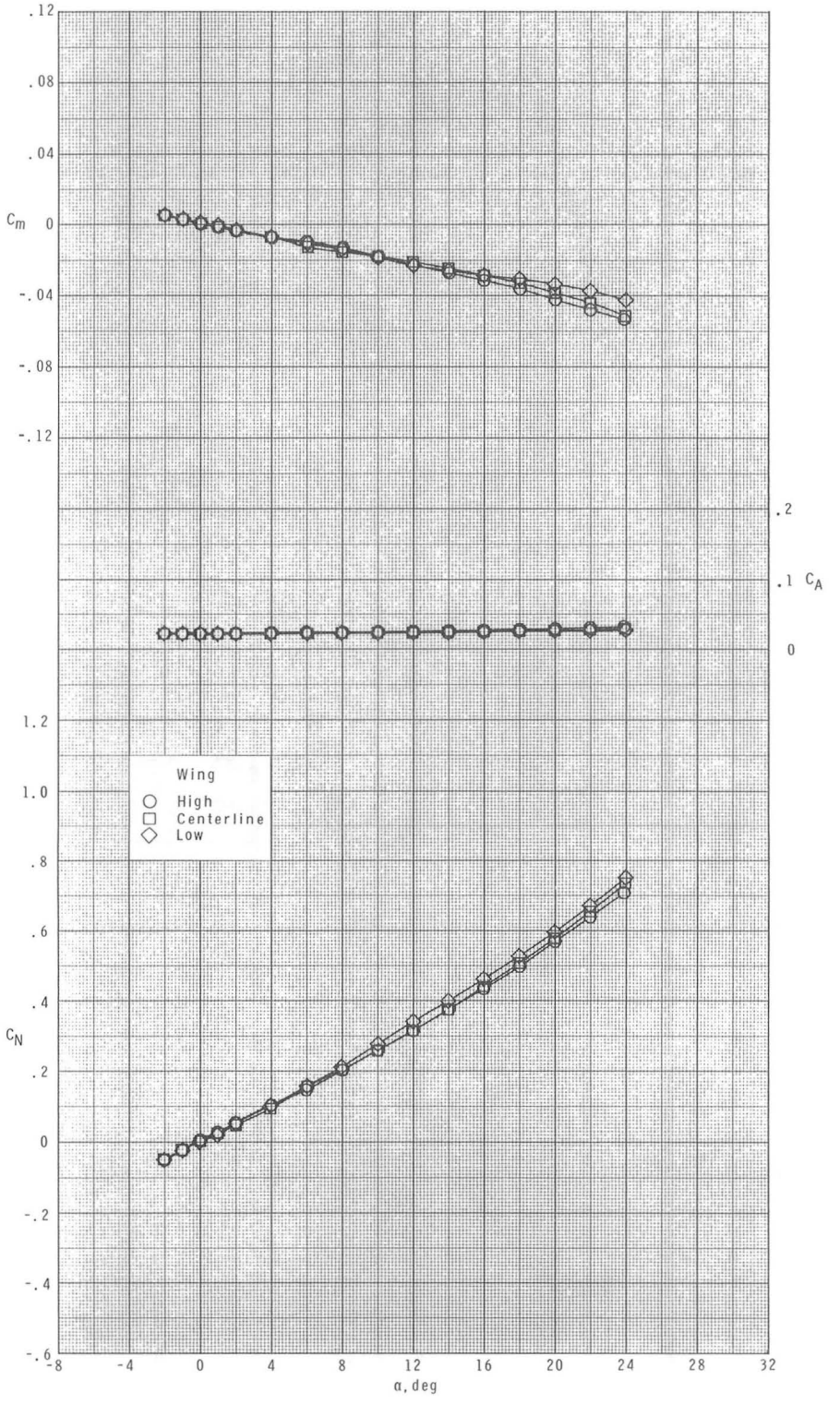

(d) M = 2.86.

Figure 8.- Continued.

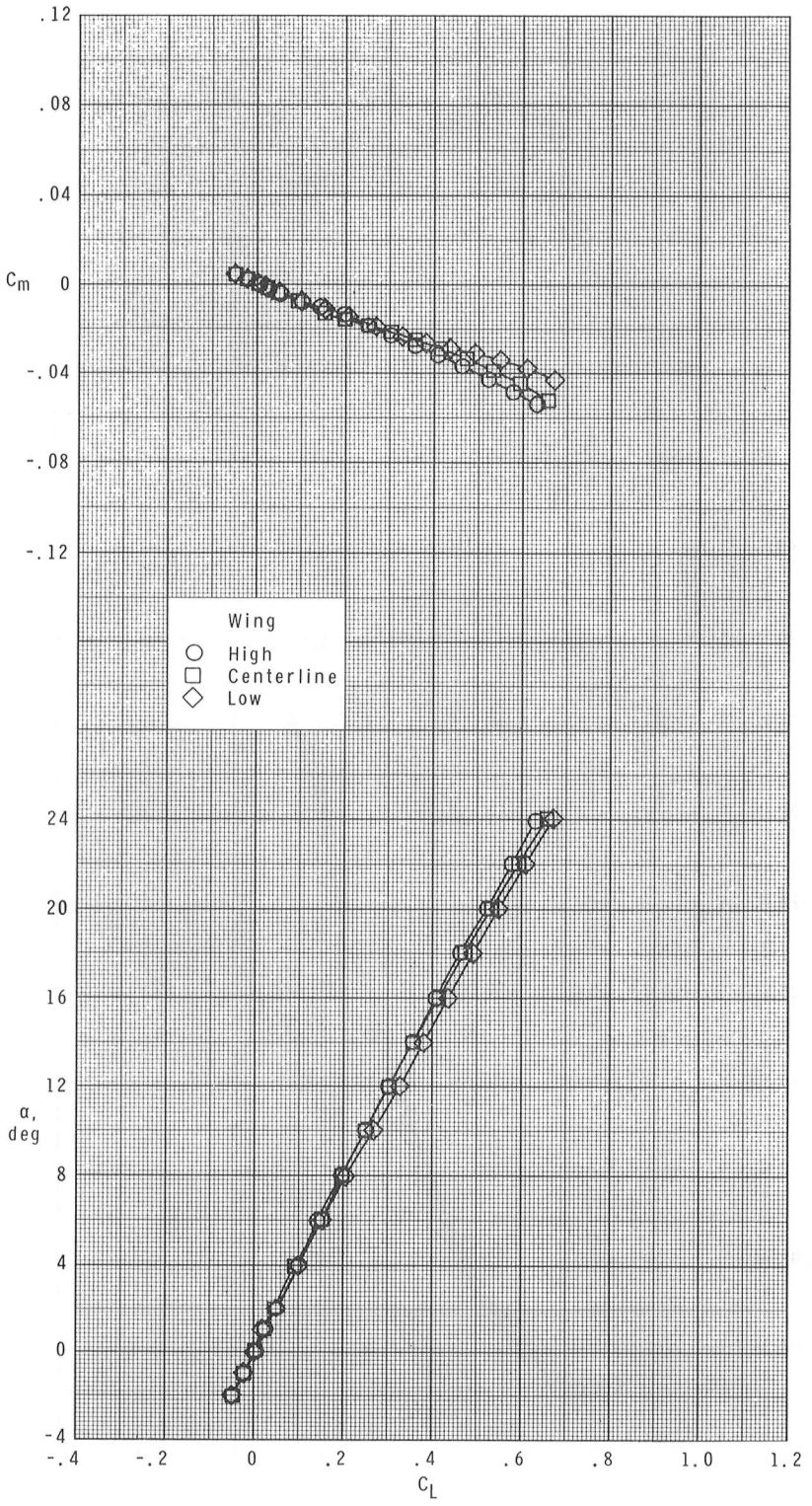

(d) Continued.

Figure 8.- Continued.

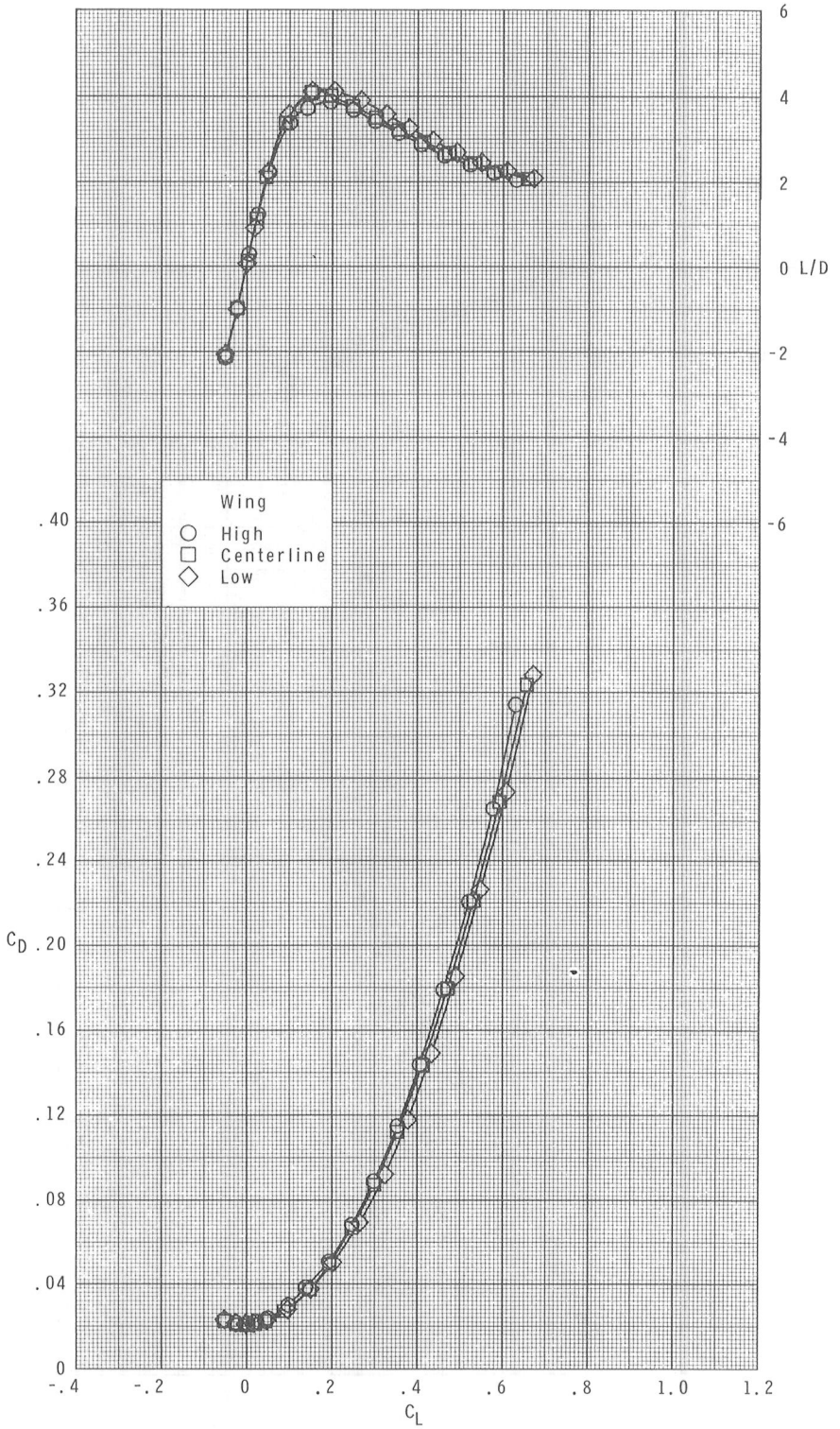

(d) Concluded.

Figure 8.- Concluded.

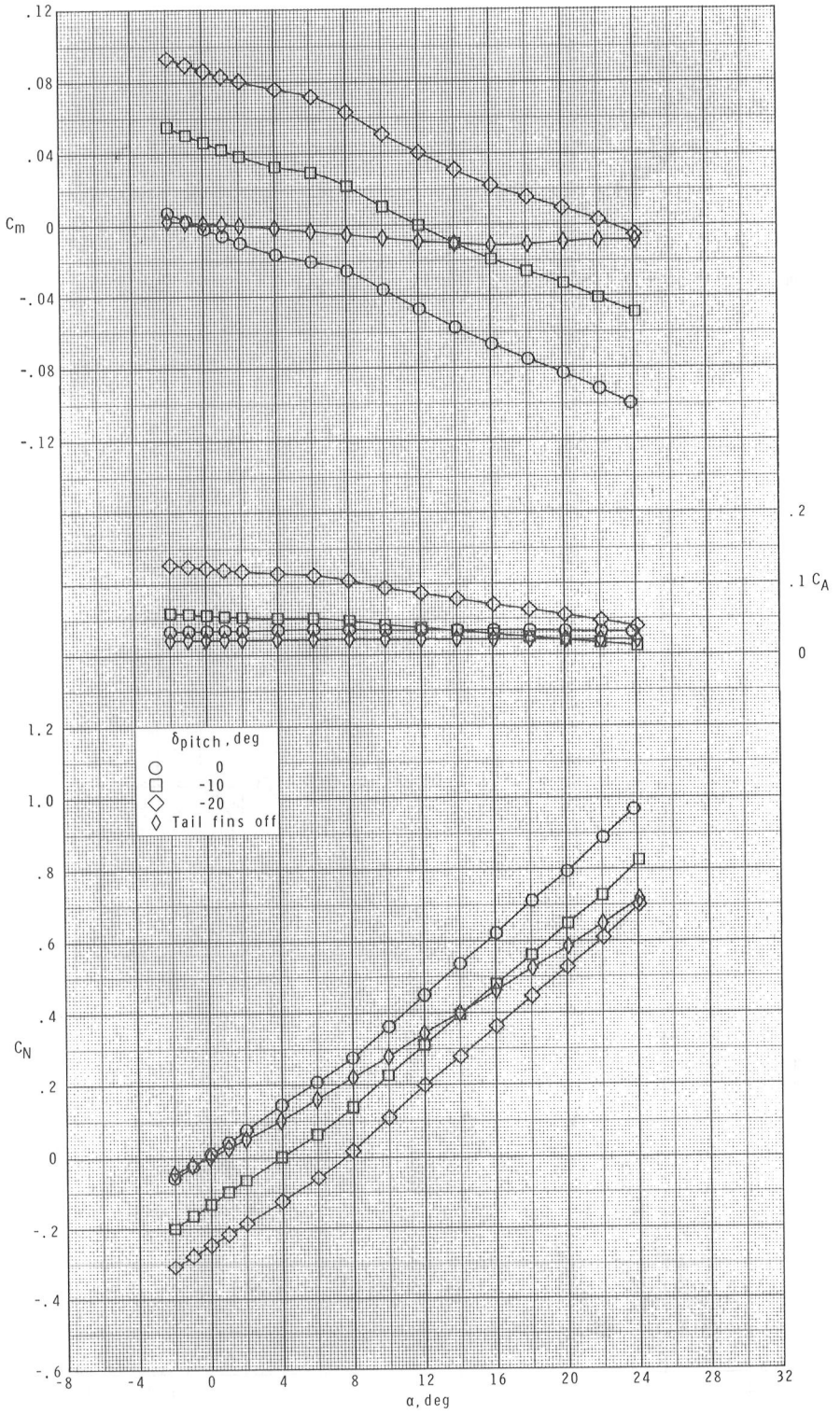

(a) M = 1.70.

Figure 9.- Effects of pitch control on longitudinal aerodynamic characteristics of the high-wing configuration.

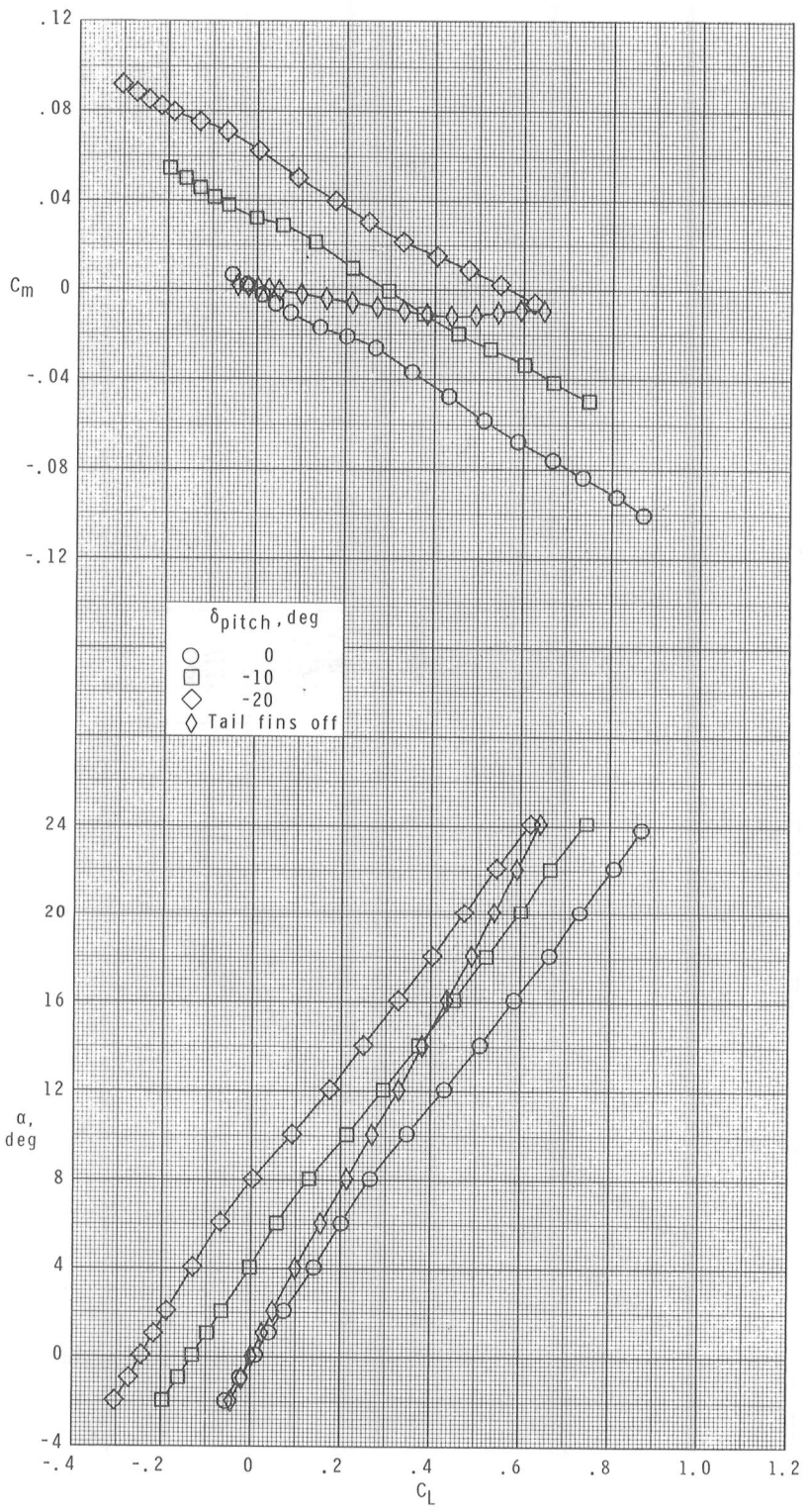

(a) Continued.

Figure 9.- Continued.

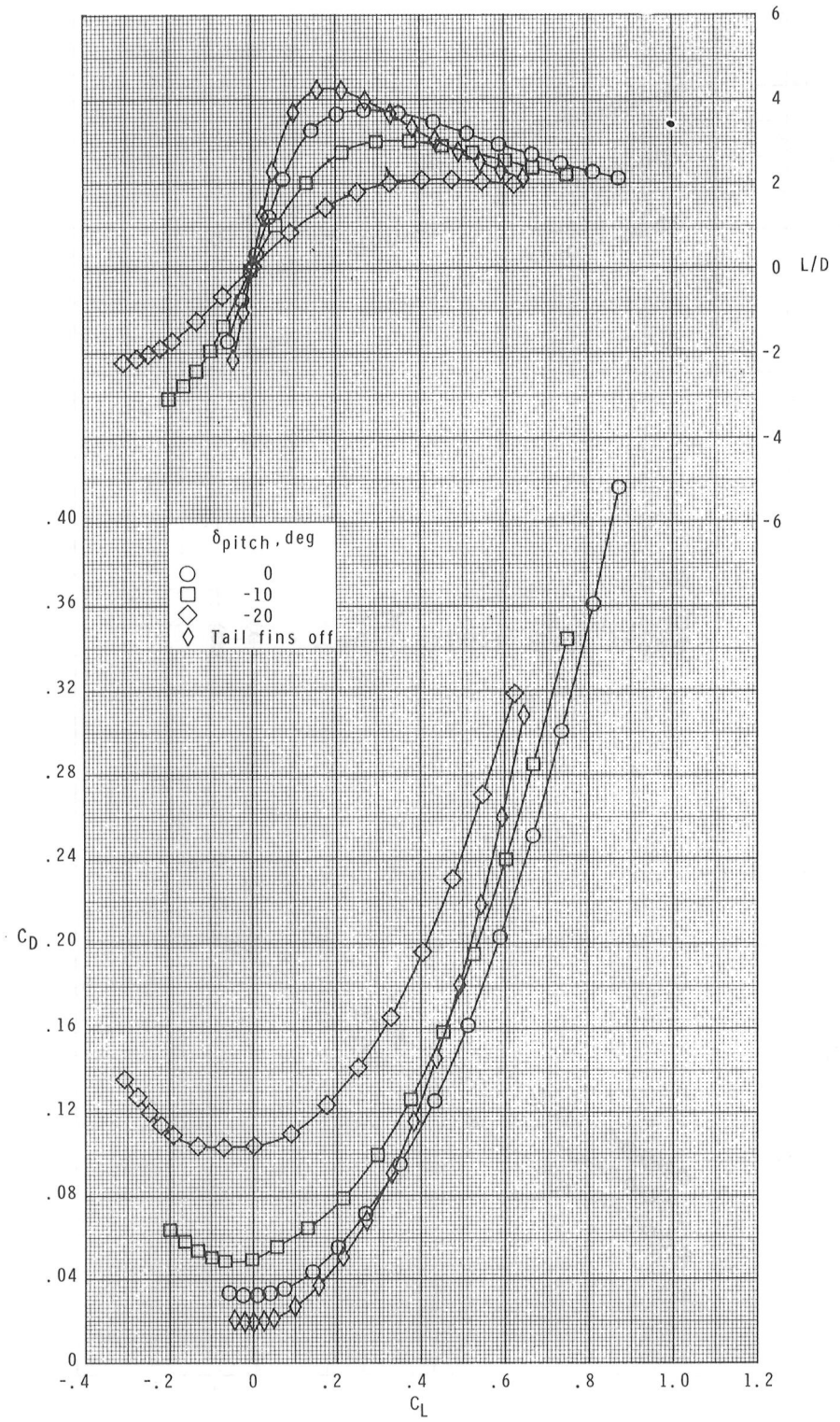

(a) Concluded.

Figure 9.- Continued.

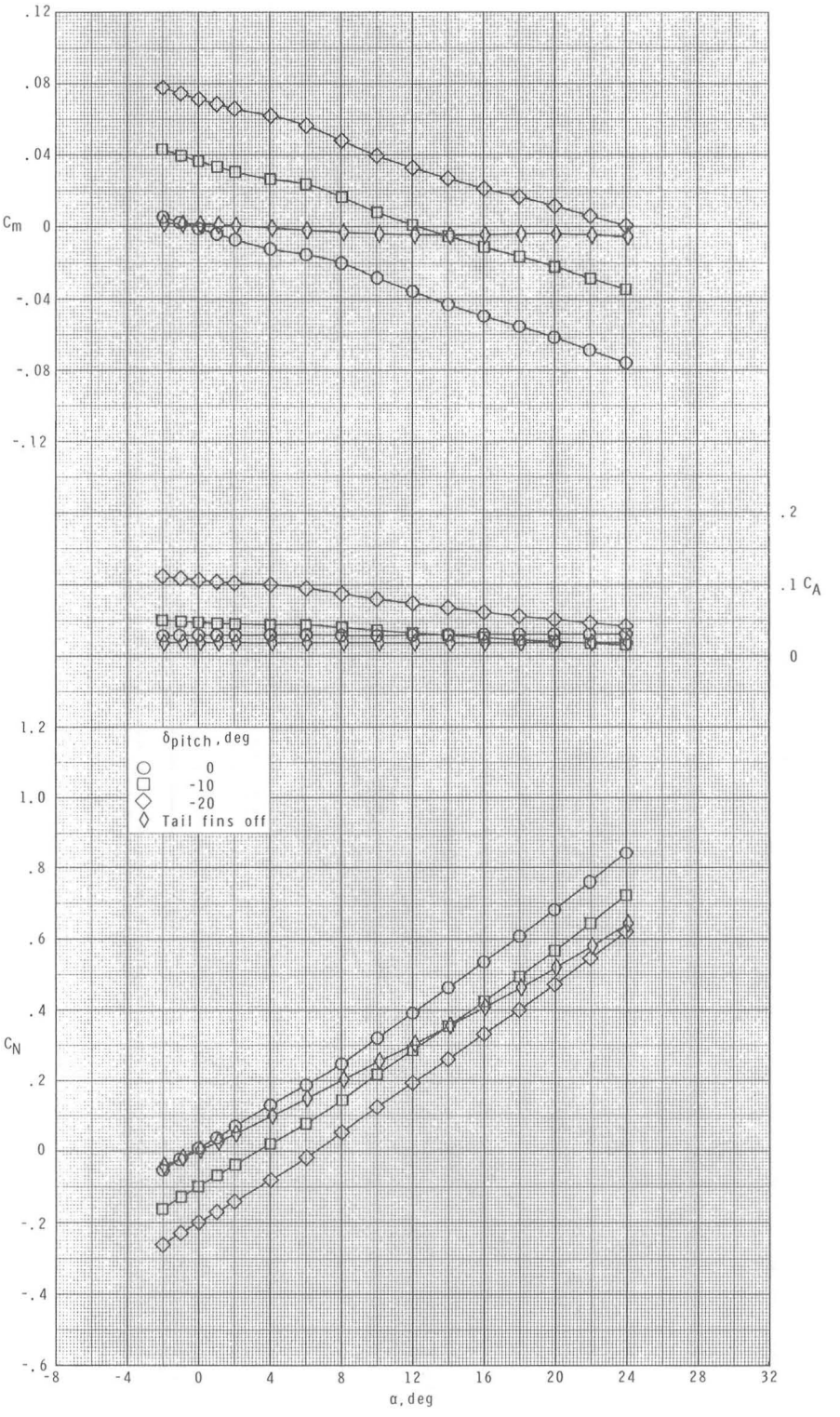

(b) M = 2.16.

Figure 9.- Continued.

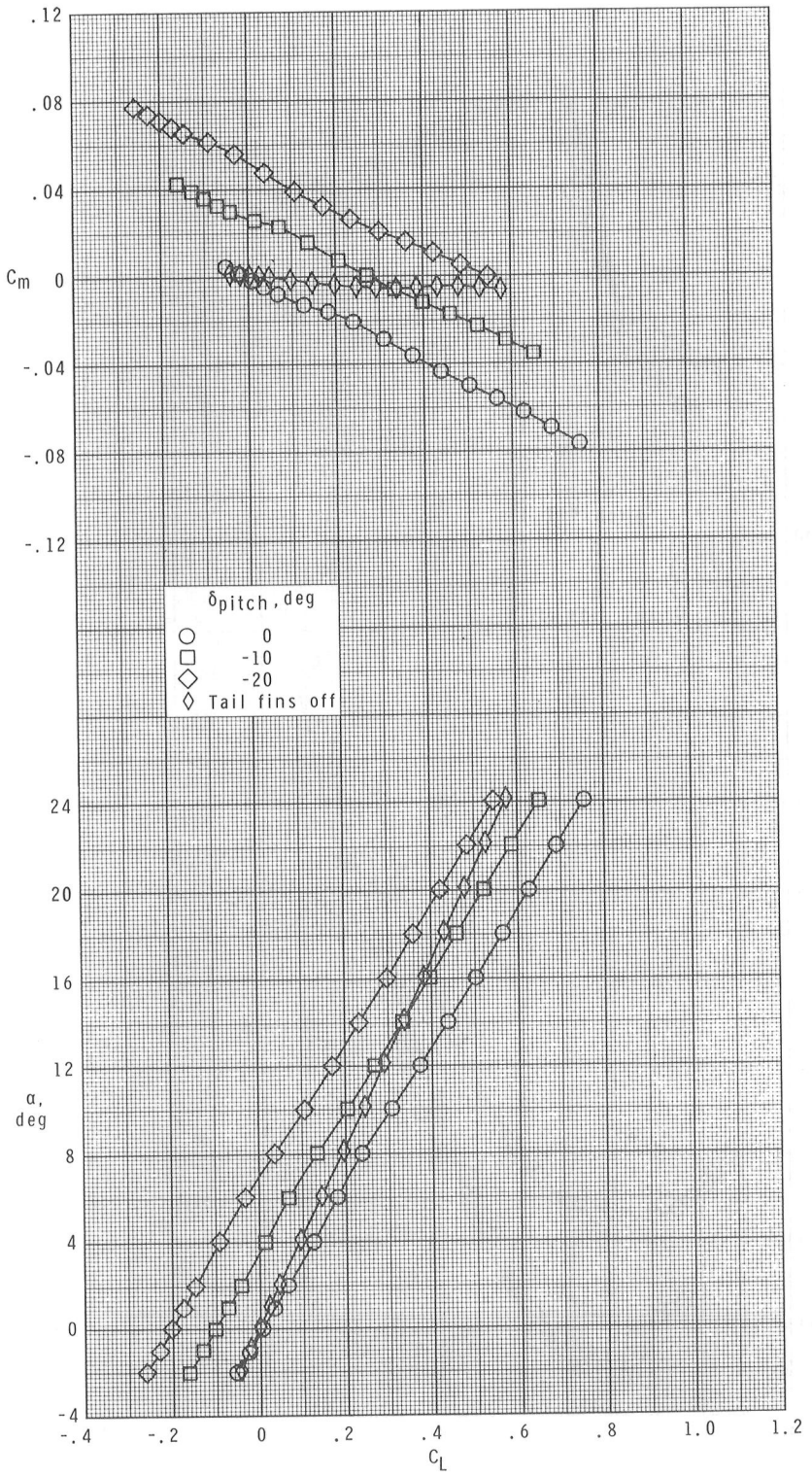

(b) Continued.

Figure 9.- Continued.

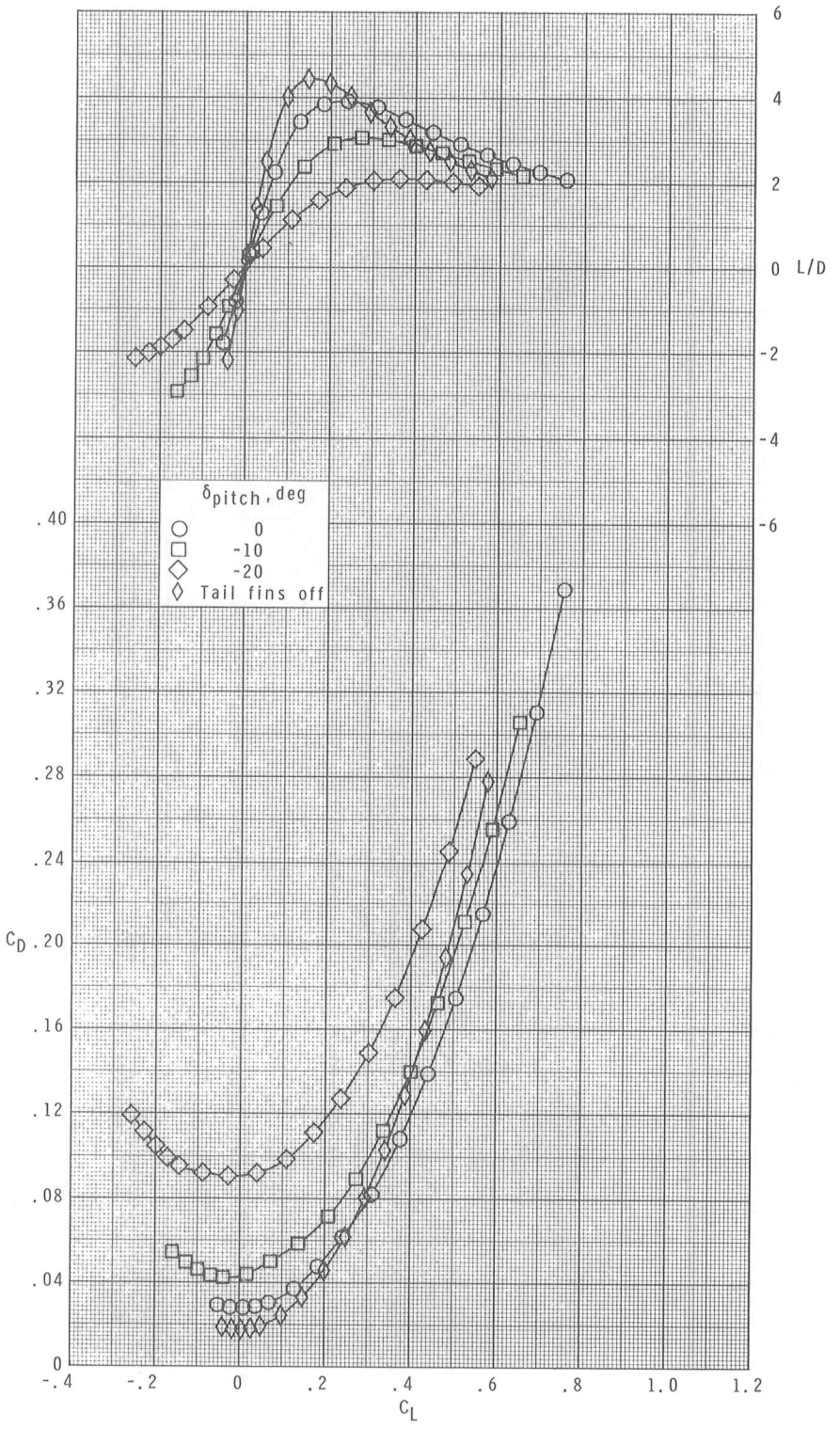

(b) Concluded.

Figure 9.- Continued.

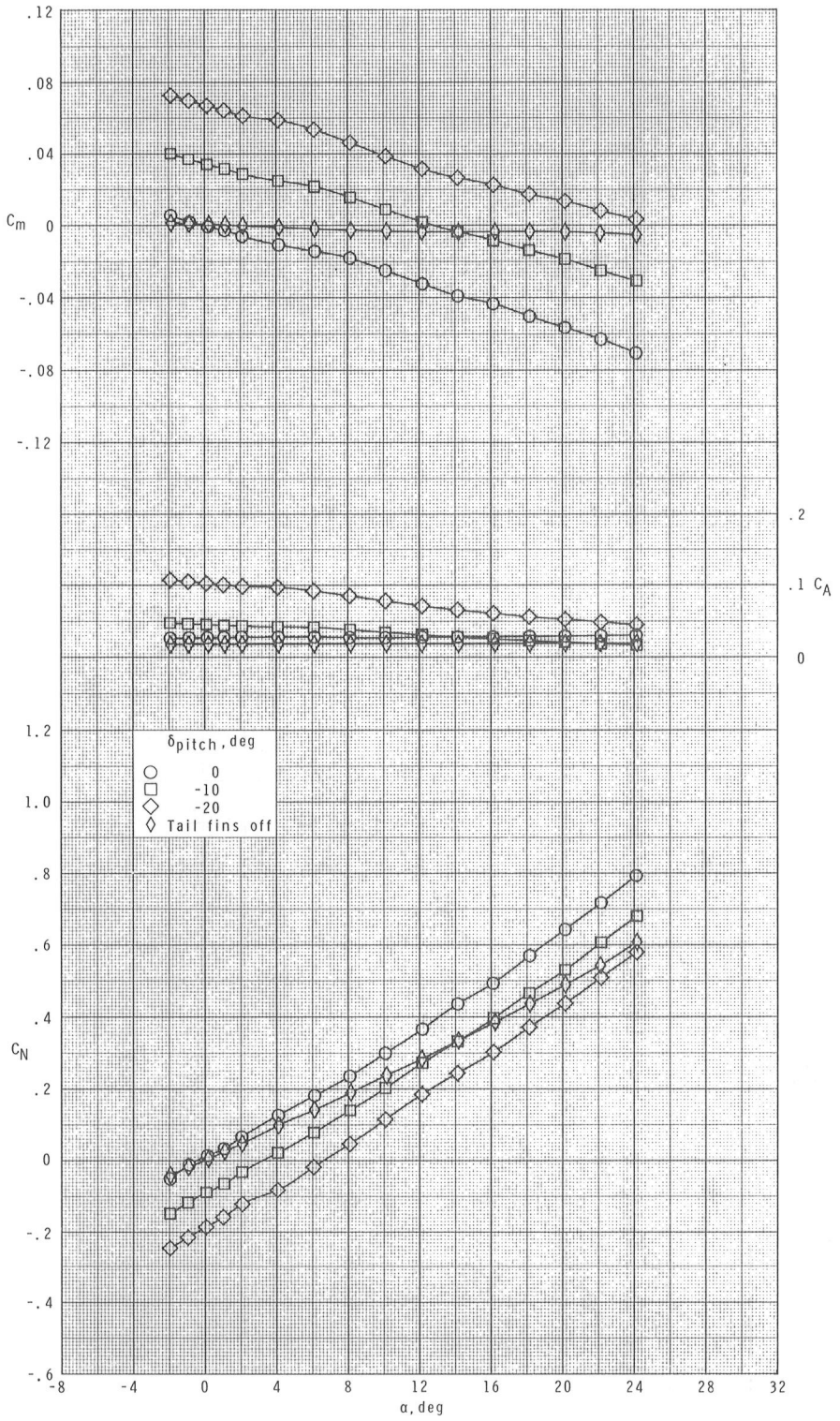

(c) M ≃ 2.36.

Figure 9.- Continued.

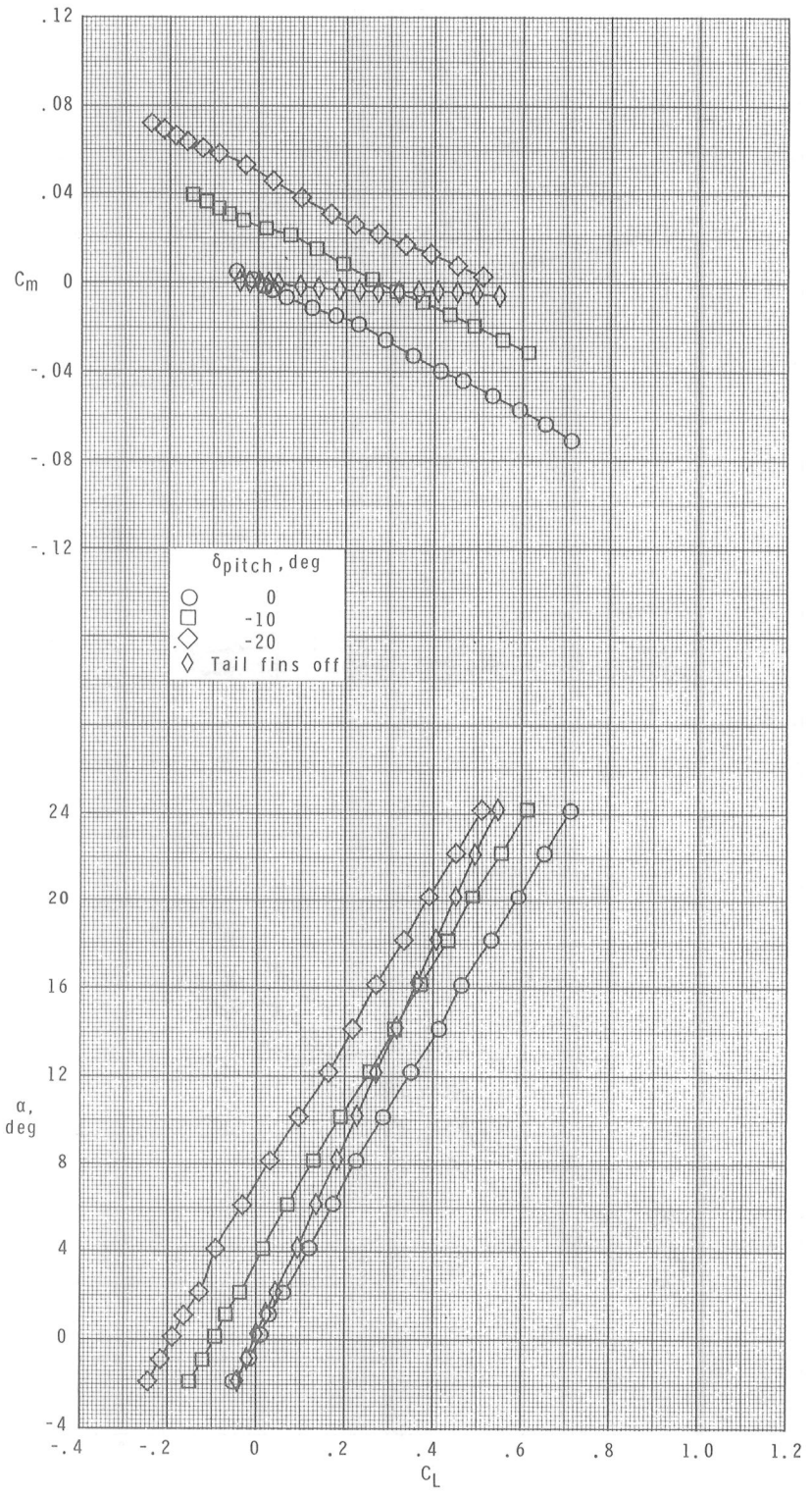

(c) Continued.

Figure 9.- Continued.

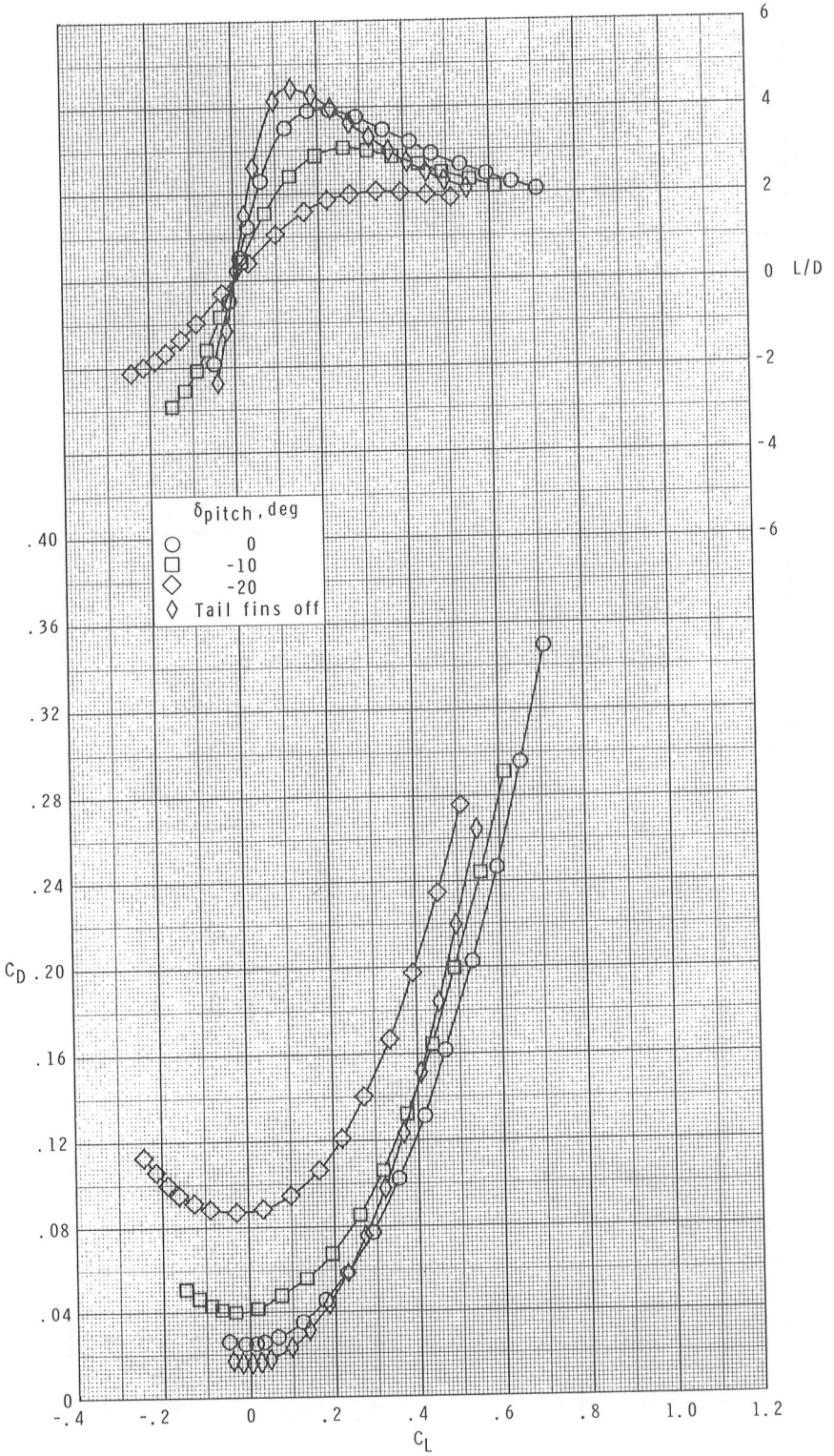

(c) Concluded.

Figure 9.- Continued.

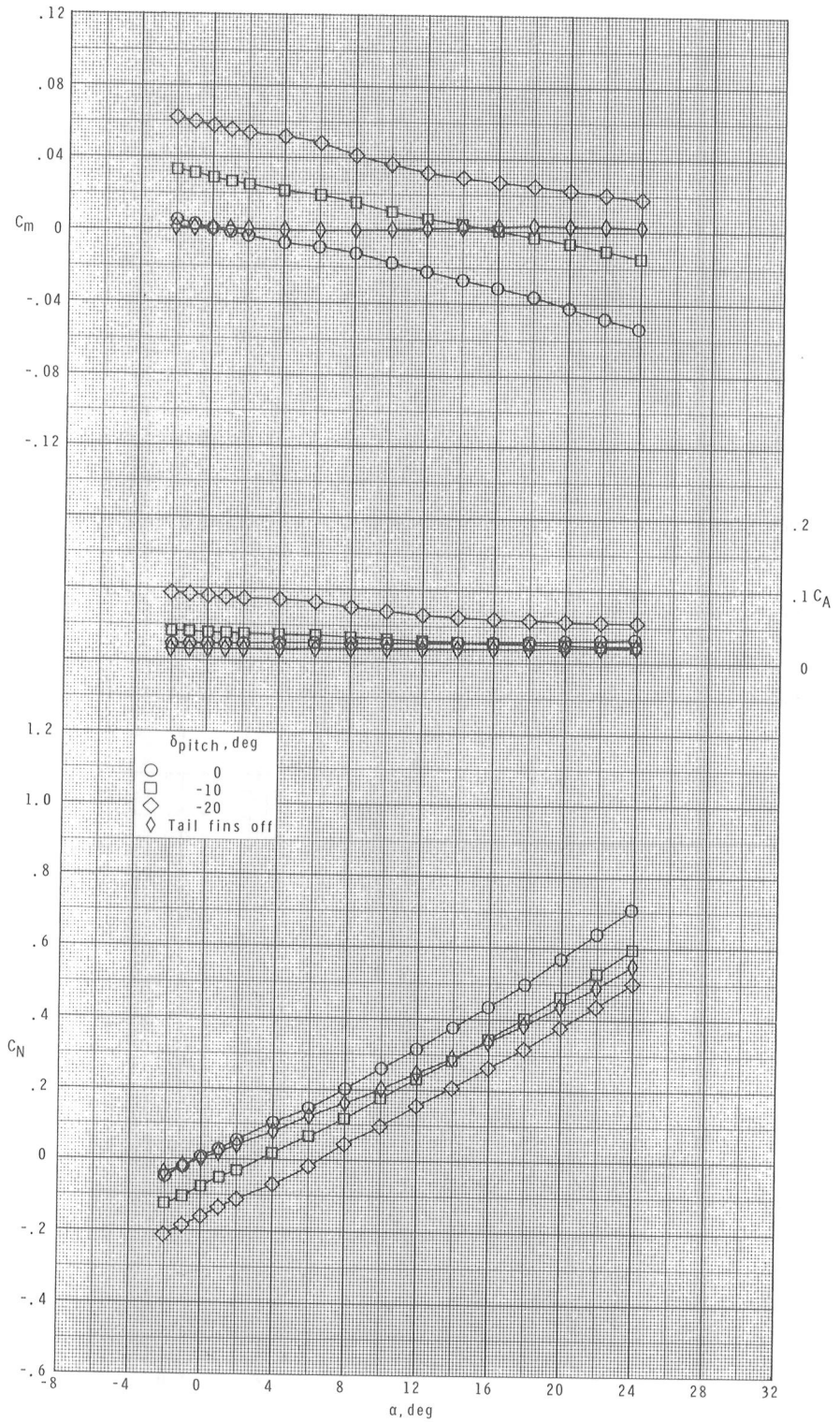

(d) M = 2.86.

Figure 9.- Continued.

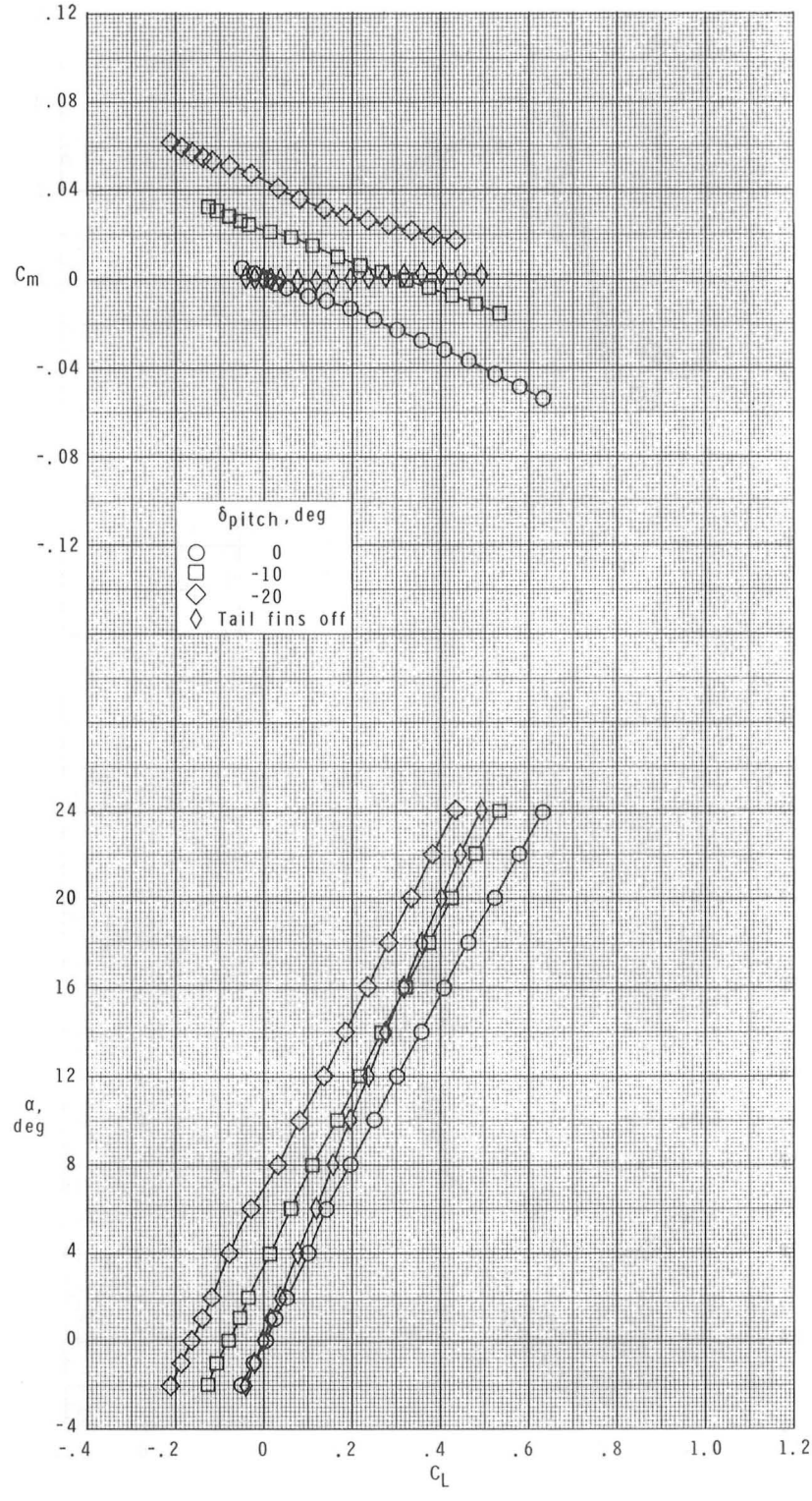

(d) Continued.

Figure 9.- Continued.

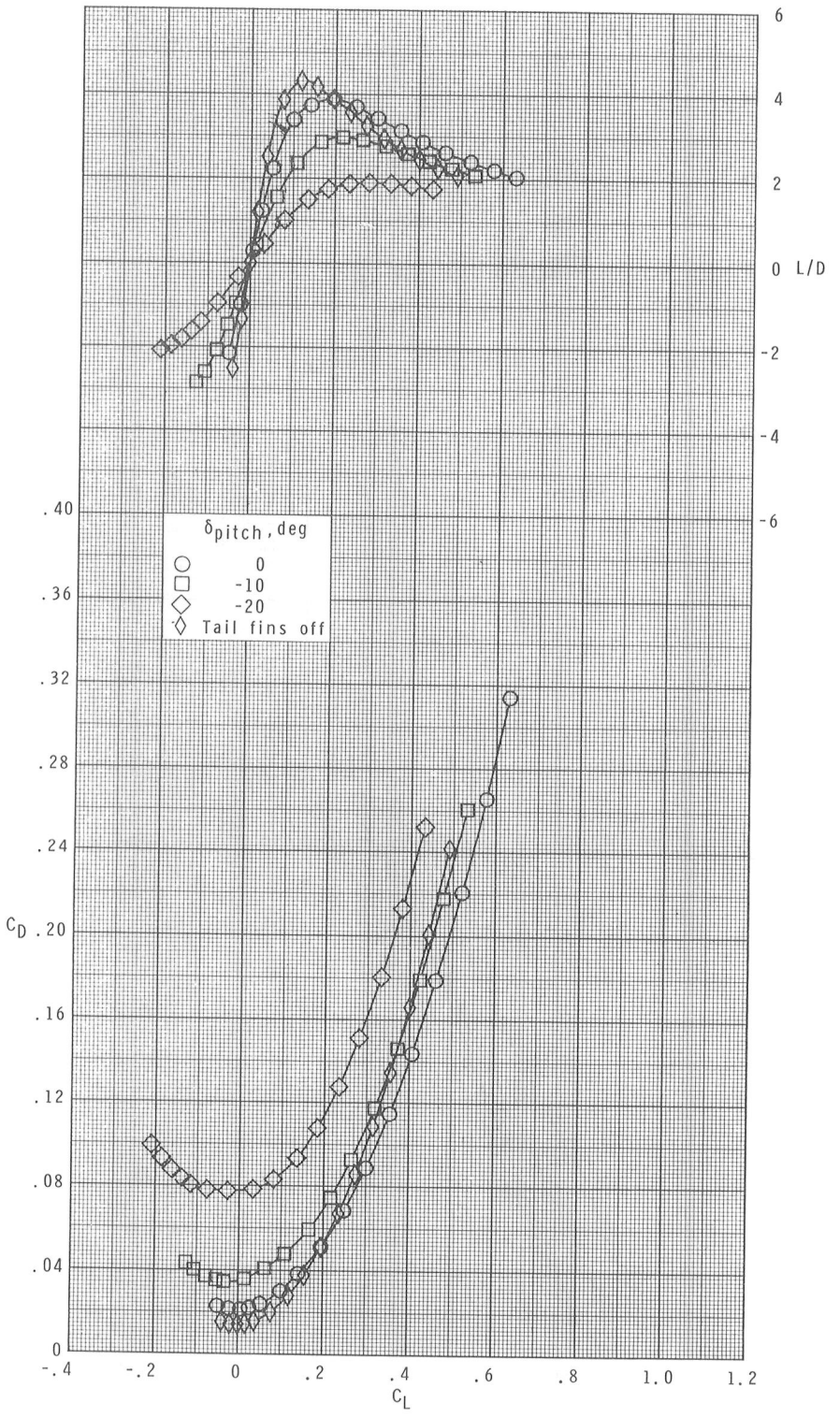

(d) Concluded.

Figure 9.- Concluded.

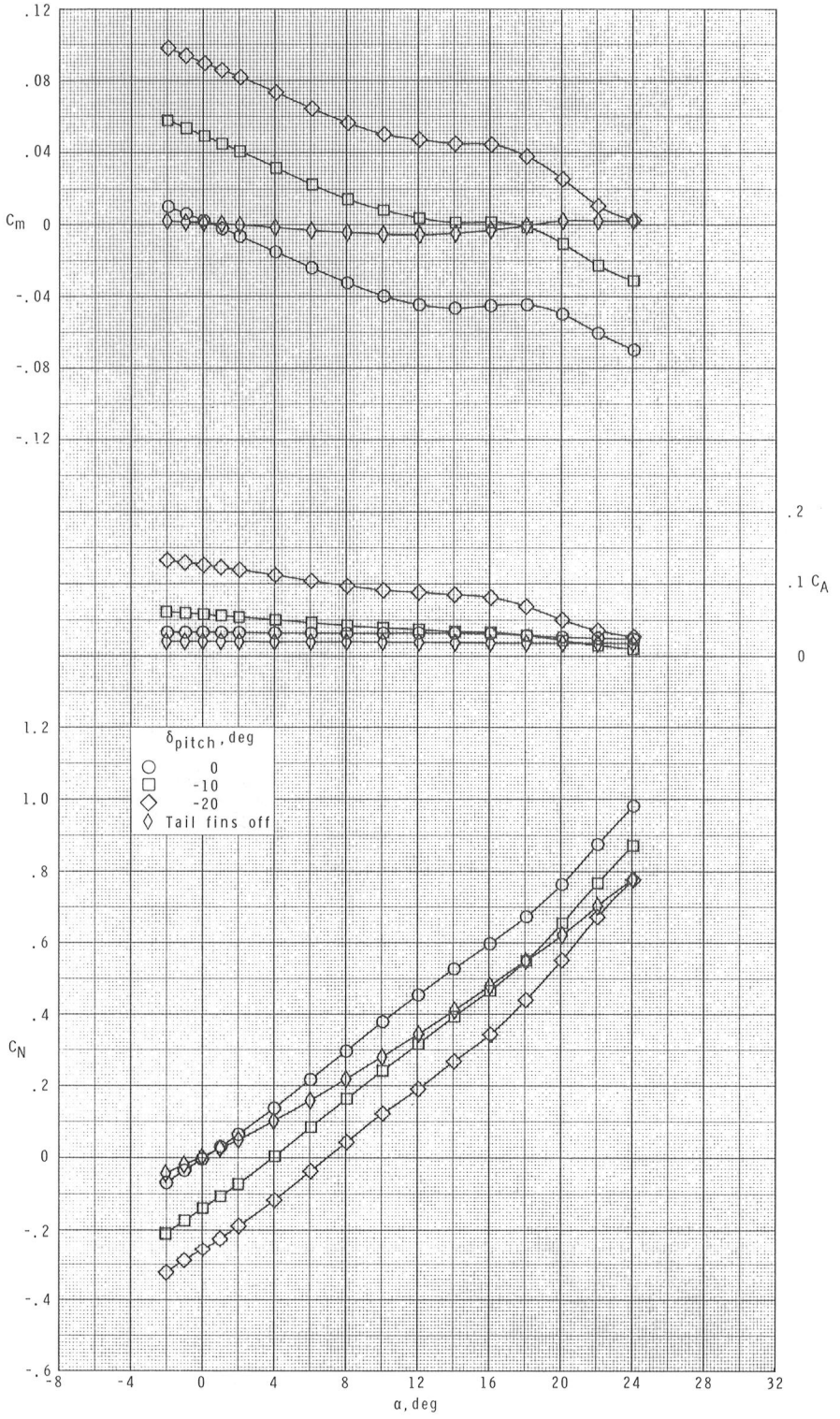

(a) M = 1.70.

Figure 10.- Effects of pitch control on longitudinal aerodynamic characteristics of the low-wing configuration.

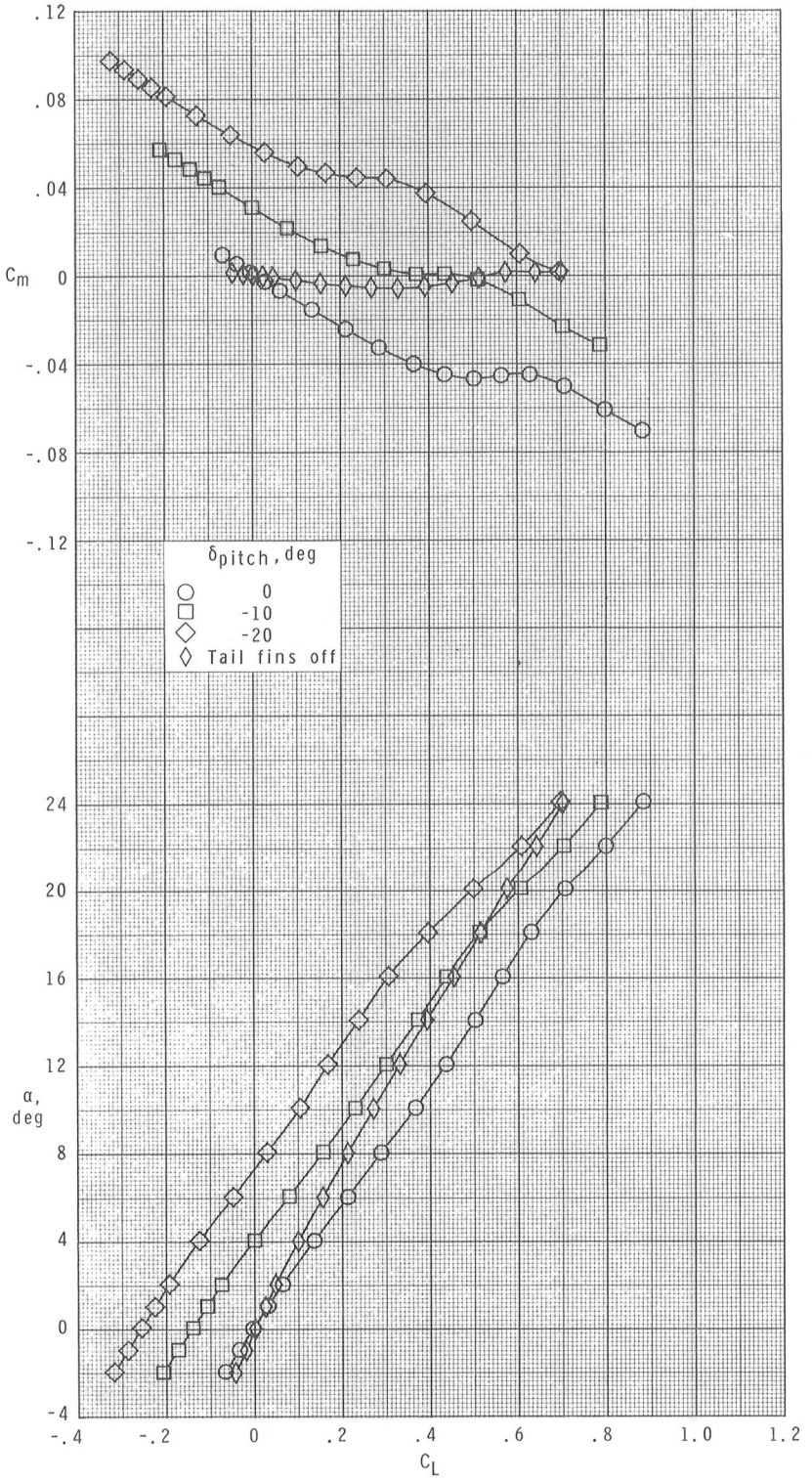

(a) Continued.

Figure 10.- Continued.

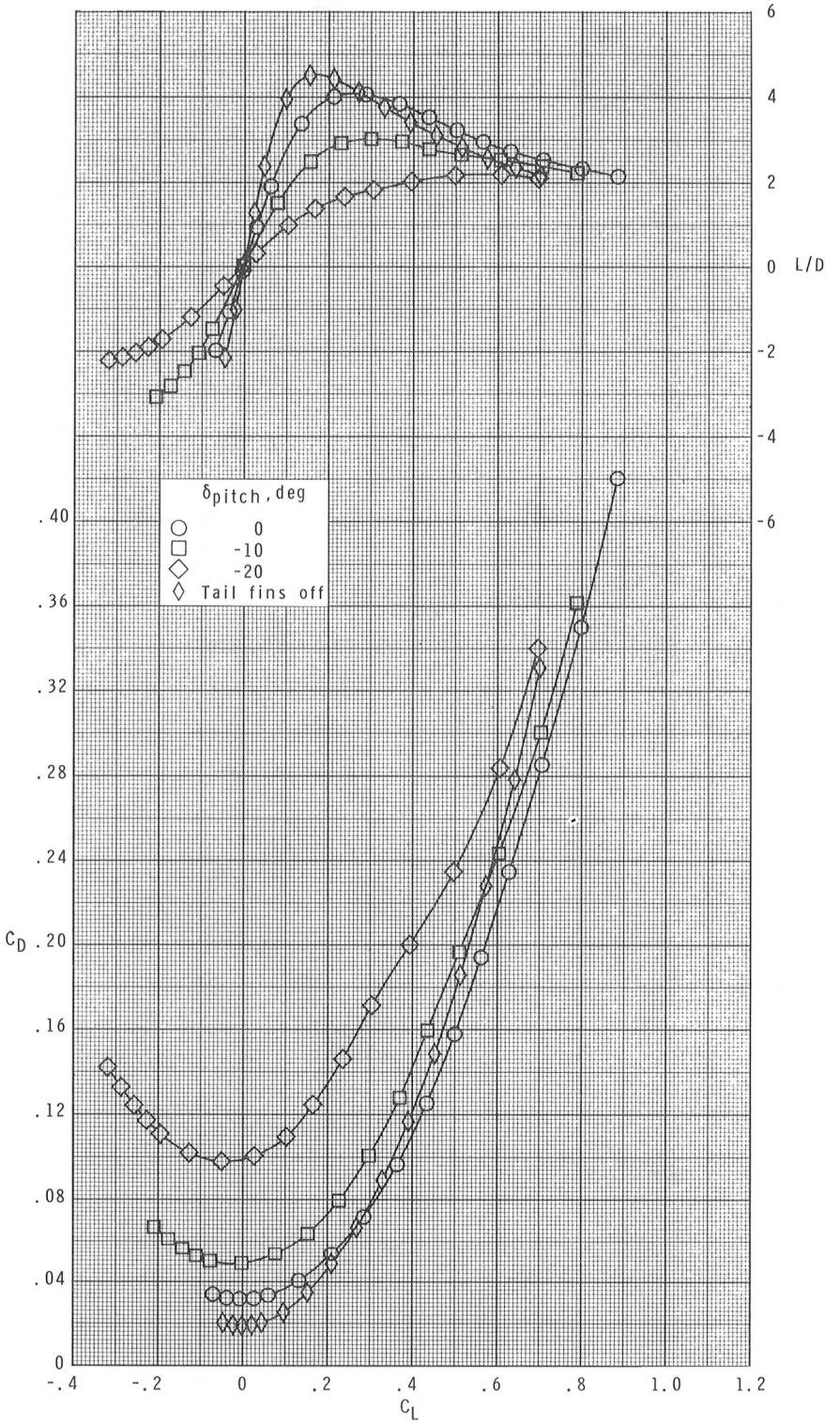

(a) Concluded.

Figure 10.- Continued.

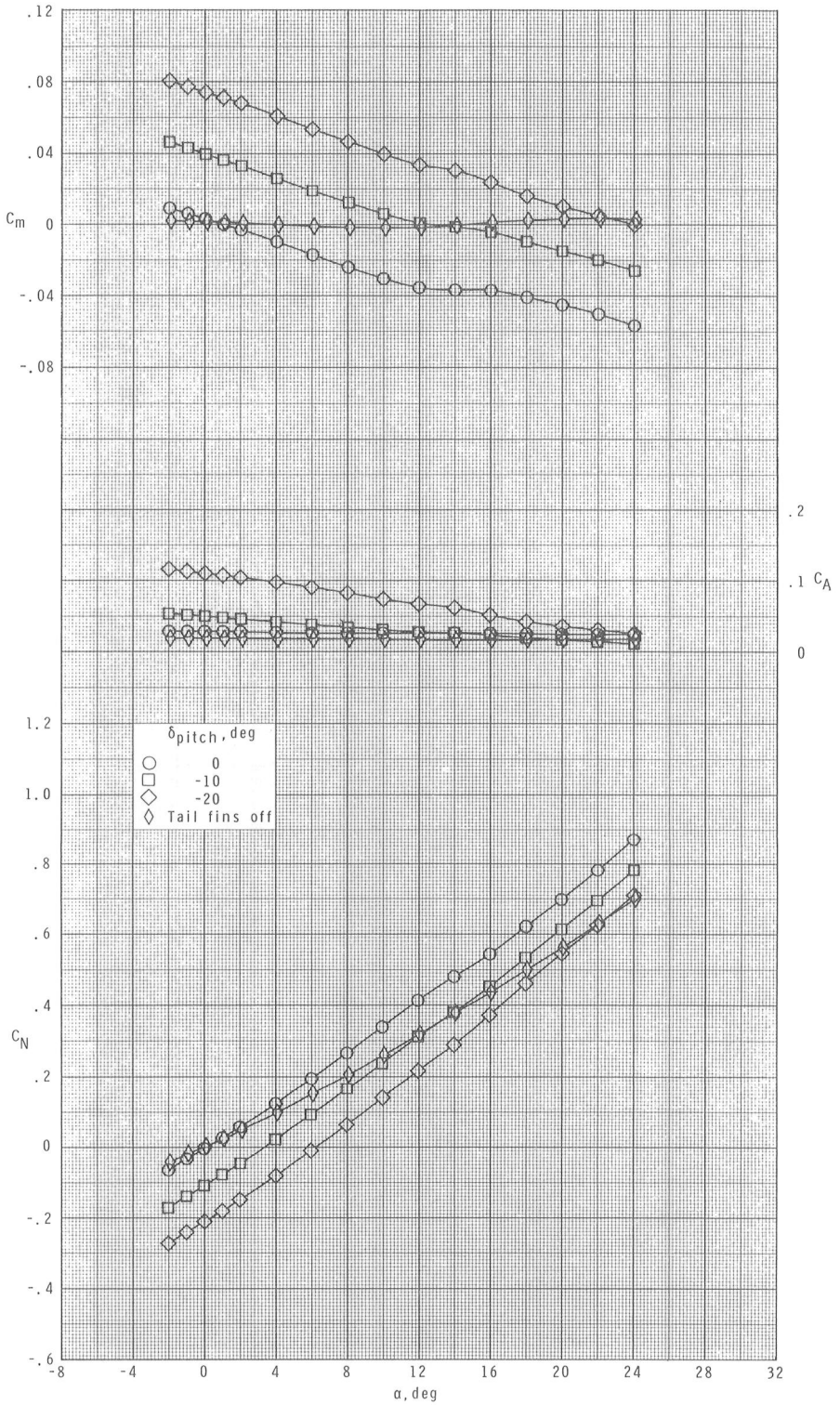

(b) M = 2.16.

Figure 10.- Continued.

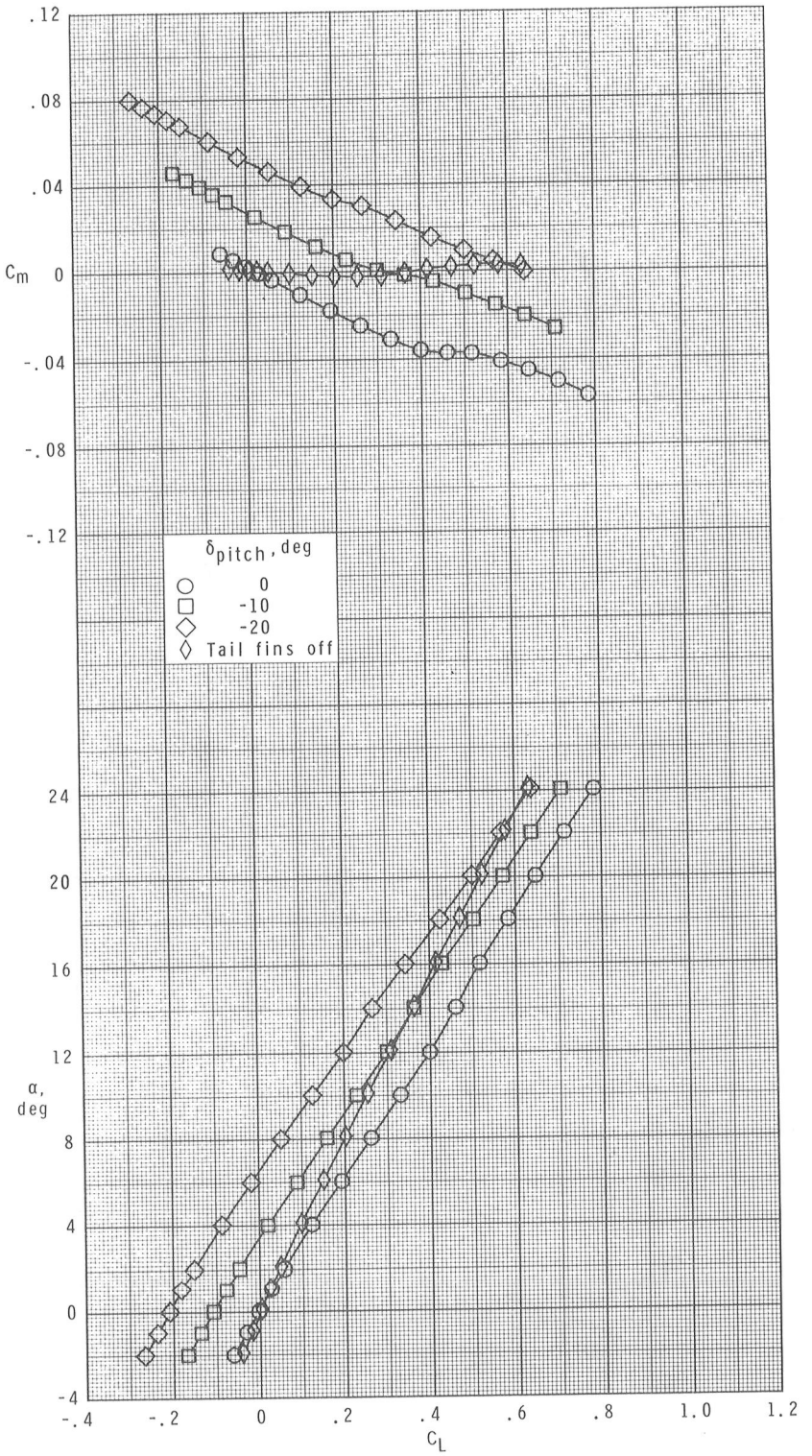

(b) Continued.

Figure 10.- Continued.

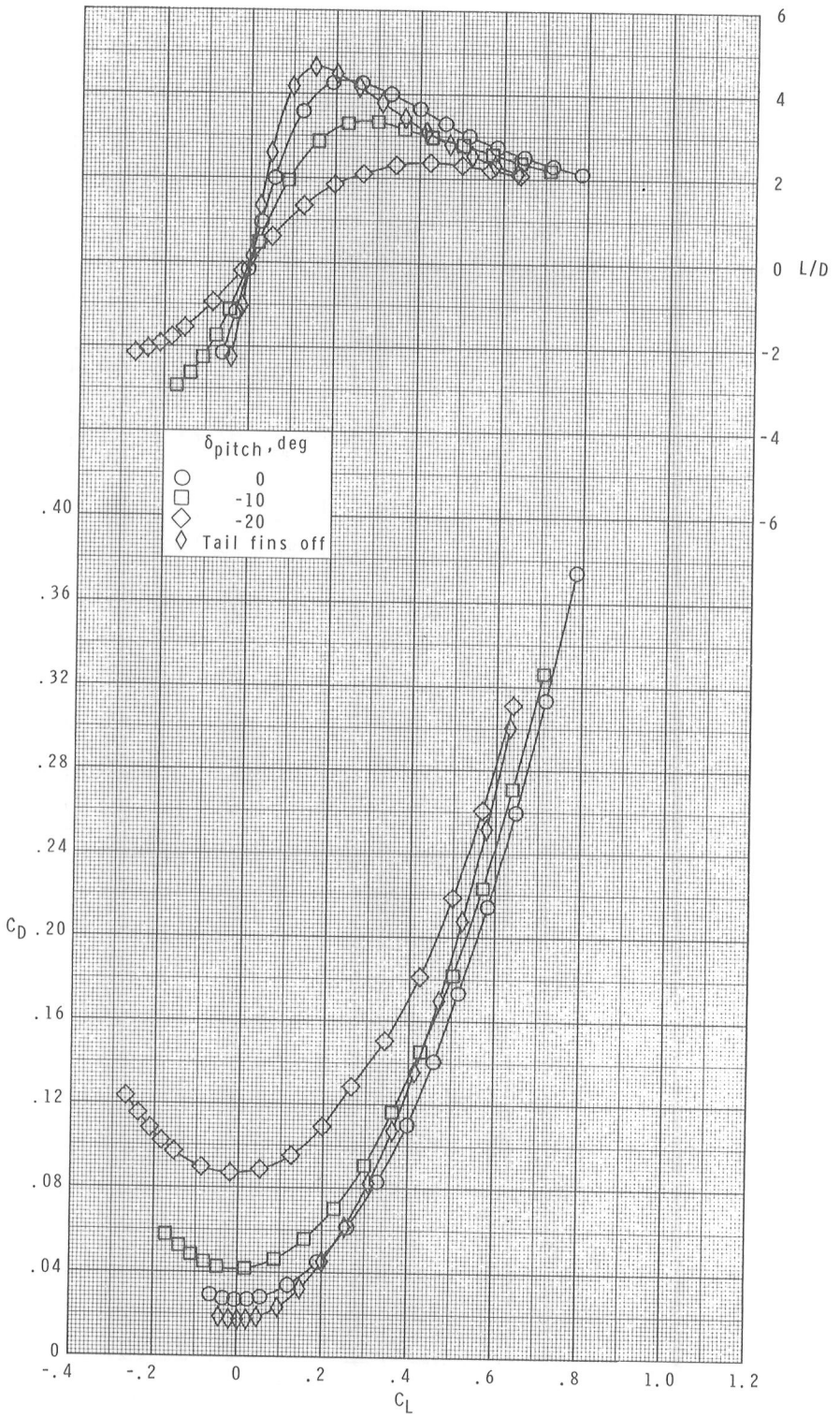

(b) Concluded.

Figure 10.- Continued.

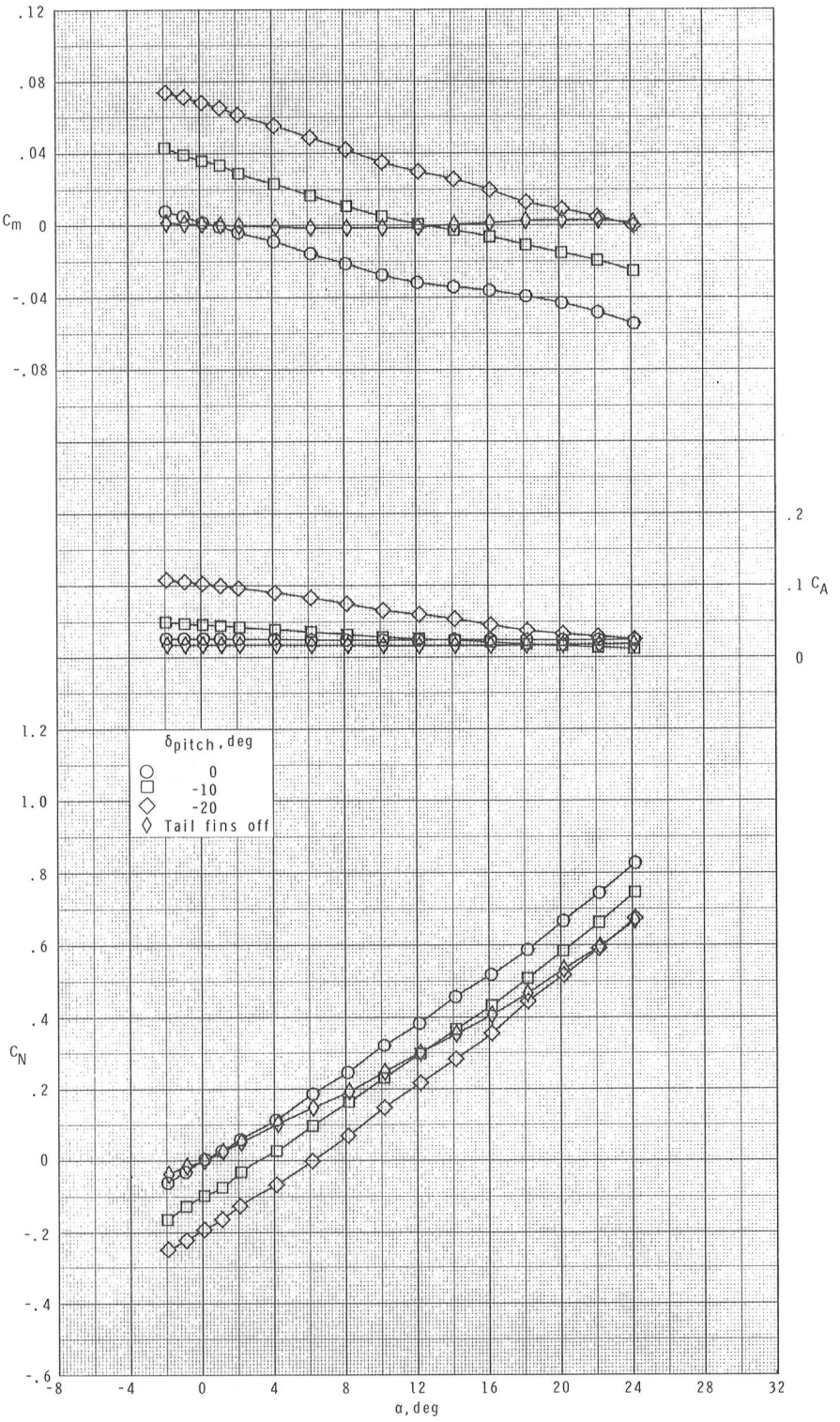

(c) M = 2.36.

Figure 10.- Continued.

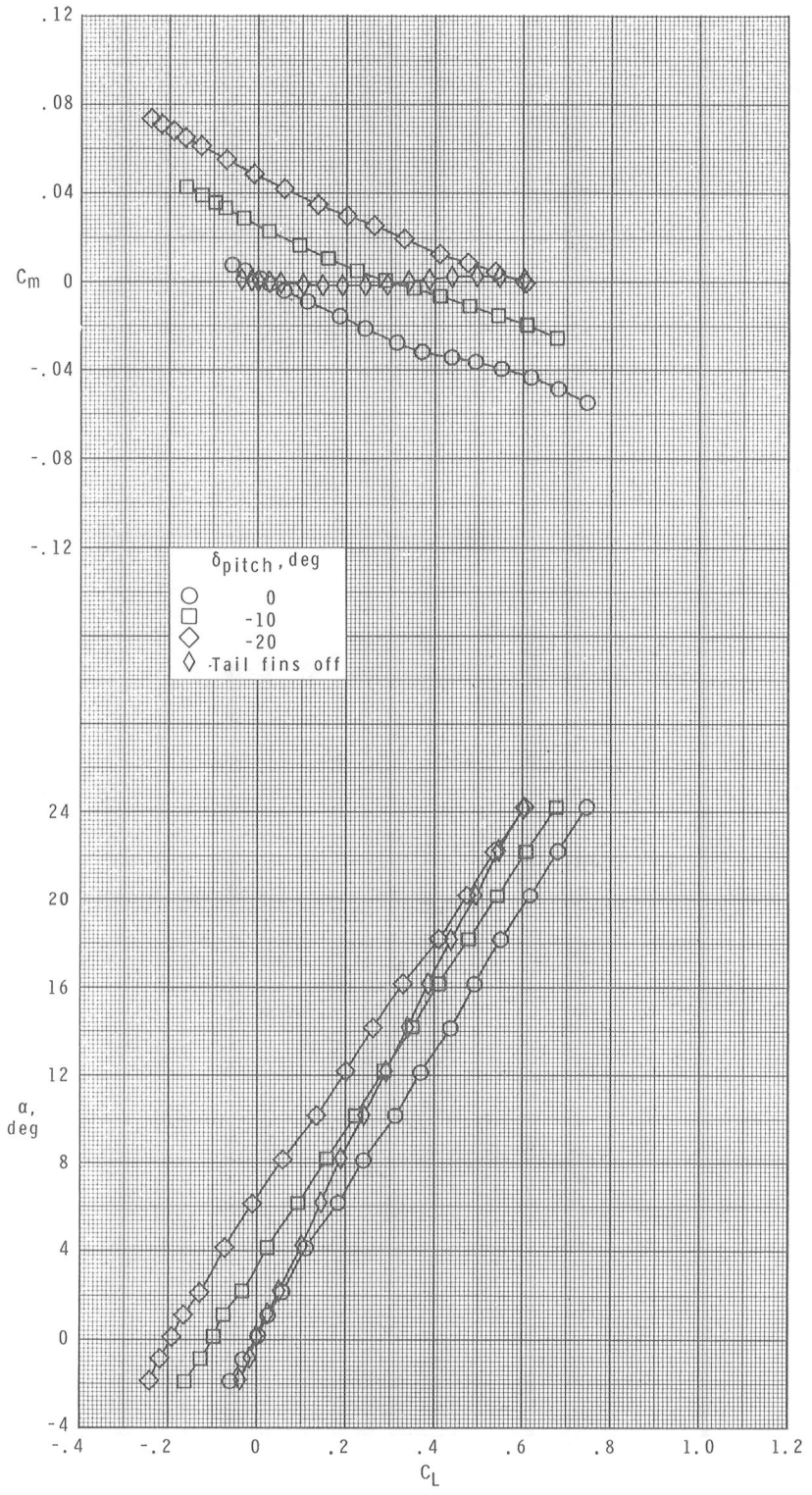

(c) Continued.

Figure 10.- Continued.

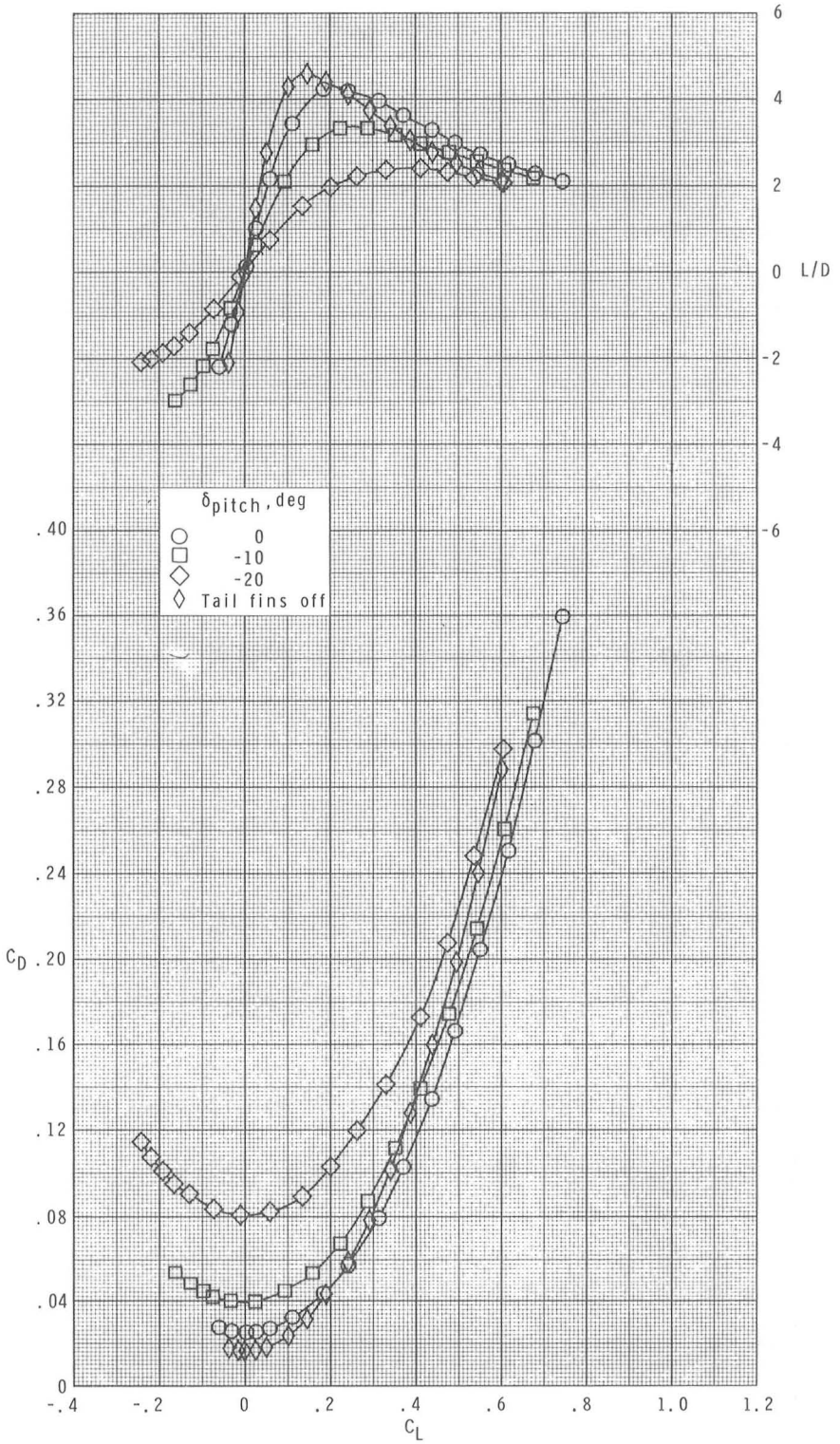

(c) Concluded.

Figure 10.- Continued.

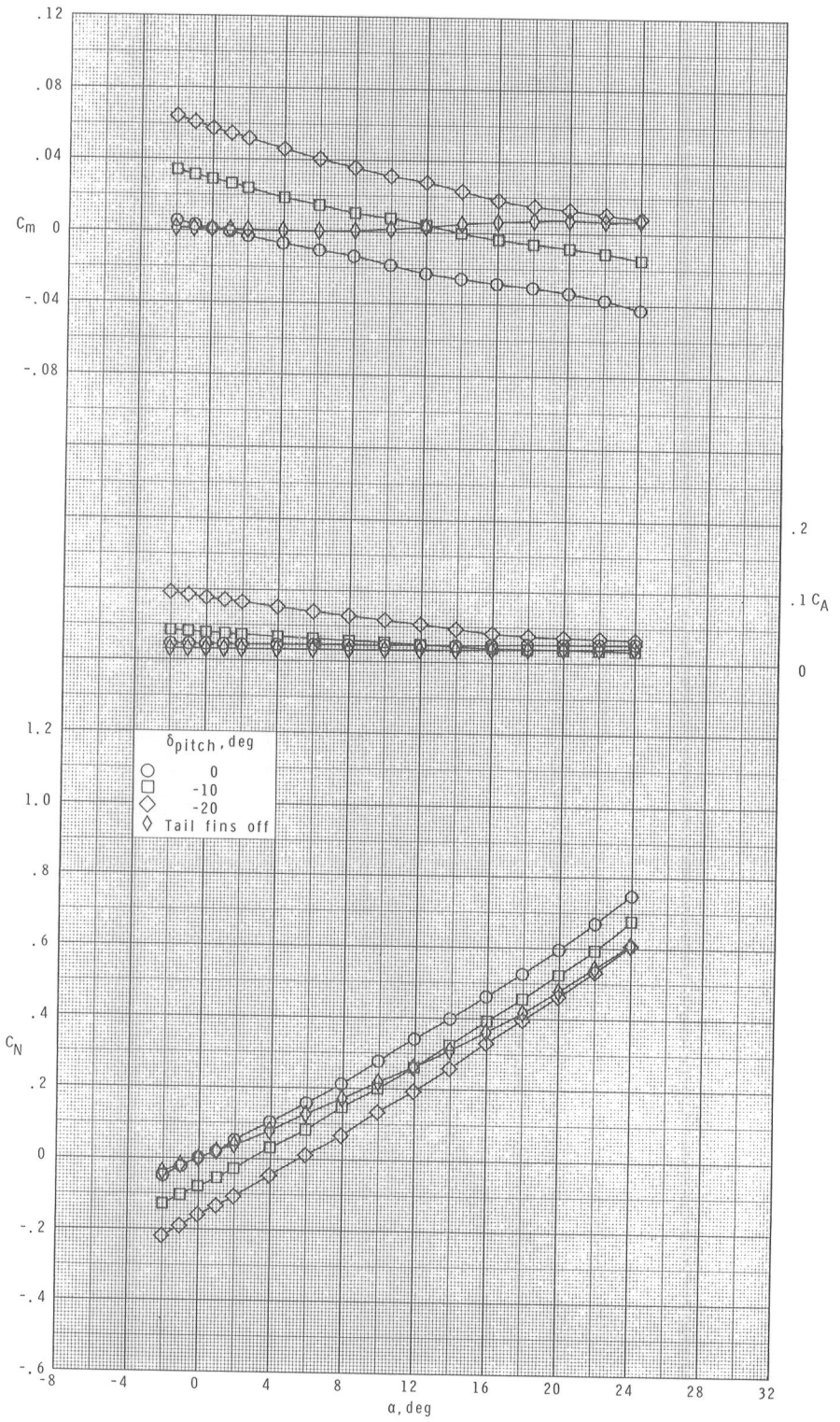

(d) M = 2.86.

Figure 10.- Continued.

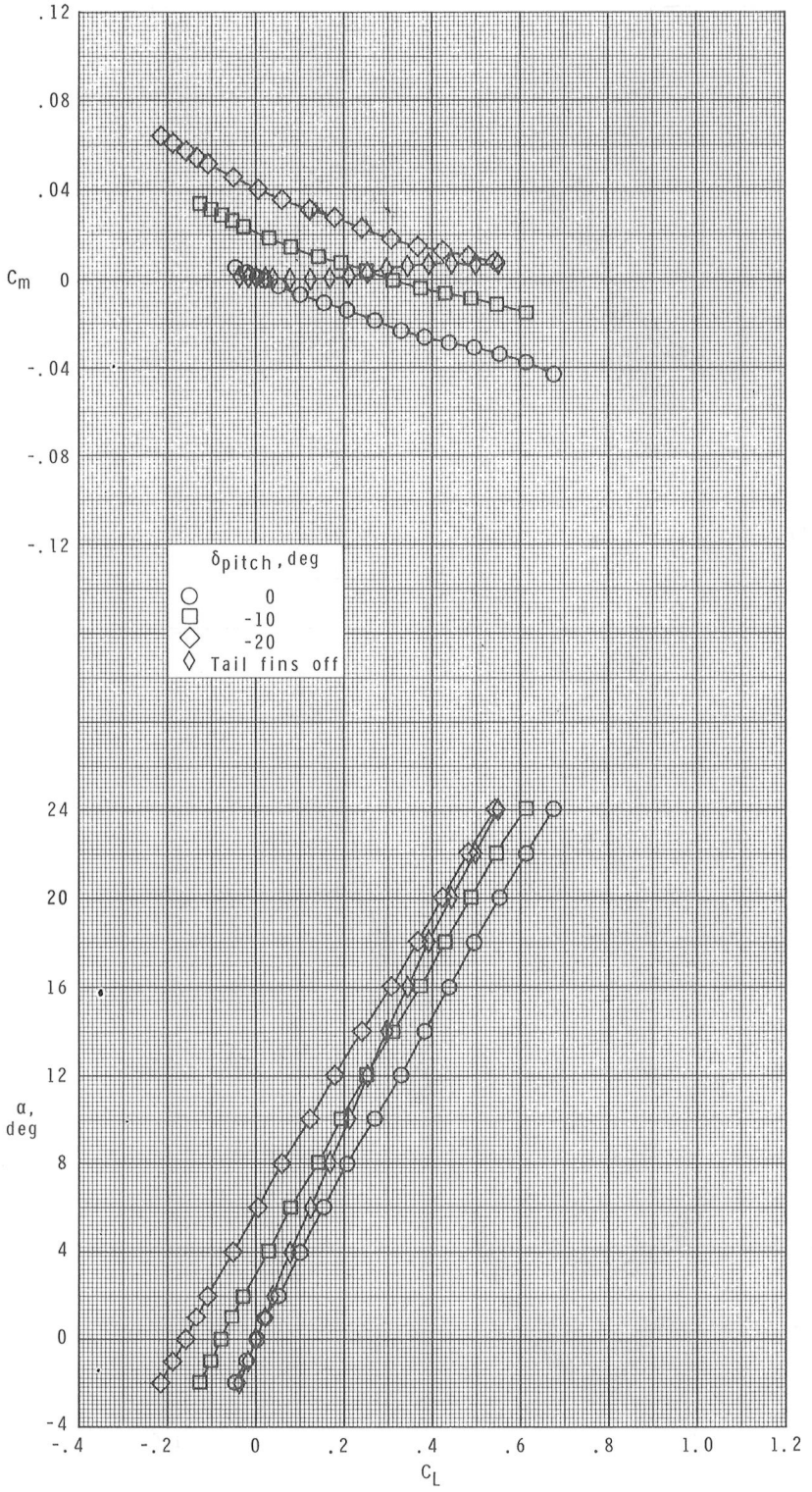

(d) Continued.

Figure 10.- Continued.

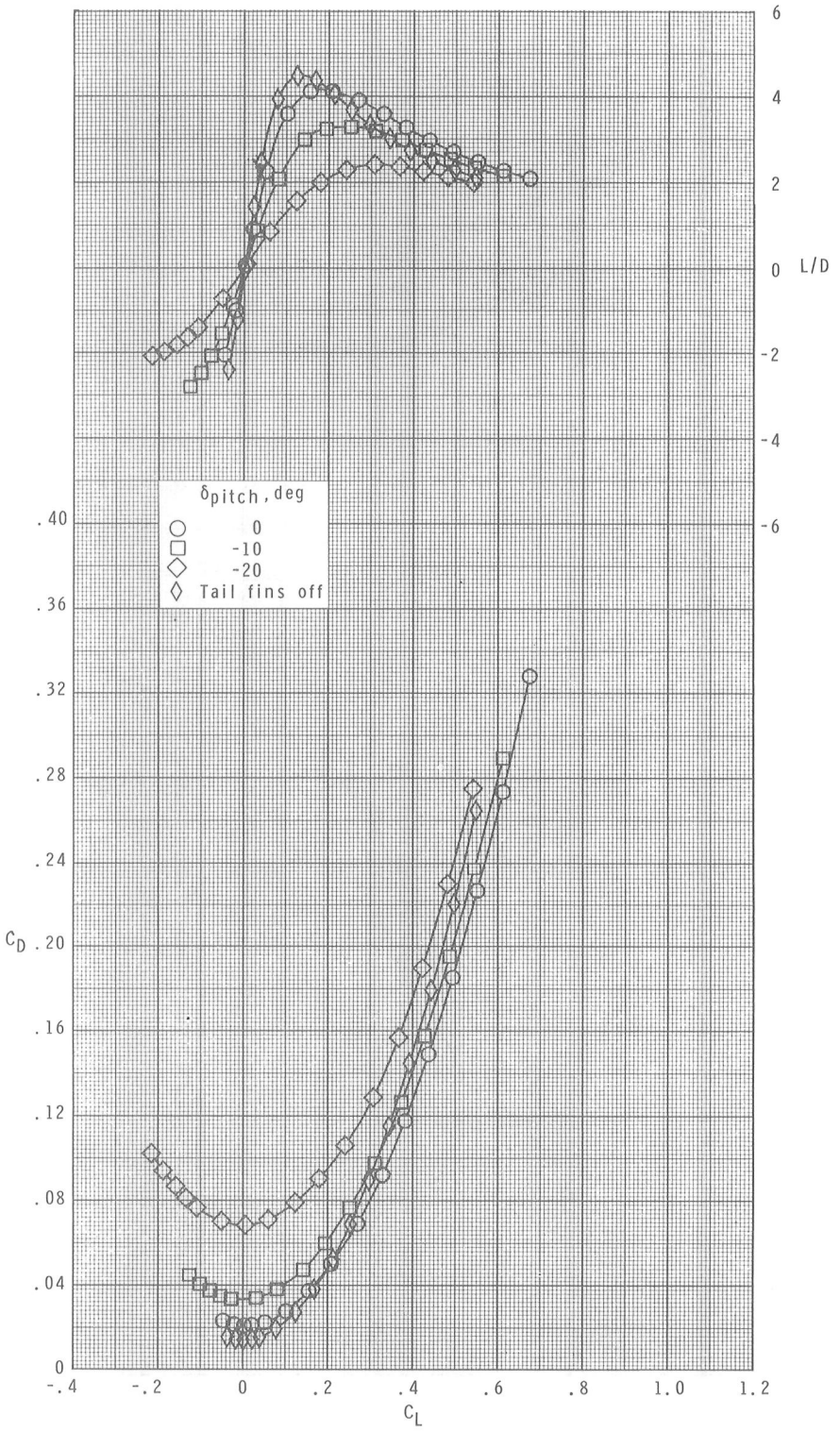

(d) Concluded.

Figure 10.- Concluded.

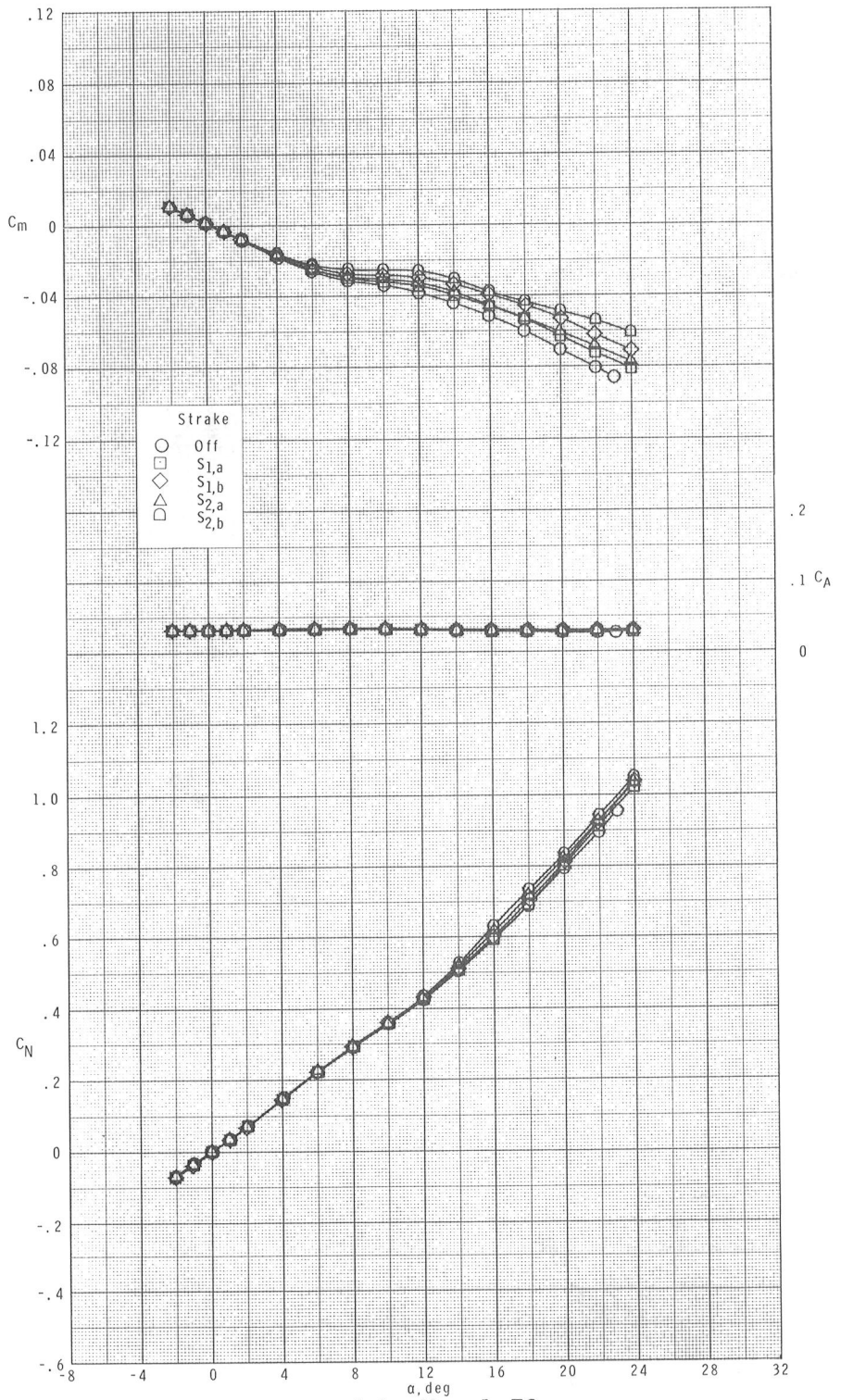

(a) M = 1.70.

Figure 11.- Effects of strake length and width on longitudinal aerodynamic characteristics of the centerline-aft-wing configuration for nose and nose-body strakes.

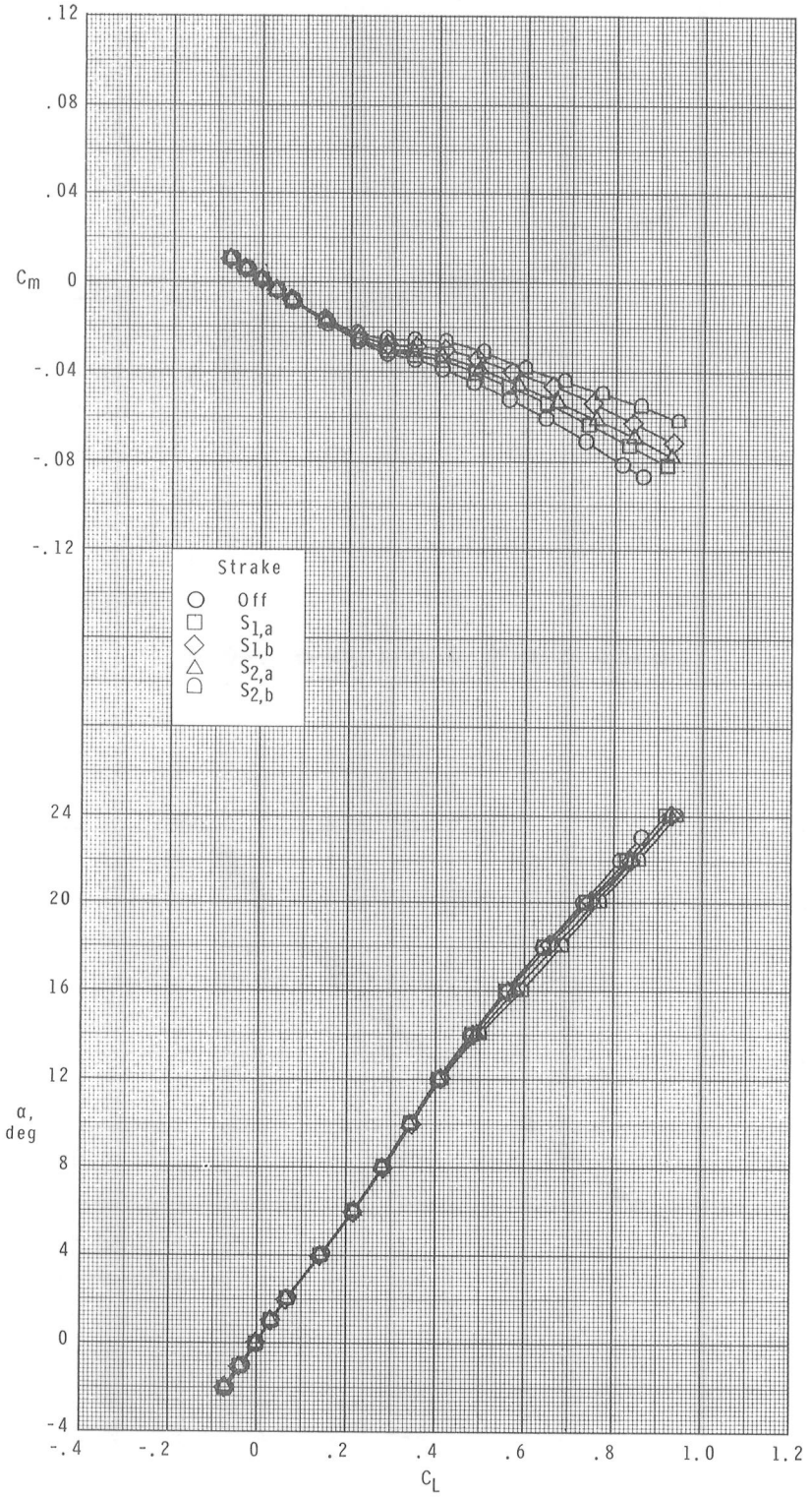

(a) Continued.

Figure 11.- Continued.

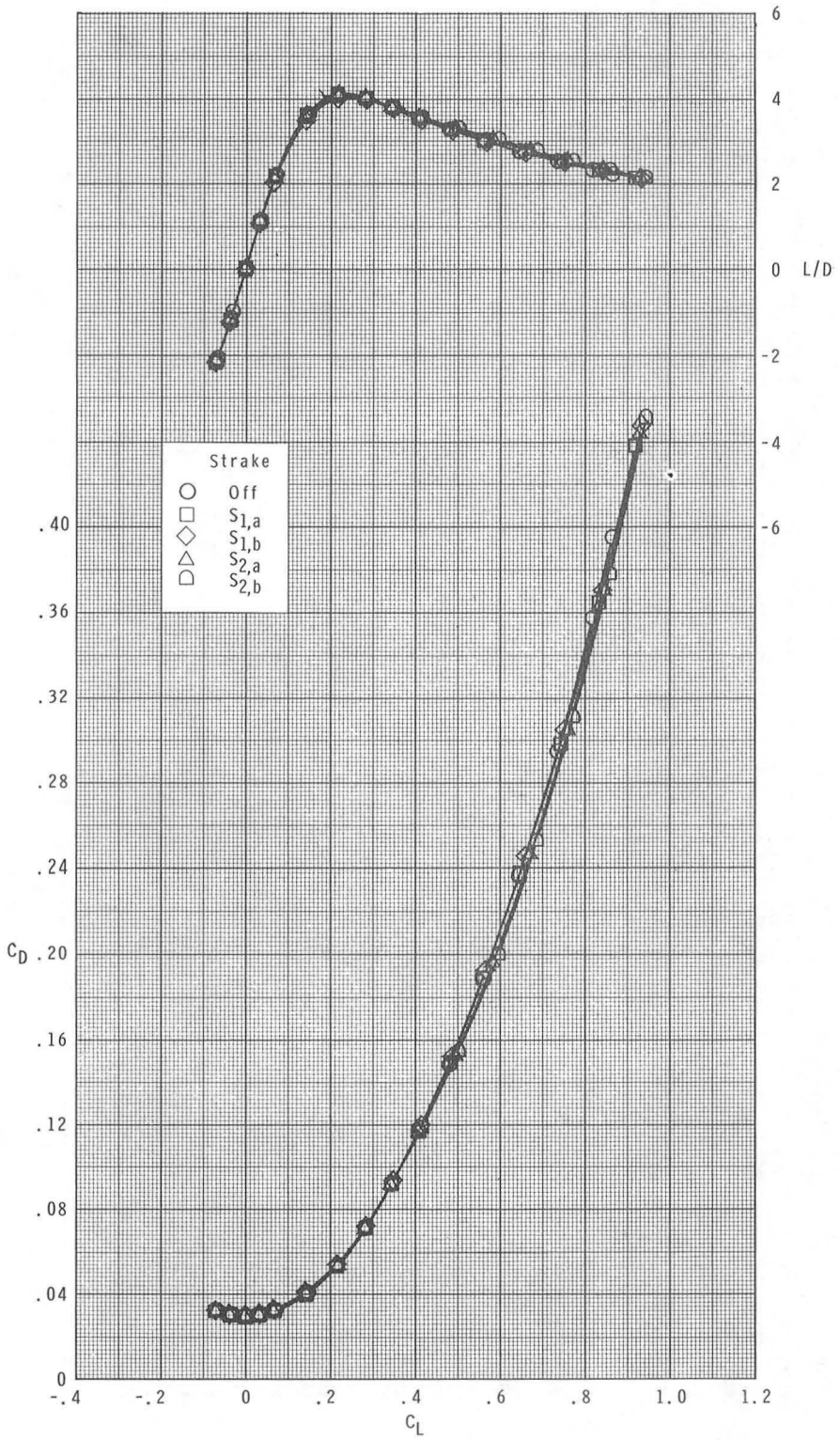

(a) Concluded.

Figure 11.- Continued.

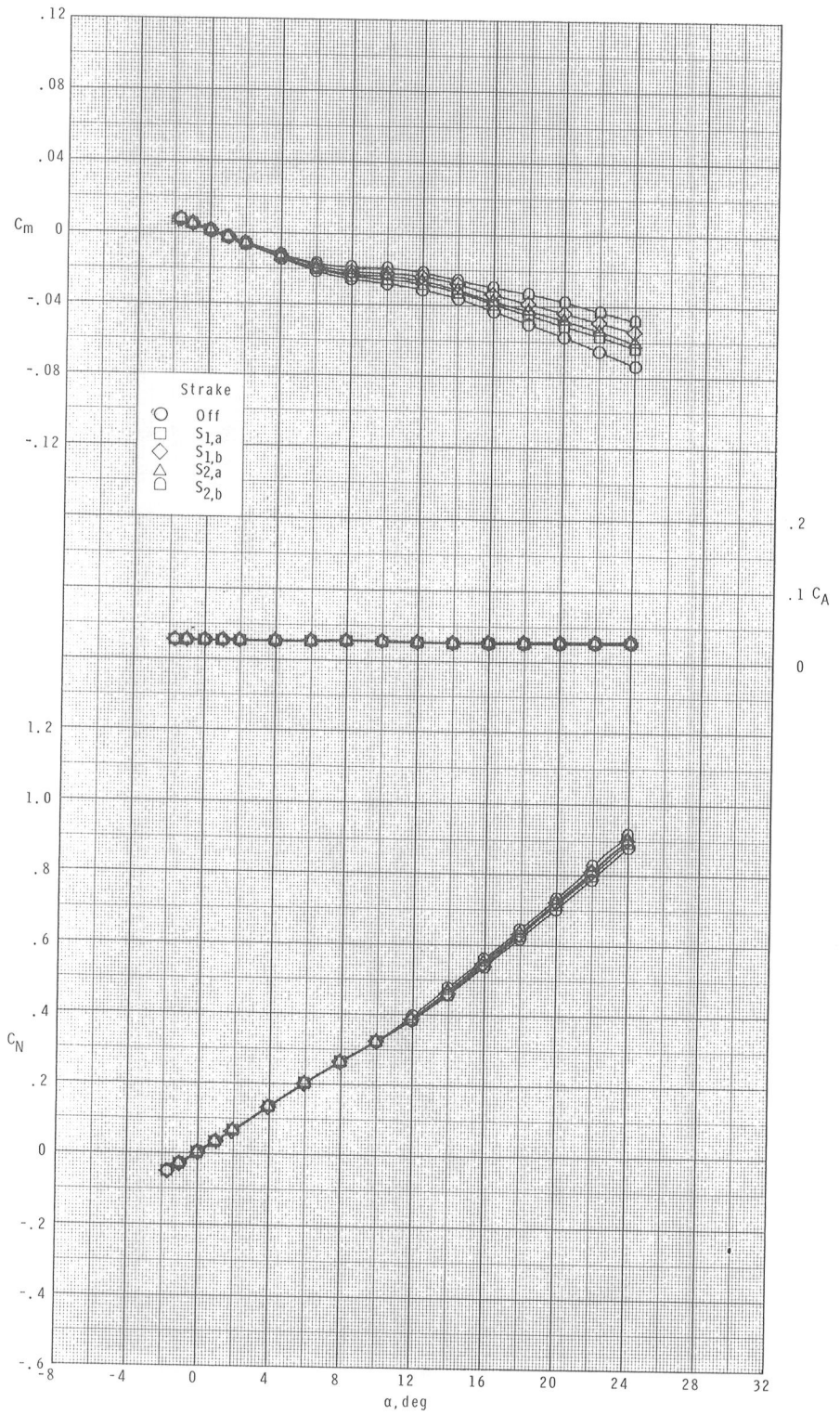

(b) M = 2.16.

Figure 11.- Continued.

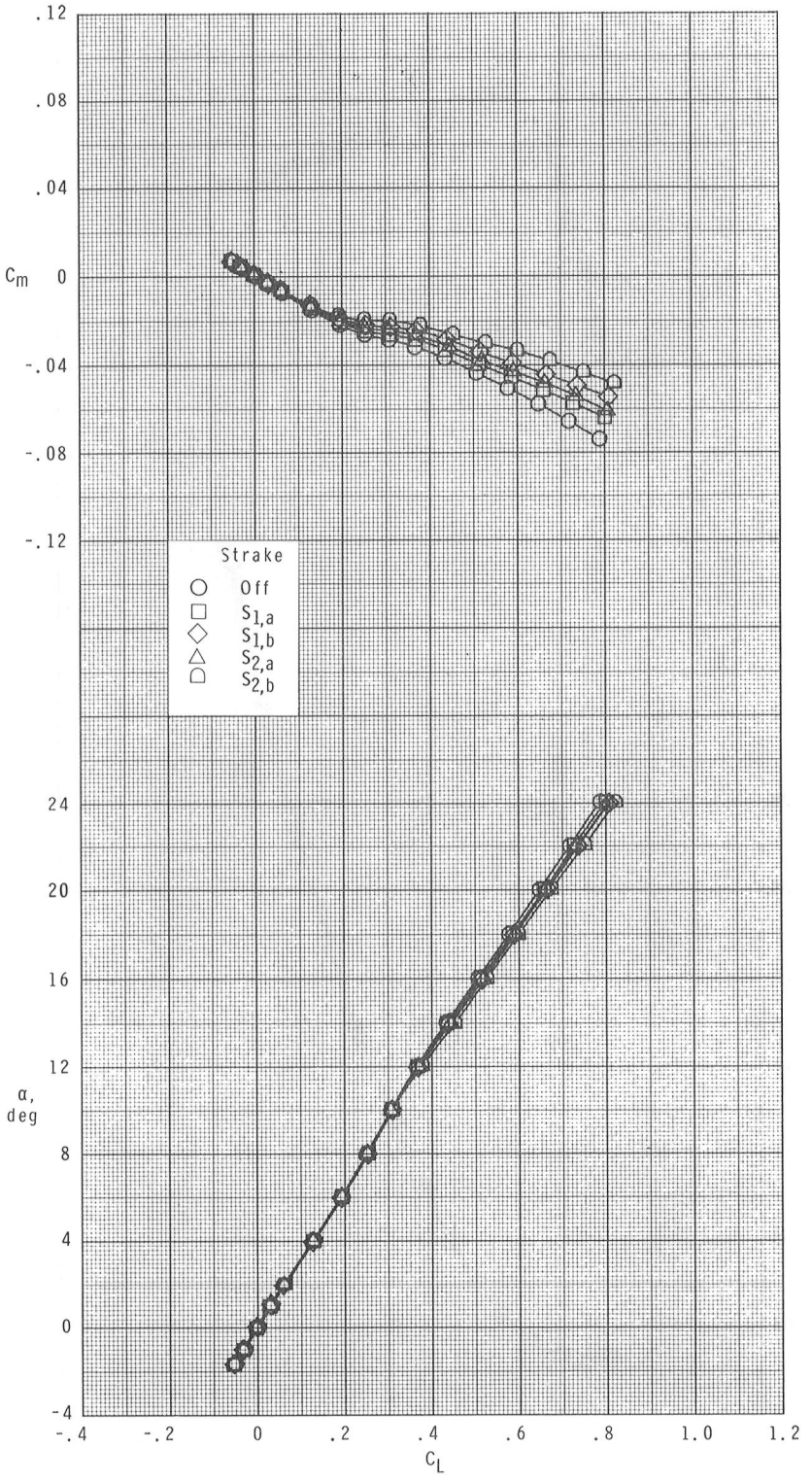

(b) Continued.

Figure 11.- Continued.

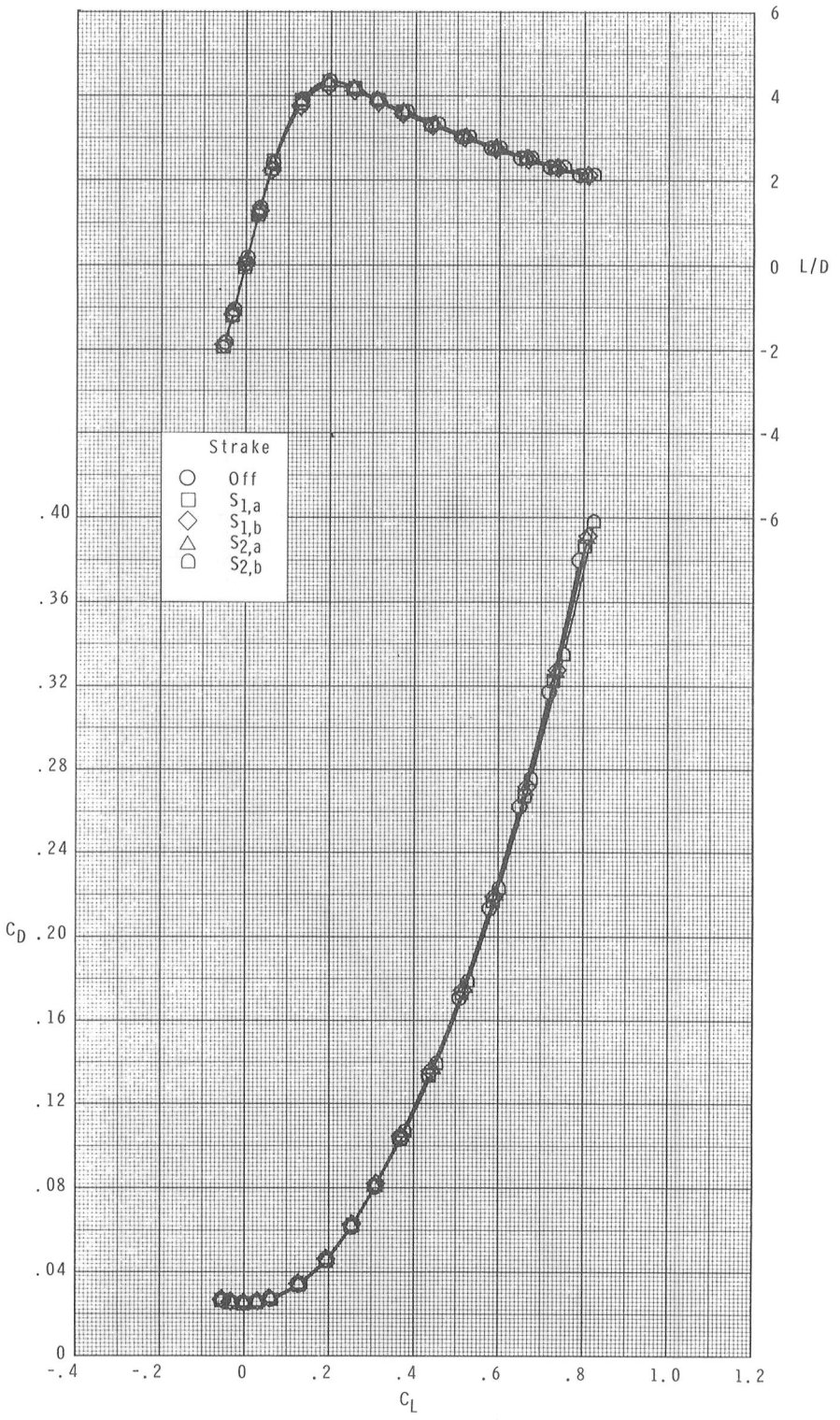

(b) Concluded.

Figure 11.- Continued.

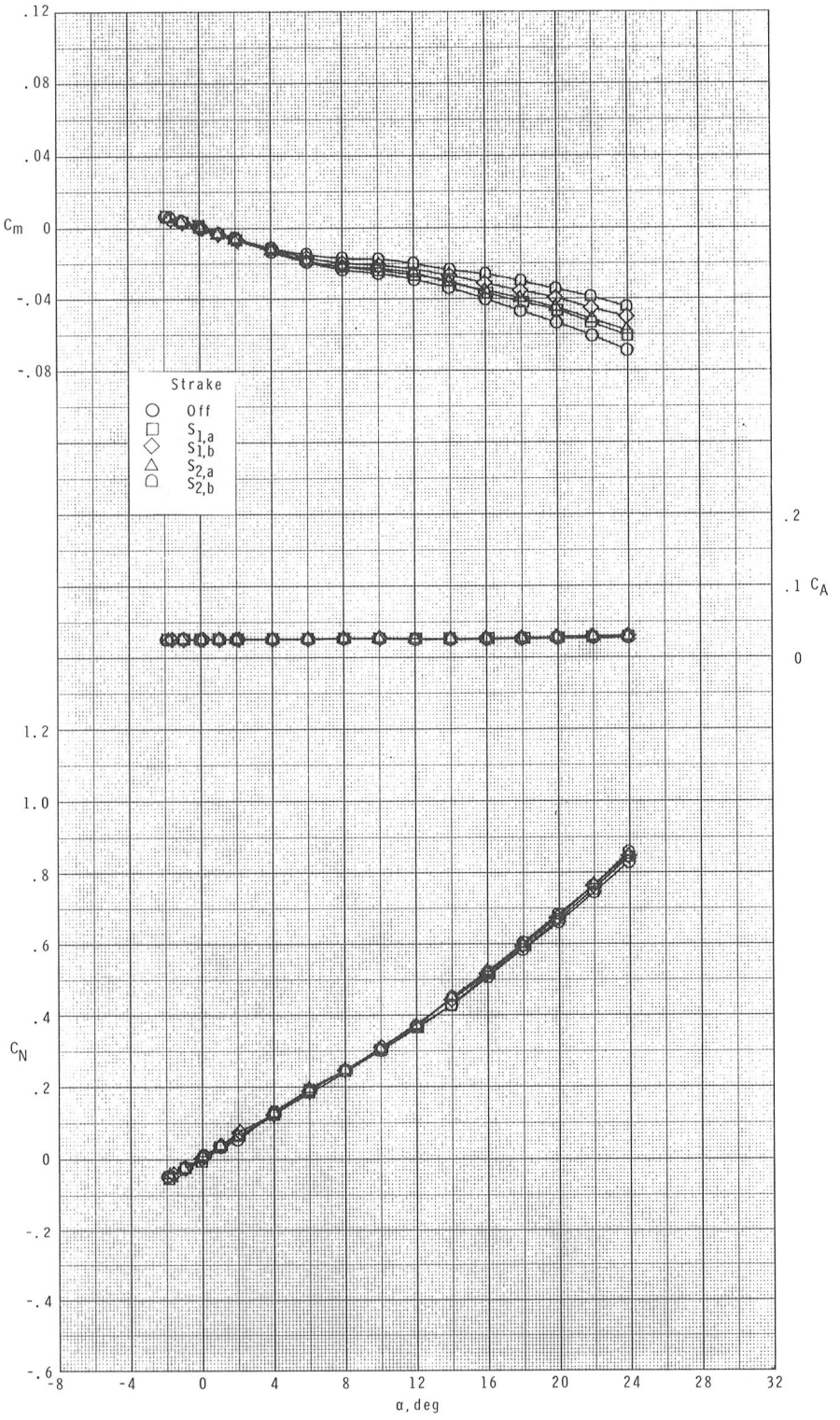

(c) M = 2.36.

Figure 11.- Continued.

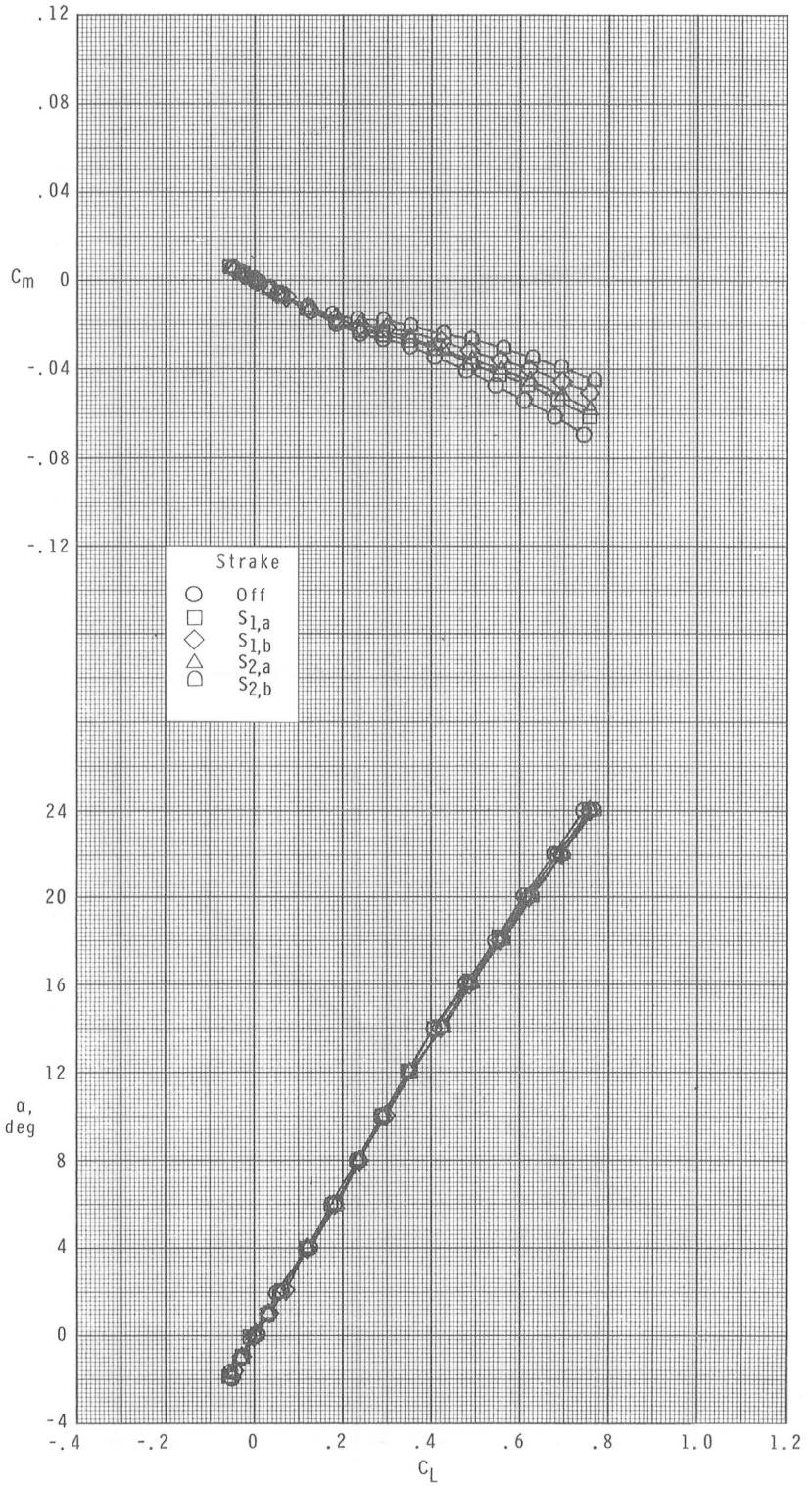

(c) Continued.

Figure 11.- Continued.

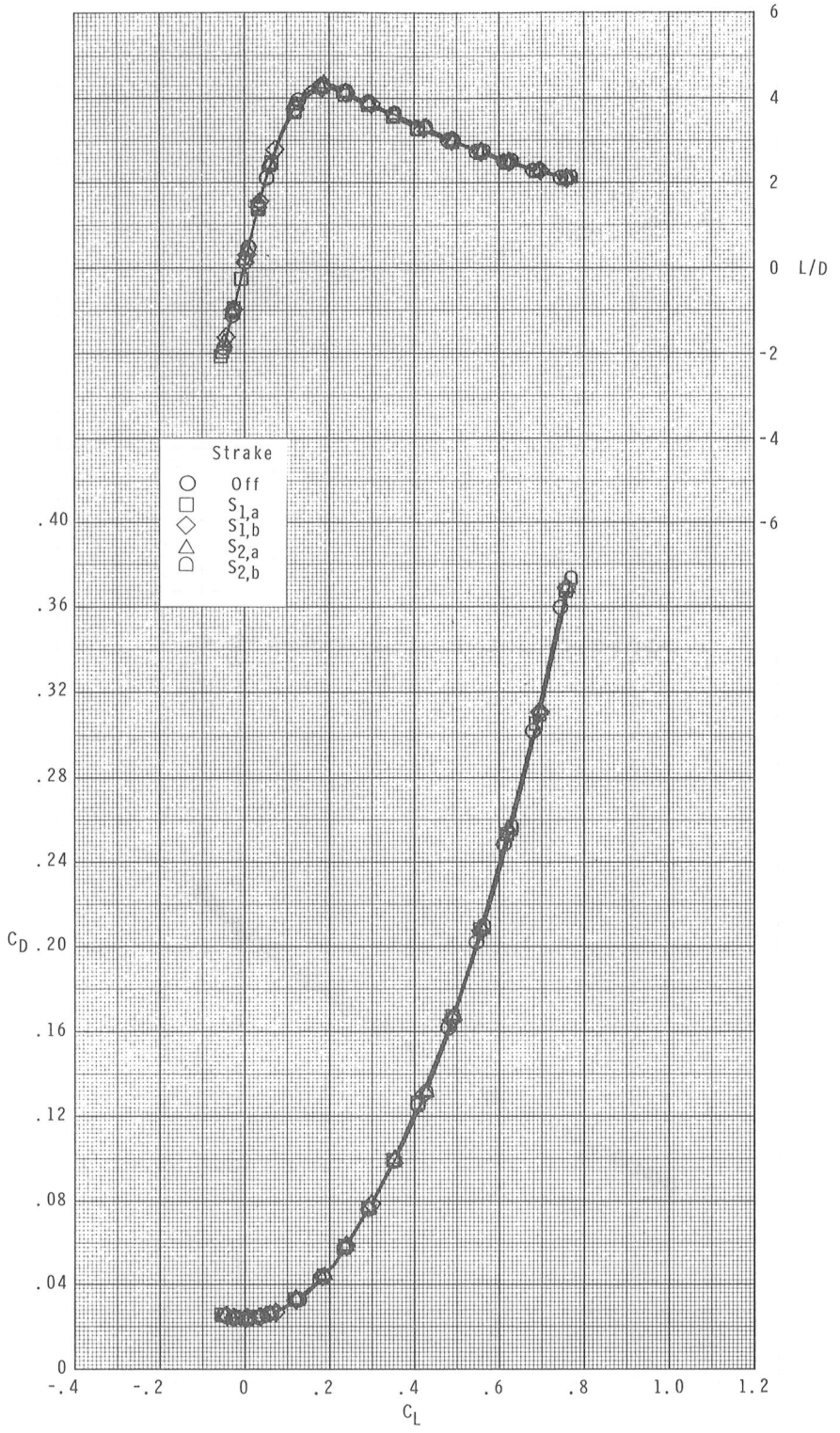

(c) Concluded.

Figure 11.- Continued.

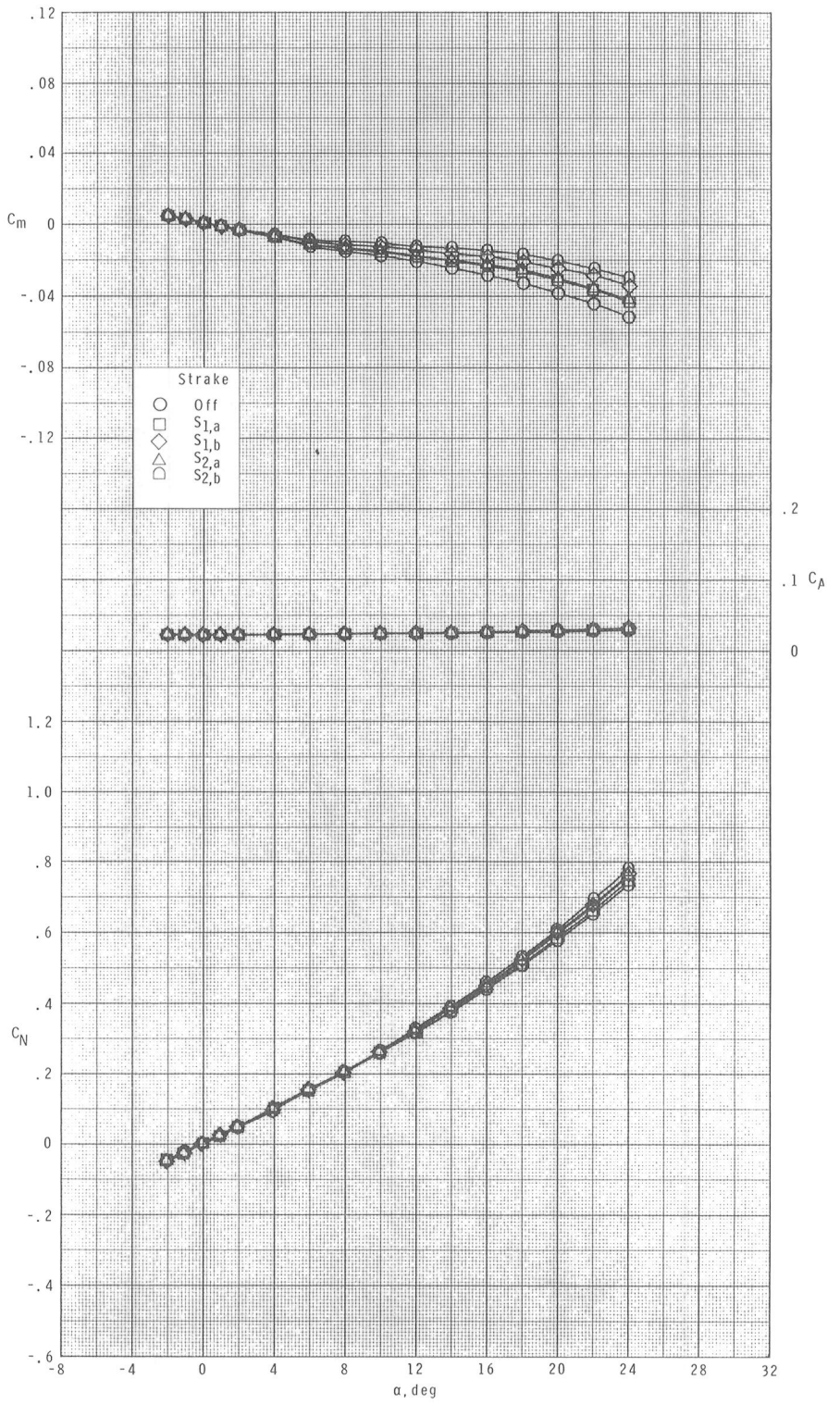

(d) M = 2.86.

Figure 11.- Continued.

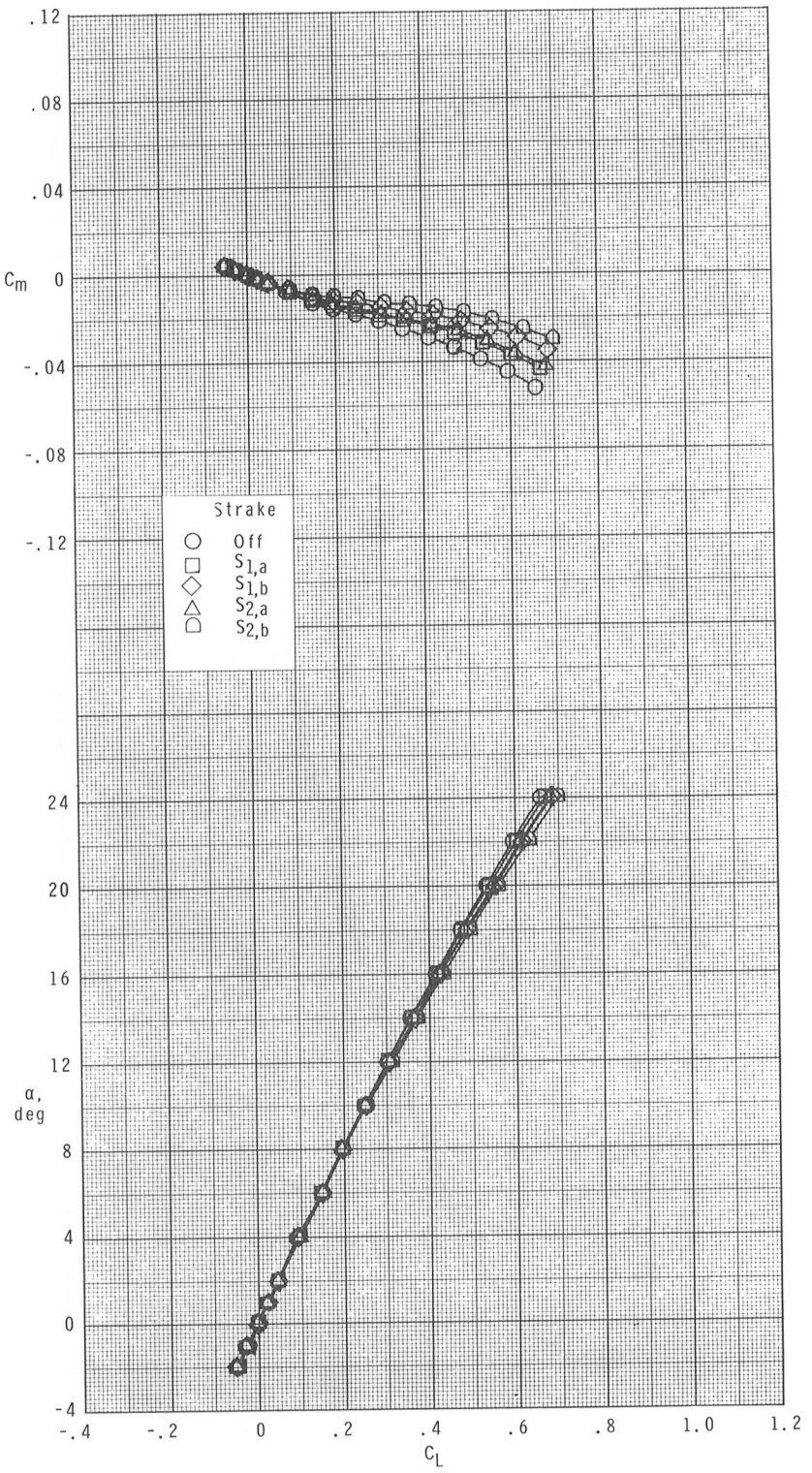

(d) Continued.

Figure 11.- Continued.

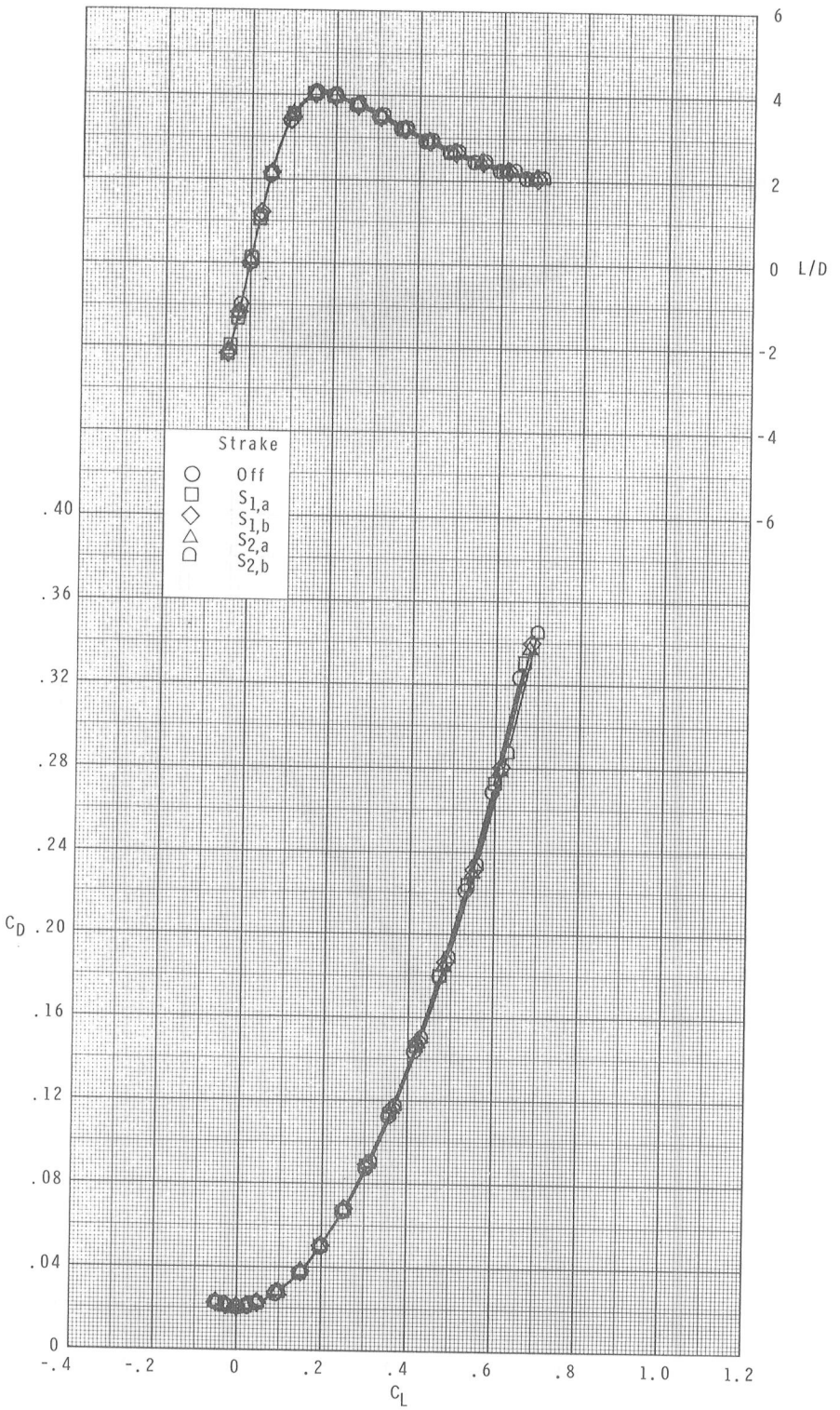

(d) Concluded.

Figure 11.- Concluded.

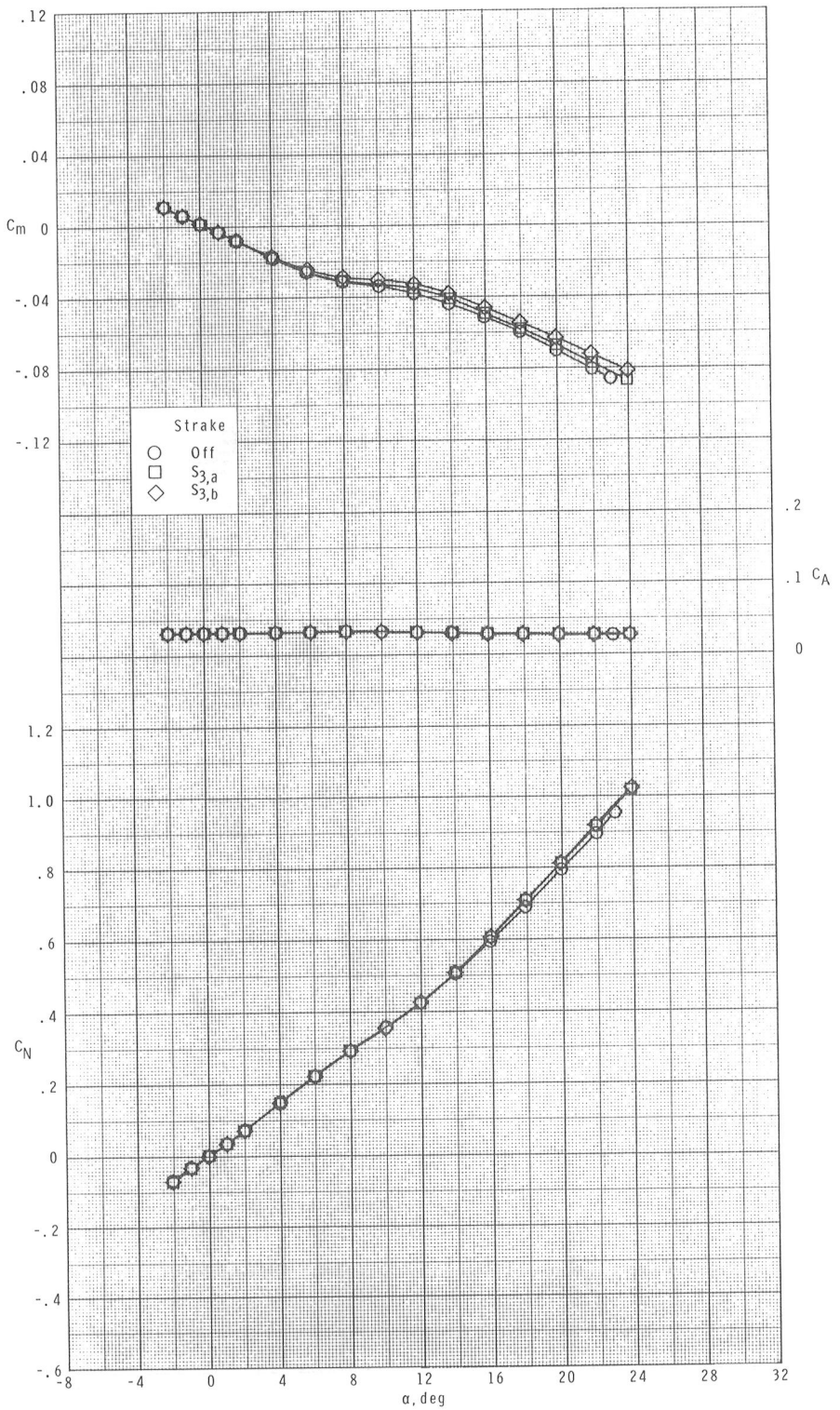

(a) M = 1.70.

Figure 12.- Effects of strake length and width on longitudinal aerodynamic characteristics of the centerline-aft-wing configuration for body strake.

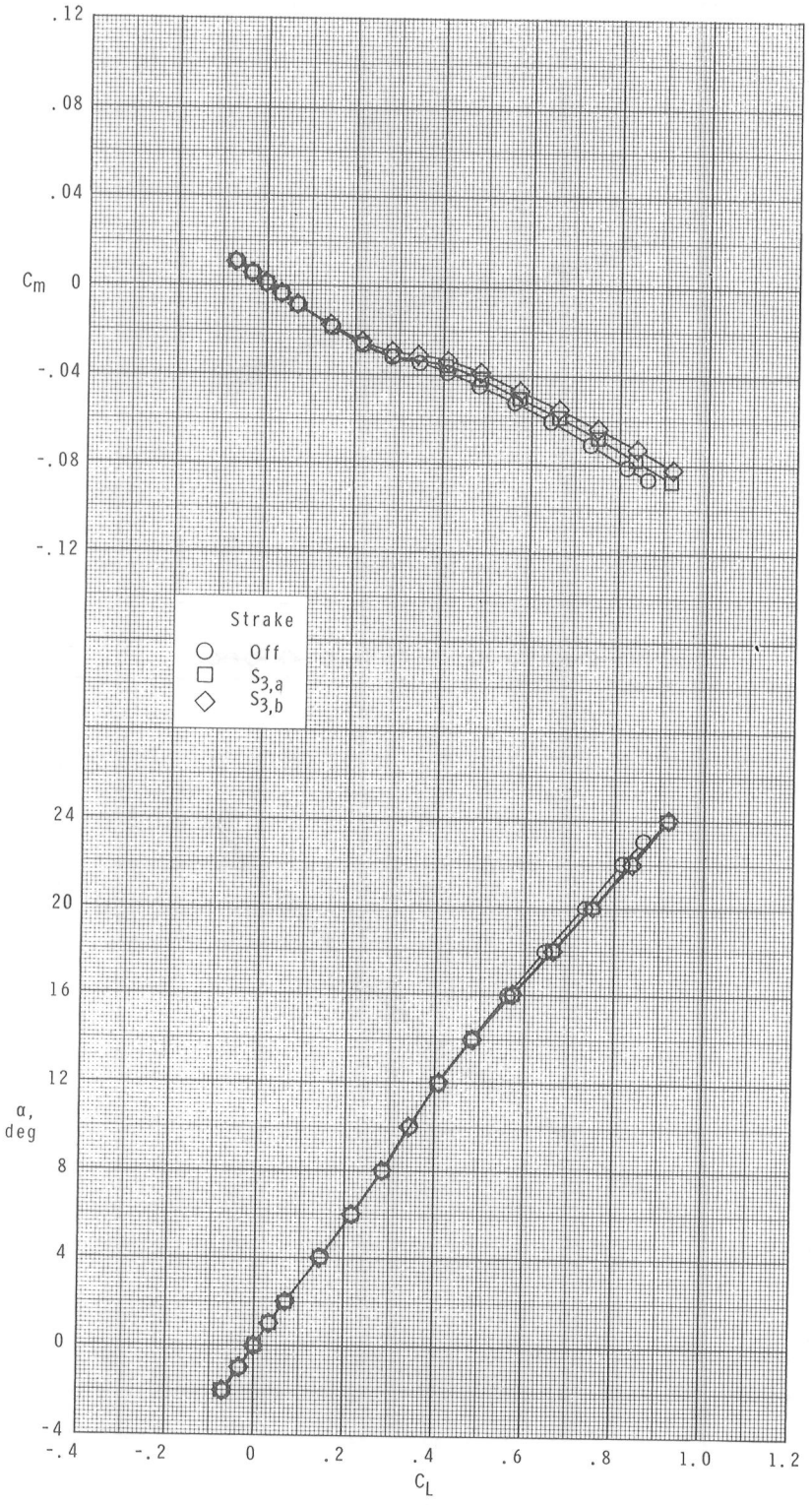

(a) Continued.

Figure 12.- Continued.

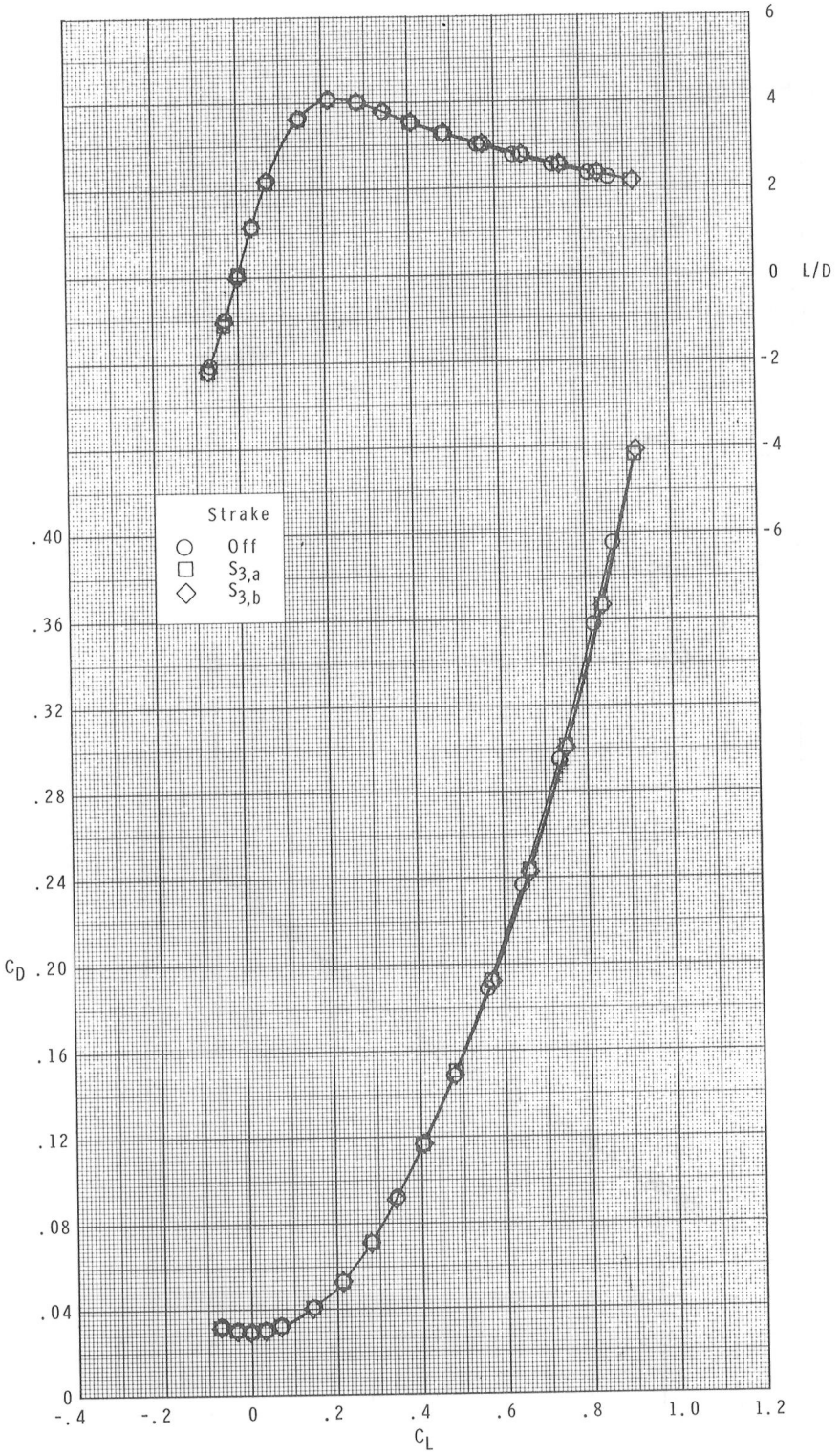

(a) Concluded.

Figure 12.- Continued.

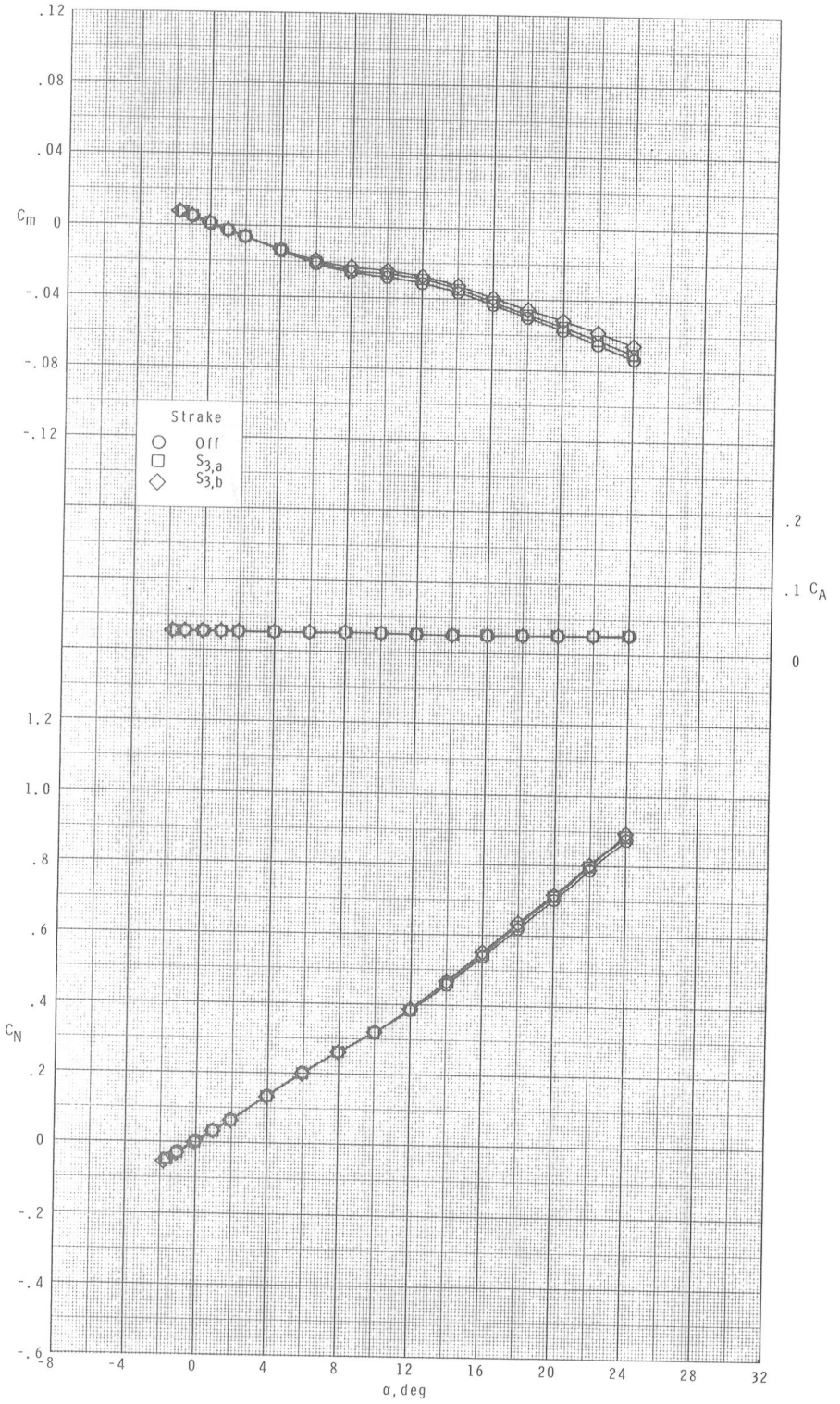

(b) M = 2.16.

Figure 12.- Continued.

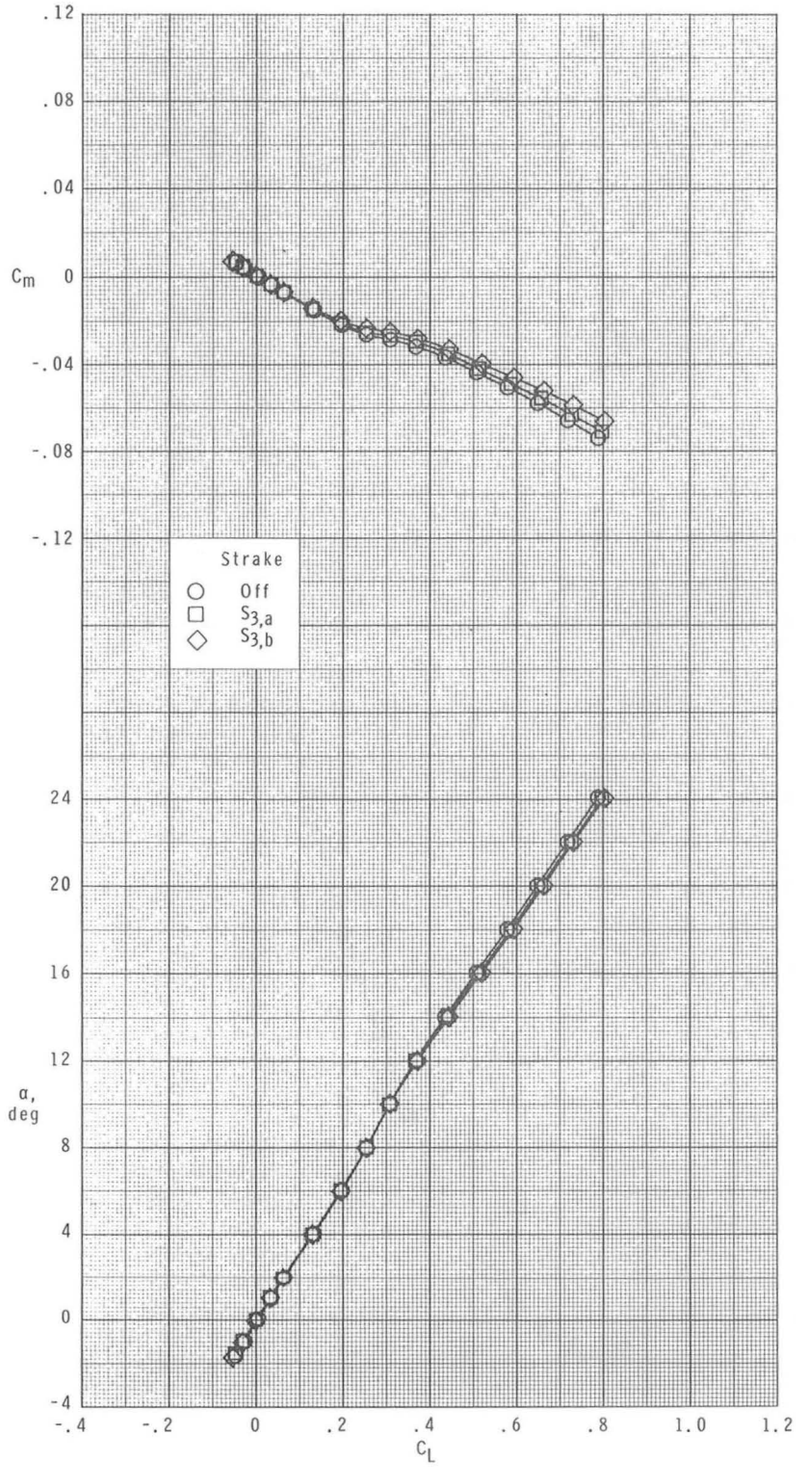

(b) Continued.

Figure 12.- Continued.

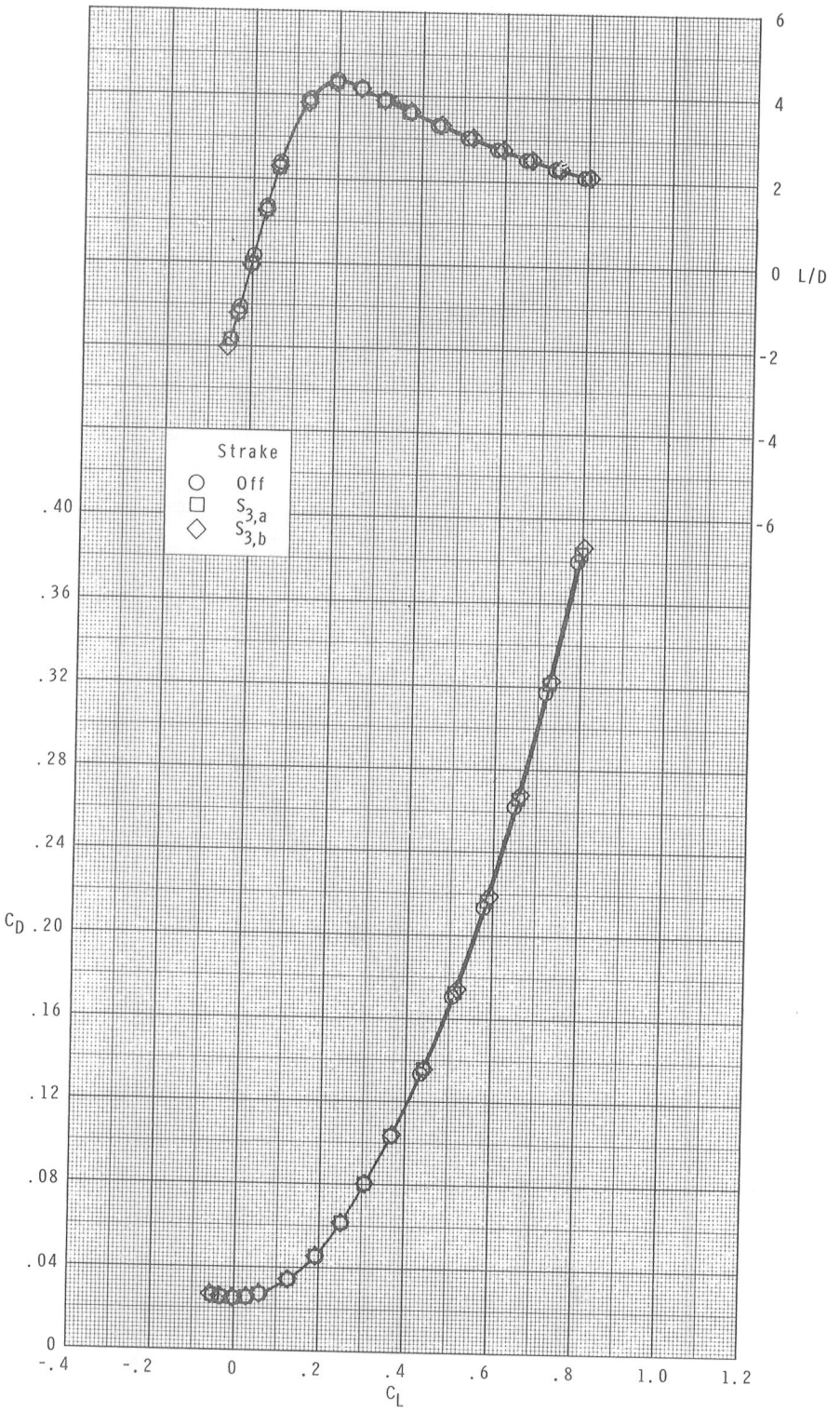

(b) Concluded.

Figure 12.- Continued.

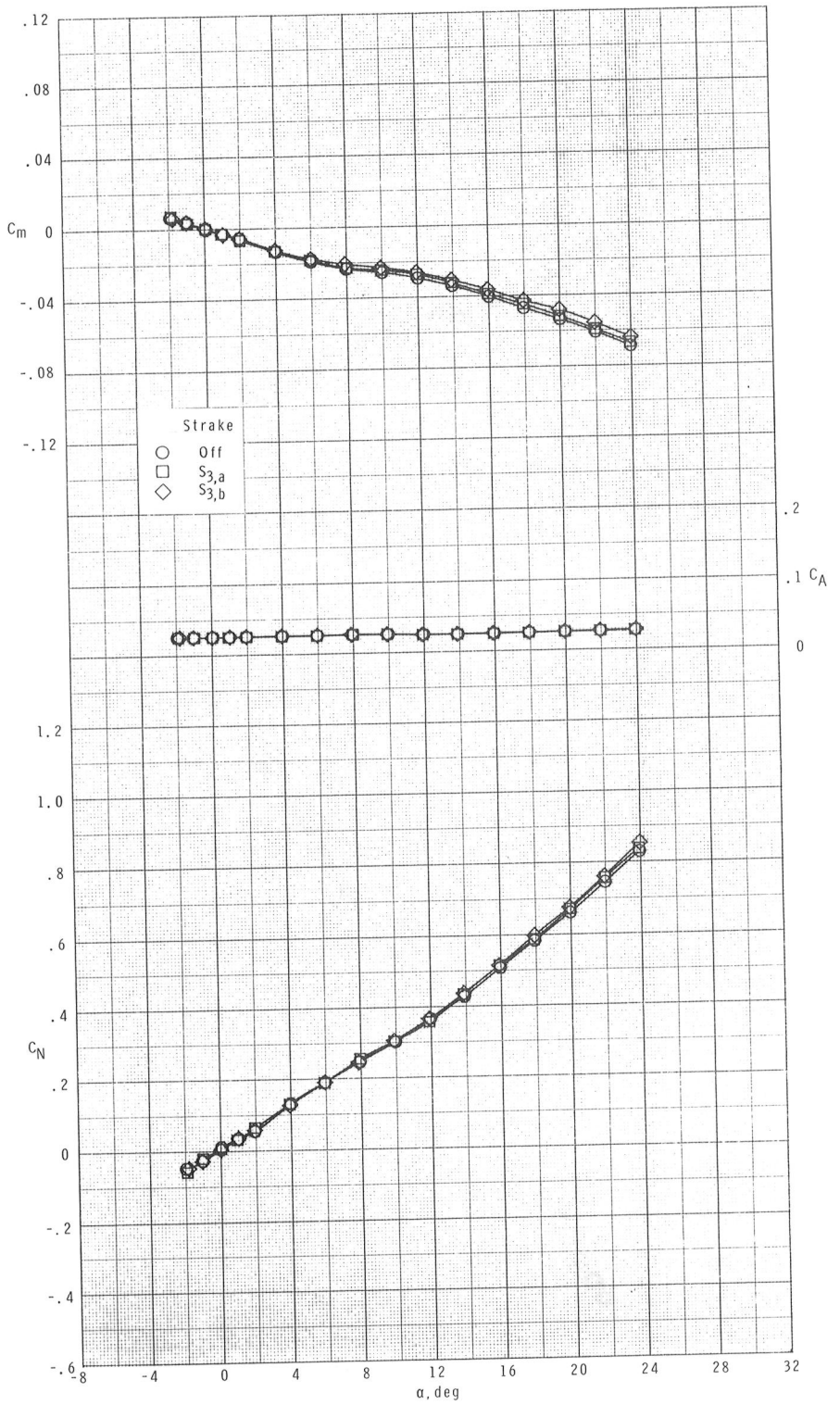

(c) M = 2.36.

Figure 12.- Continued.

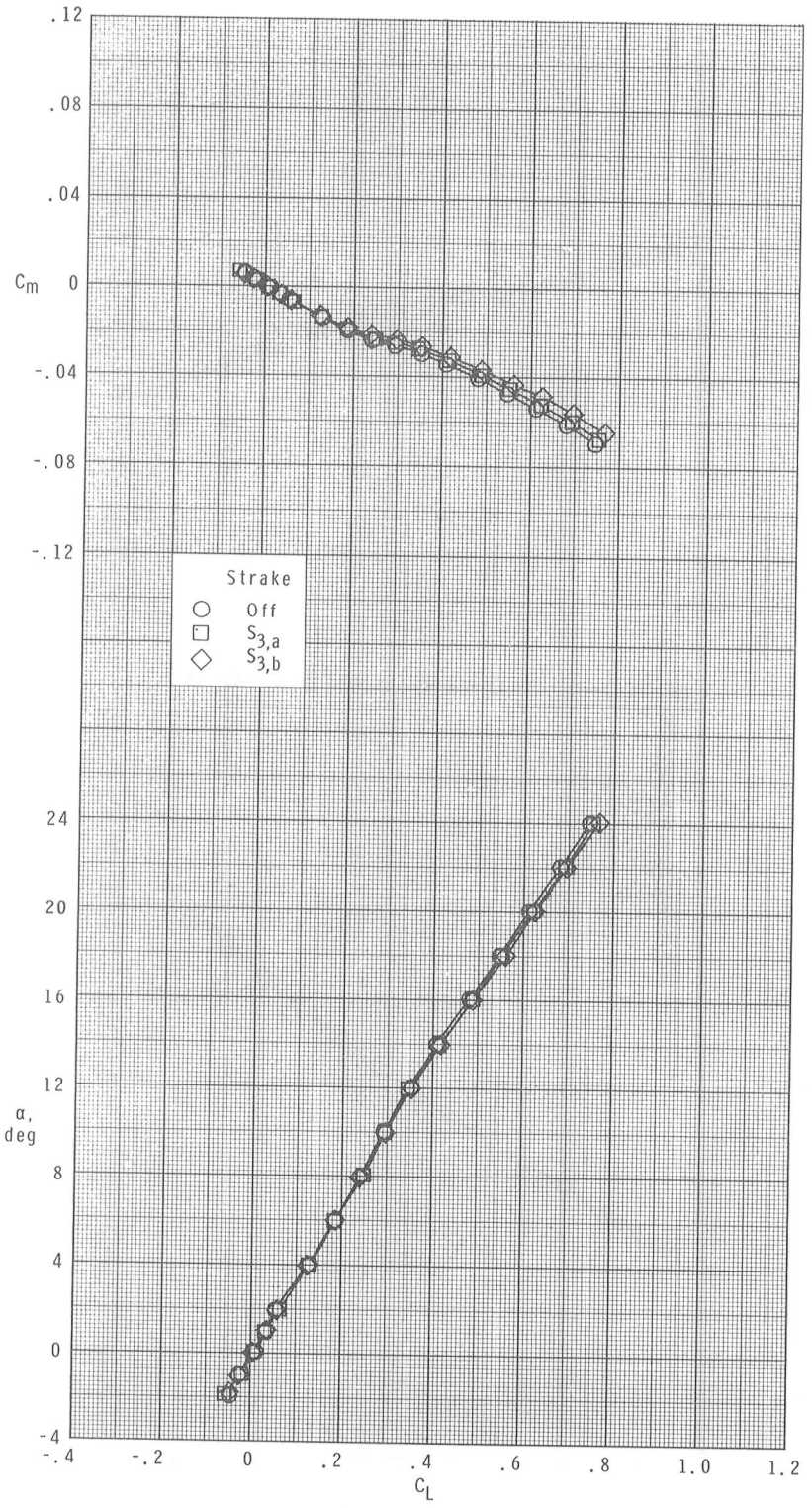

(c) Continued.

Figure 12.- Continued.

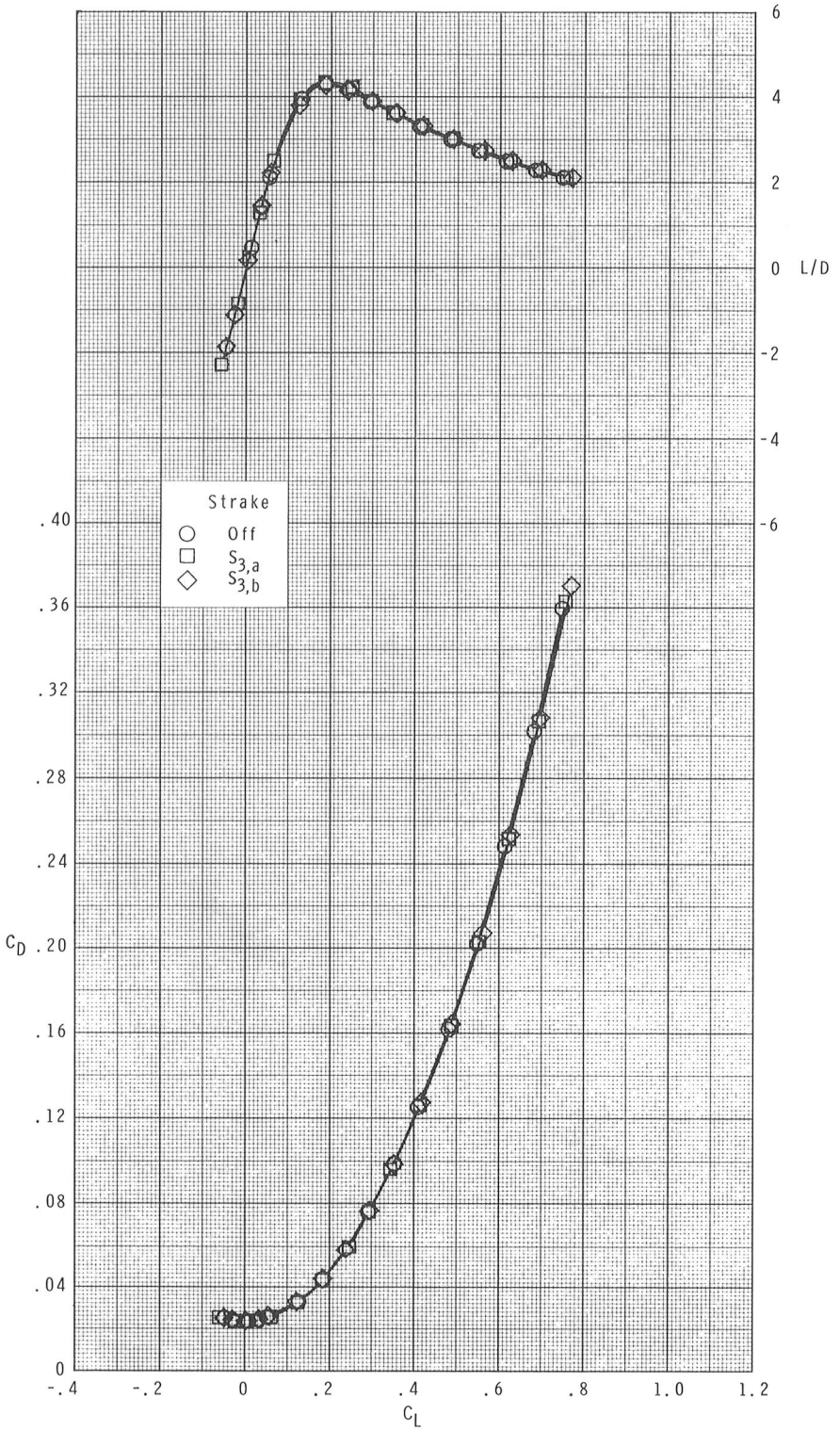

(c) Concluded.

Figure 12.- Continued.

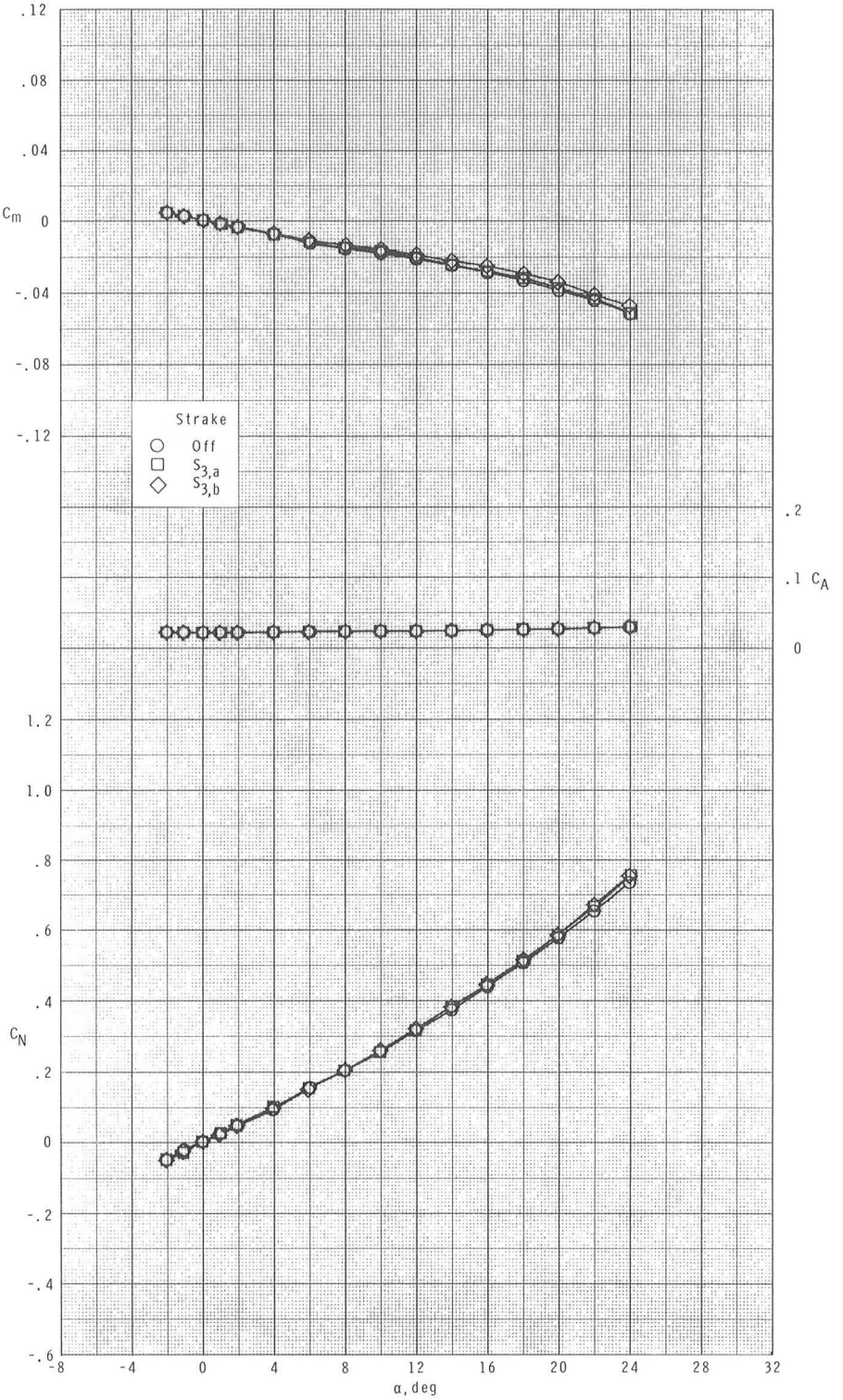

(d) M = 2.86.

Figure 12.- Continued.

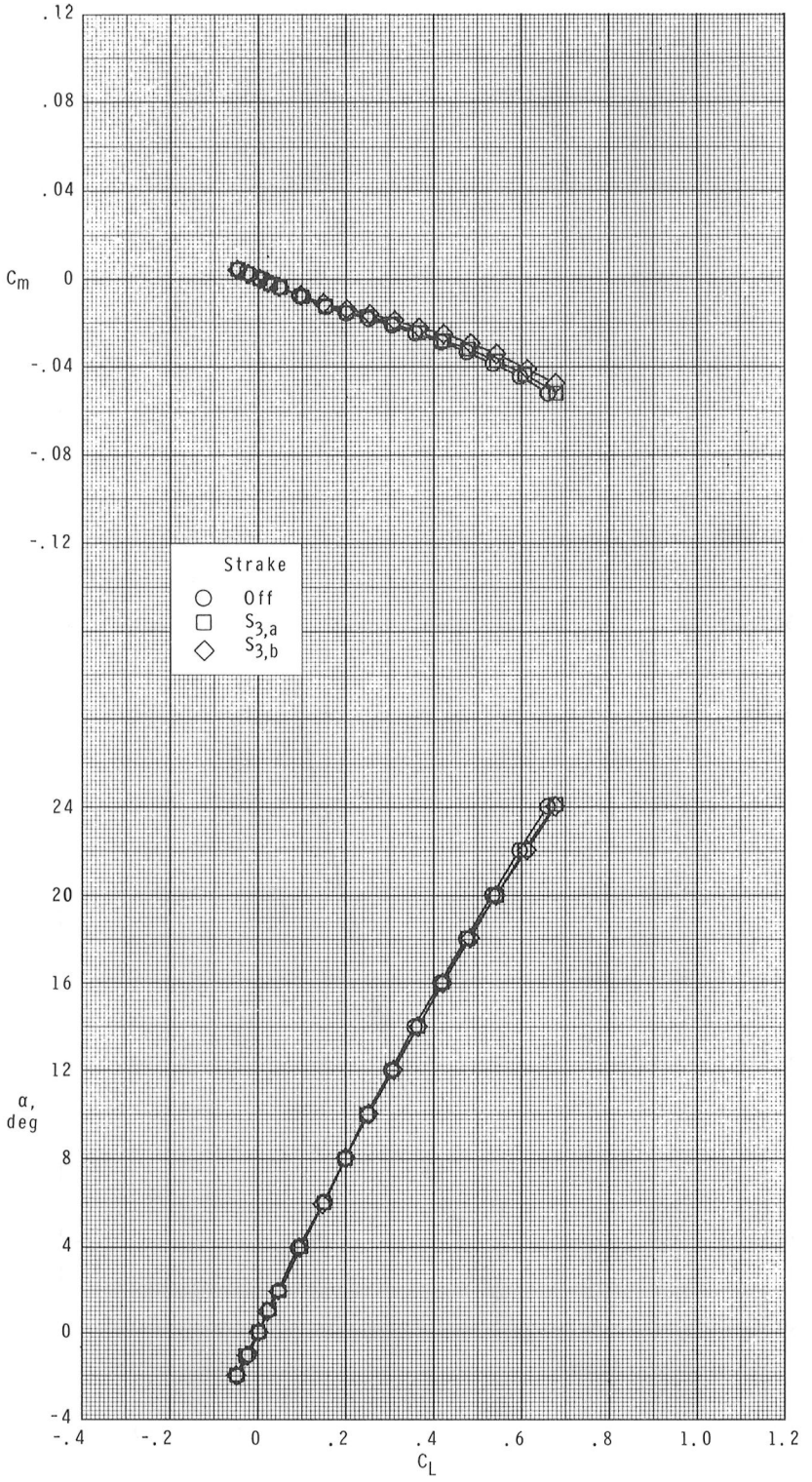

(d) Continued.

Figure 12.- Continued.

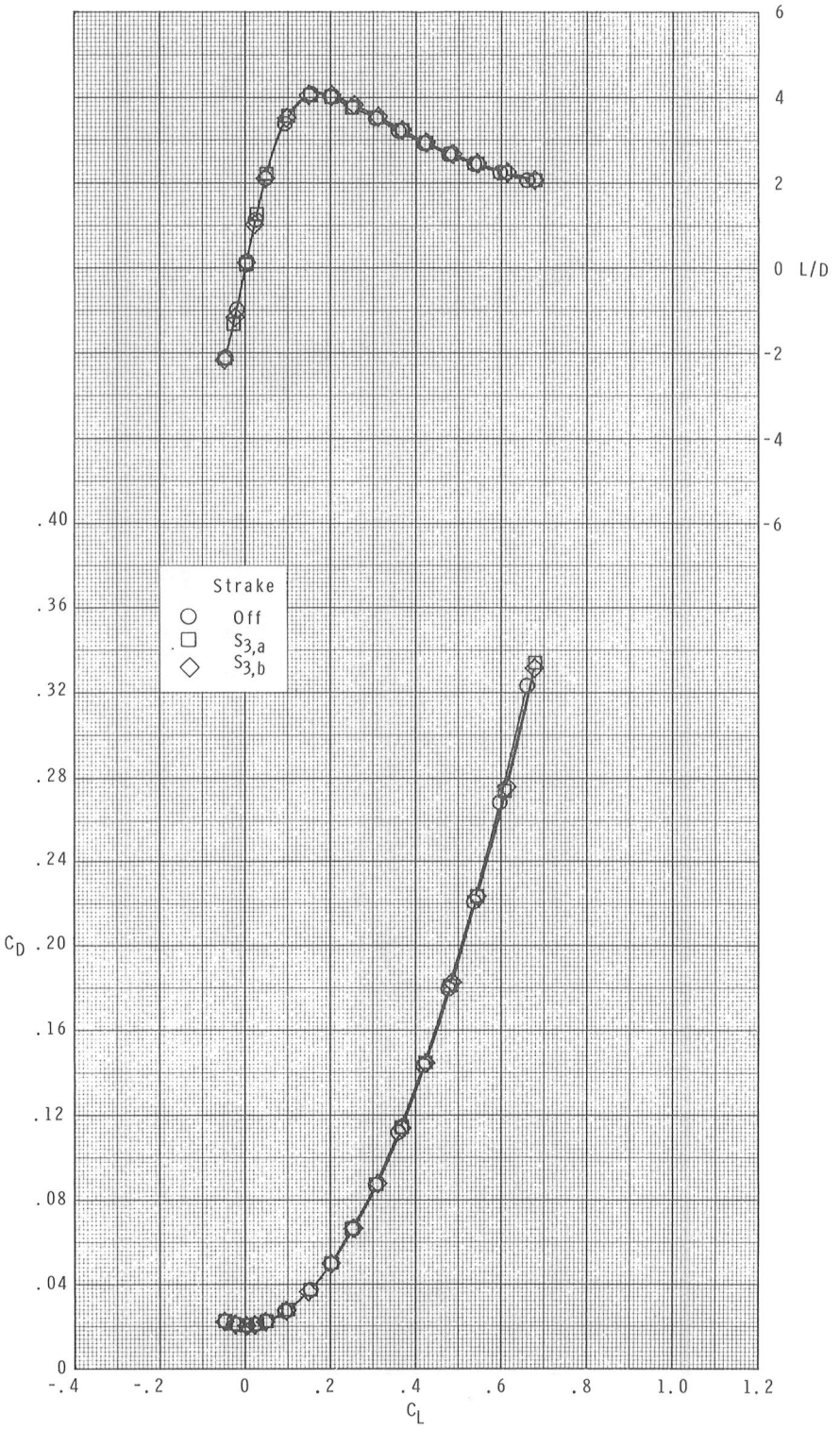

(d) Concluded.

Figure 12.- Concluded.

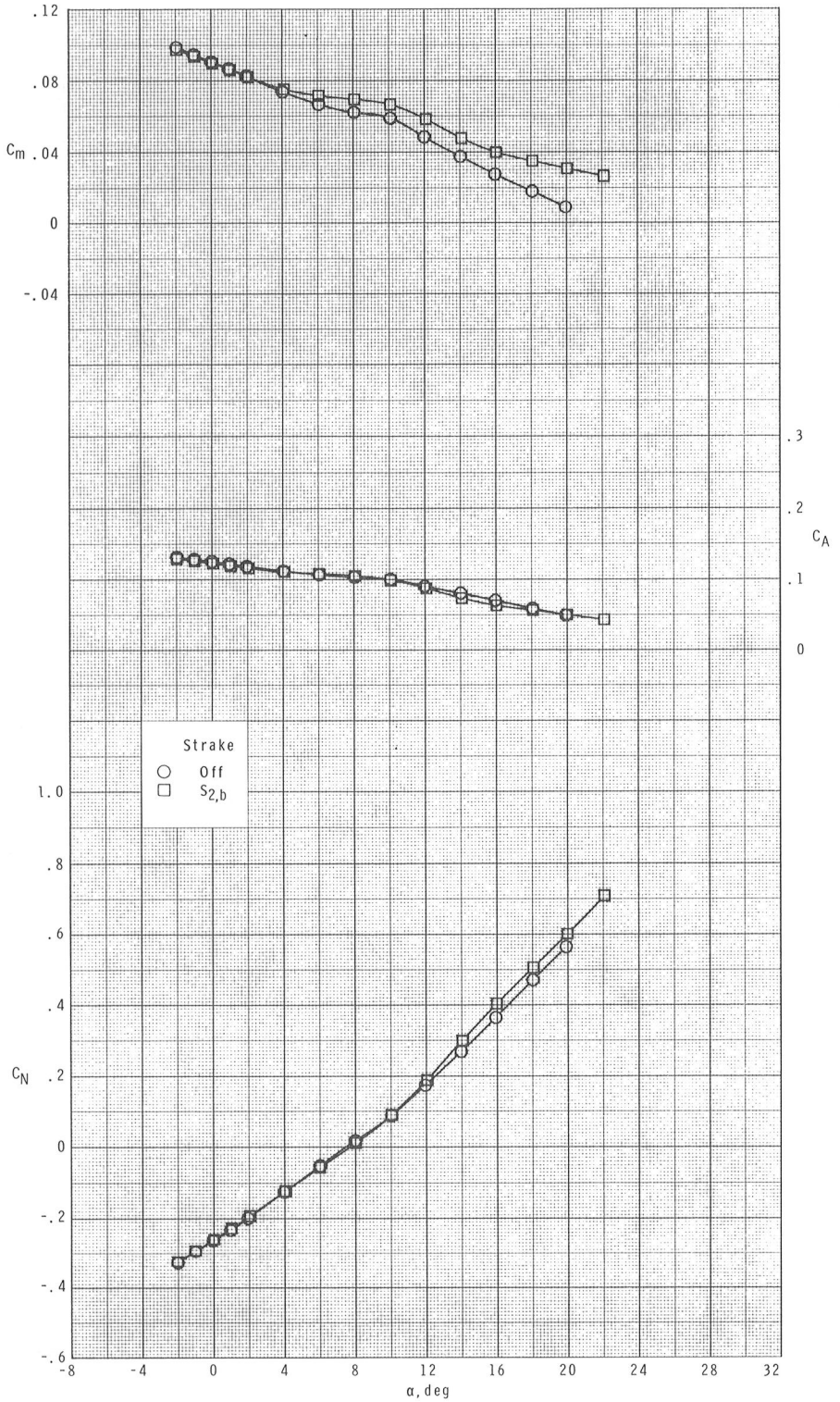

(a) M = 1.70.

Figure 13.- Effects of nose-body strake on pitch-control characteristics of the centerline-aft-wing configuration. $\delta_{pitch} = -20^{o}$.

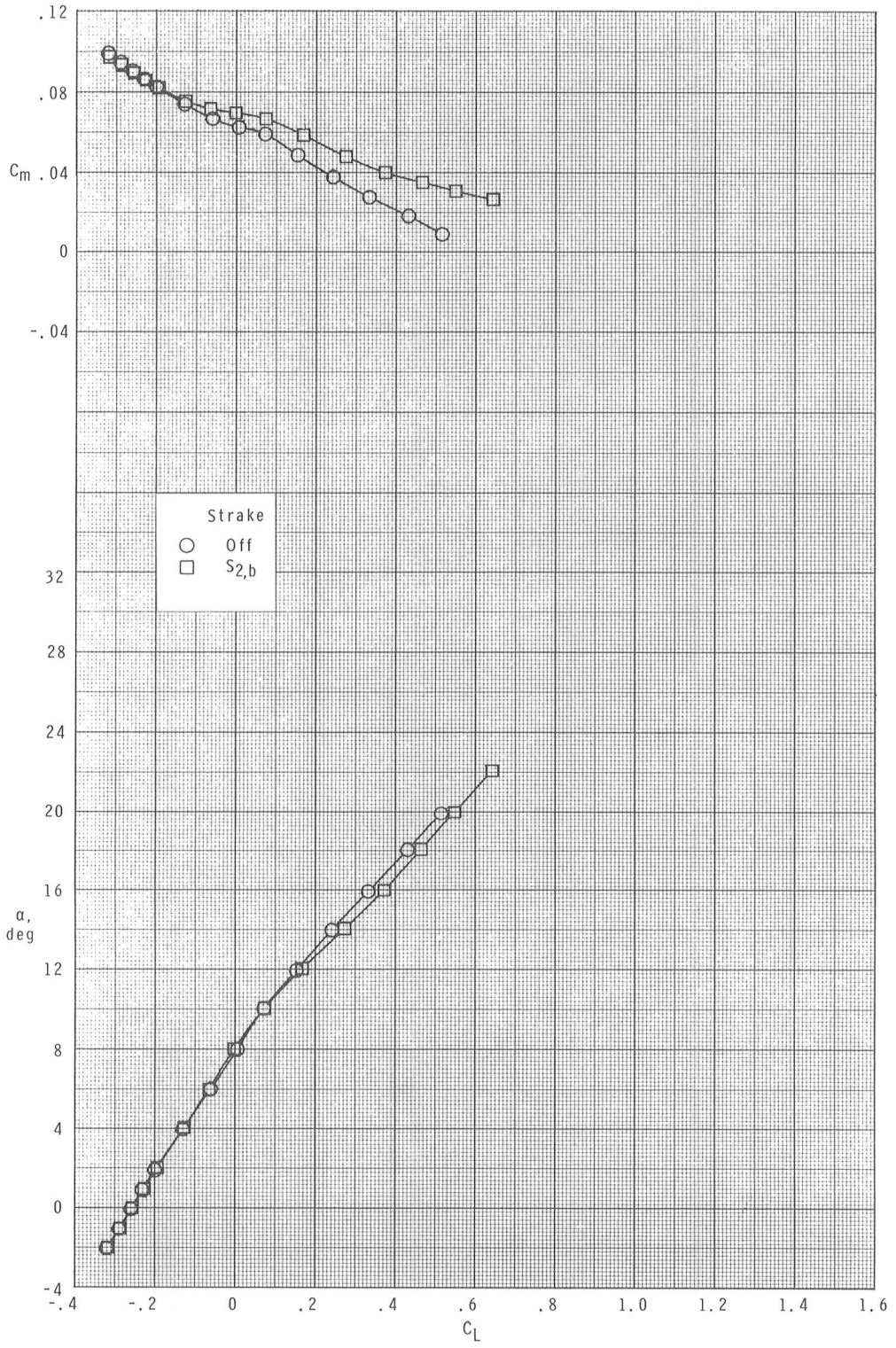

(a) Continued.

Figure 13.- Continued.

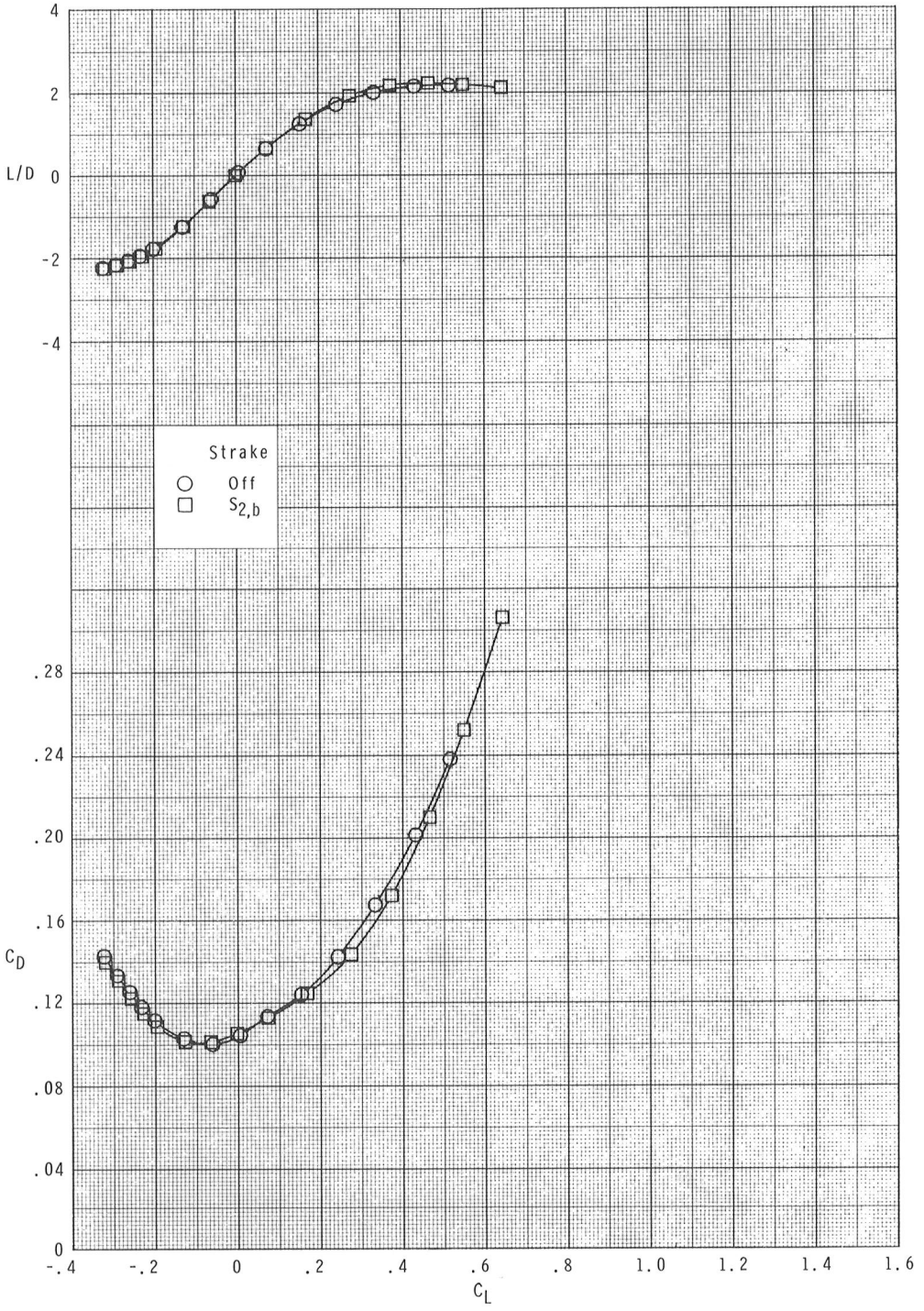

(a) Concluded.

Figure 13.- Continued.

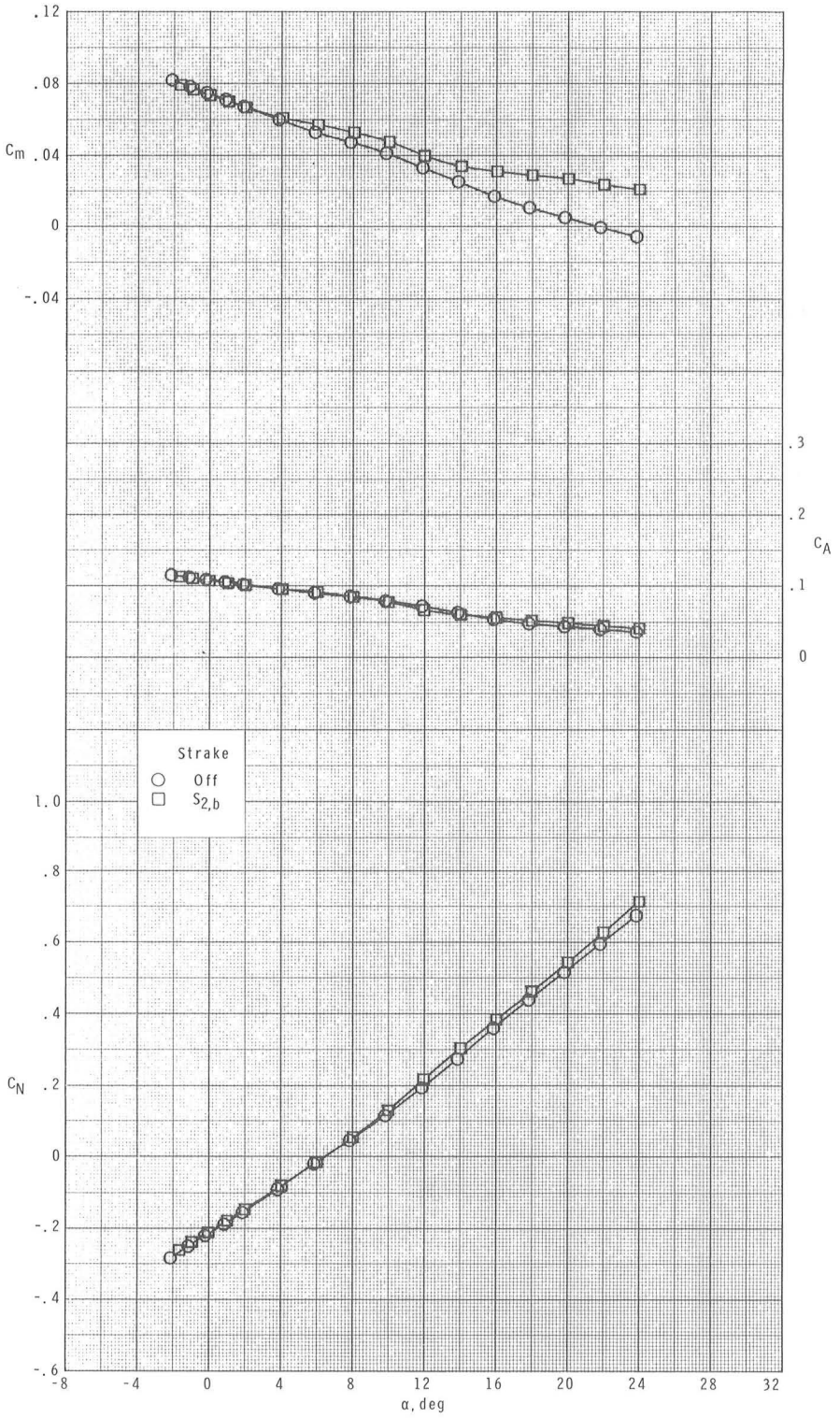

(b) M = 2.16.

Figure 13.- Continued.

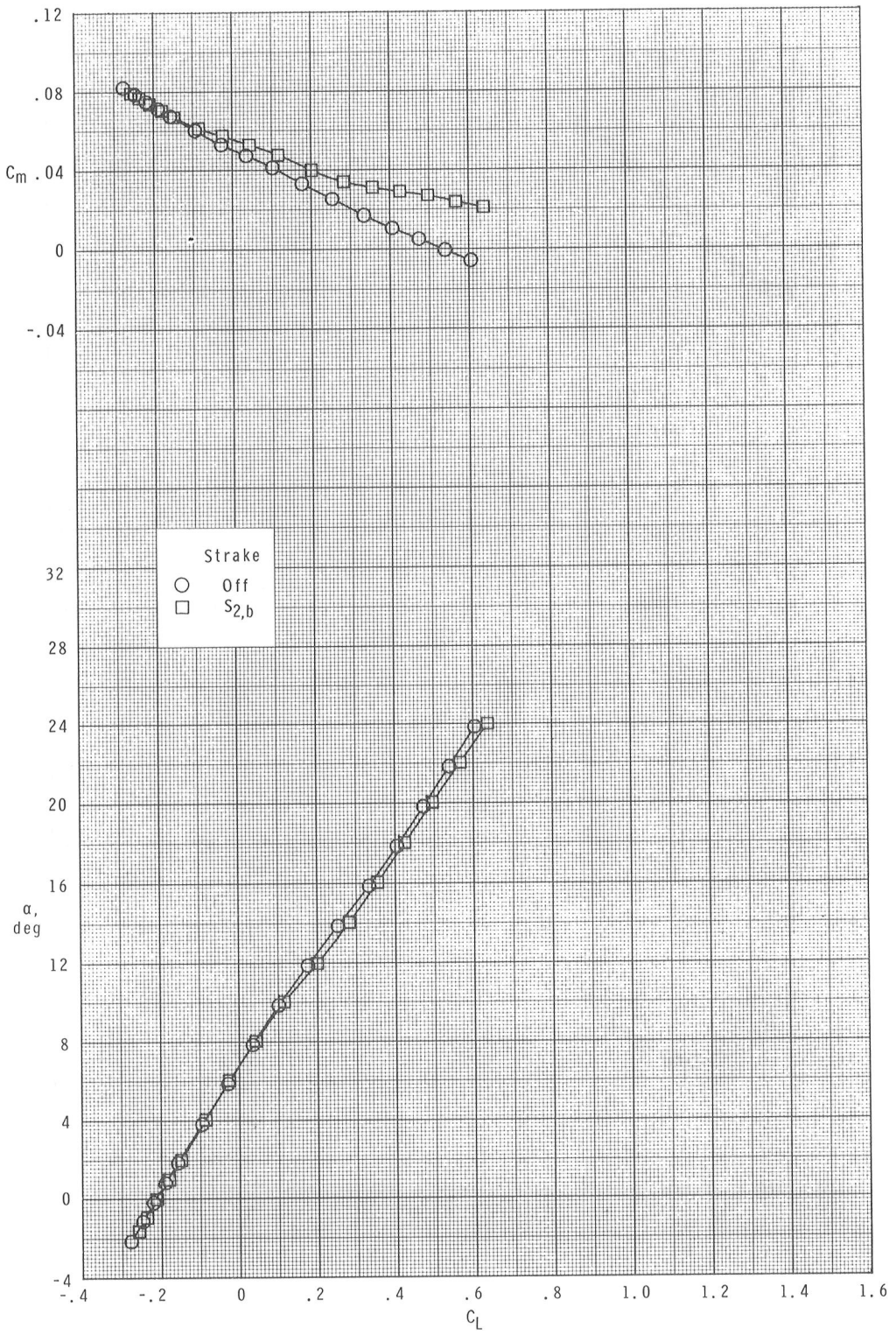

(b) Continued.

Figure 13.- Continued.

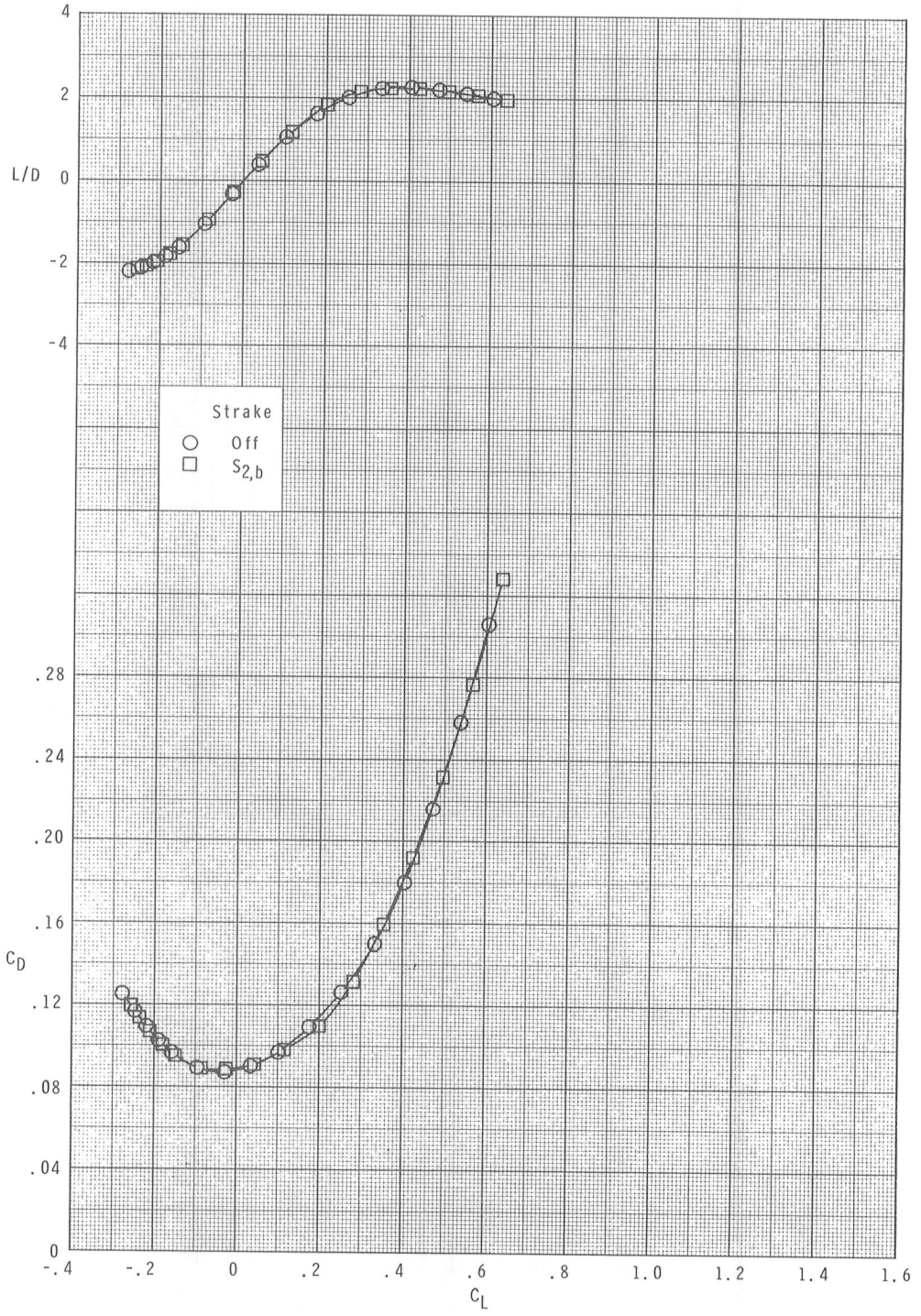

(b) Concluded.

Figure 13.- Continued.

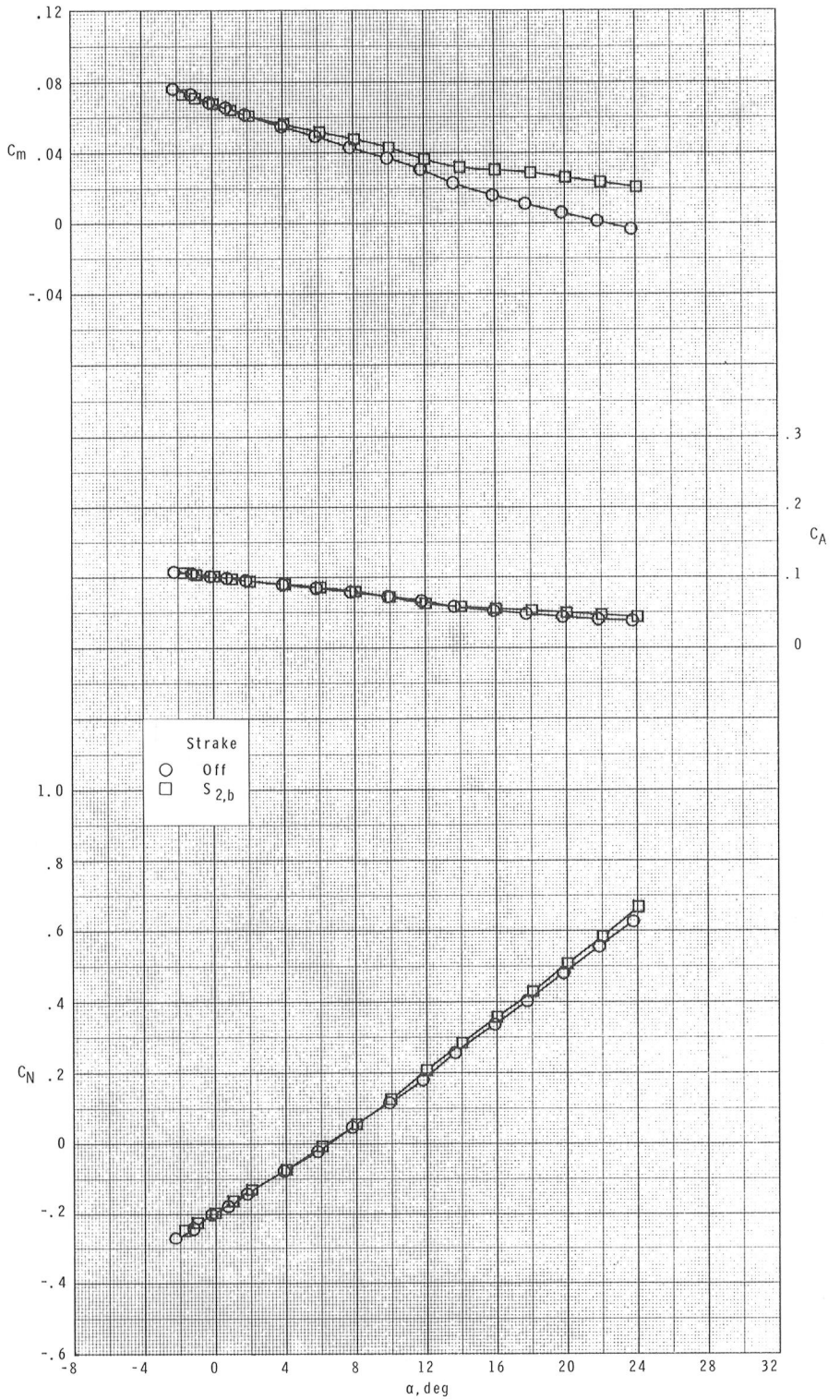

(c) M = 2.36.

Figure 13.- Continued.

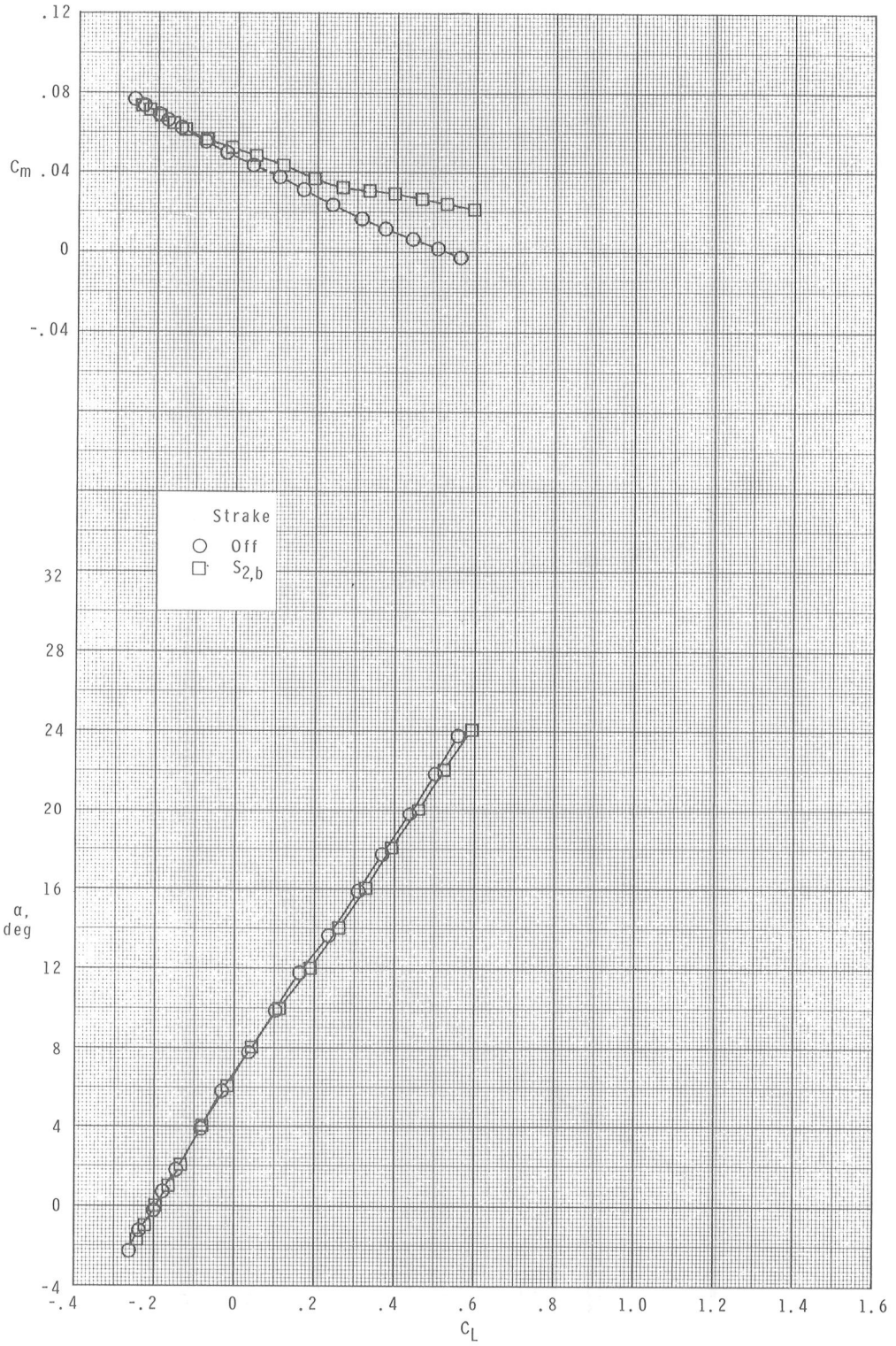

(c) Continued.

Figure 13.- Continued.

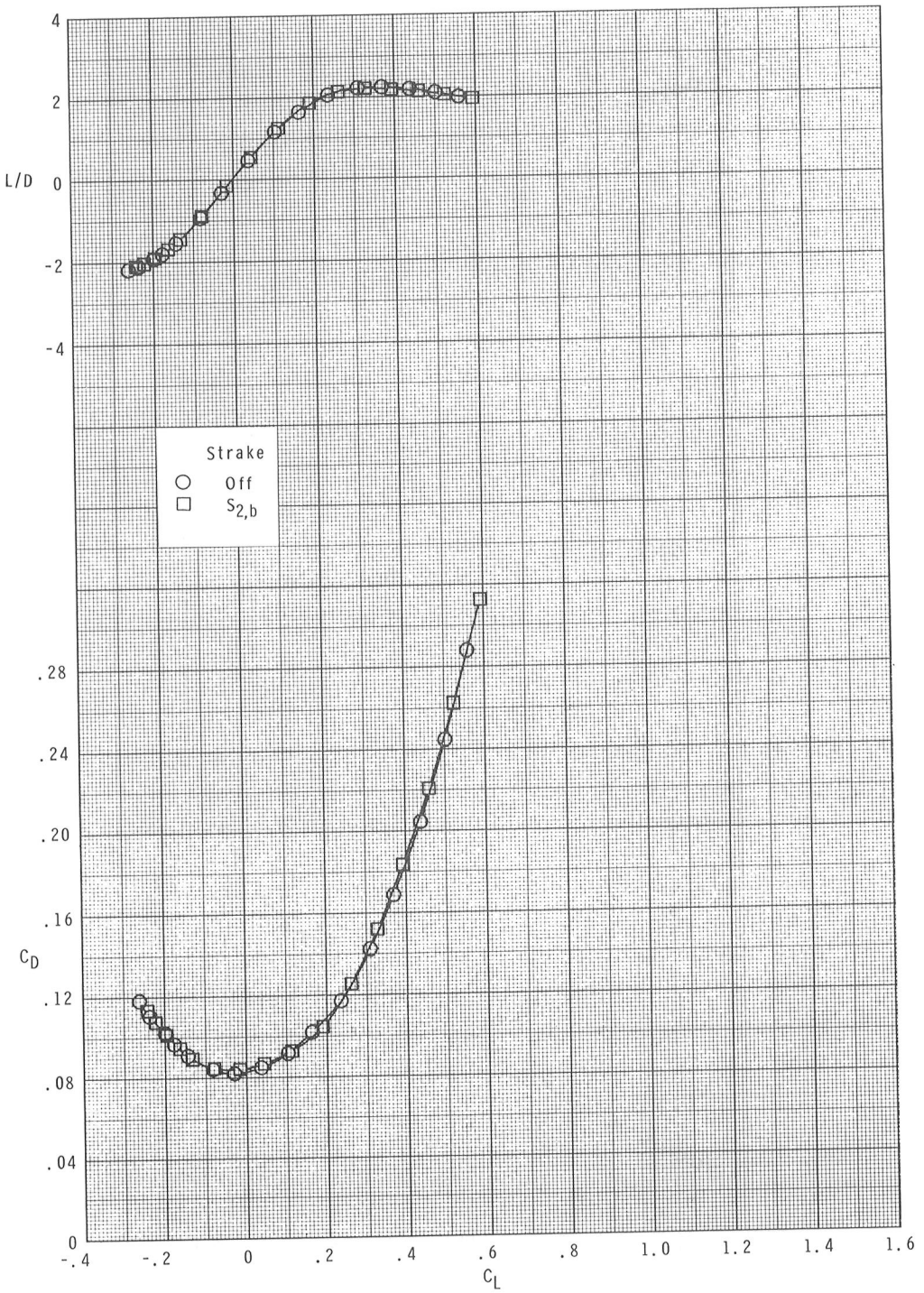

(c) Concluded.

Figure 13.- Continued.

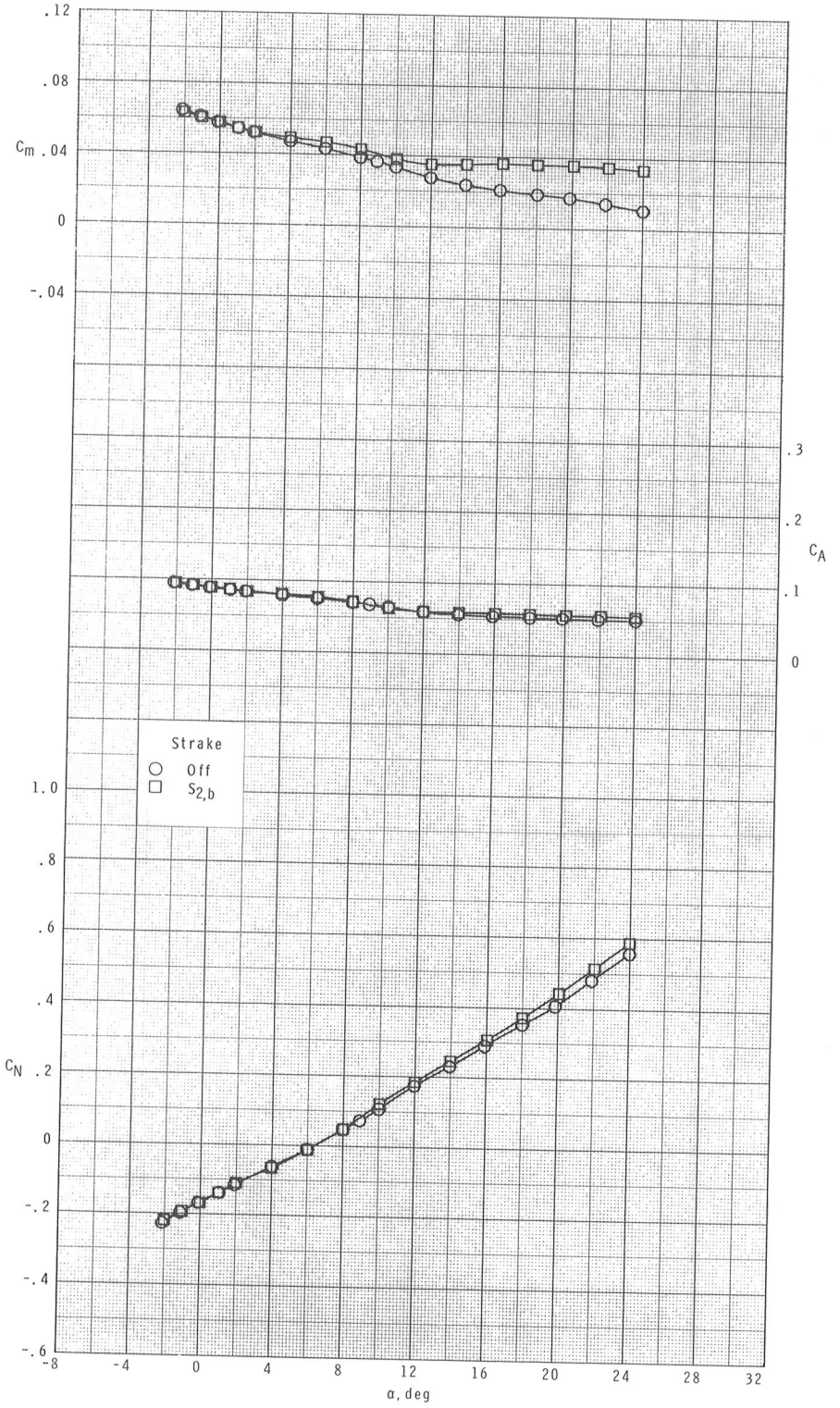

(d) M = 2.86.

Figure 13.- Continued.

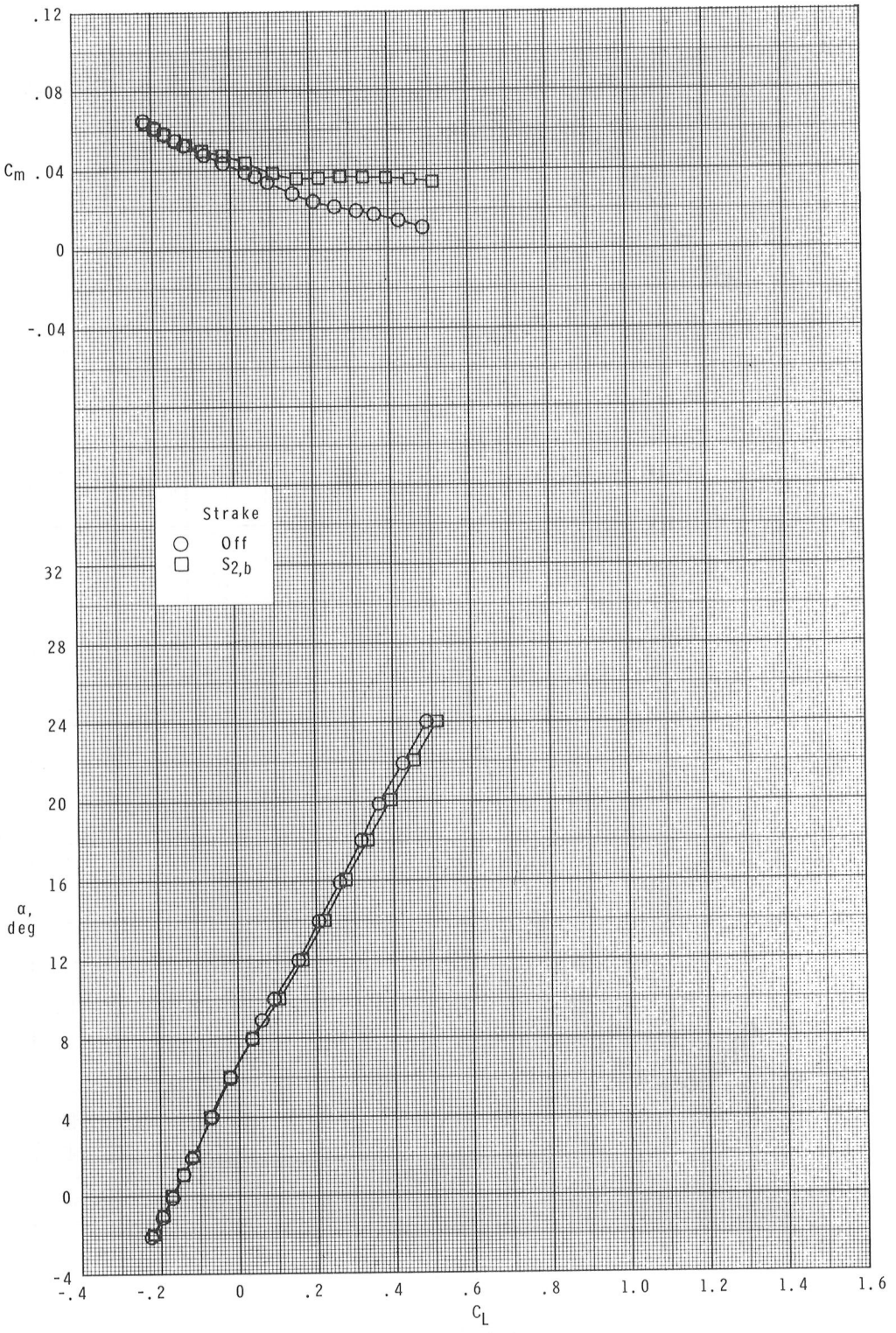

(d) Continued.

Figure 13.- Continued.

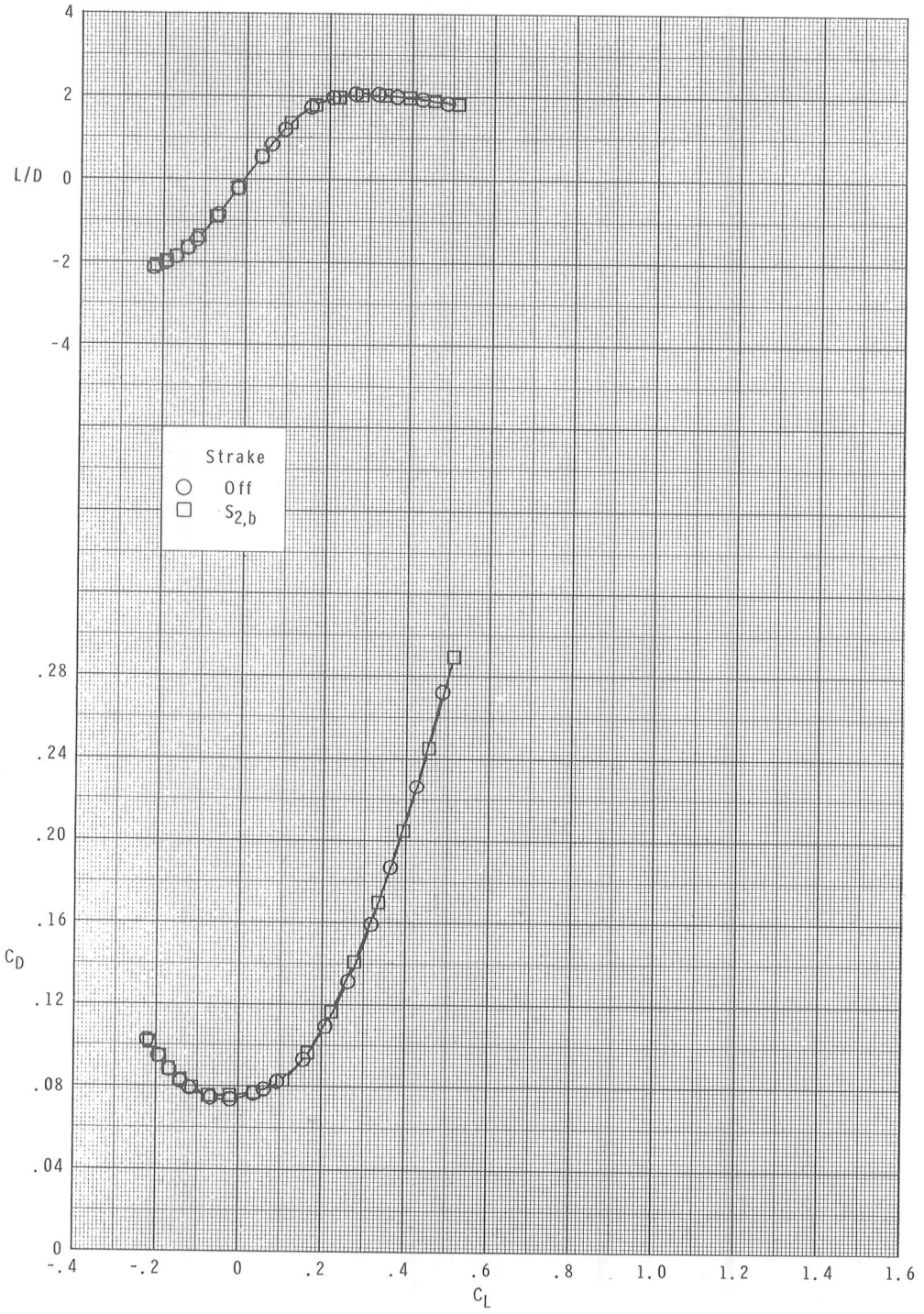

(d) Concluded.

Figure 13.- Concluded.

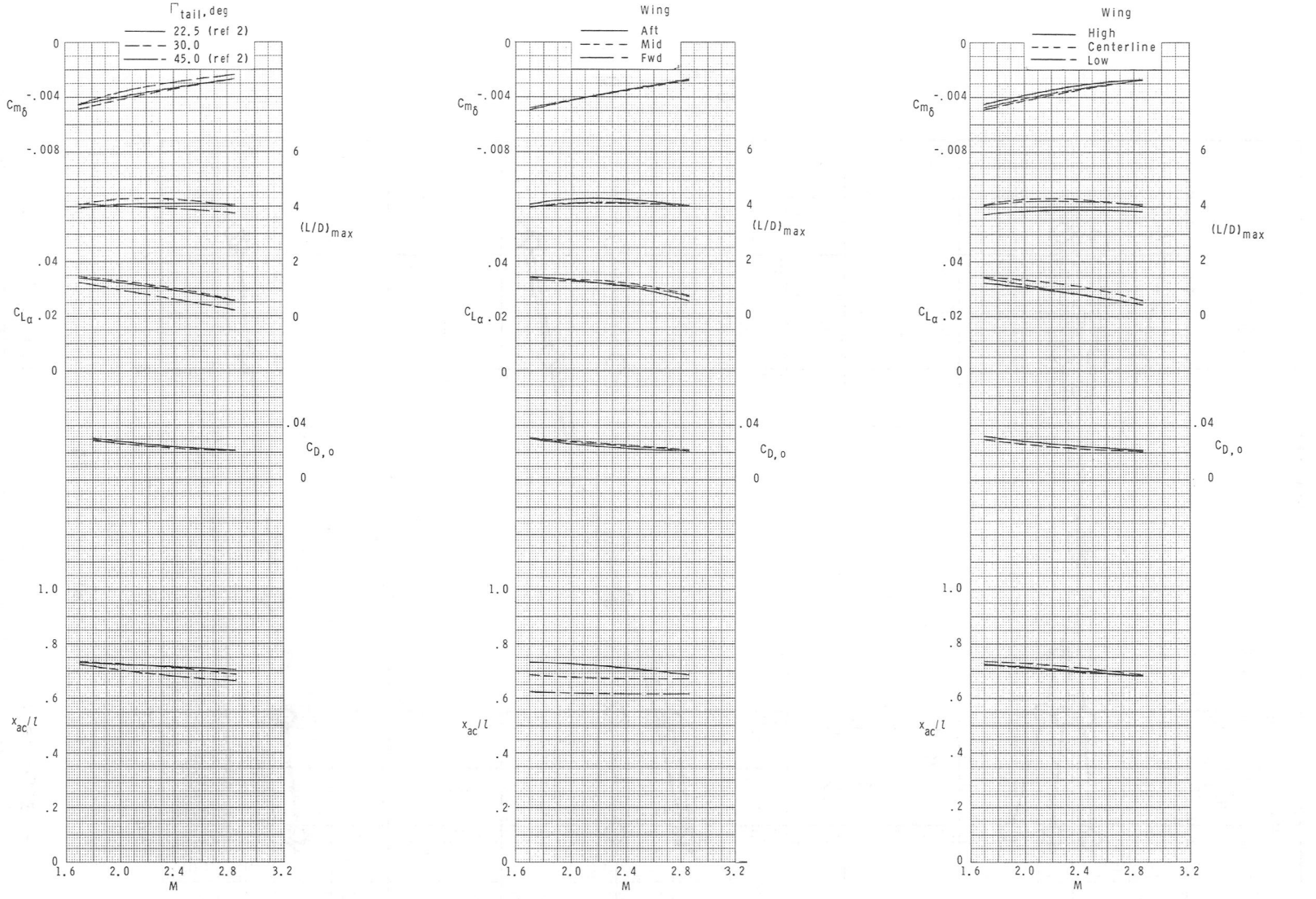

(a) Effect of tail-fin dihedral angle; centerline-aft-wing configuration.

(b) Effect of wing longitudinal location; centerline wing; $\Gamma_{tail} = 30.0^{o}$.

(c) Effect of wing vertical location; aft wing; $\Gamma_{tail} = 30.0^{o}$.

Figure 14.- Summary of longitudinal aerodynamic characteristics.

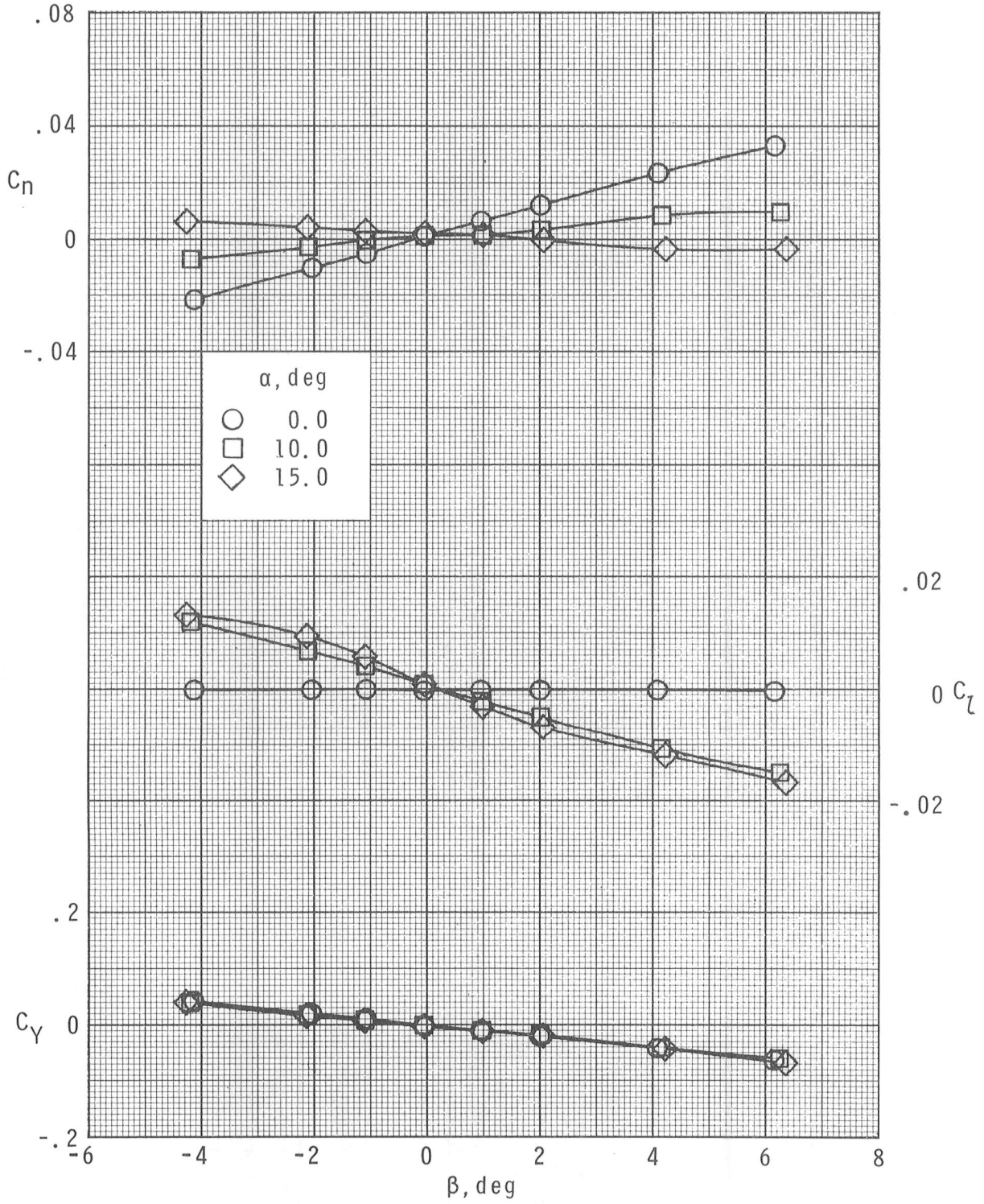

(a) M = 1.70.

Figure 15.- Effects of angle of attack on lateral and directional aerodynamic characteristics with sideslip angle of the centerline-aft-wing configurations.

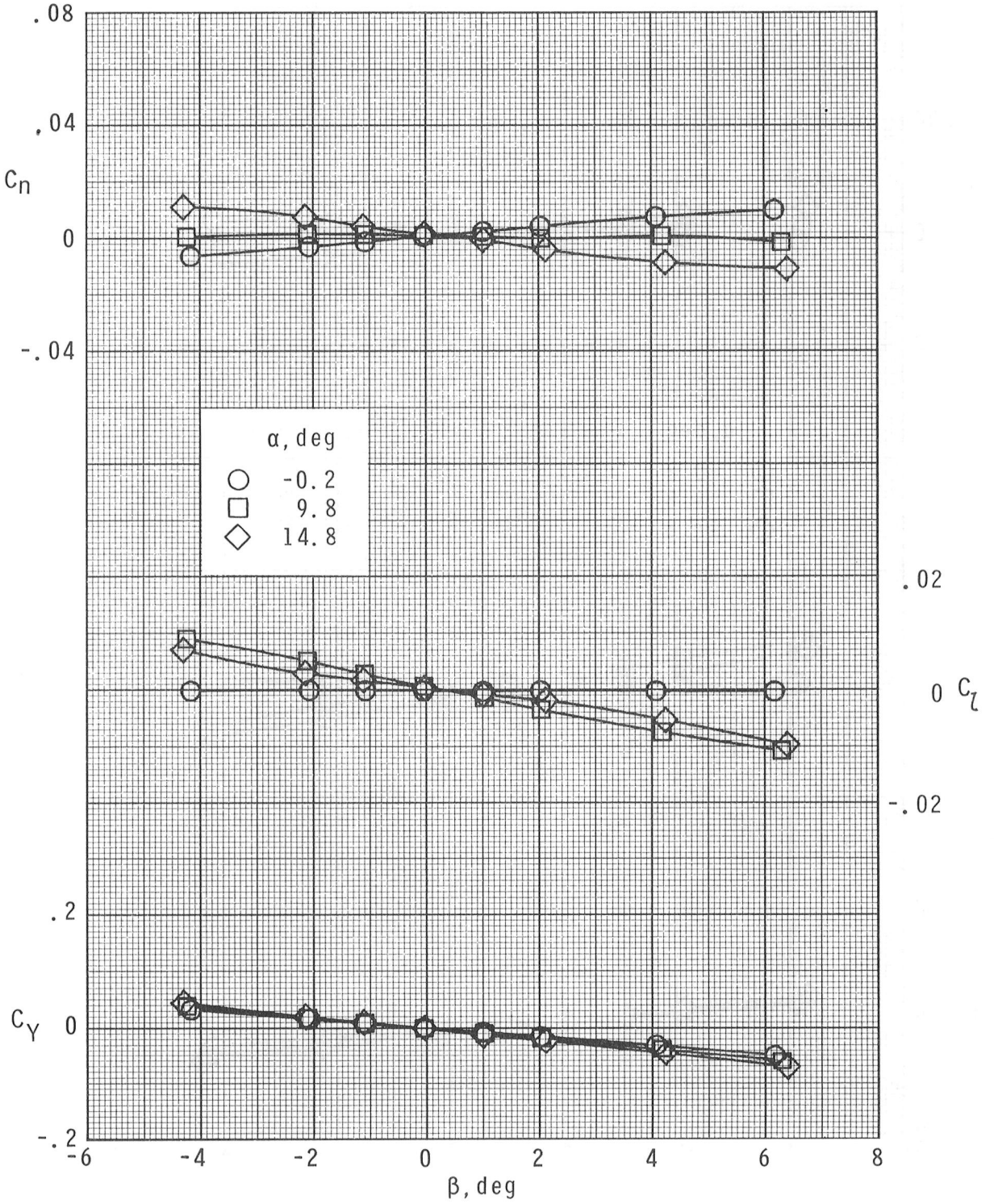

(b) M = 2.16.

Figure 15.- Continued.

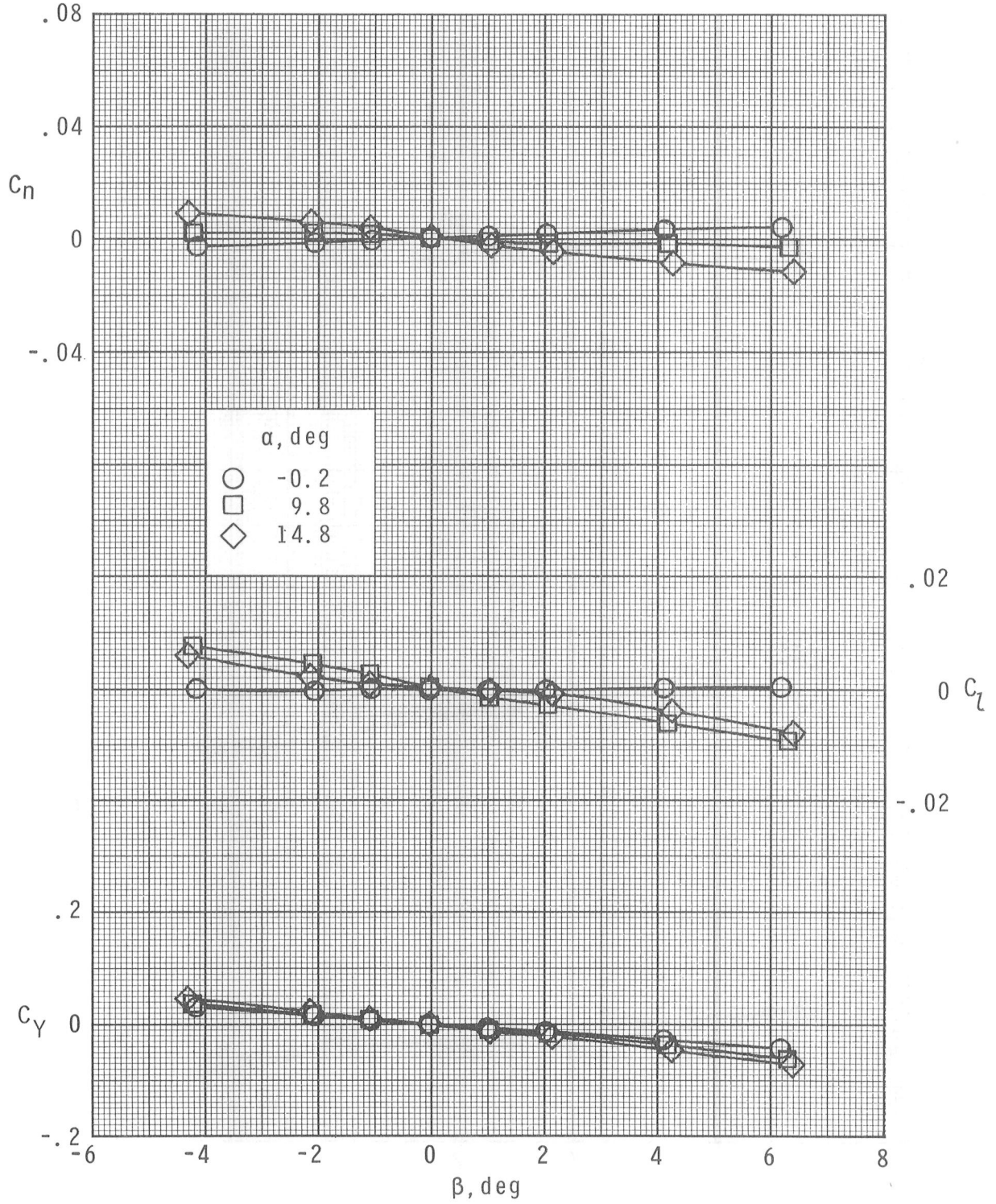

(c) M = 2.36.

Figure 15.- Continued.

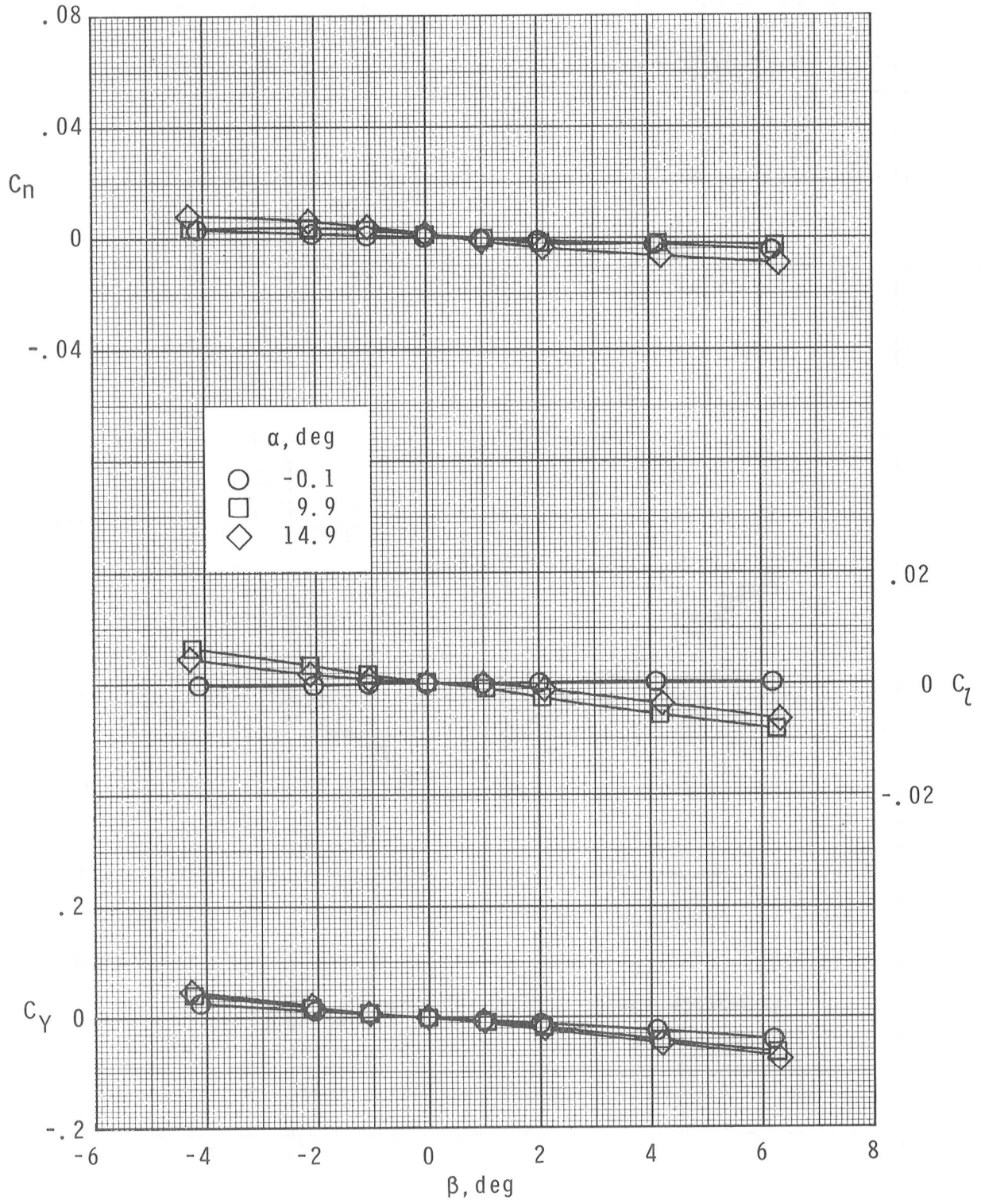

(d) M = 2.86.

Figure 15.- Concluded.

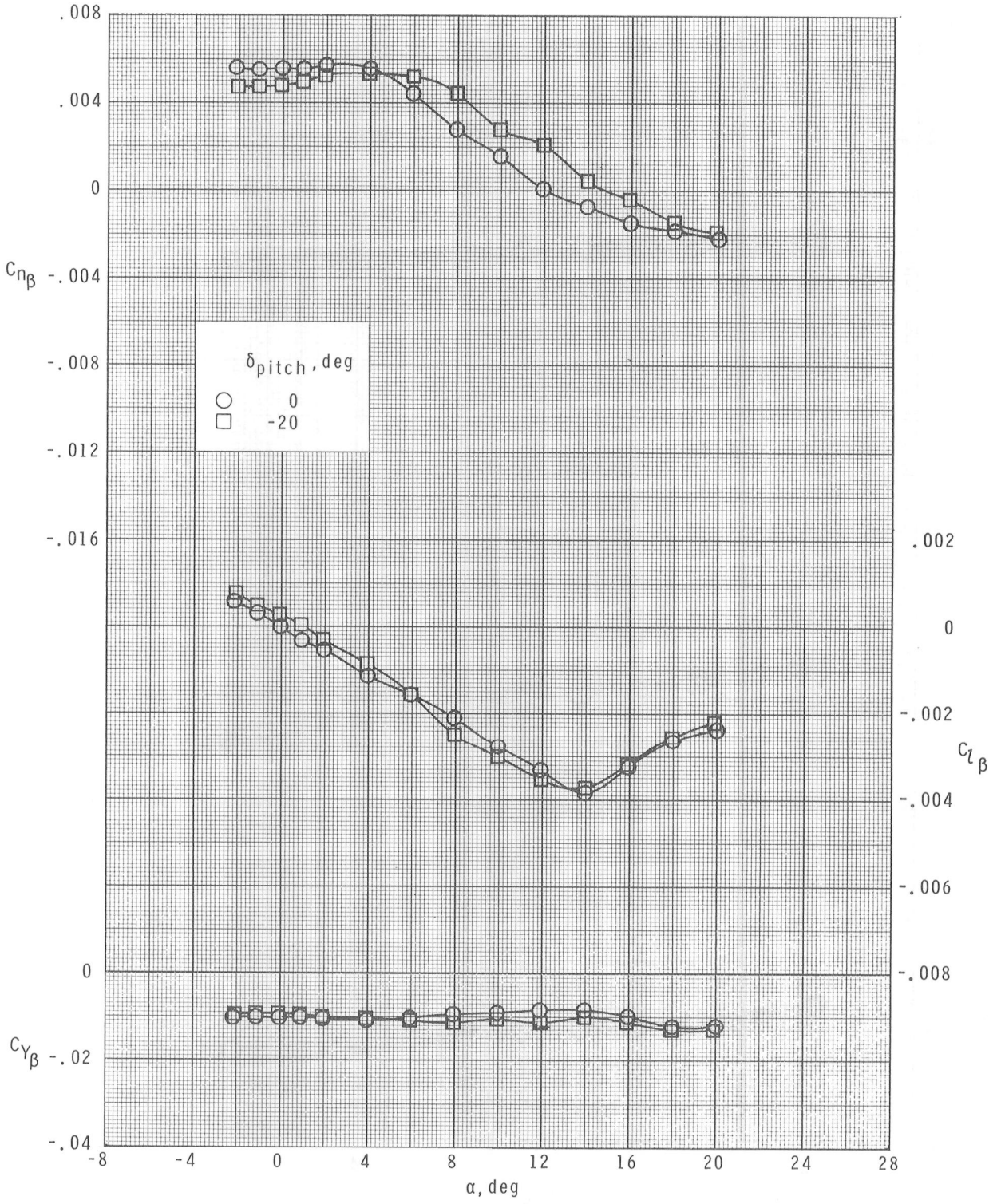

(a) M = 1.70.

Figure 16.- Effects of pitch control on lateral and directional parameters of the centerline-aft-wing configuration.

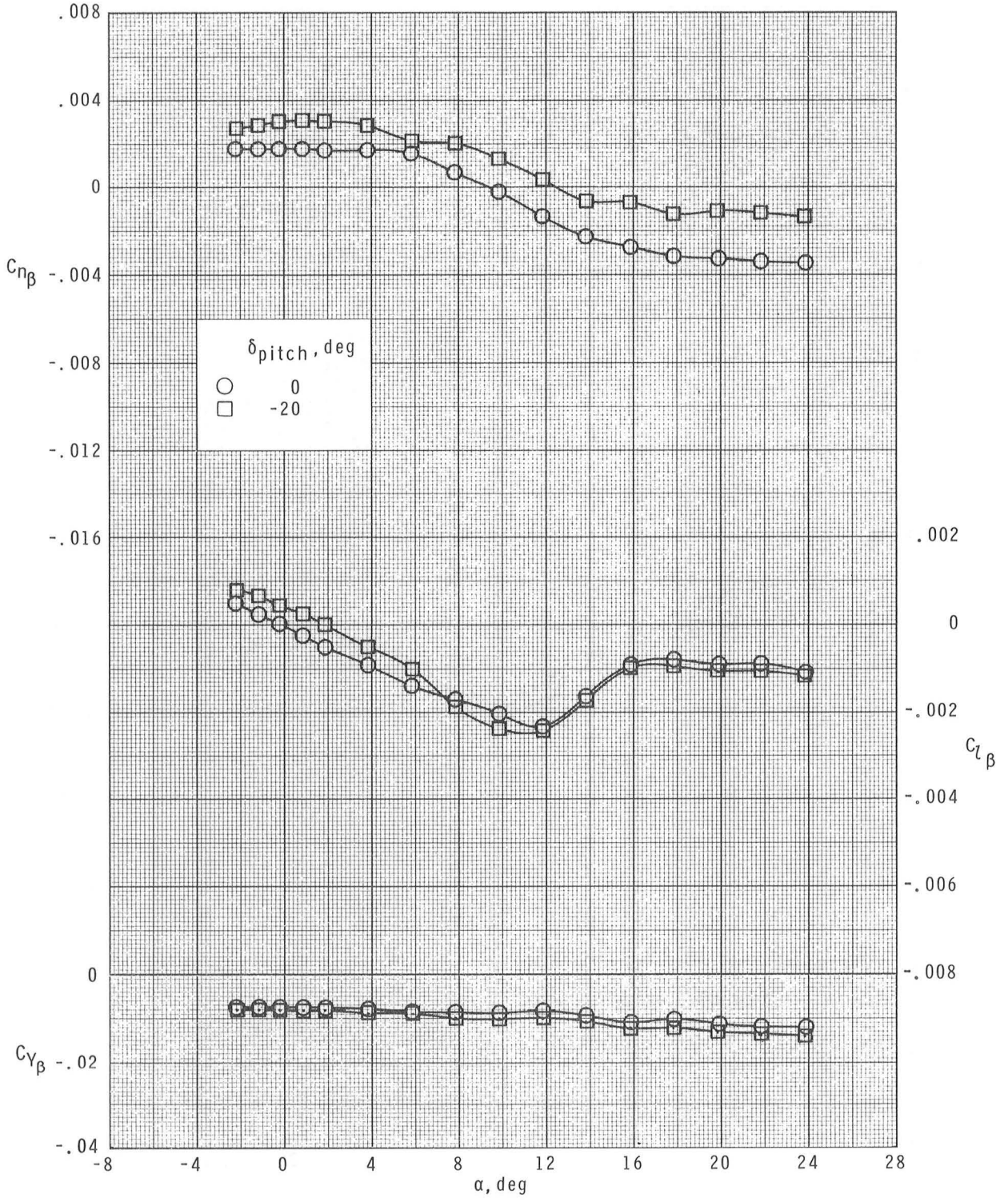

(b) M = 2.16.

Figure 16.- Continued.

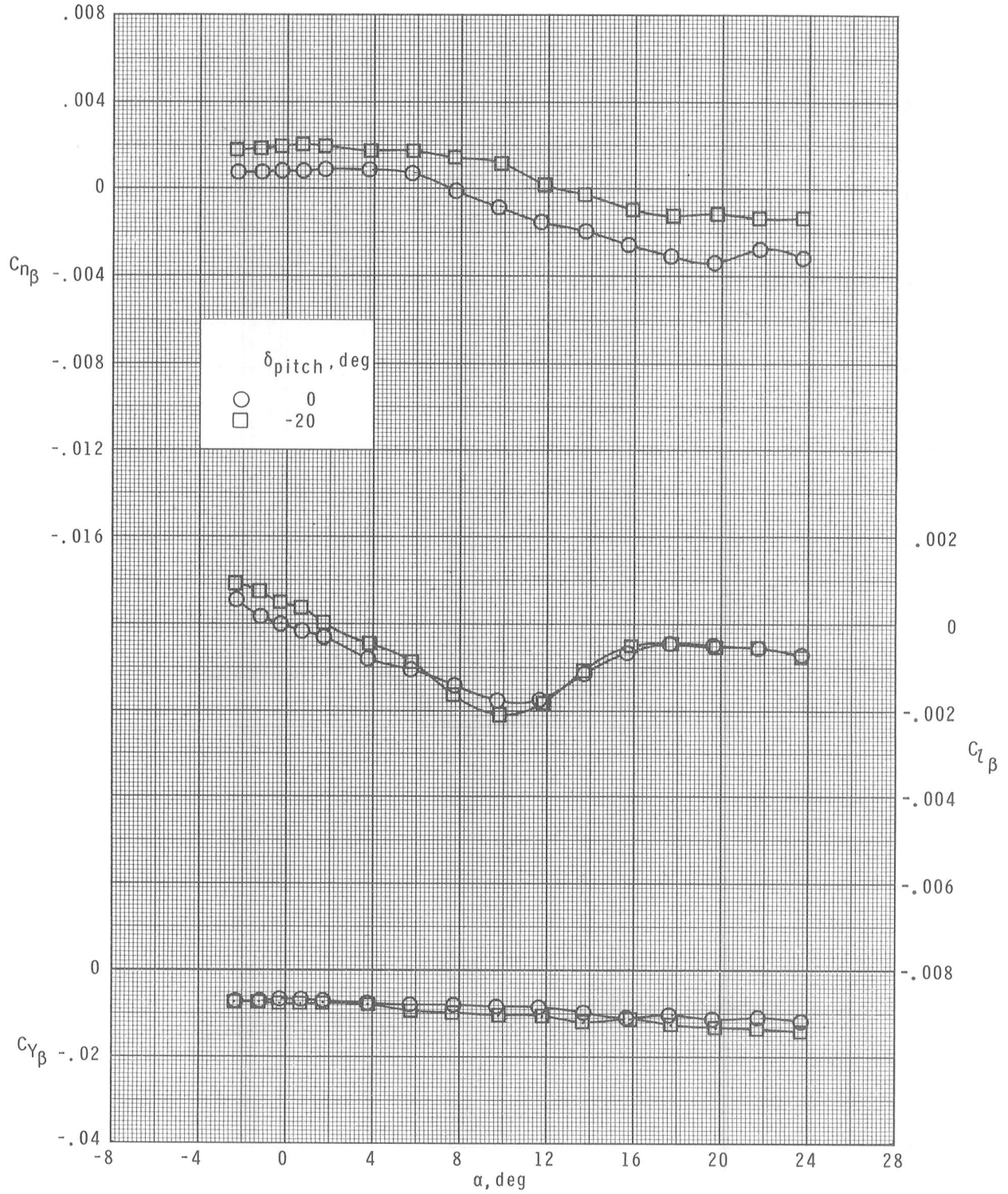

(c) M = 2.36.

Figure 16.- Continued.

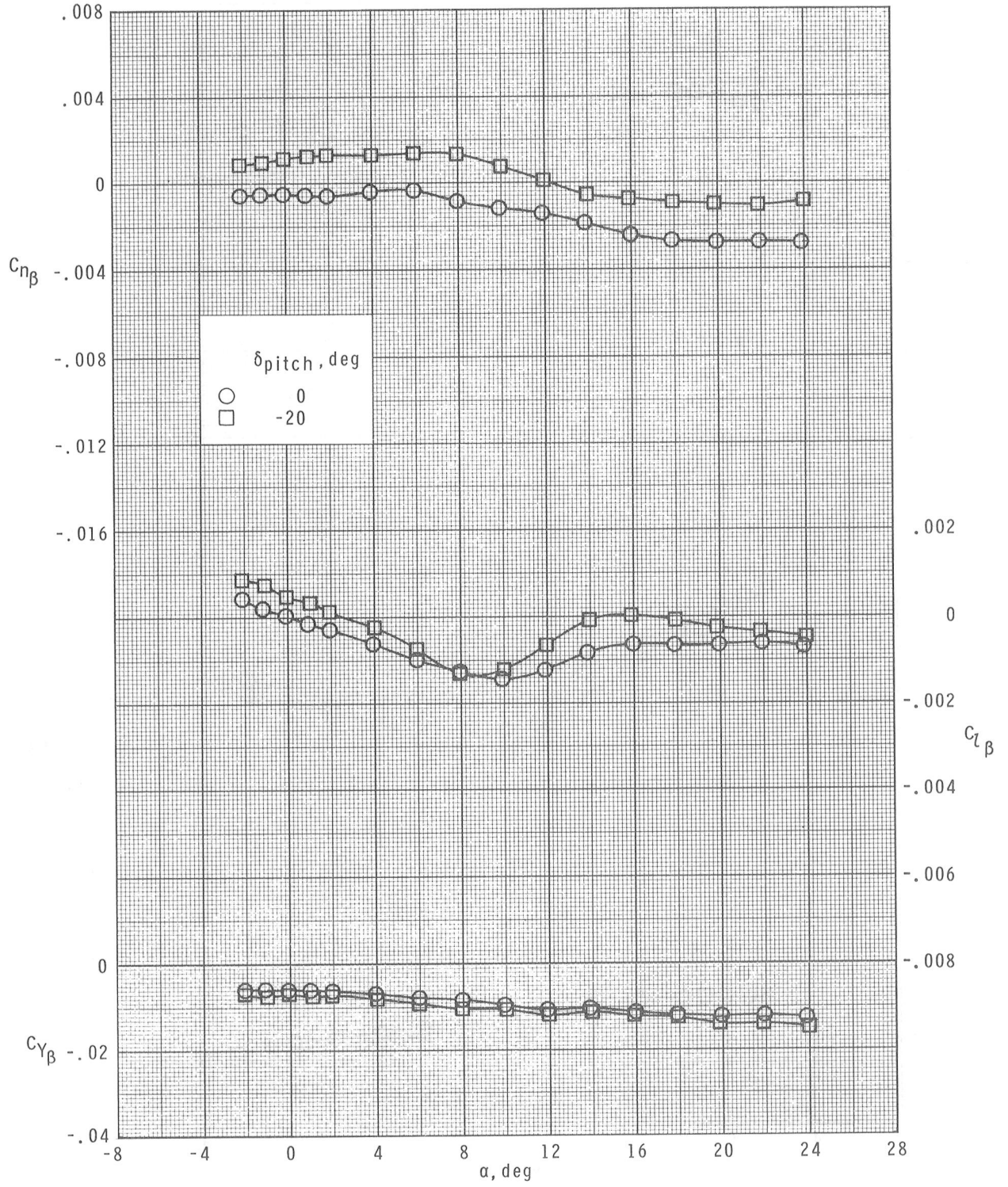

(d) M = 2.86.

Figure 16.- Concluded.

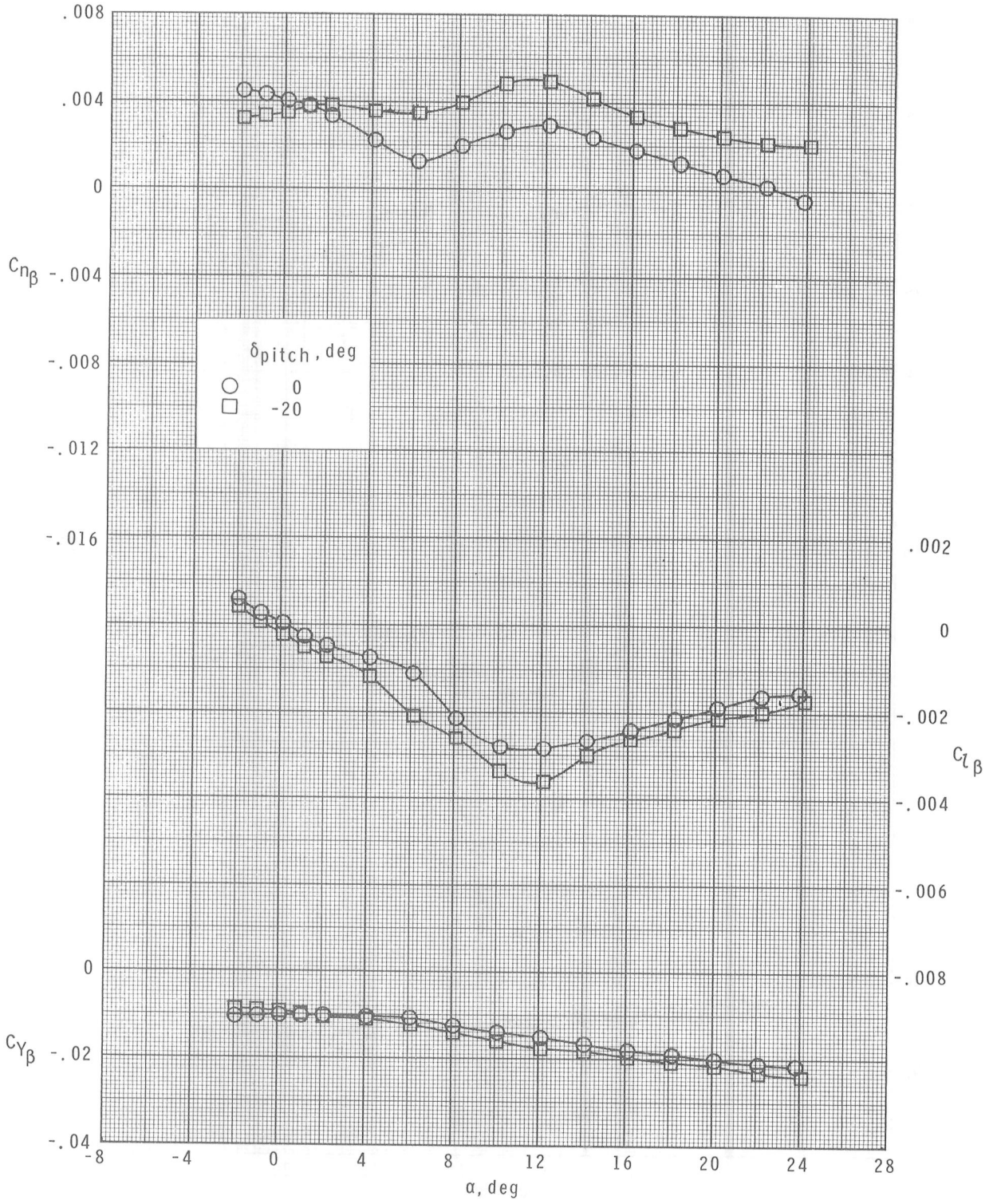

(a) M = 1.70.

Figure 17.- Effects of pitch control on lateral and directional parameters of the high-aft-wing configuration.

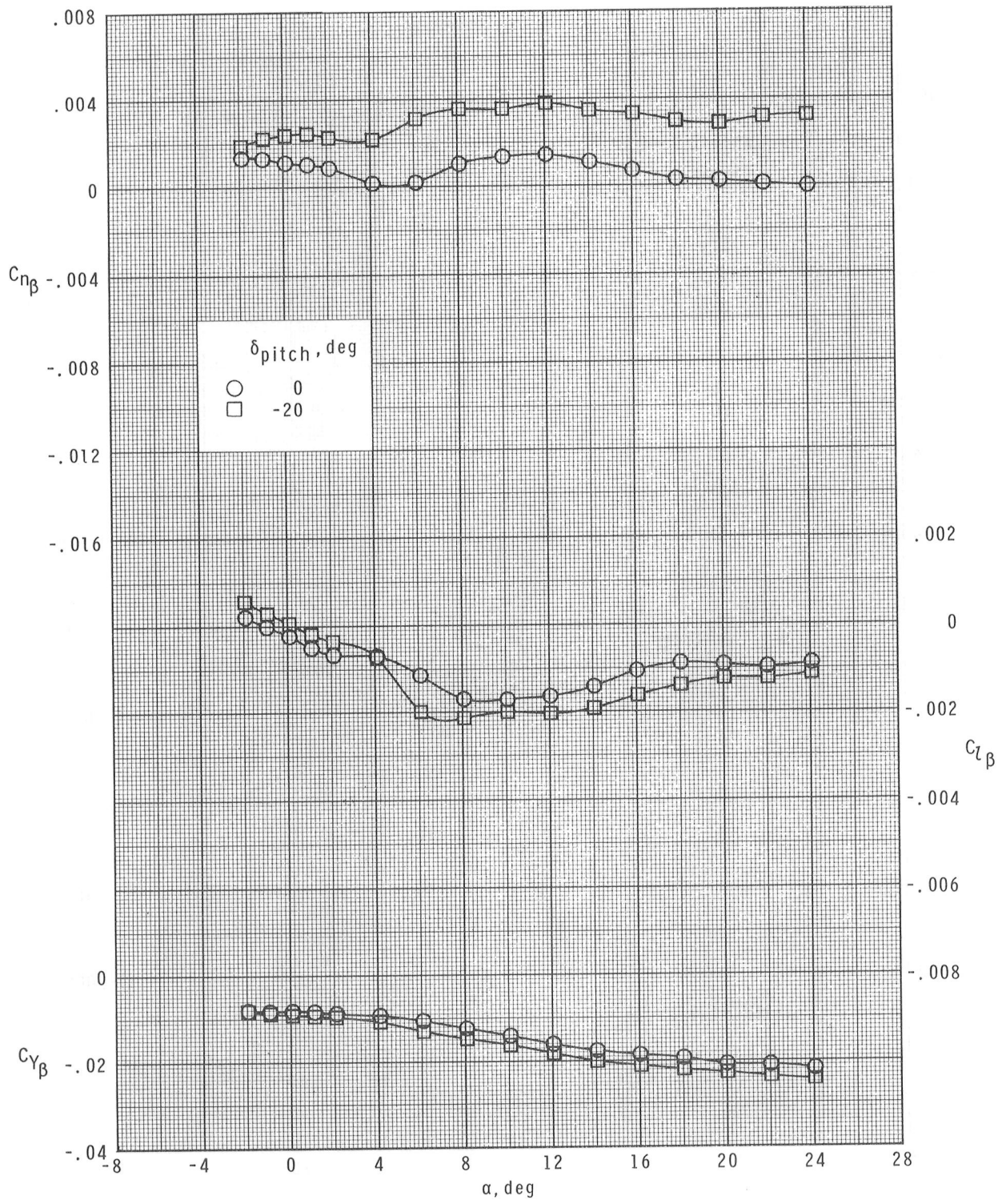

(b) M = 2.16.

Figure 17.- Continued.

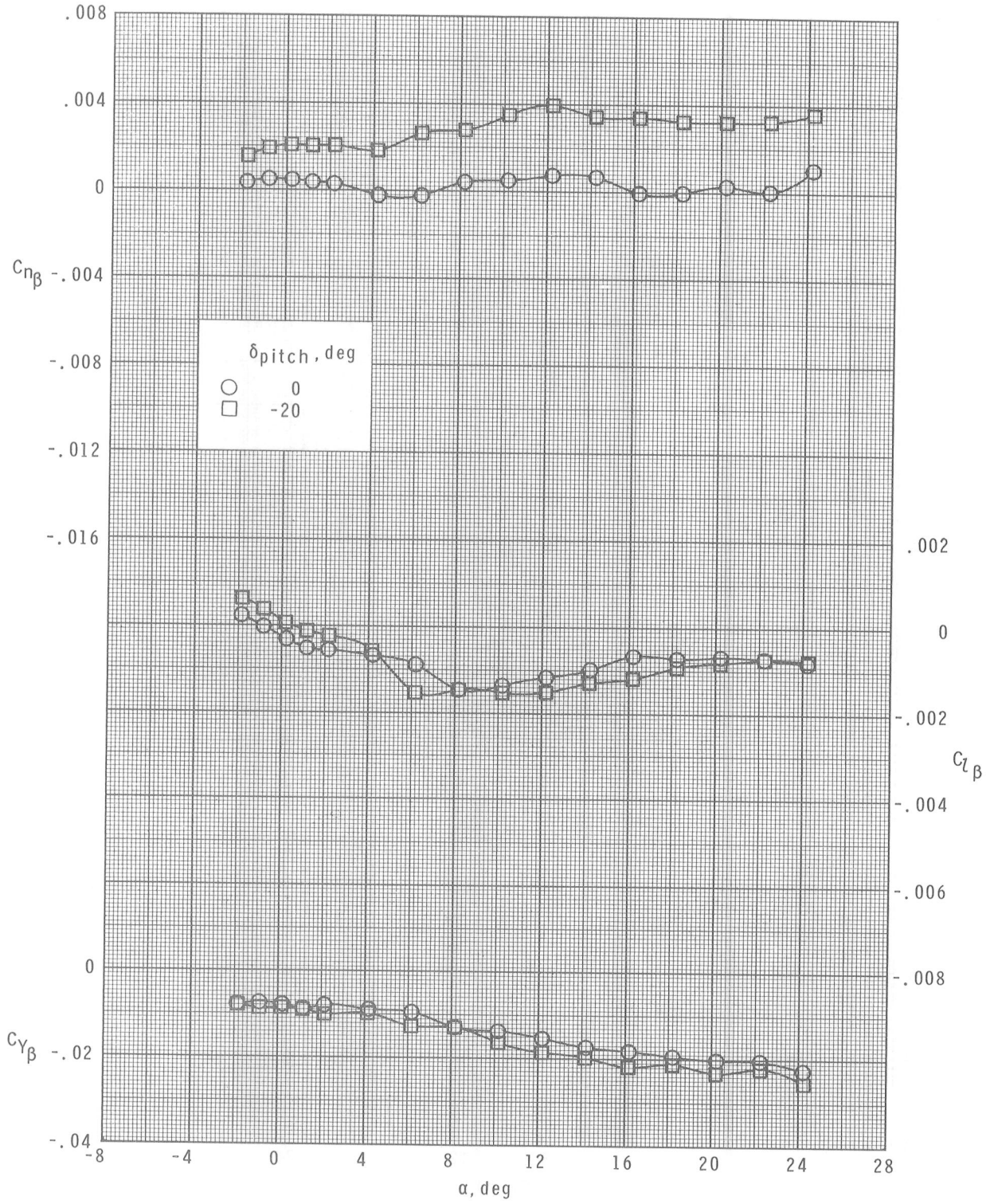

(c) M = 2.36.

Figure 17.- Continued.

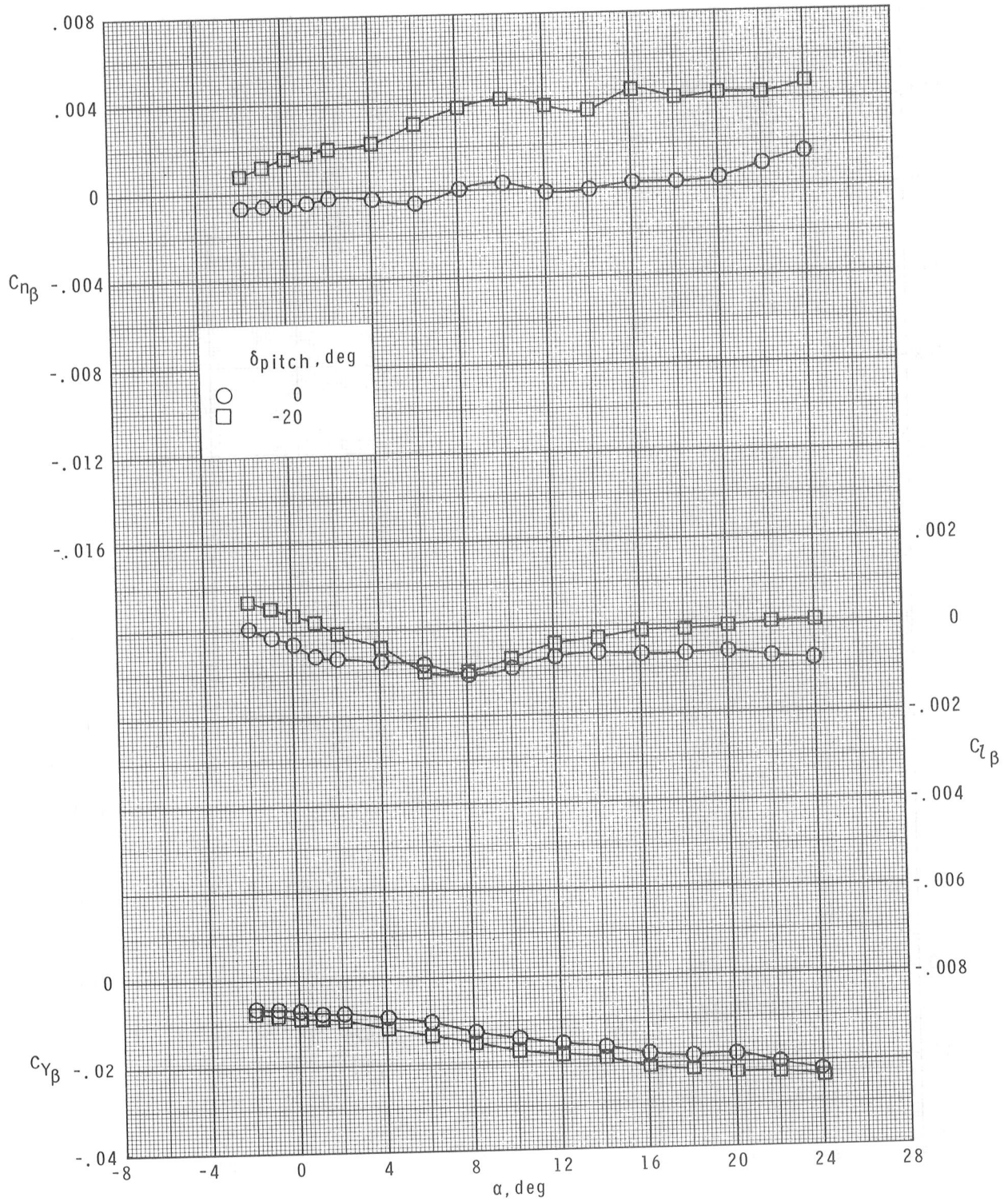

(d) M = 2.86.

Figure 17.- Concluded.

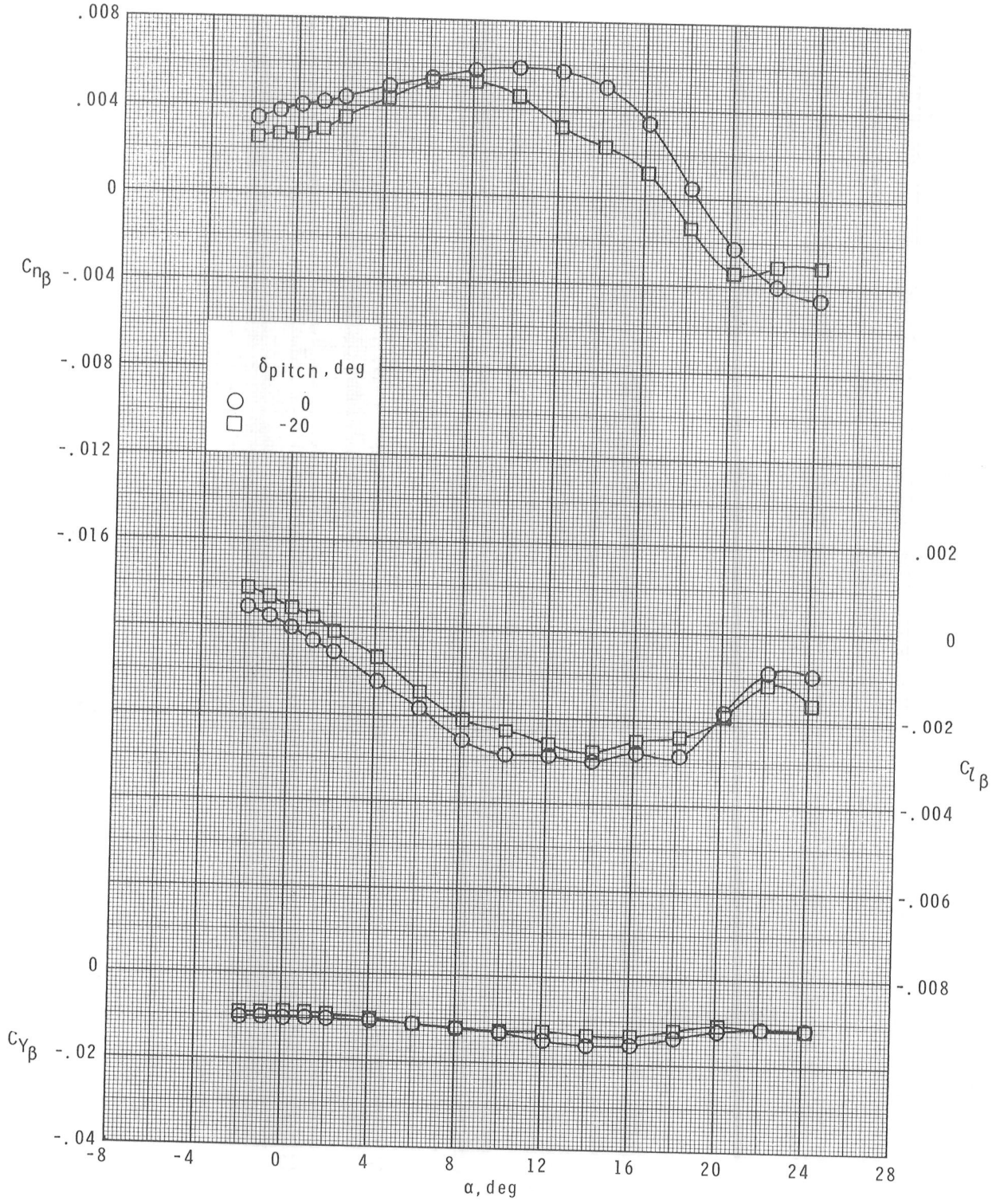

(a) M = 1.70.

Figure 18.- Effects of pitch control on lateral and directional parameters of the low-aft-wing configuration.

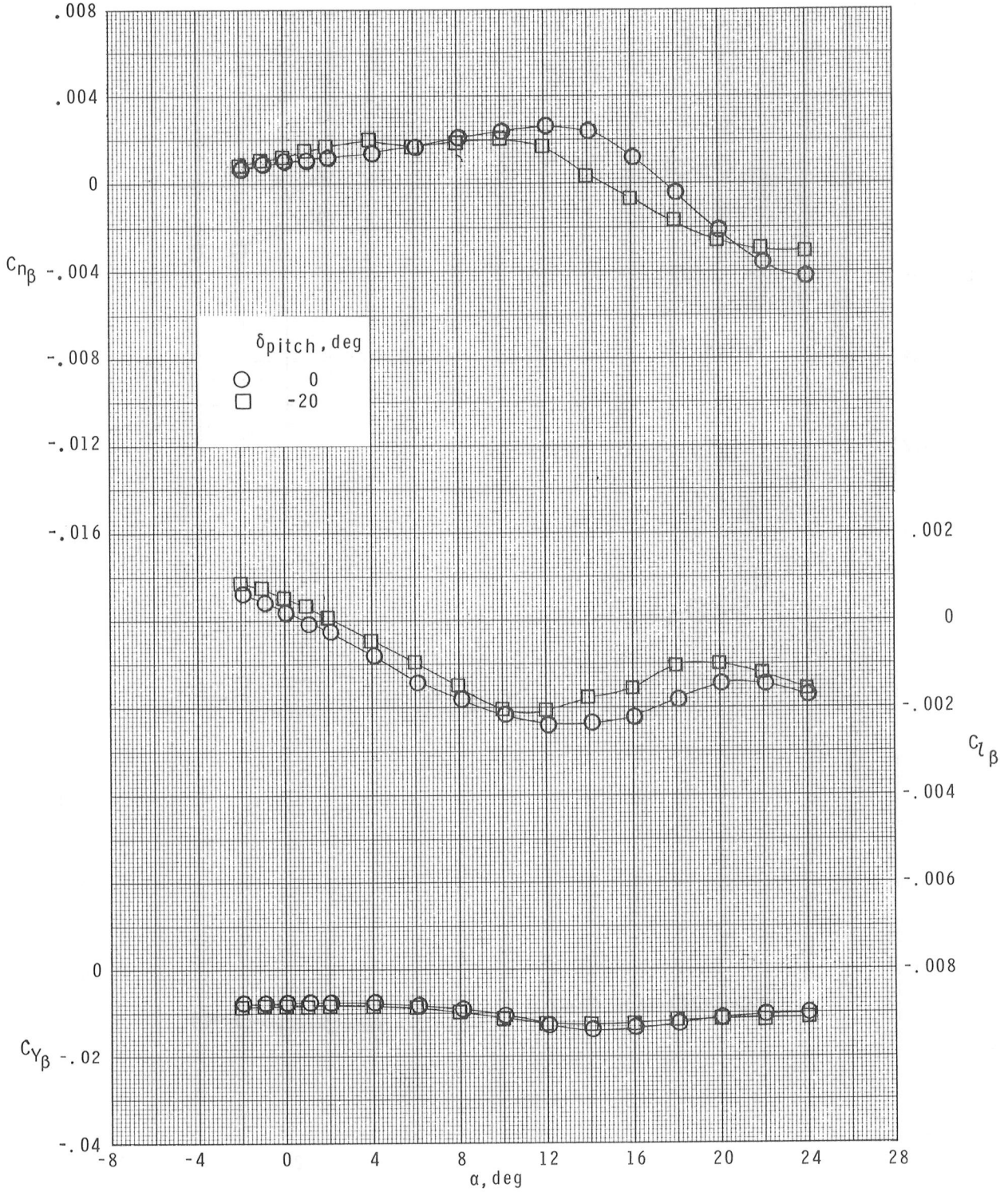

(b) M = 2.16.

Figure 18.- Continued.

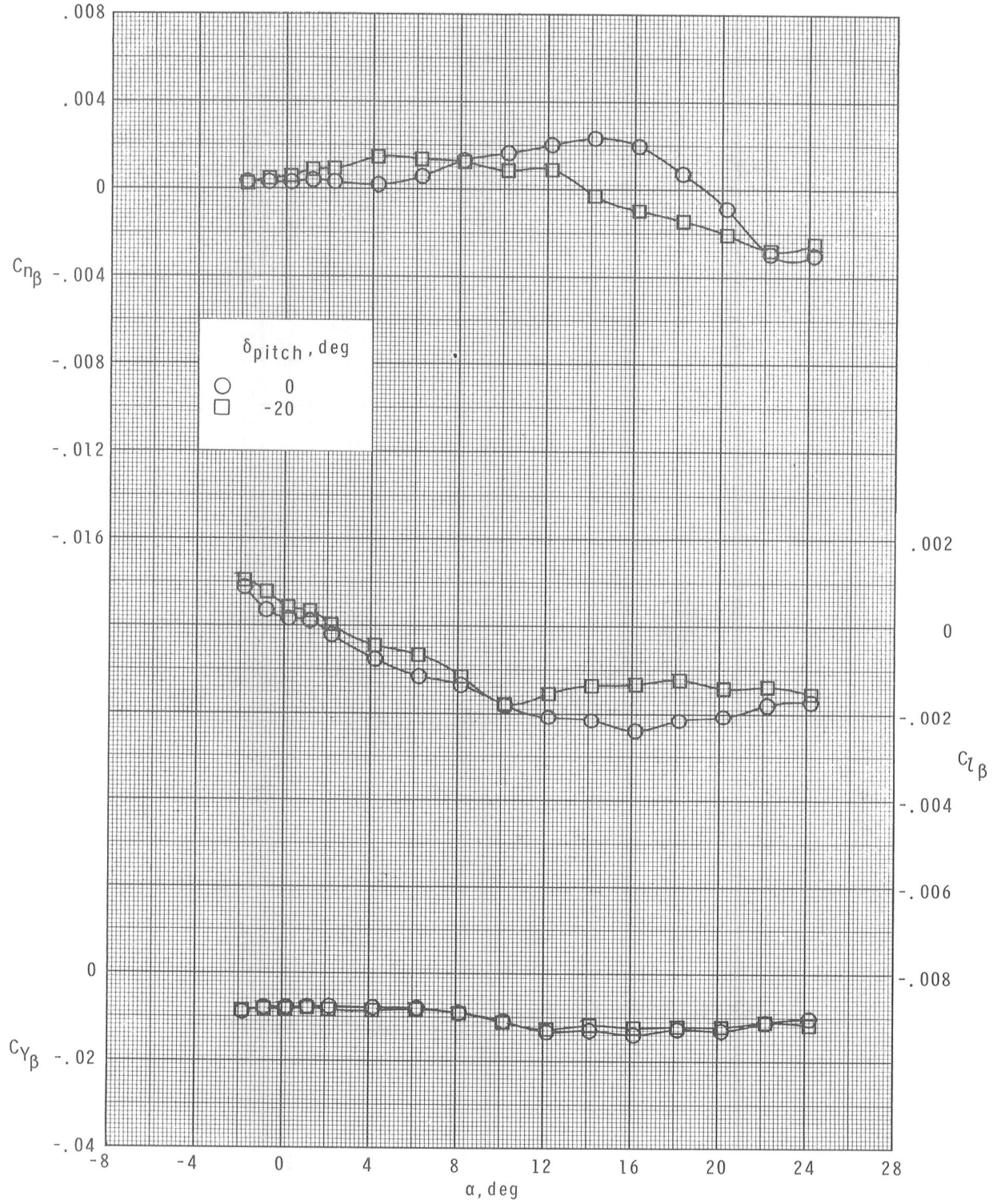

(c) M = 2.36.

Figure 18.- Continued.

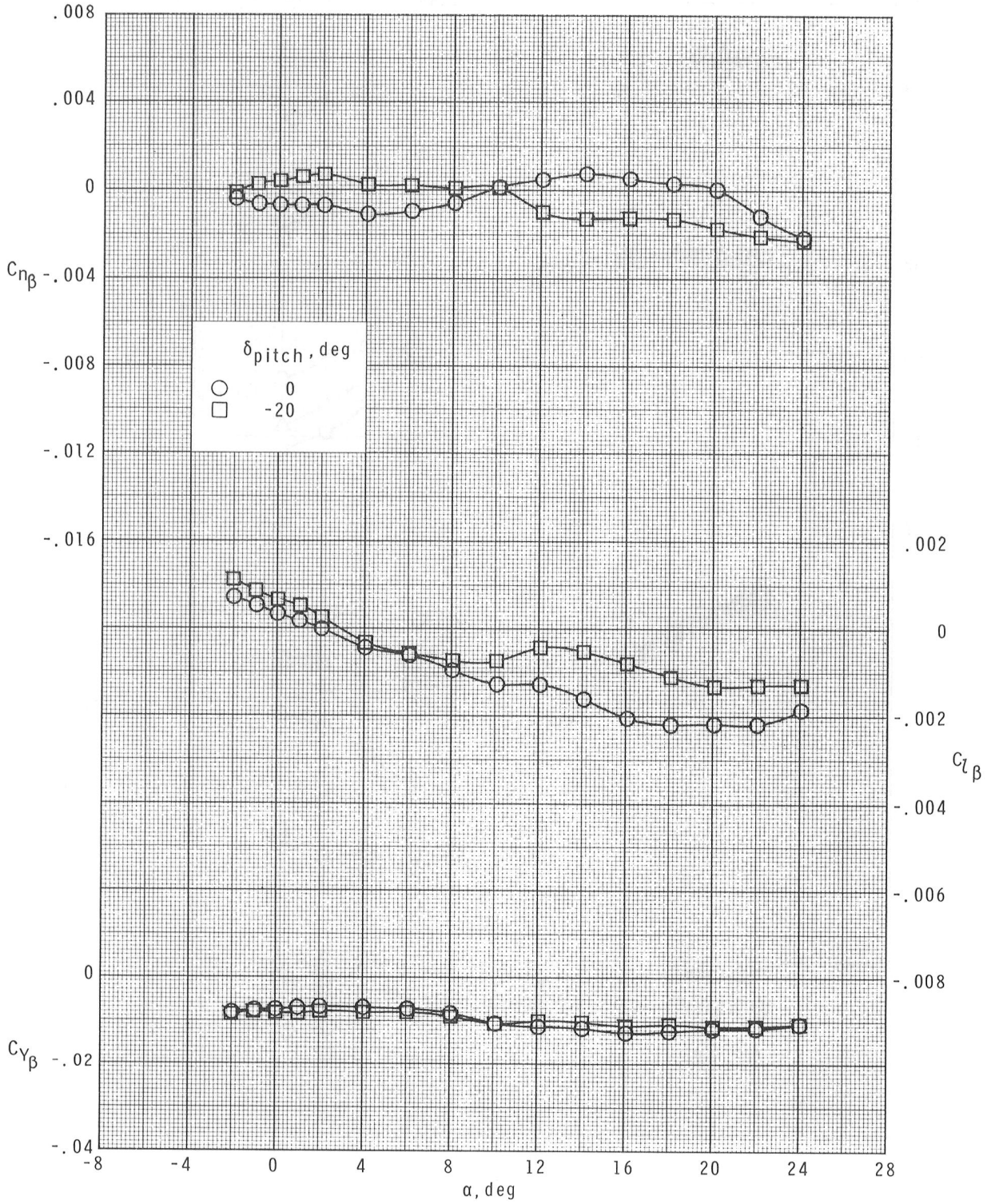

(d) M = 2.86.

Figure 18.- Concluded.

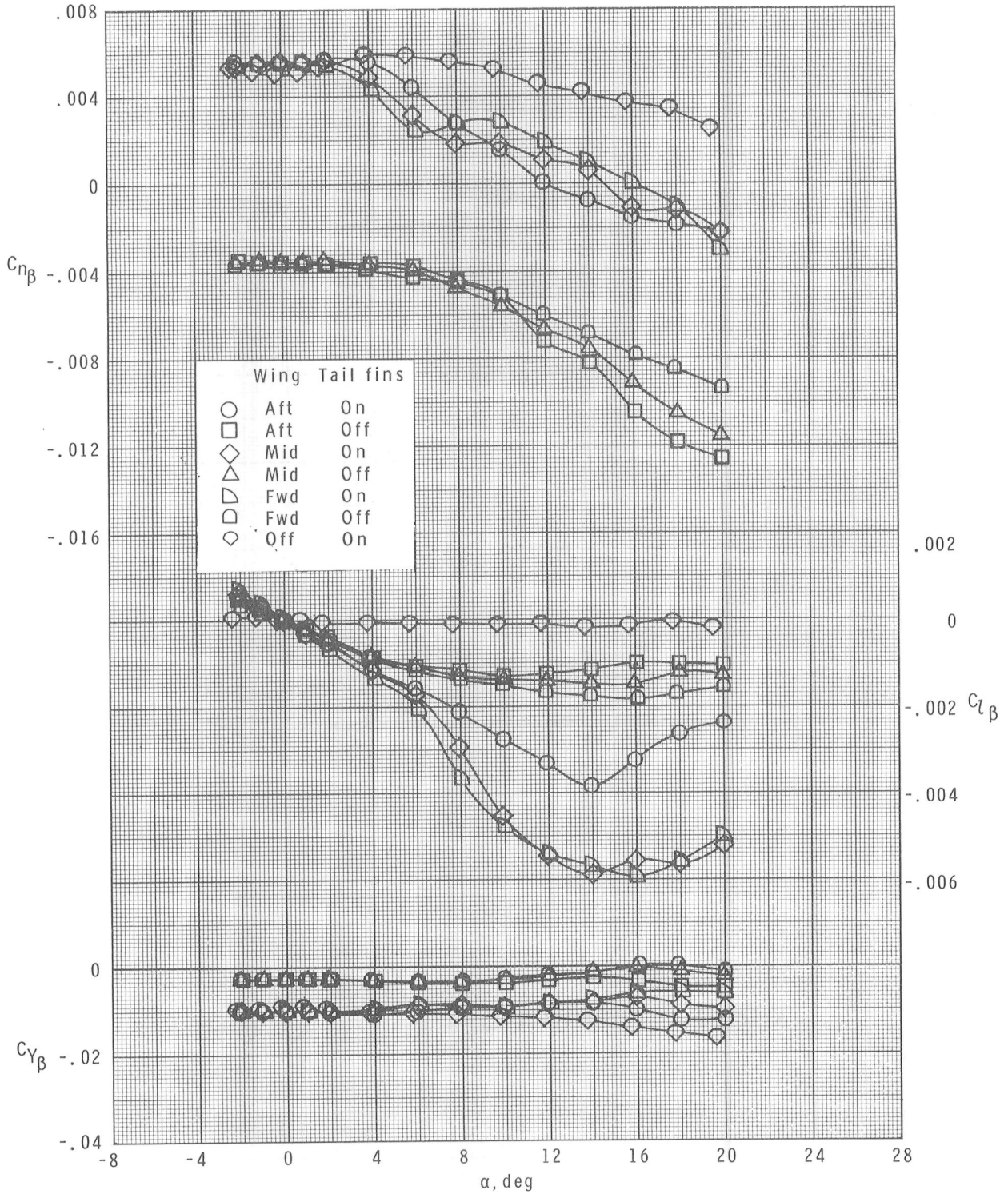

(a) M = 1.70.

Figure 19.- Effects of wing longitudinal location and tail fins on lateral and directional parameters of the centerline-wing configurations. Zero control deflection.

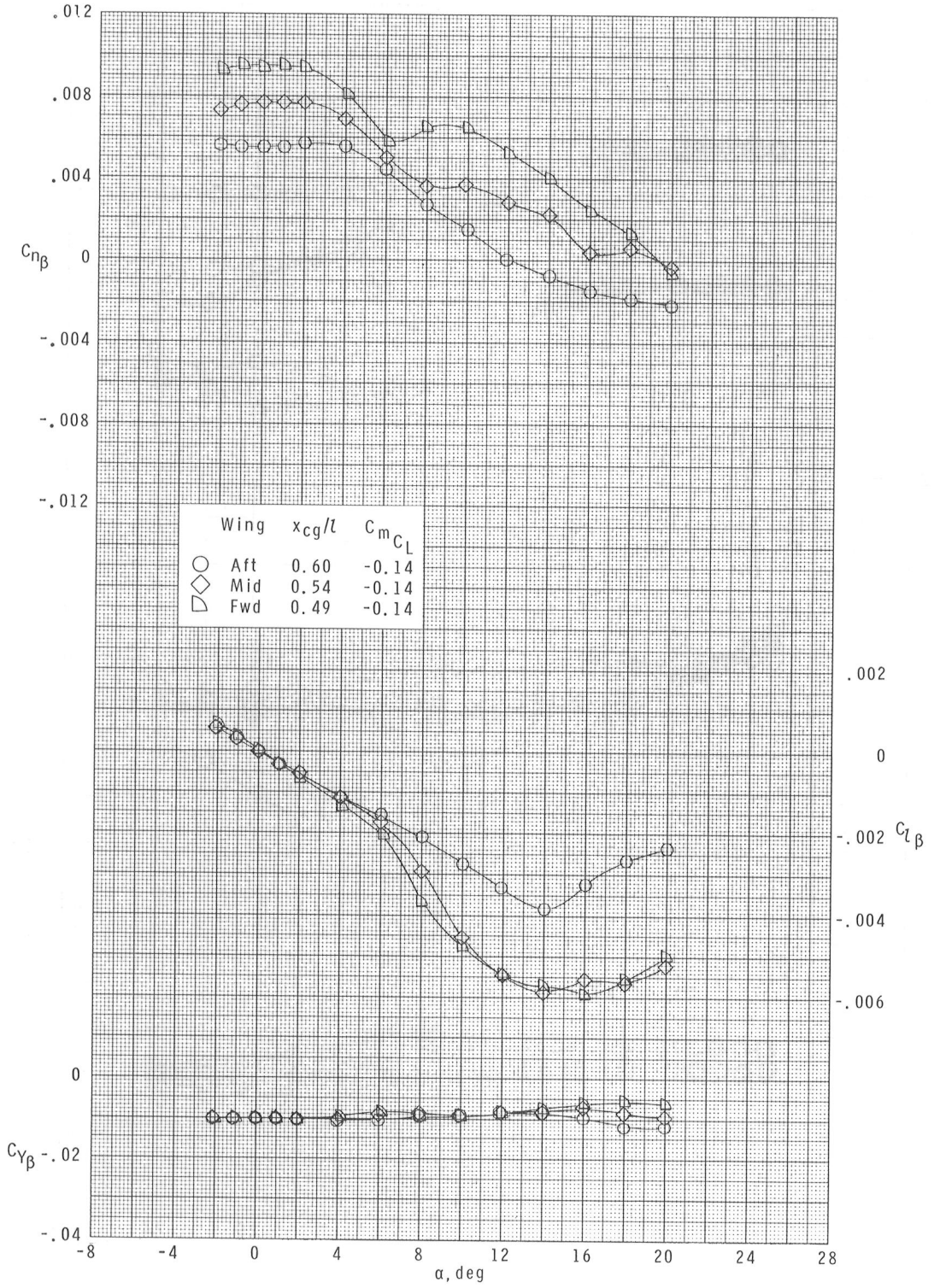

(a) Concluded.

Figure 19.- Continued.

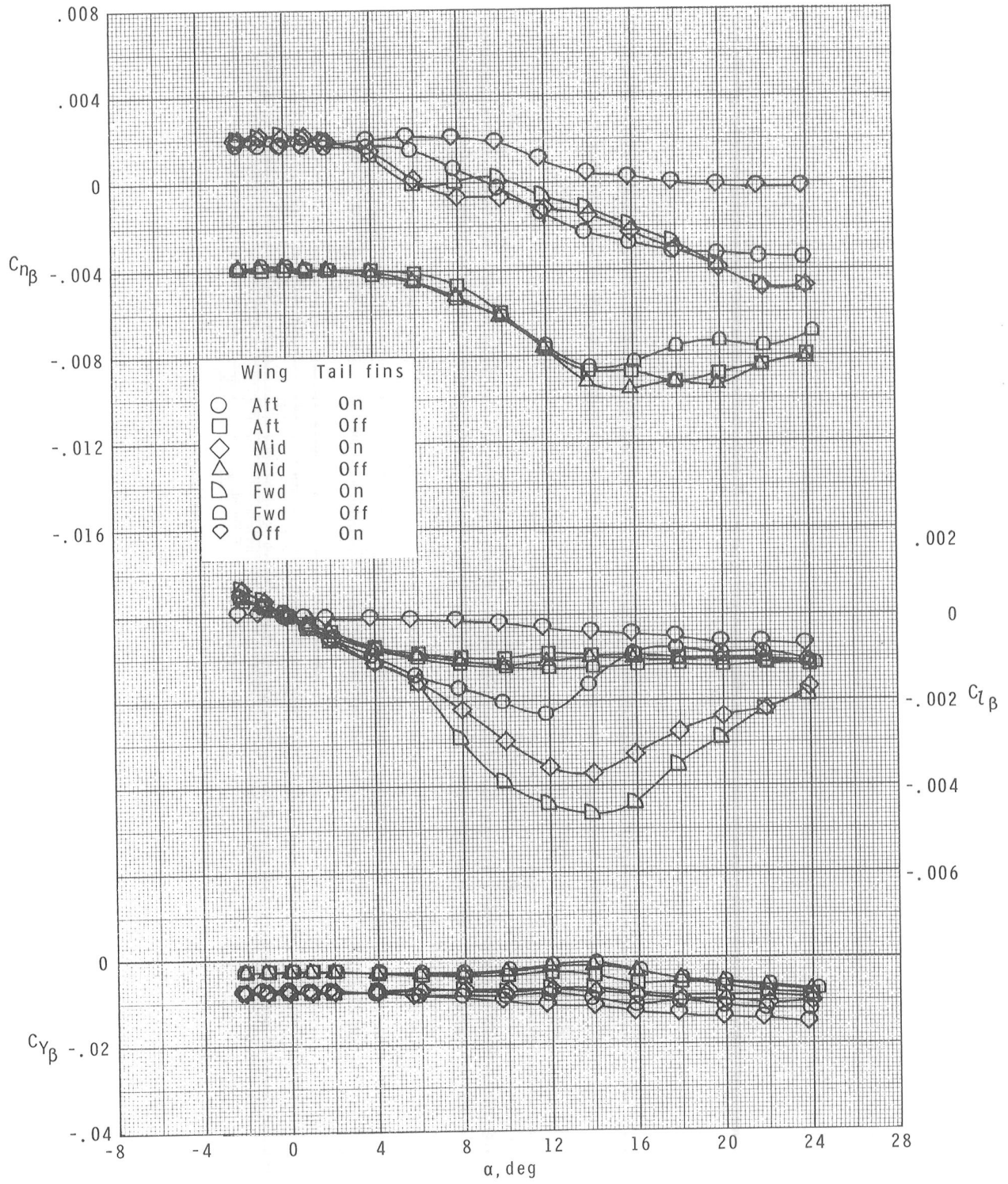

(b) M = 2.16.

Figure 19.- Continued.

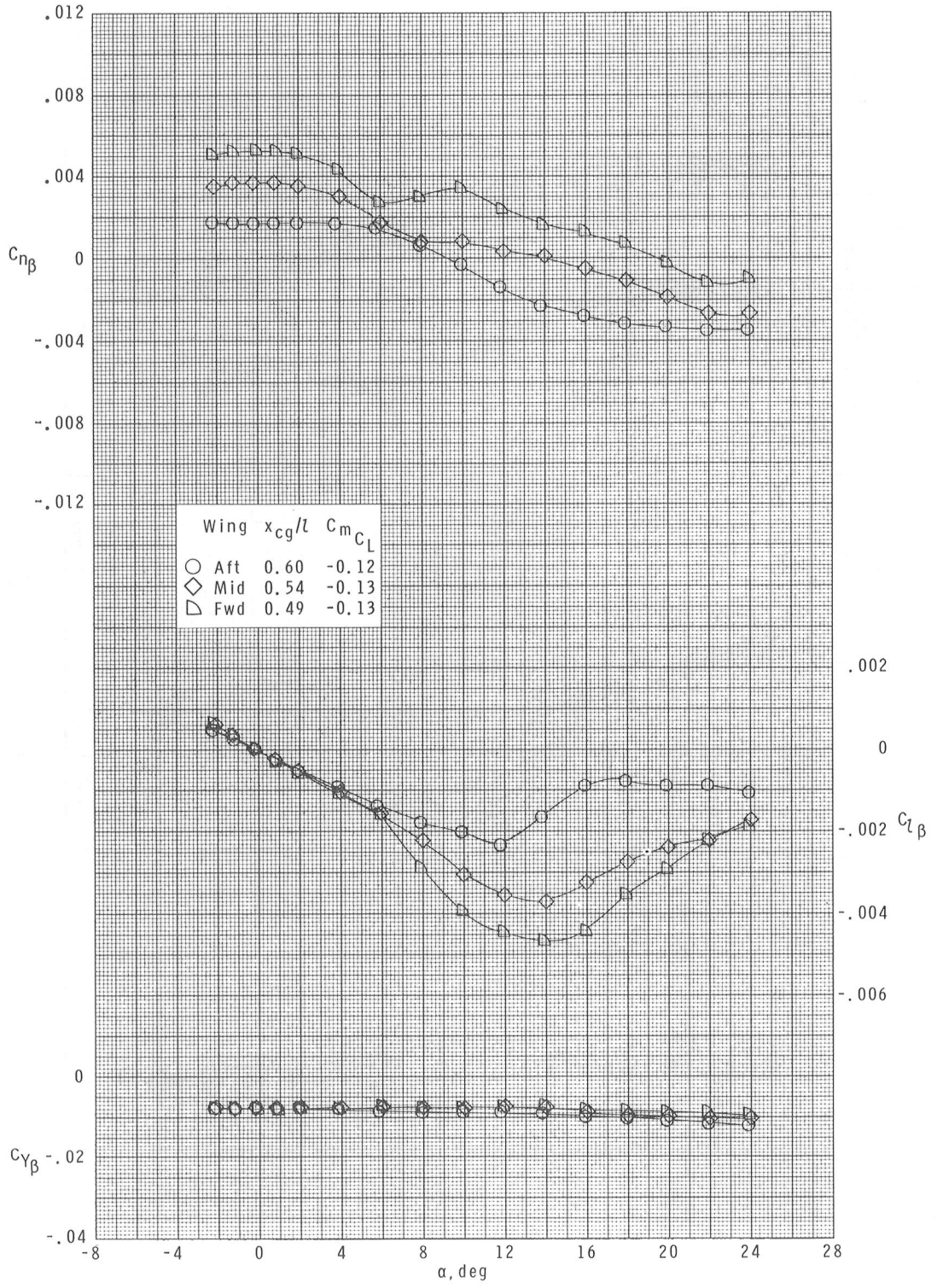

(b) Concluded.

Figure 19.- Continued.

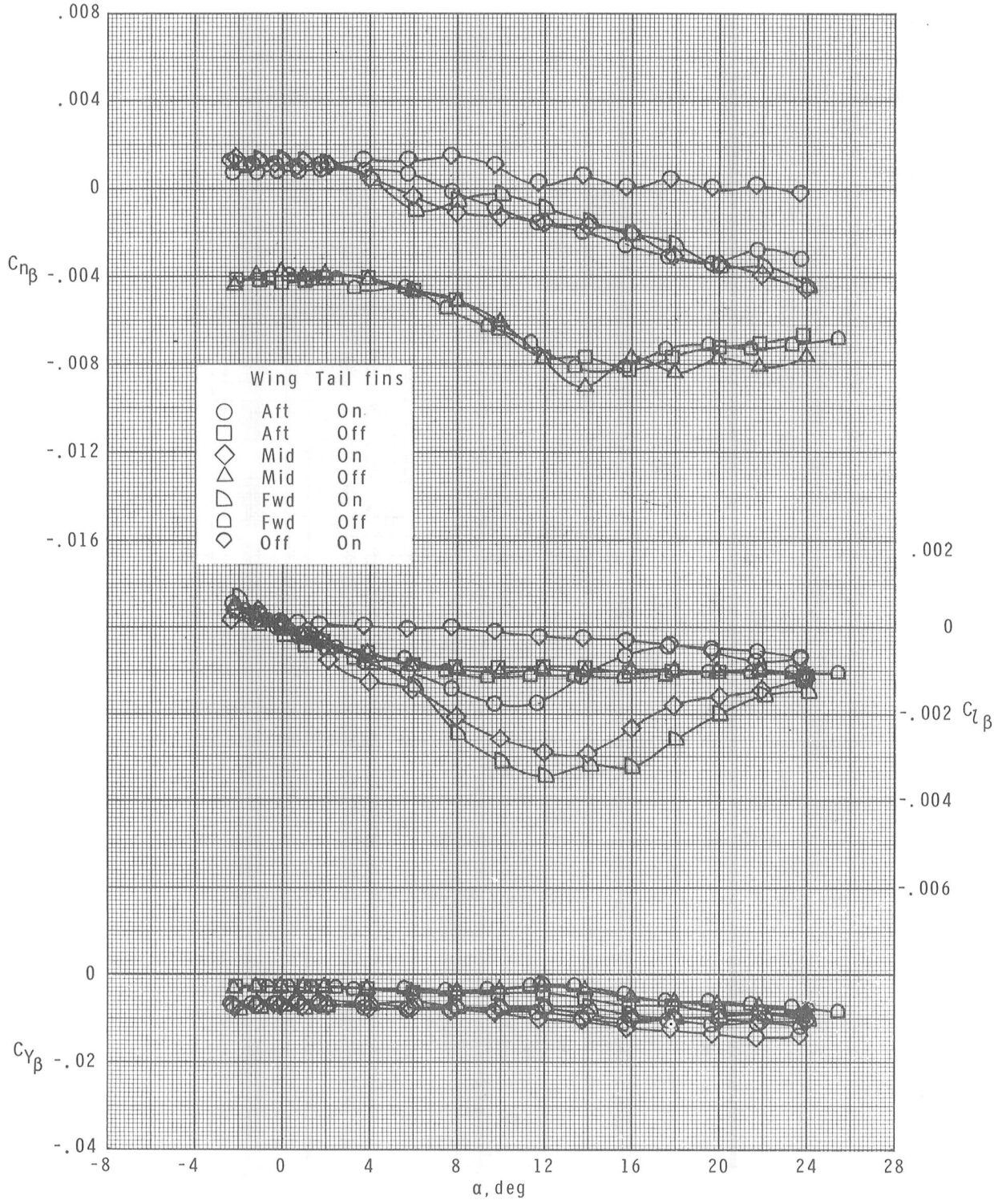

(c) M = 2.36.

Figure 19.- Continued.

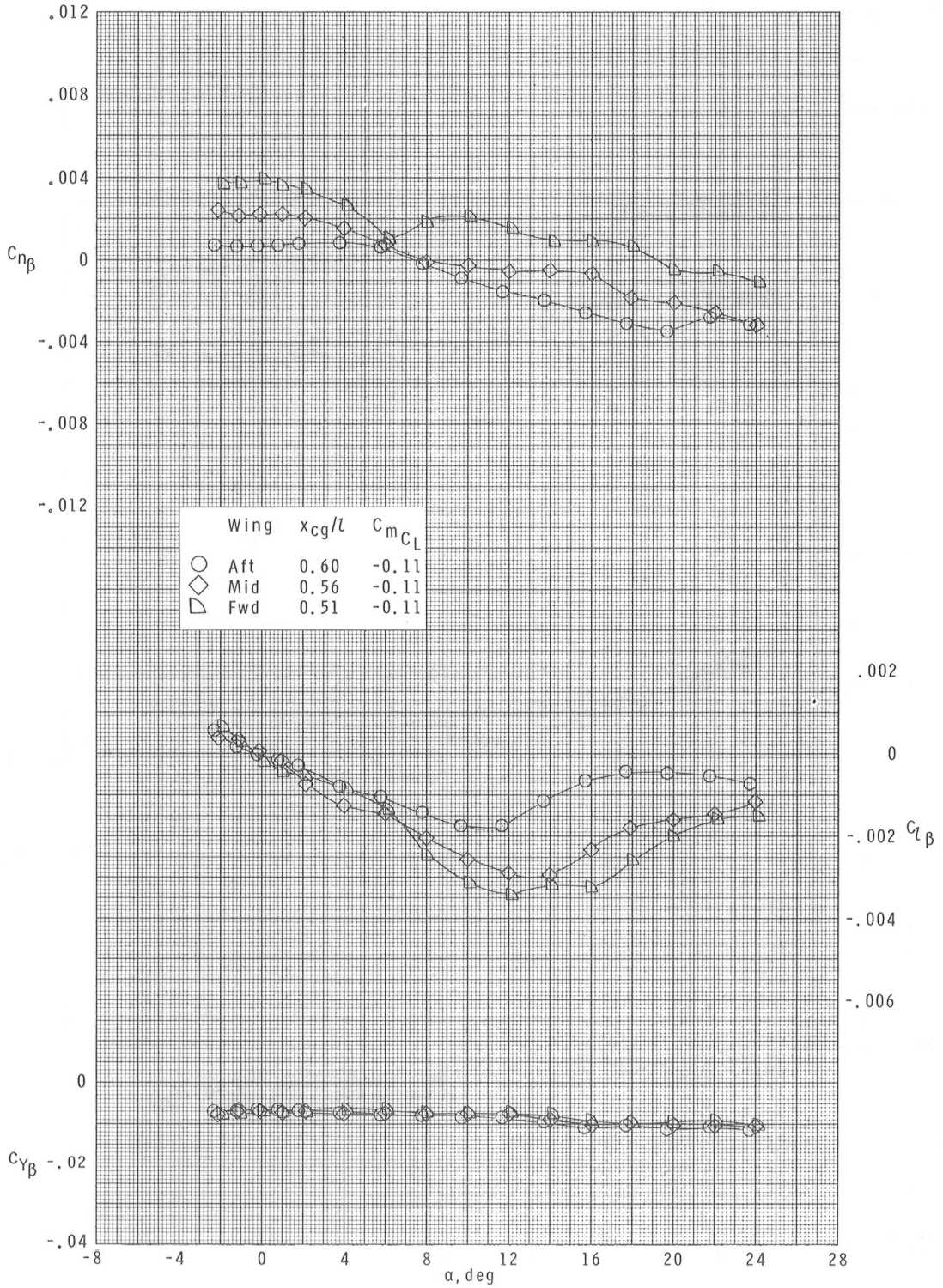

(c) Concluded.

Figure 19.- Continued.

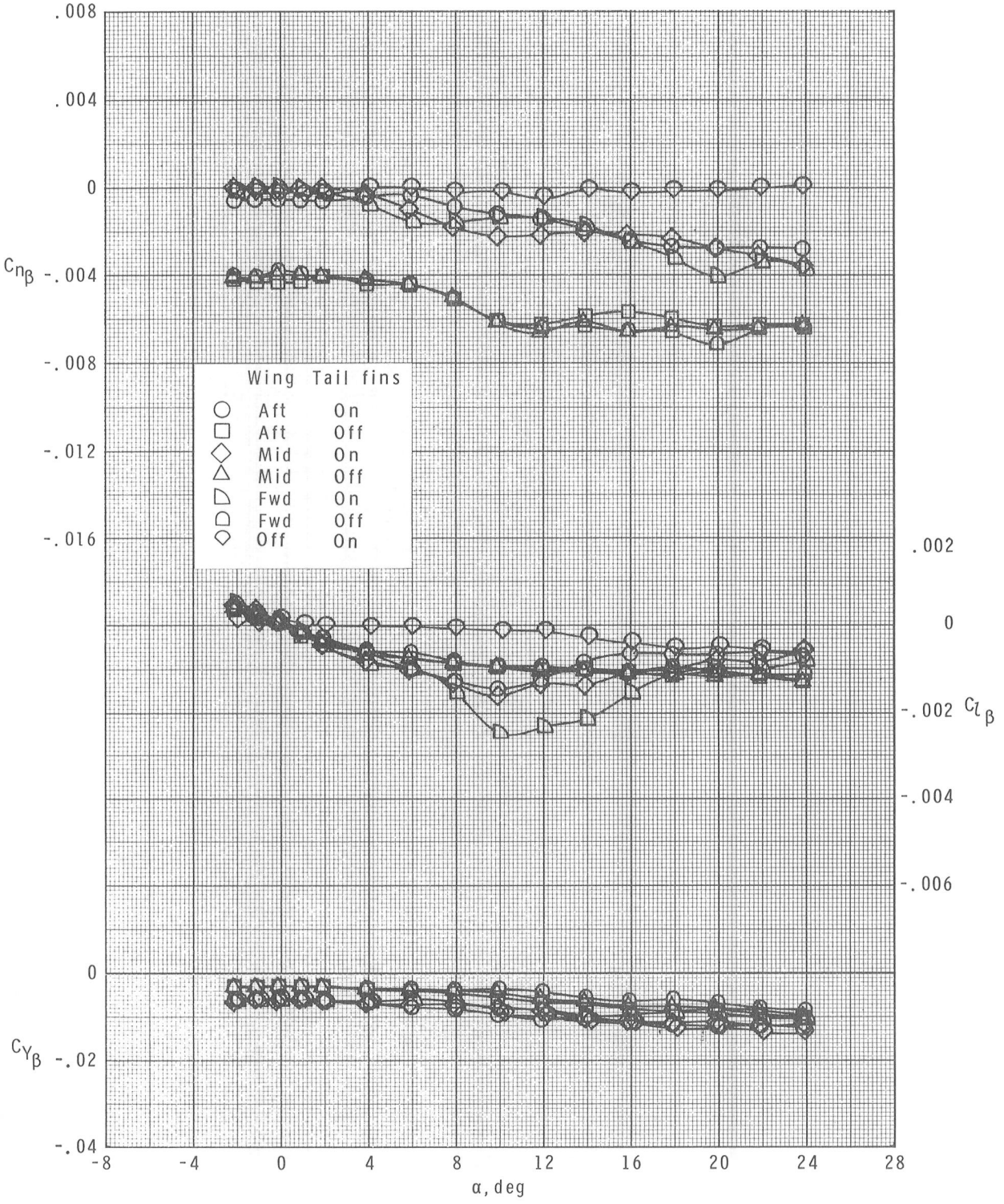

(d) M = 2.86.

Figure 19.- Concluded.

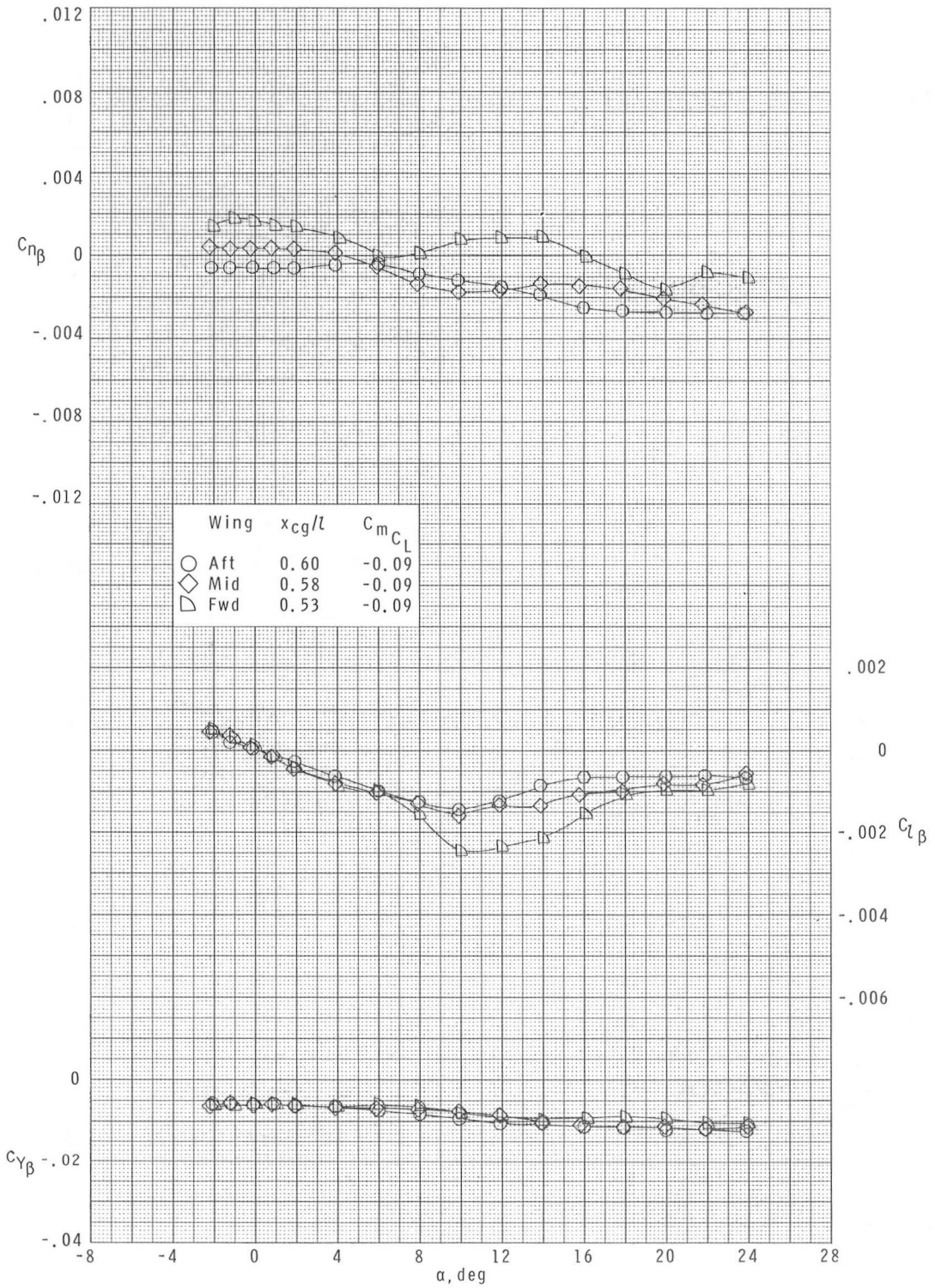

(d) Concluded.

Figure 19.- Concluded.

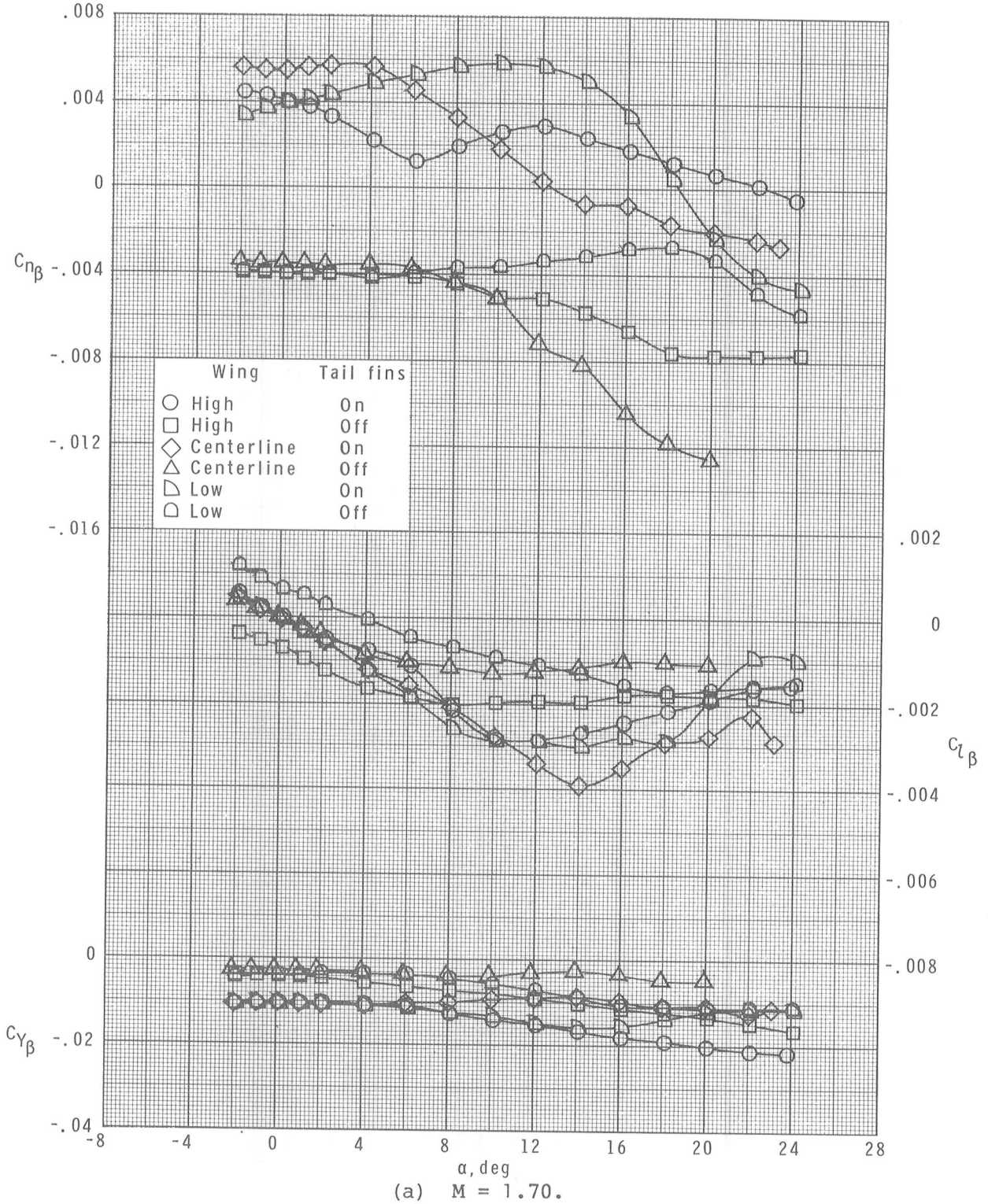

(a) M = 1.70.

Figure 20.- Effects of wing vertical location and tail fins on lateral and directional parameters of the aft-wing configurations. Zero control deflection.

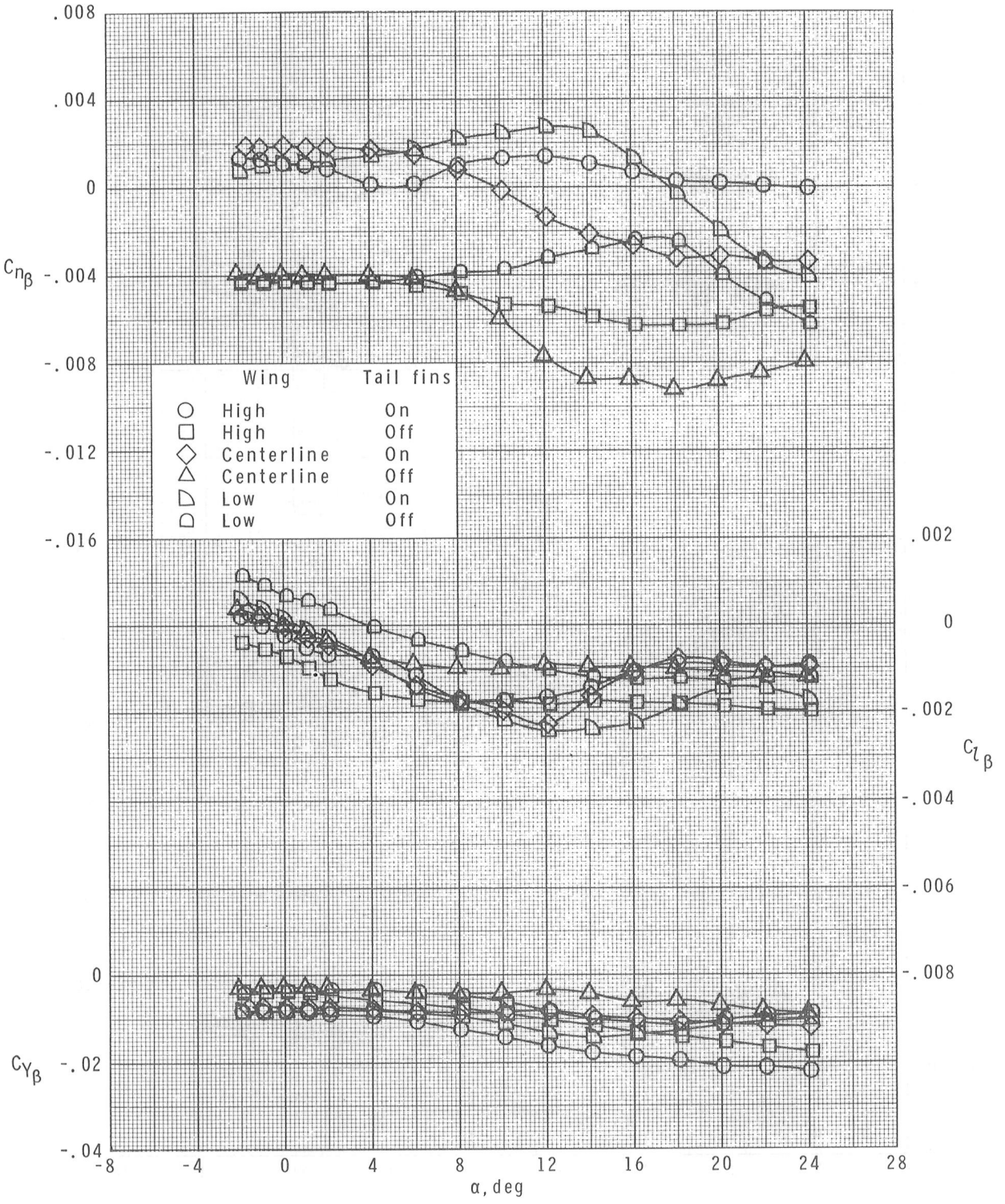

(b) M = 2.16.

Figure 20.- Continued.

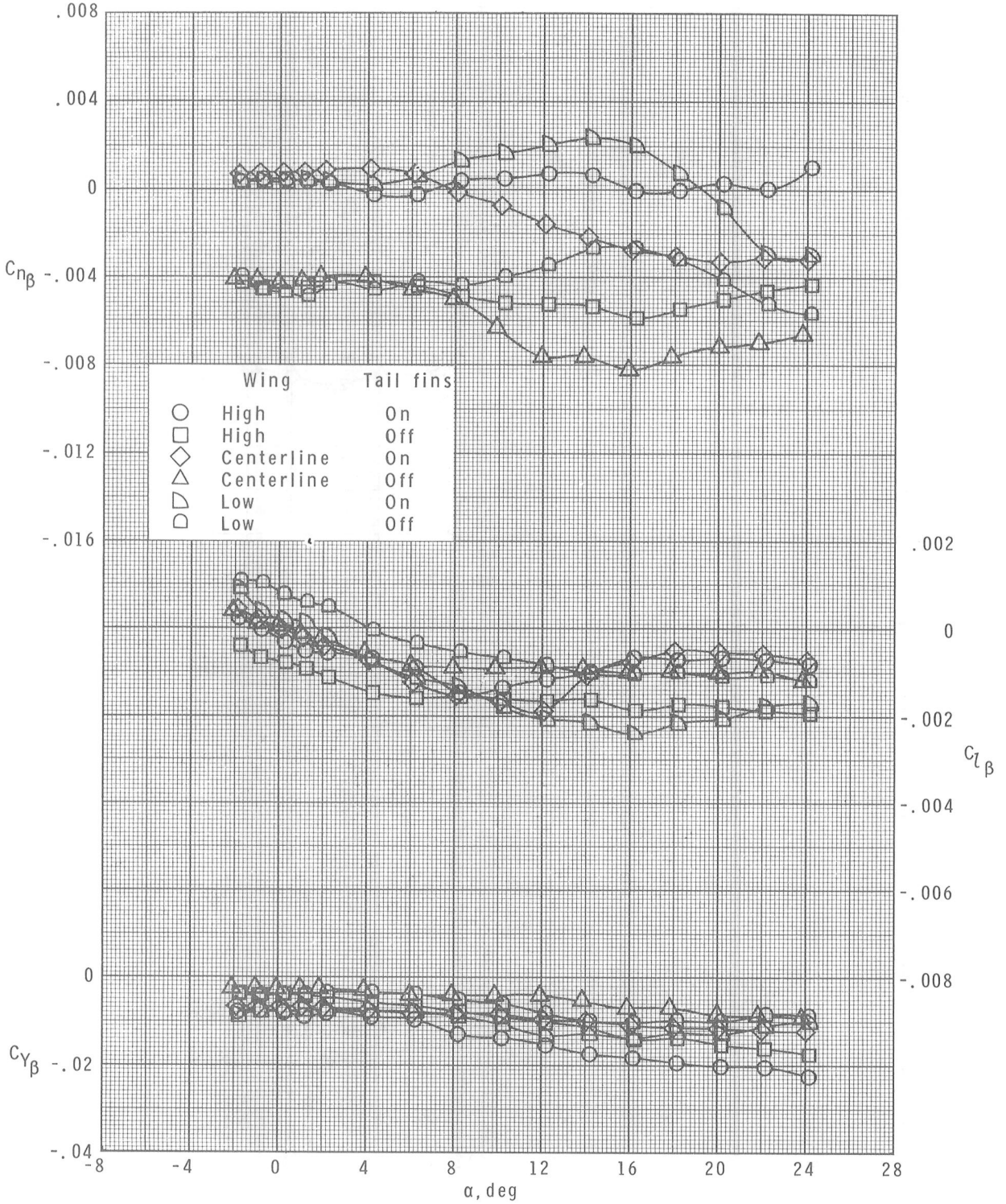

(c) M = 2.36.

Figure 20.- Continued.

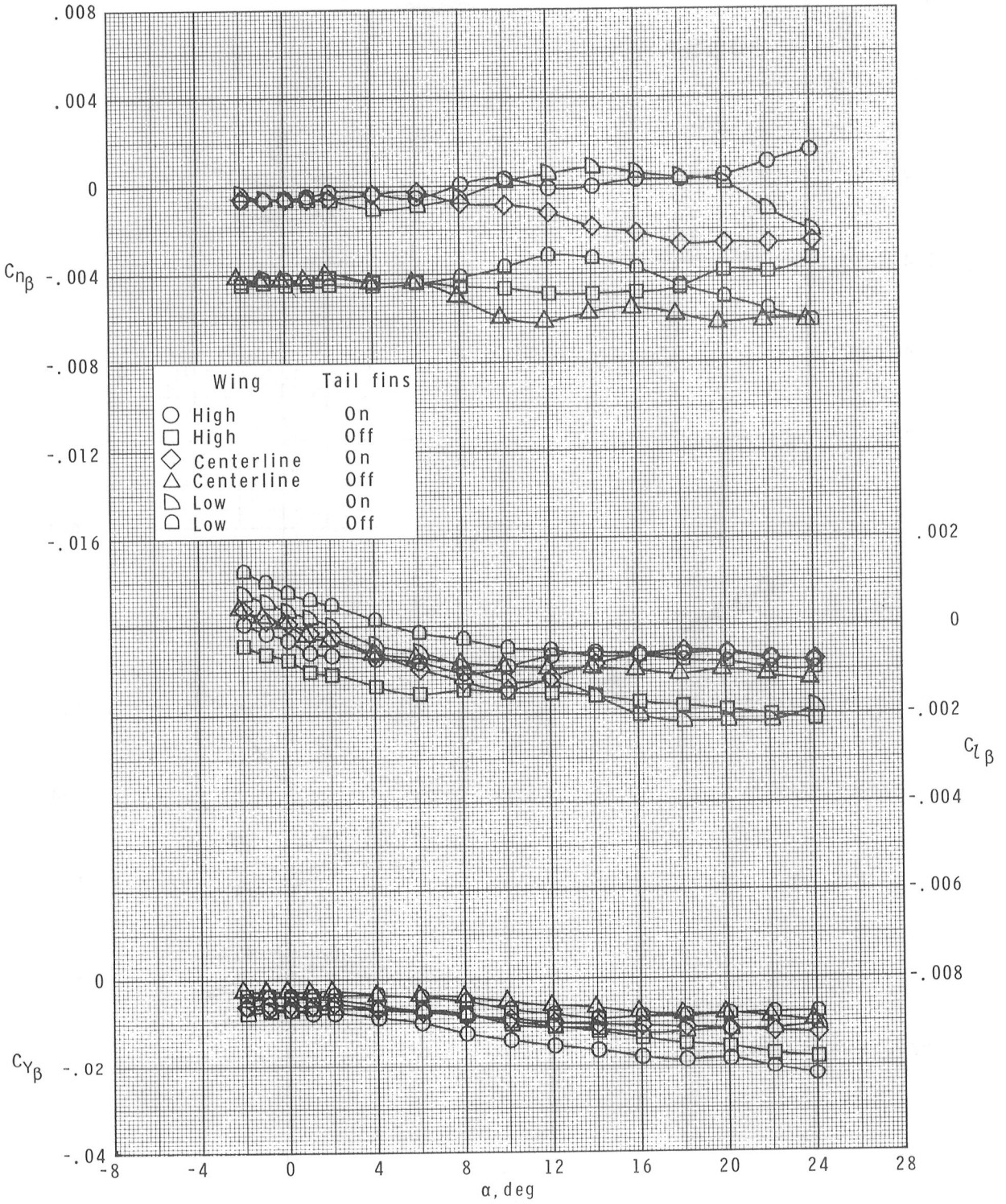

(d) M = 2.86.

Figure 20.- Concluded.

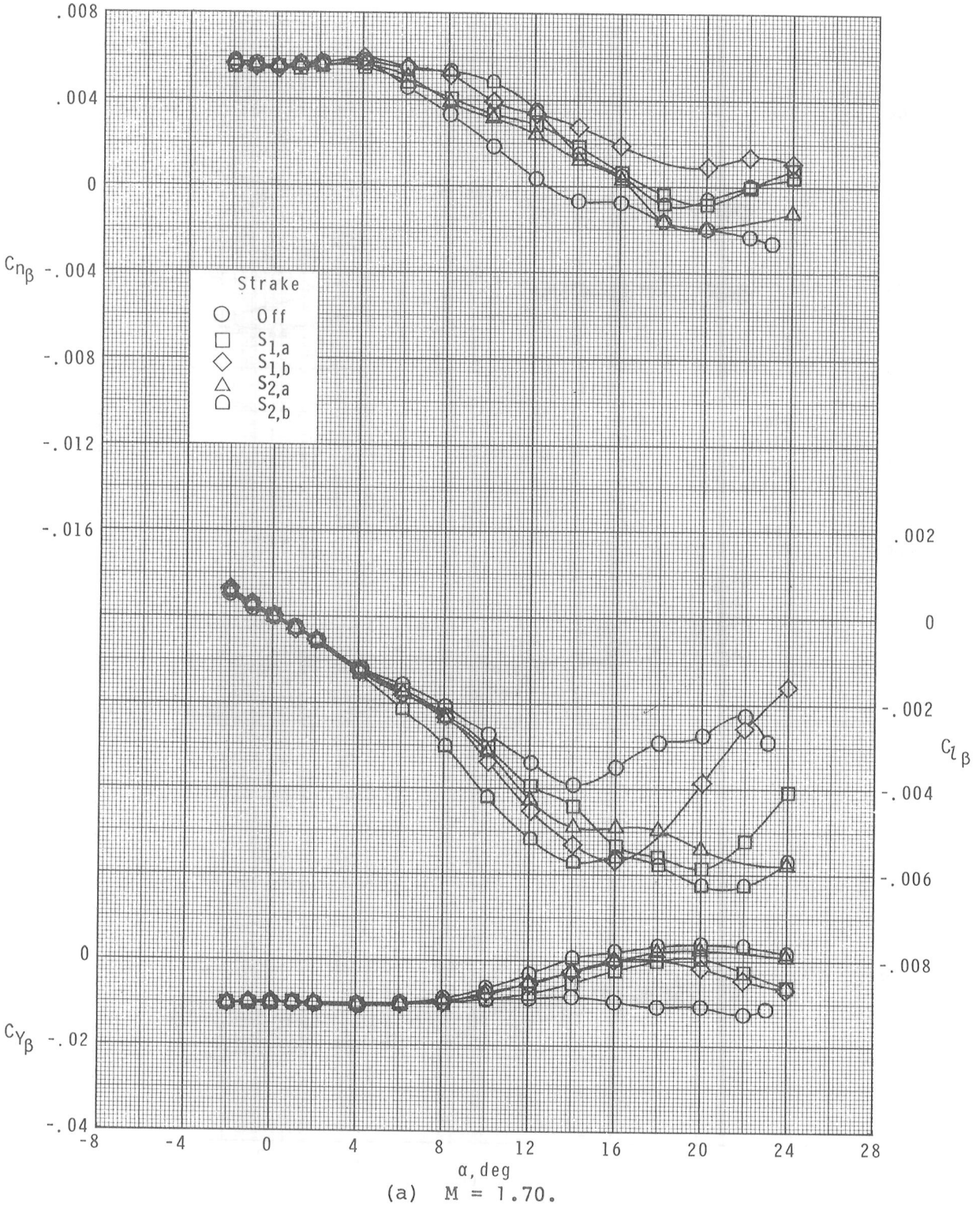

(a) M = 1.70.

Figure 21.- Effects of strake length and width on lateral and directional parameters of the centerline-aft-wing configuration for nose and nose-body strakes. Zero control deflection.

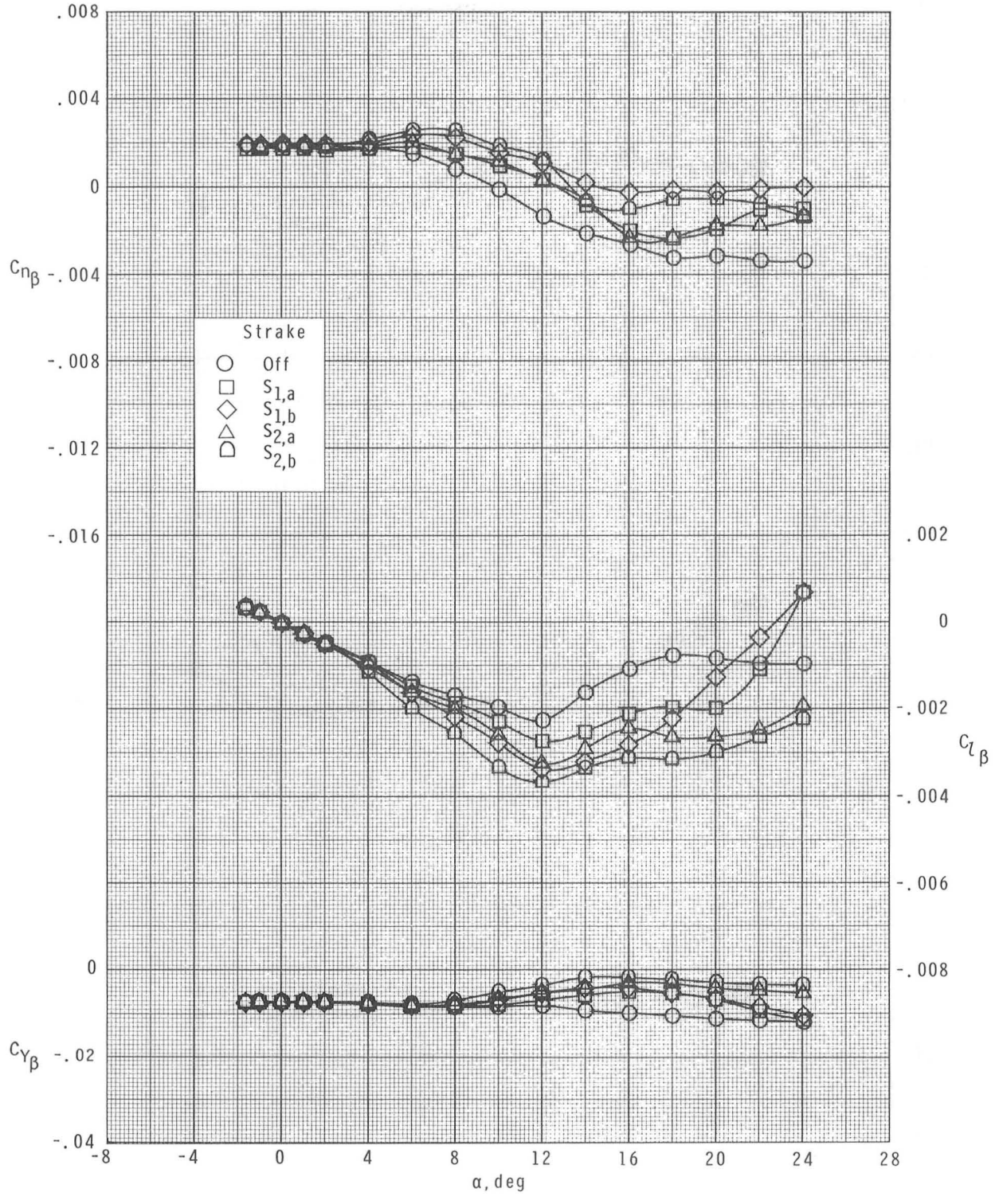

(b) M = 2.16.

Figure 21.- Continued.

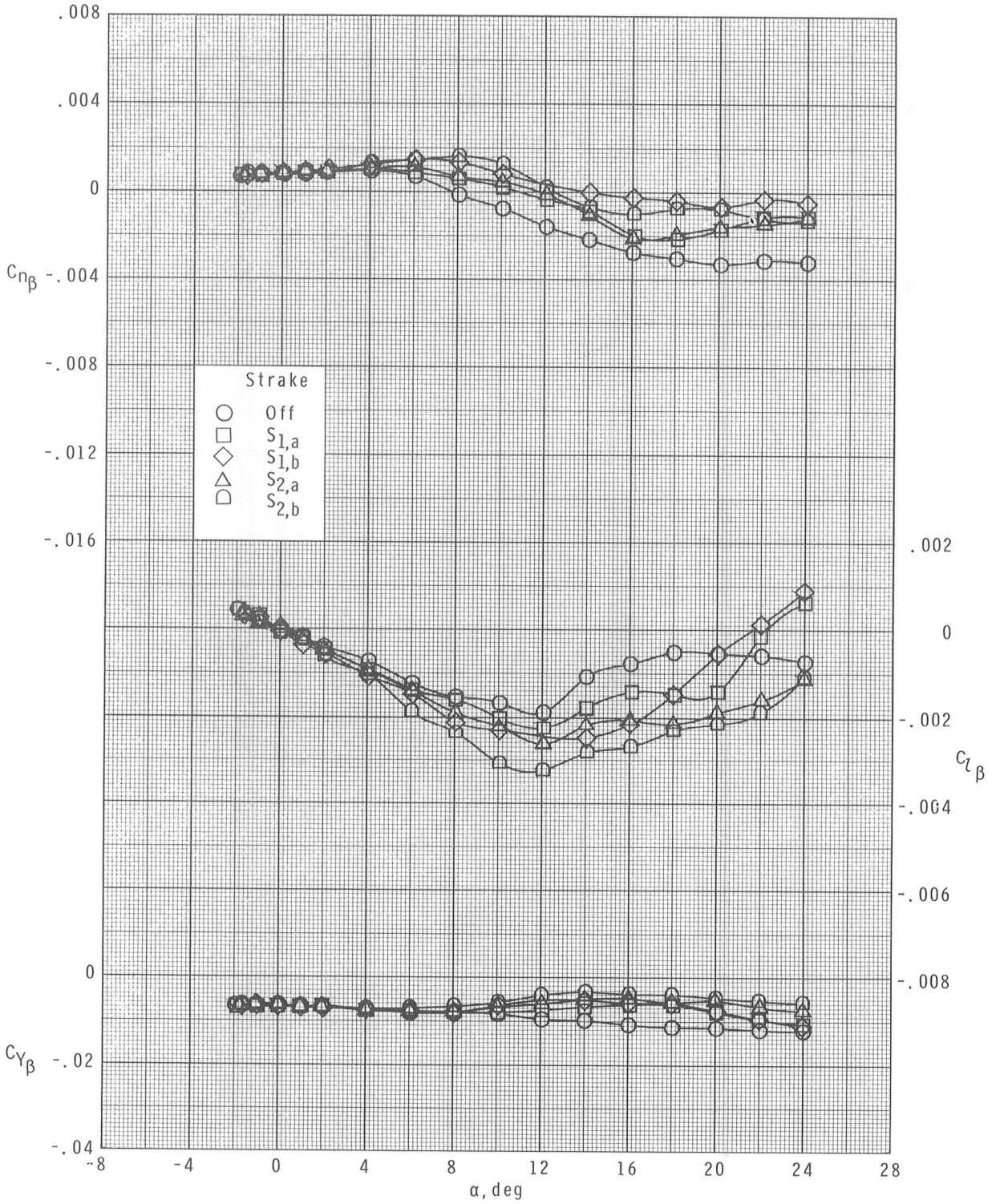

(c) M = 2.36.

Figure 21.- Continued.

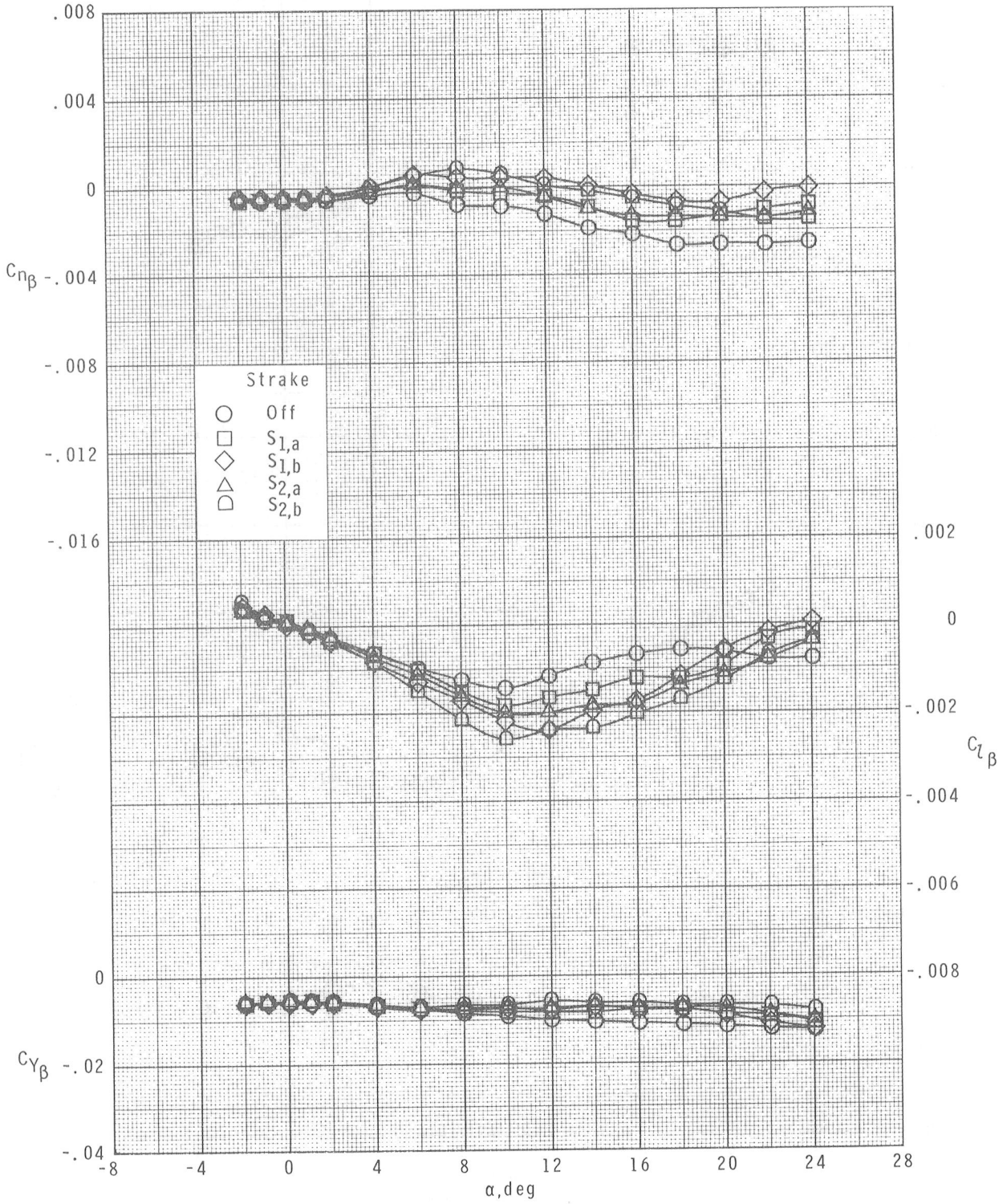

(d) M = 2.86.

Figure 21.- Concluded.

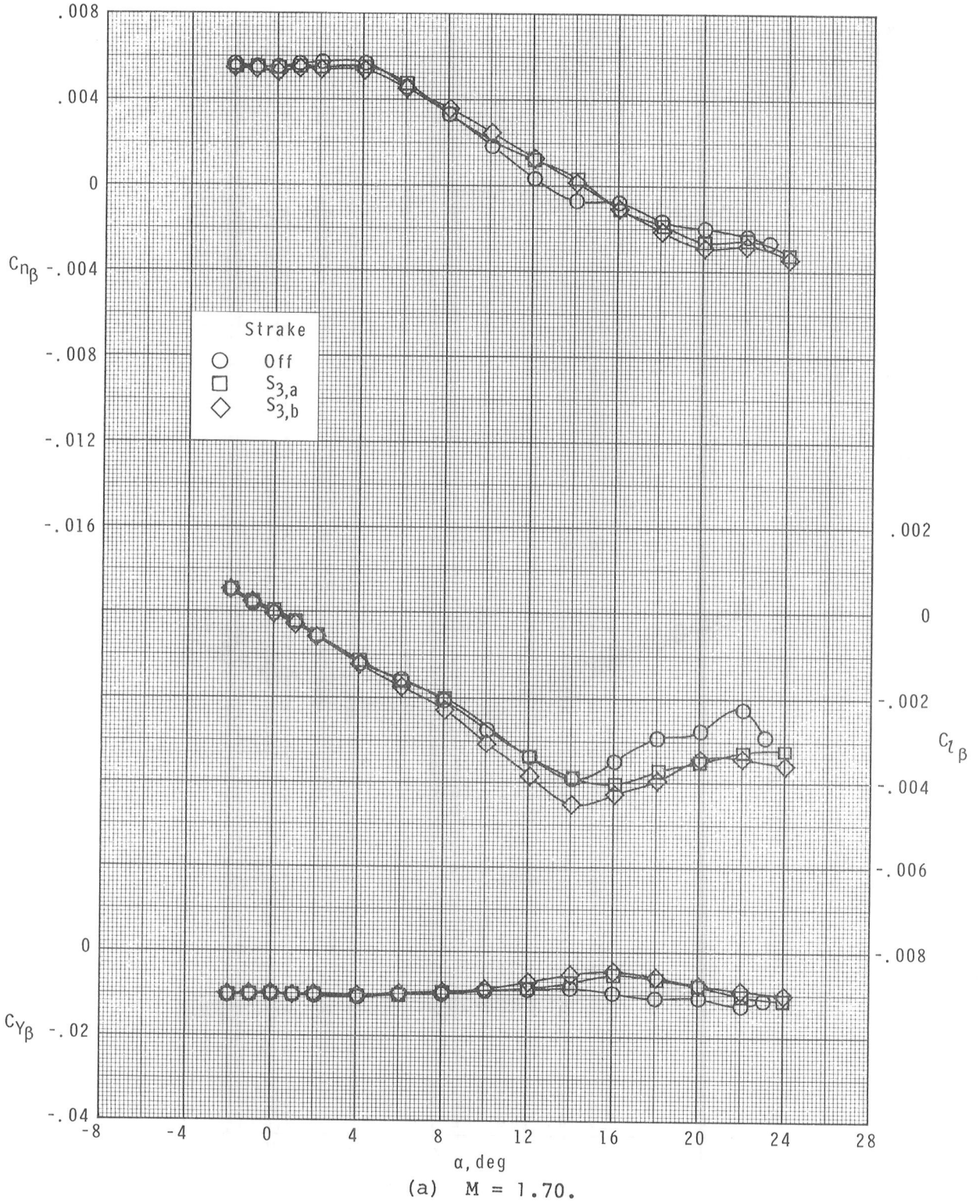

(a) M = 1.70.

Figure 22.- Effects of strake length and width on lateral and directional parameters of the centerline-aft-wing configuration for body strake. Zero control deflection.

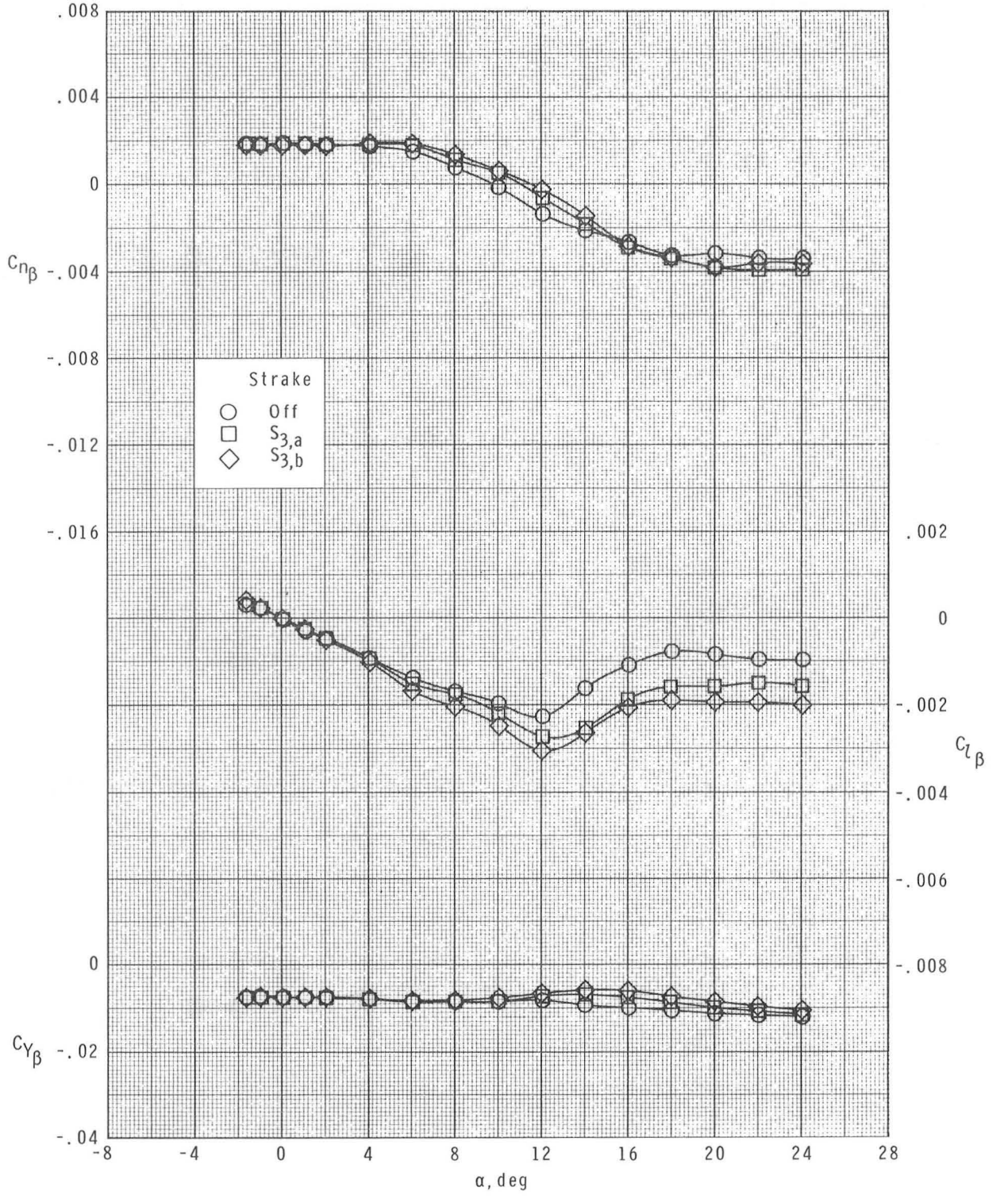

(b) M = 2.16.

Figure 22.- Continued.

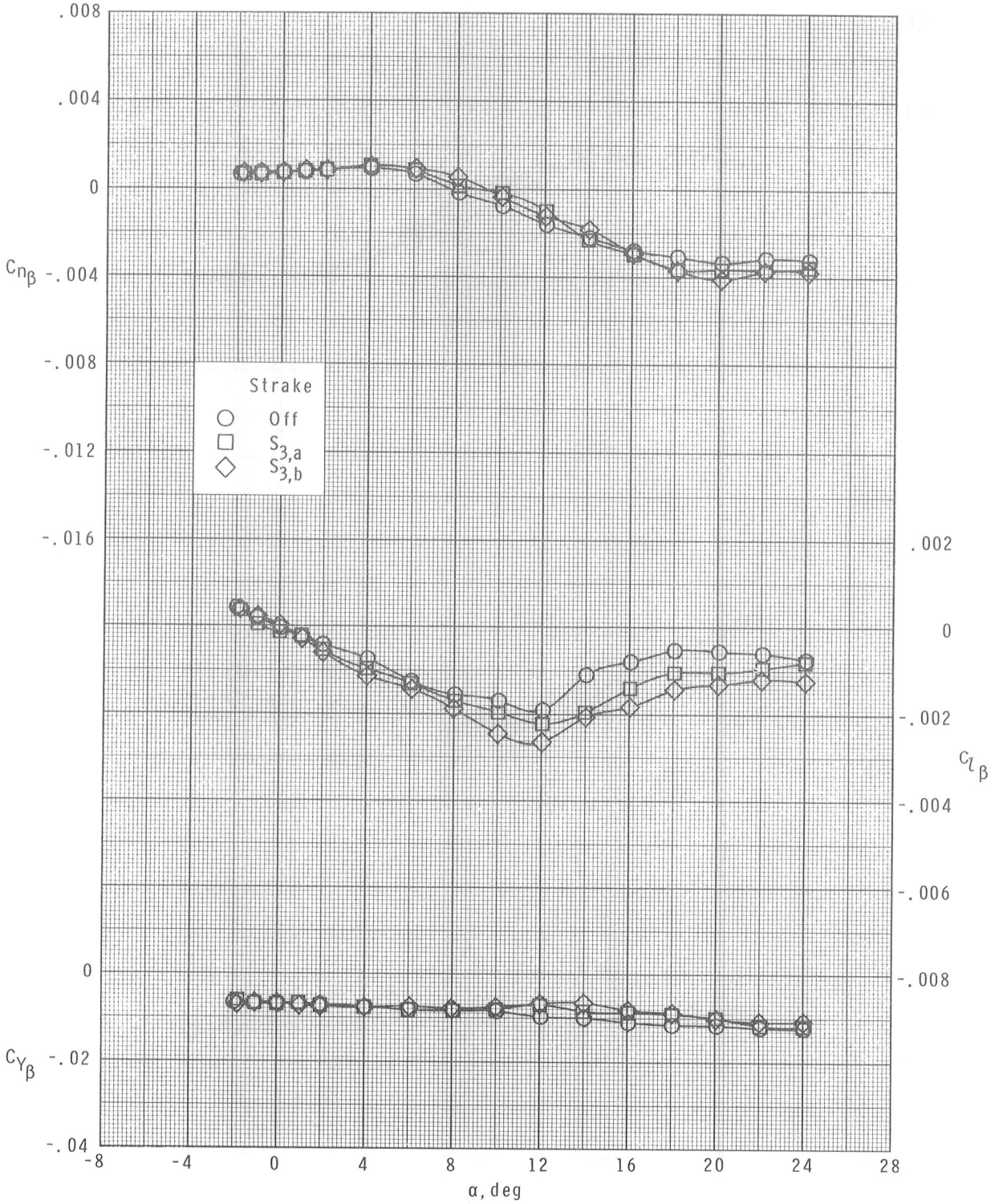

(c) M = 2.36.

Figure 22.- Continued.

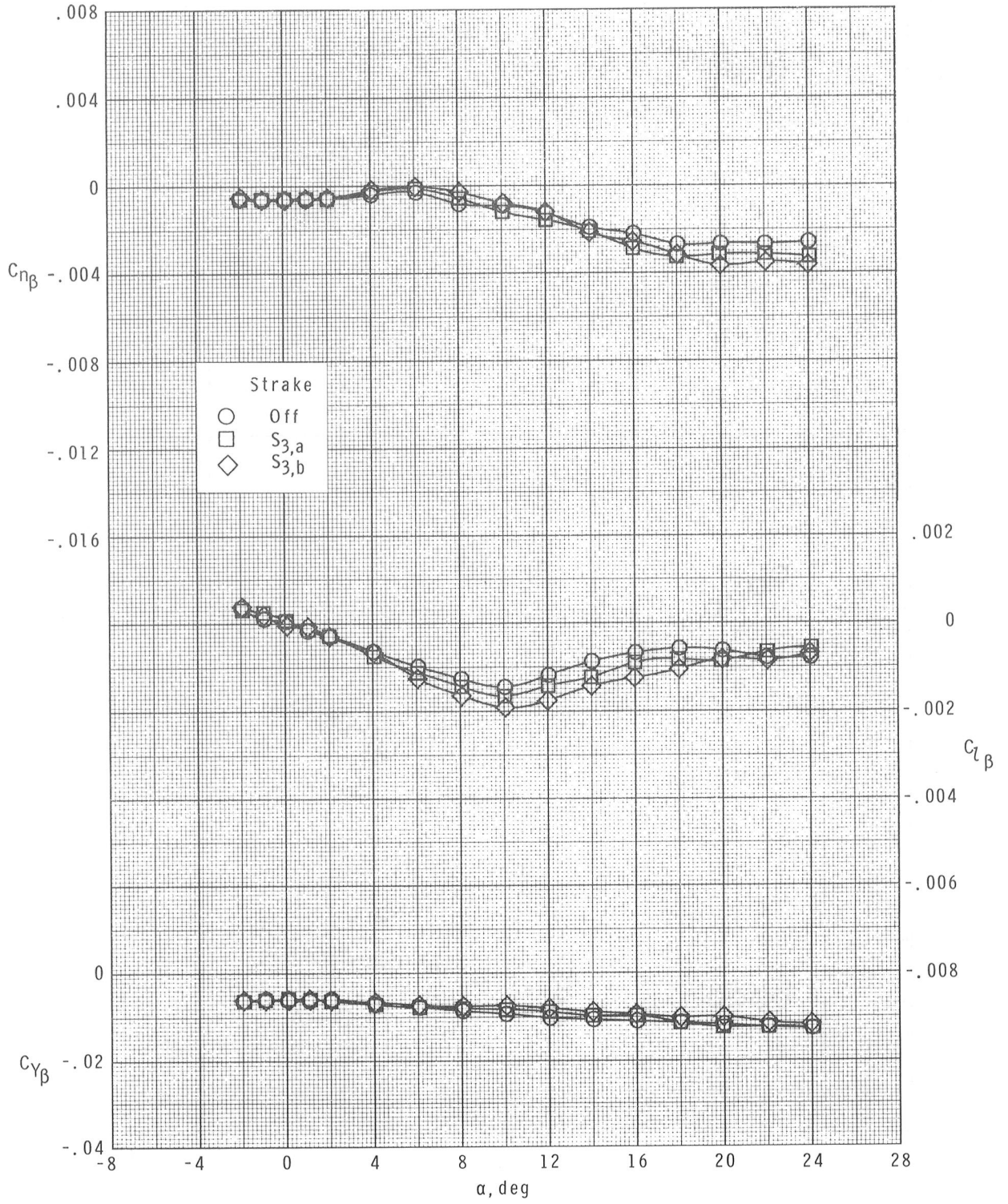

(d) M = 2.86.

Figure 22.- Concluded.

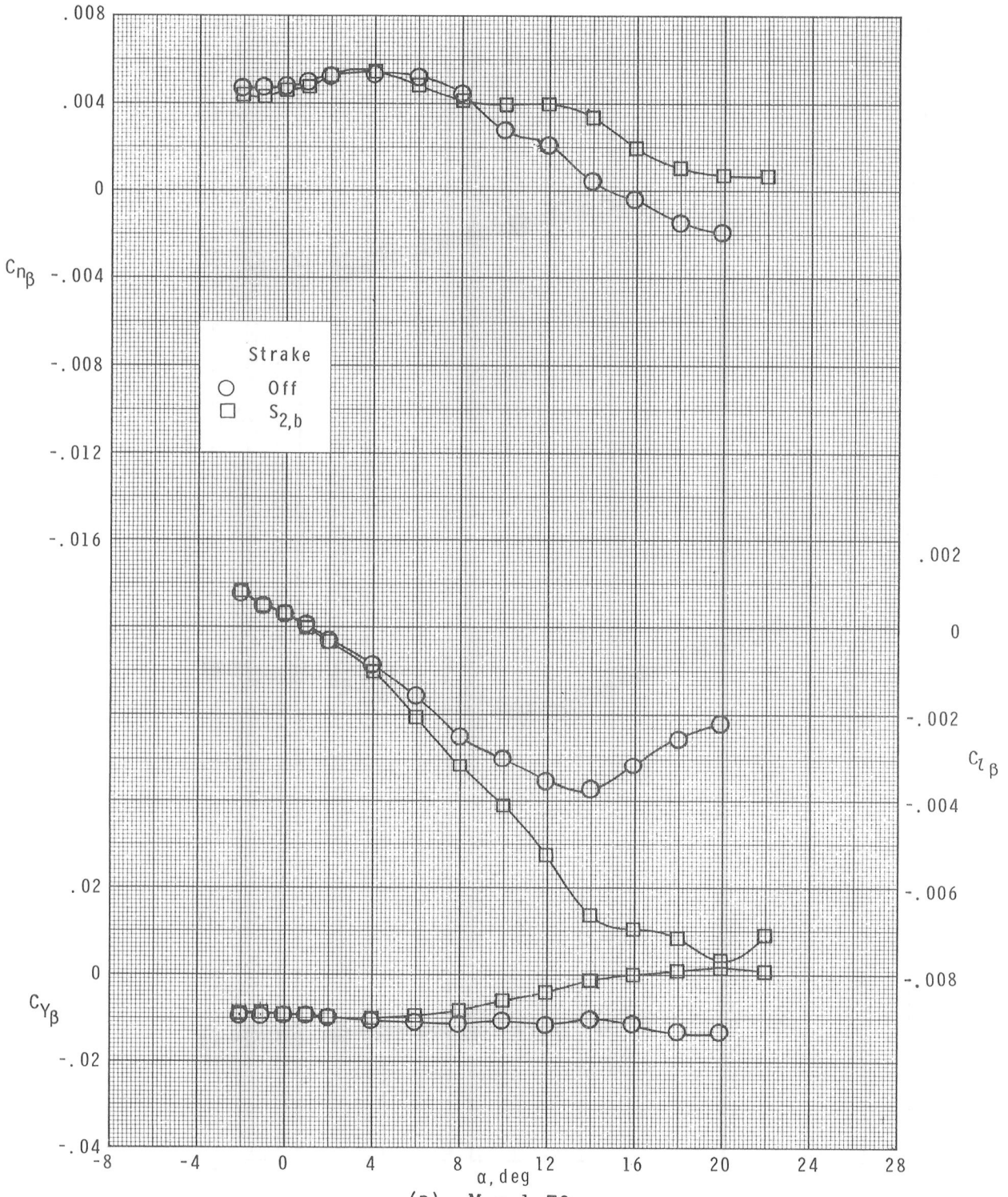

(a) M = 1.70.

Figure 23.- Effects of nose-body strake on the lateral and directional parameters of the centerline-aft-wing configuration with pitch control. $\delta_{pitch} = -20^o$.

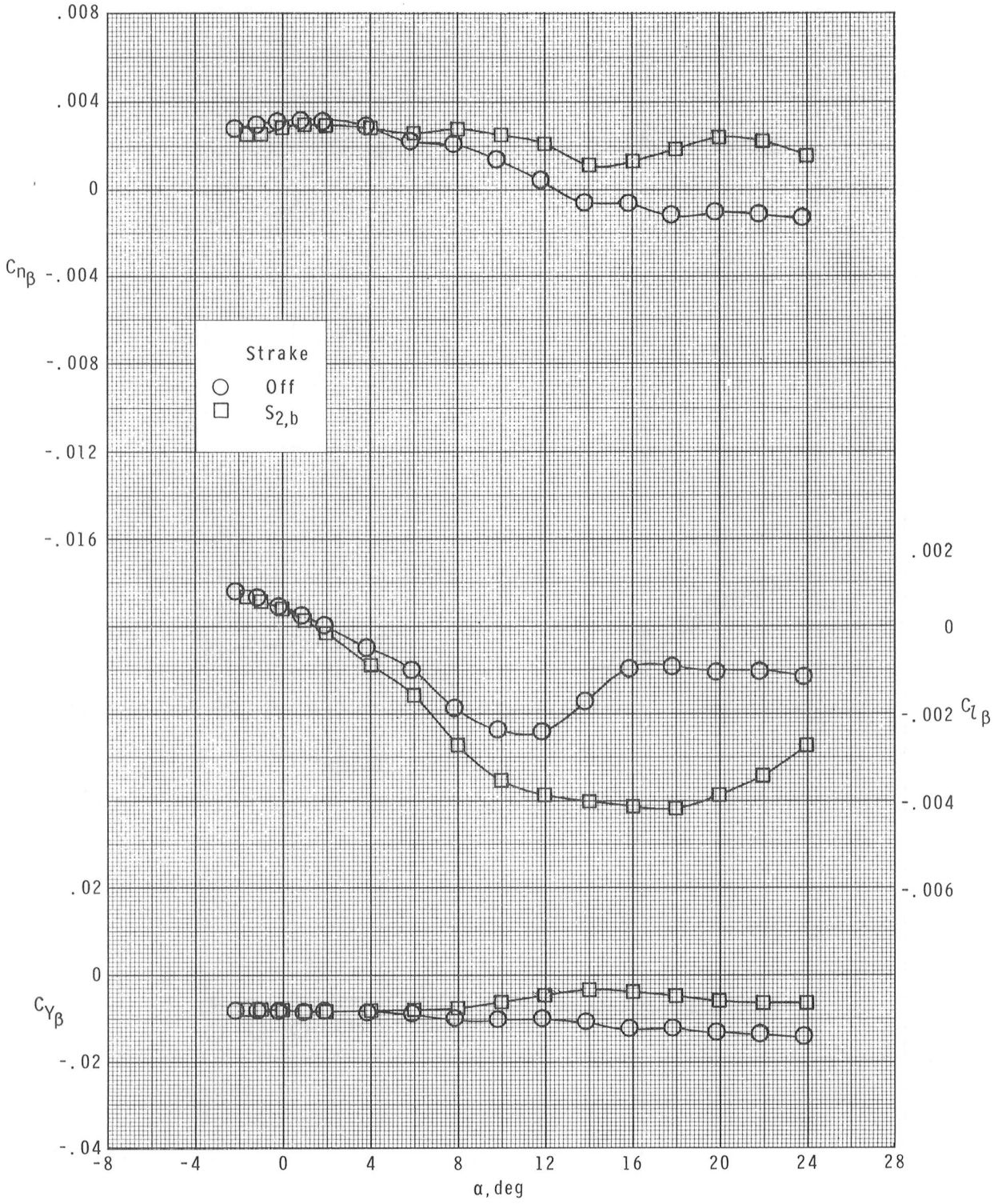

(b) M = 2.16.

Figure 23.- Continued.

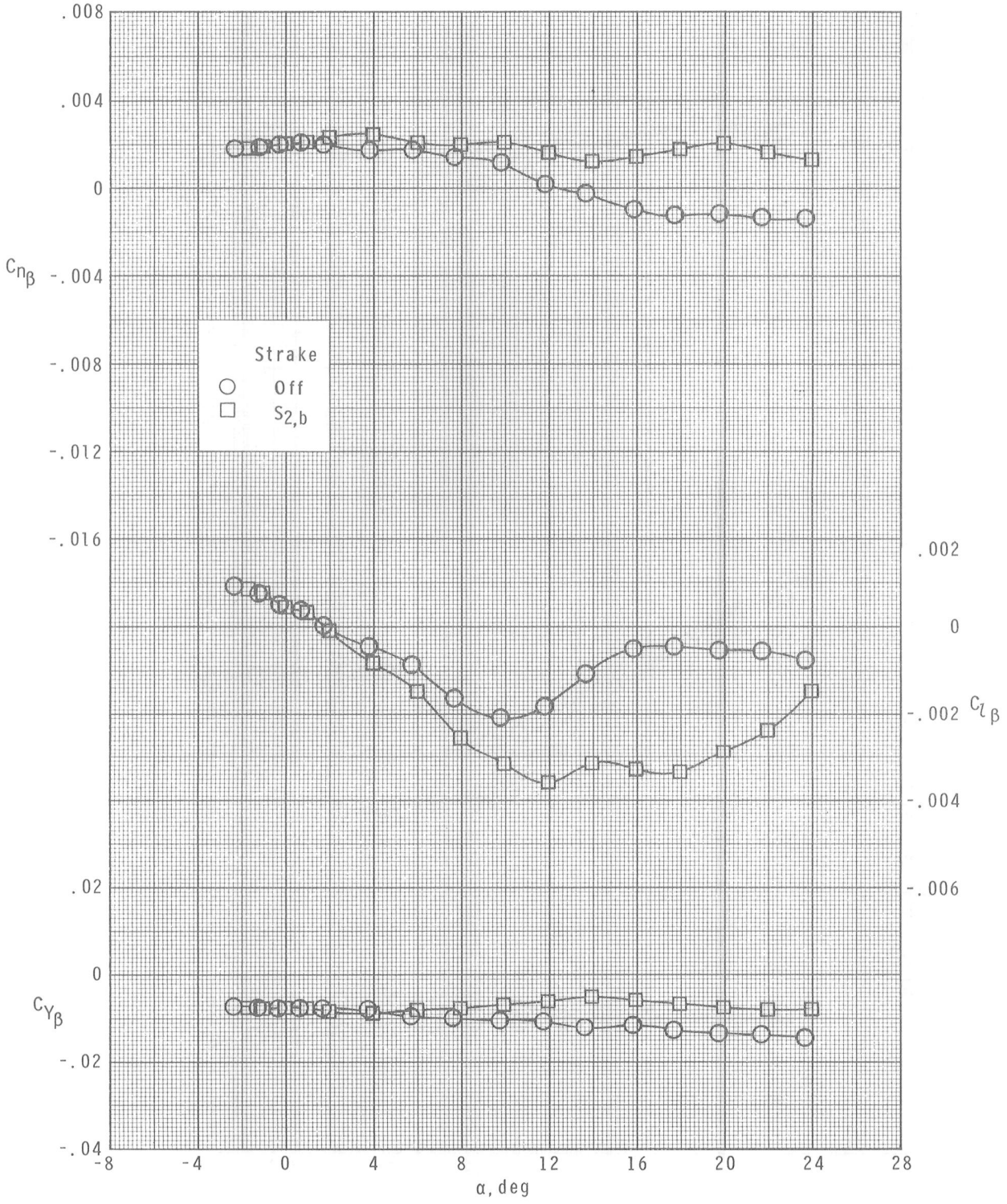

(c) M = 2.36.

Figure 23.- Continued.

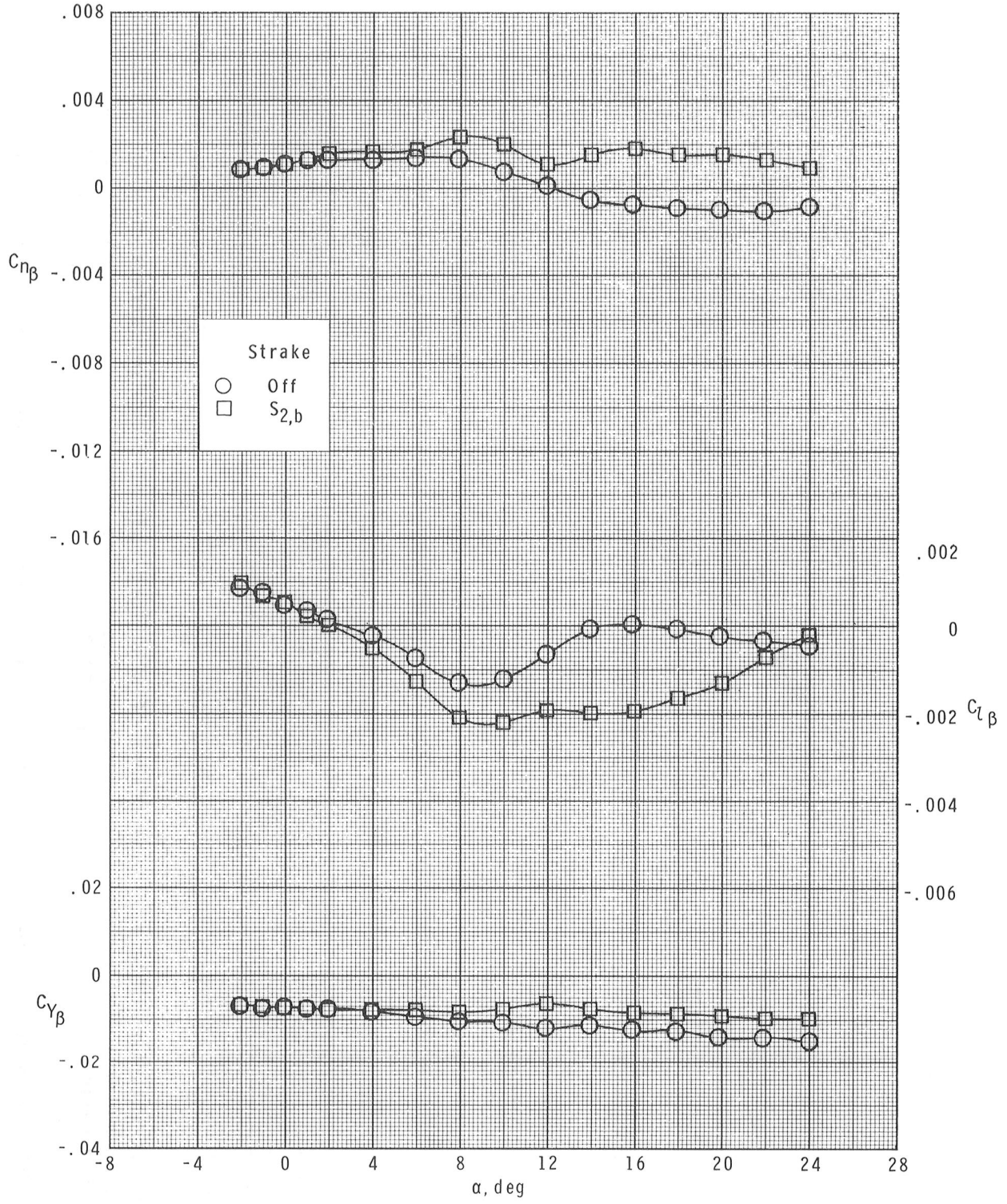

(d) M = 2.86.

Figure 23.- Concluded.

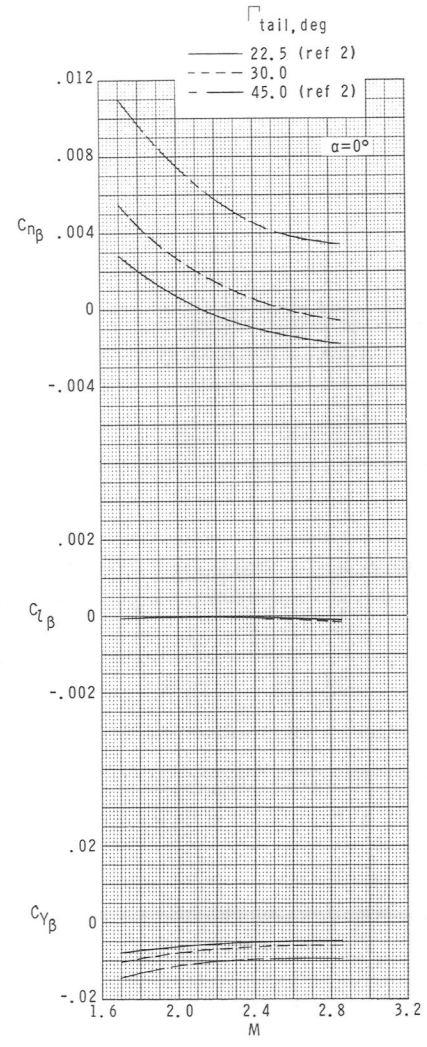

(a) Effect of tail-fin dihedral angle; centerline-aft-wing configuration.

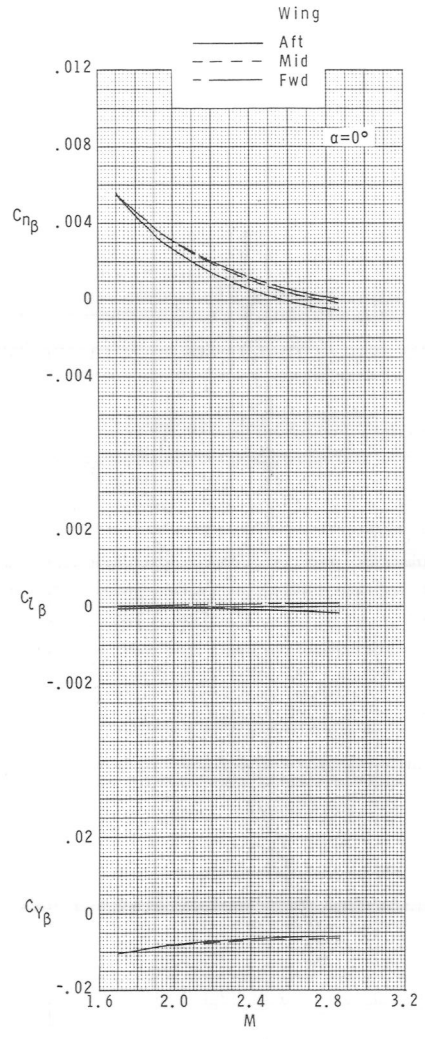

(b) Effect of wing longitudinal location; centerline wing. $\Gamma_{tail} = 30.0^{o}$.

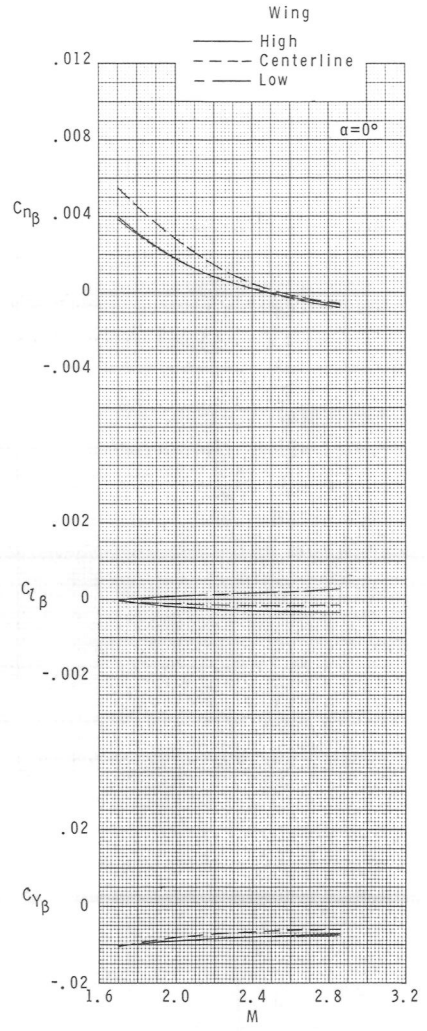

(c) Effect of wing vertical location; aft wing. $\Gamma_{tail} = 30.0^{o}$.

Figure 24.- Summary of lateral and directional aerodynamic parameters. Zero control deflection.

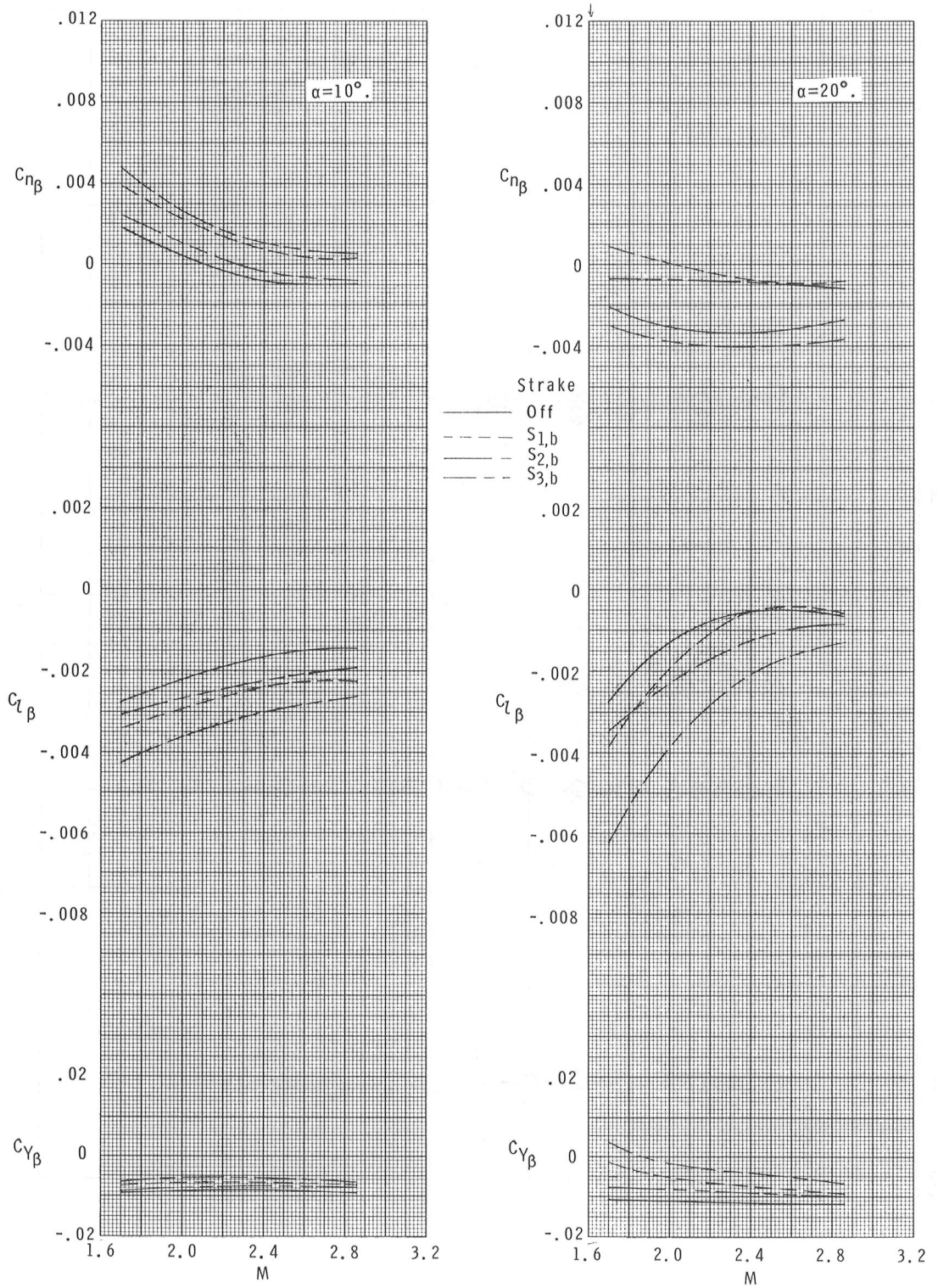

(d) Effect of strakes, centerline-aft-wing configuration. $\Gamma_{tail} = 30.0^{o}$.

Figure 24.- Concluded.

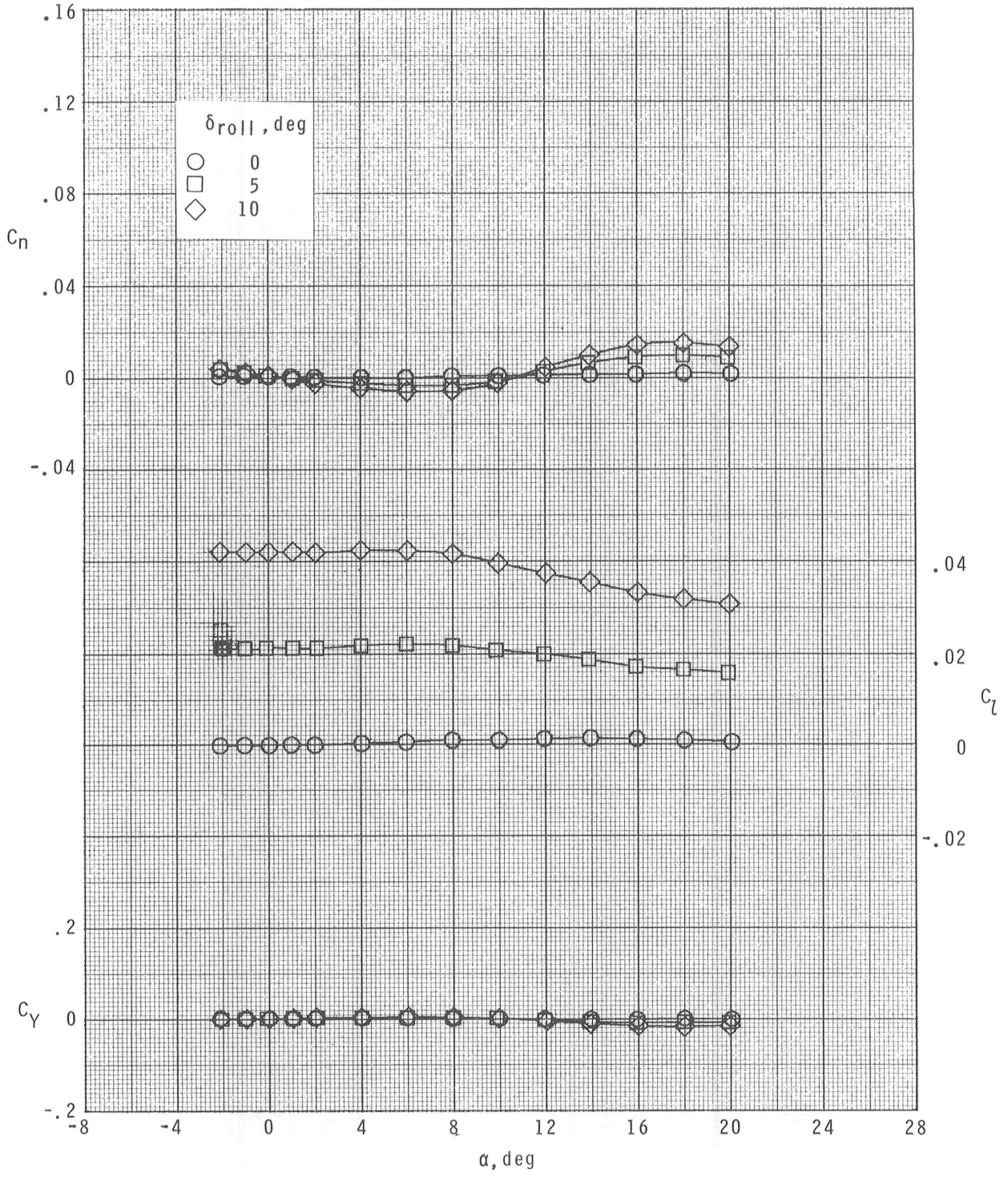

(a) M = 1.70.

Figure 25.- Roll-control characteristics of the centerline-aft-wing configurations.

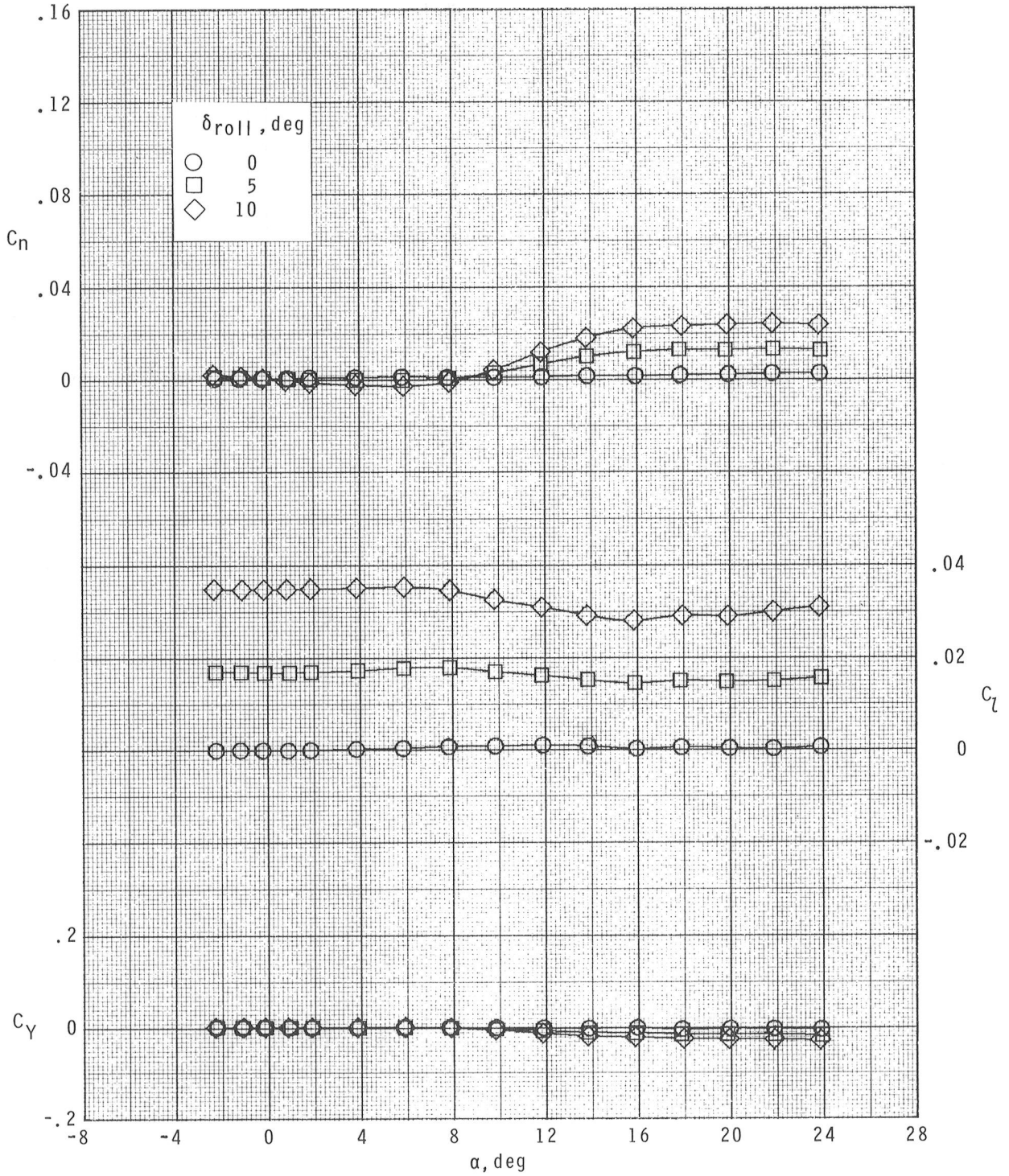

(b) M = 2.16.

Figure 25.- Continued.

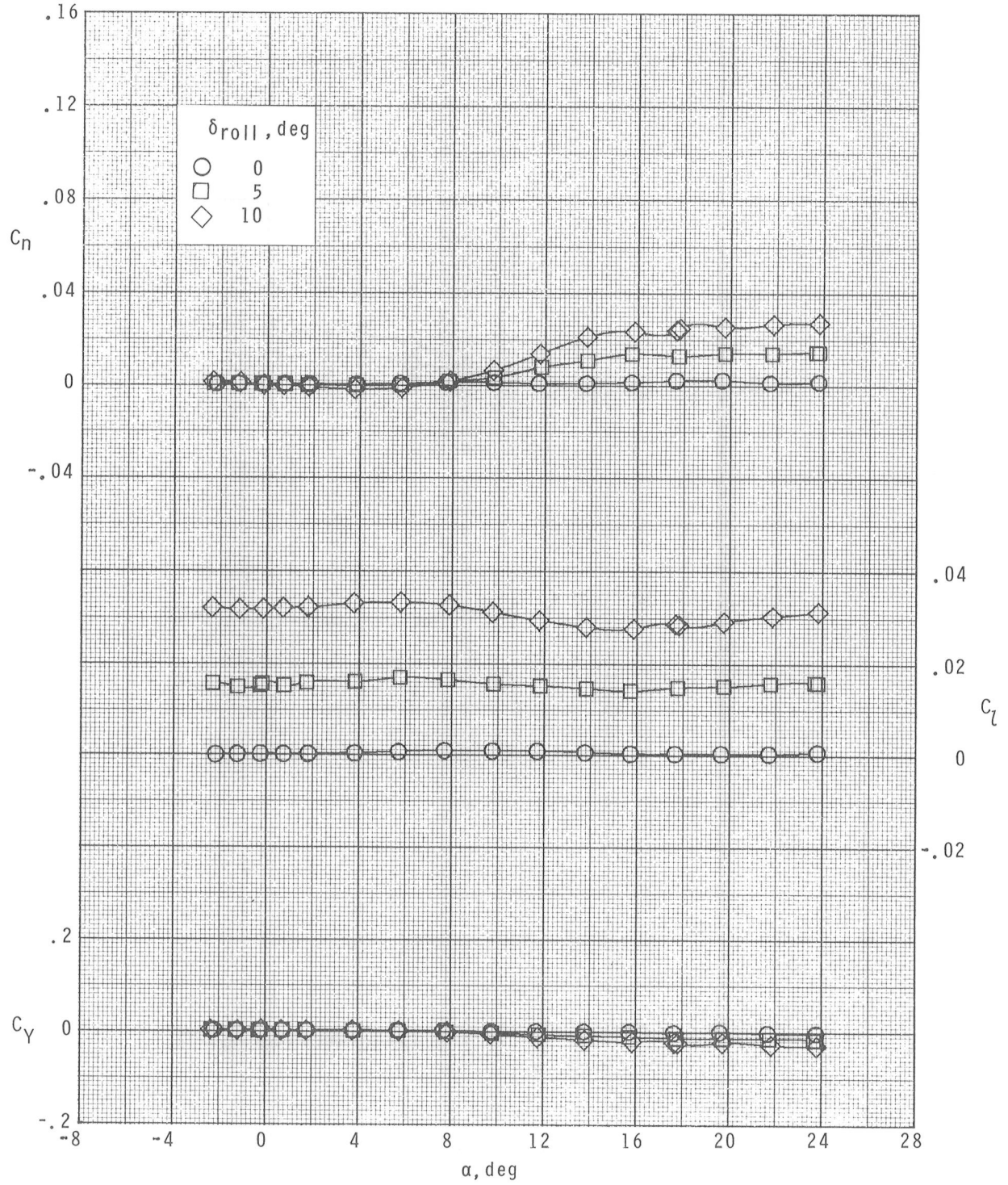

(c) M = 2.36.

Figure 25.- Continued.

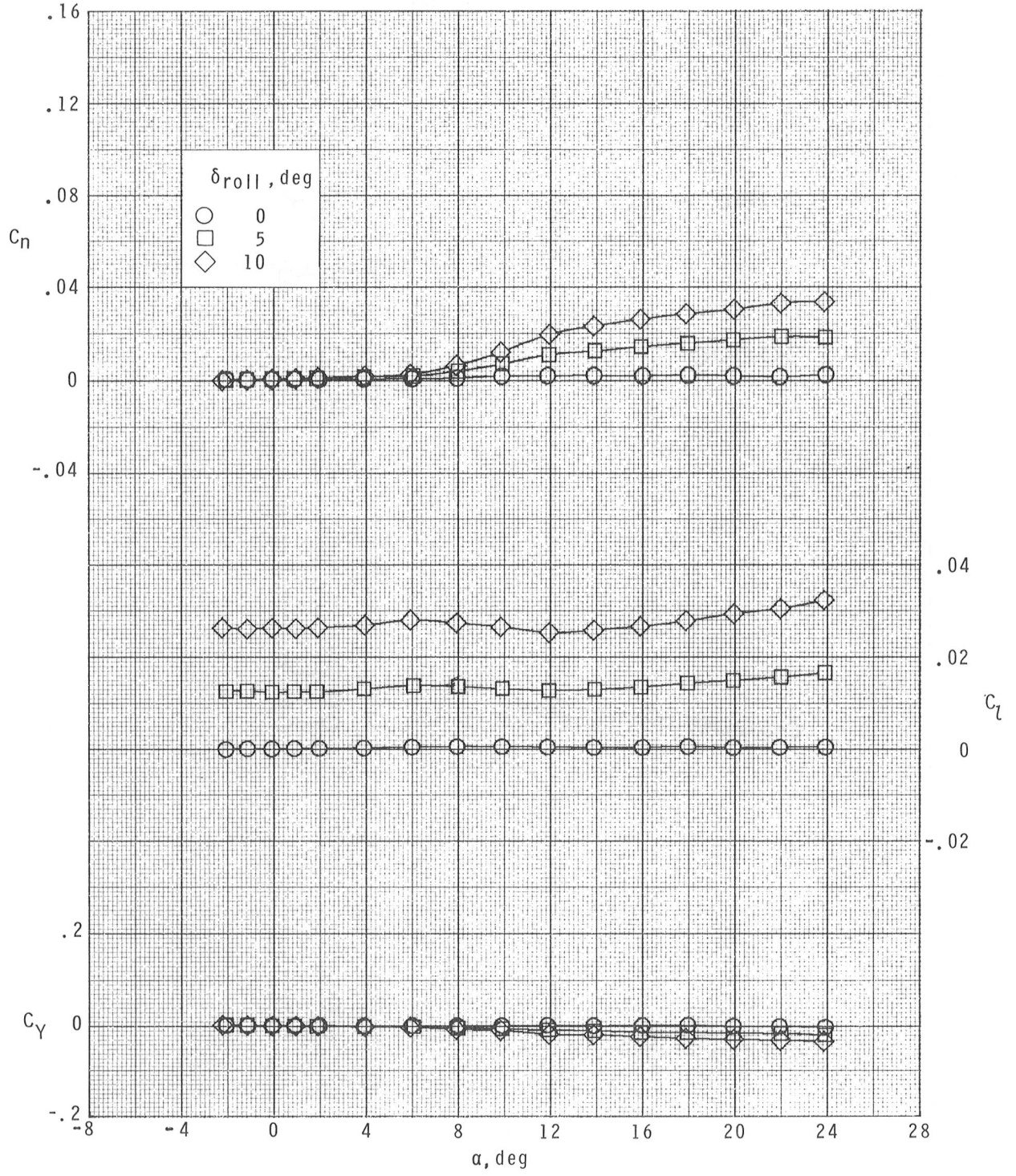

(d) M = 2.86.

Figure 25.- Concluded.

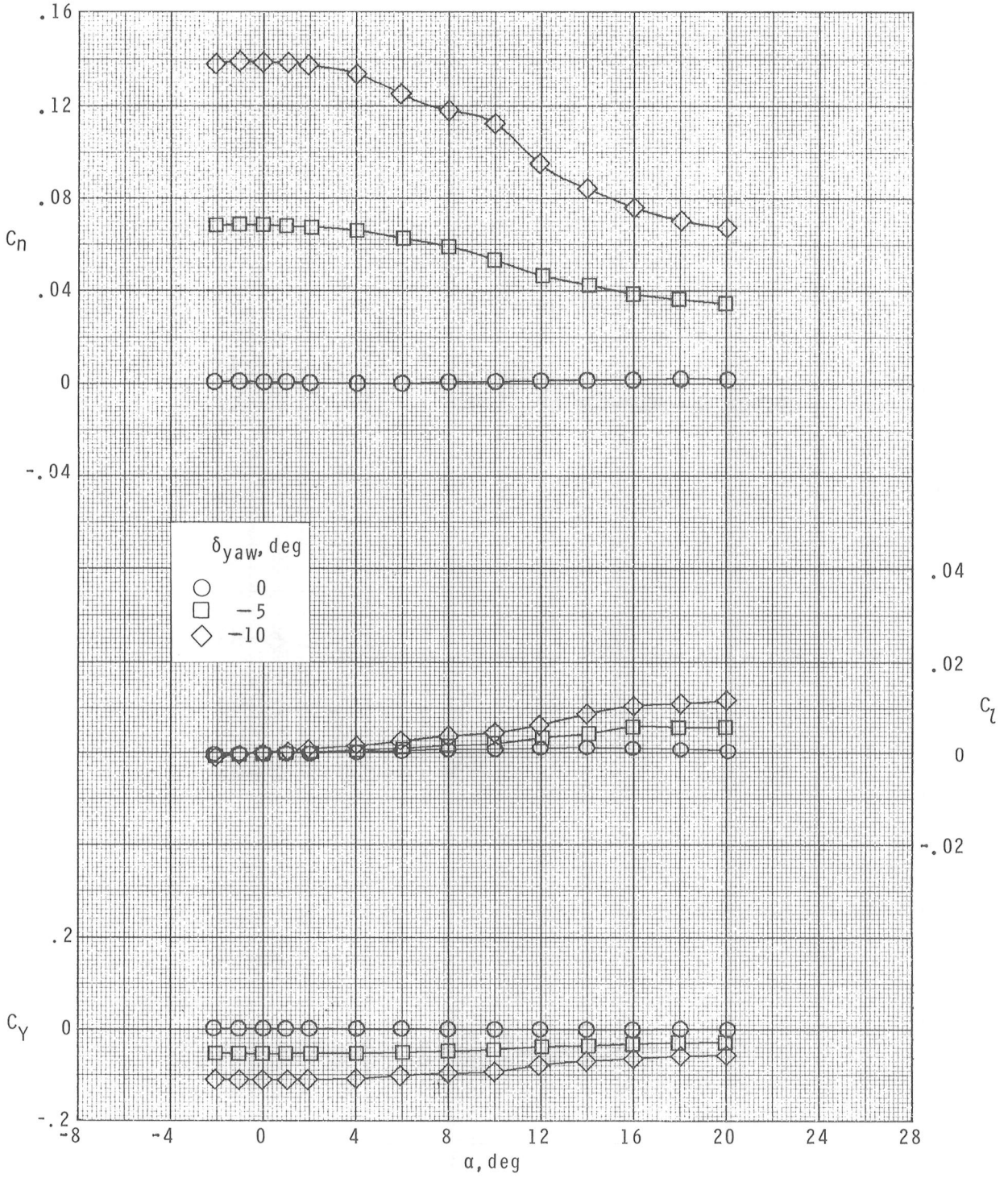

(a) M = 1.70.

Figure 26.- Yaw-control characteristics of the centerline-aft-wing configurations.

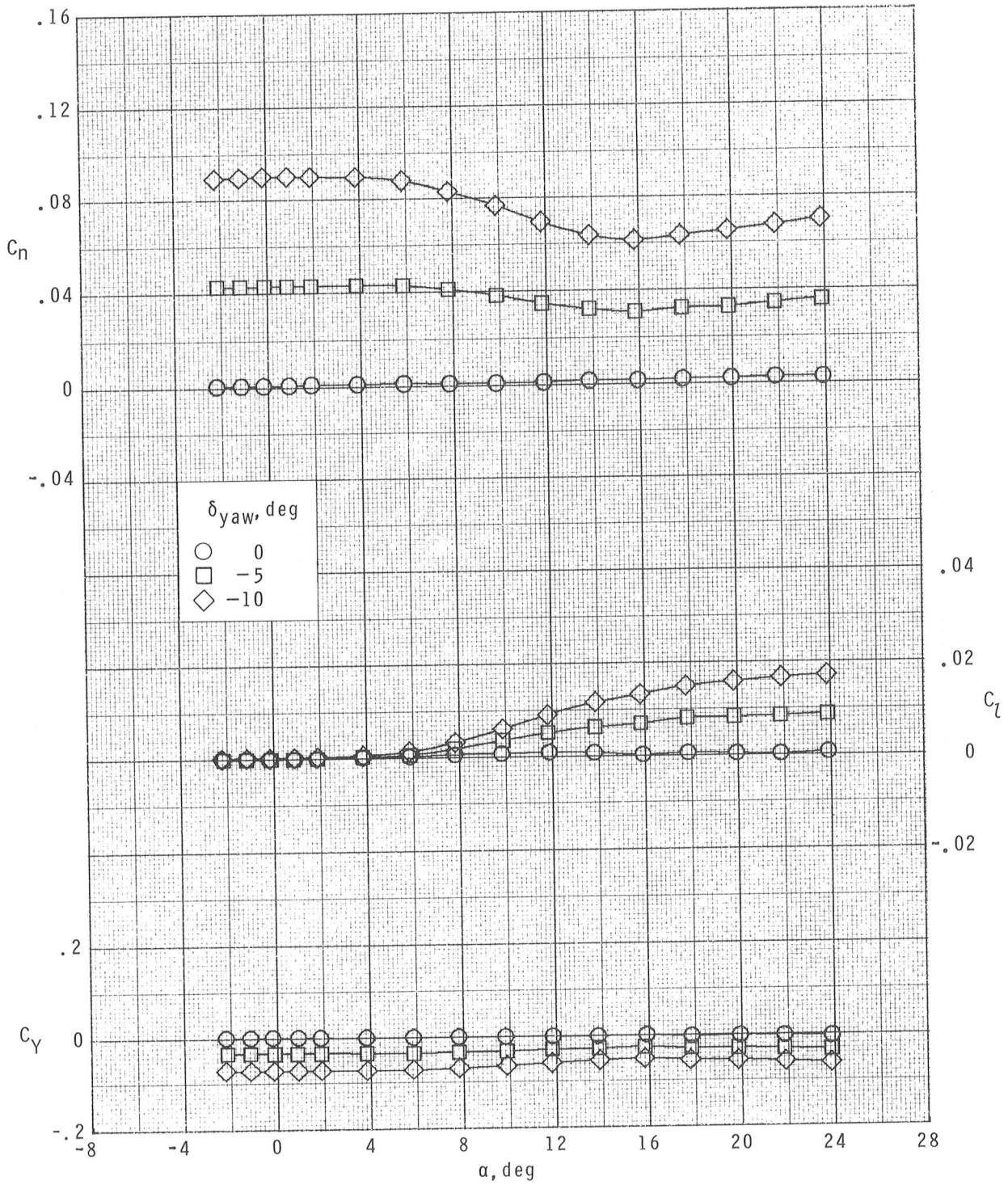

(b) M = 2.16.

Figure 26.- Continued.

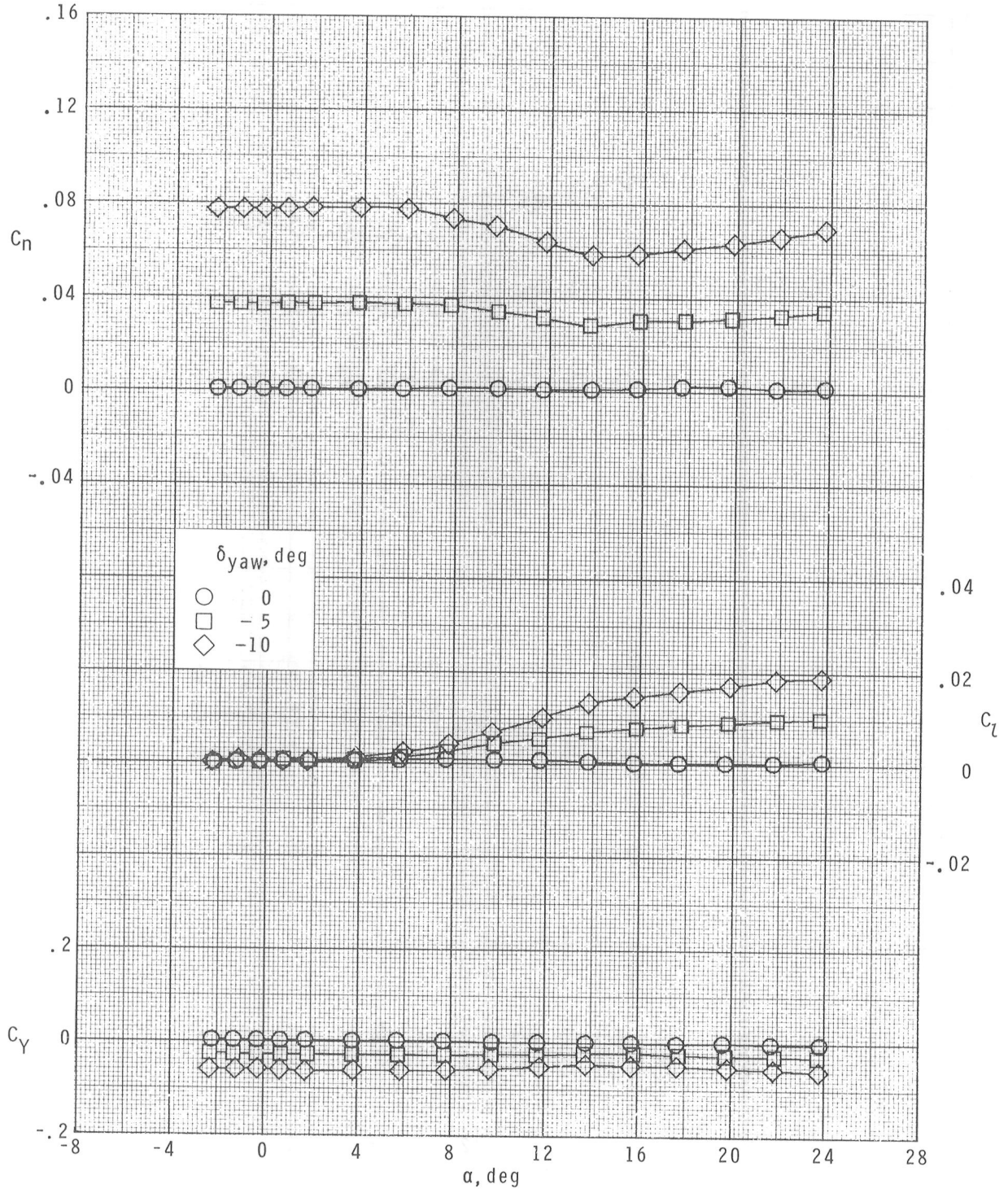

(c) M = 2.36.

Figure 26.- Continued.

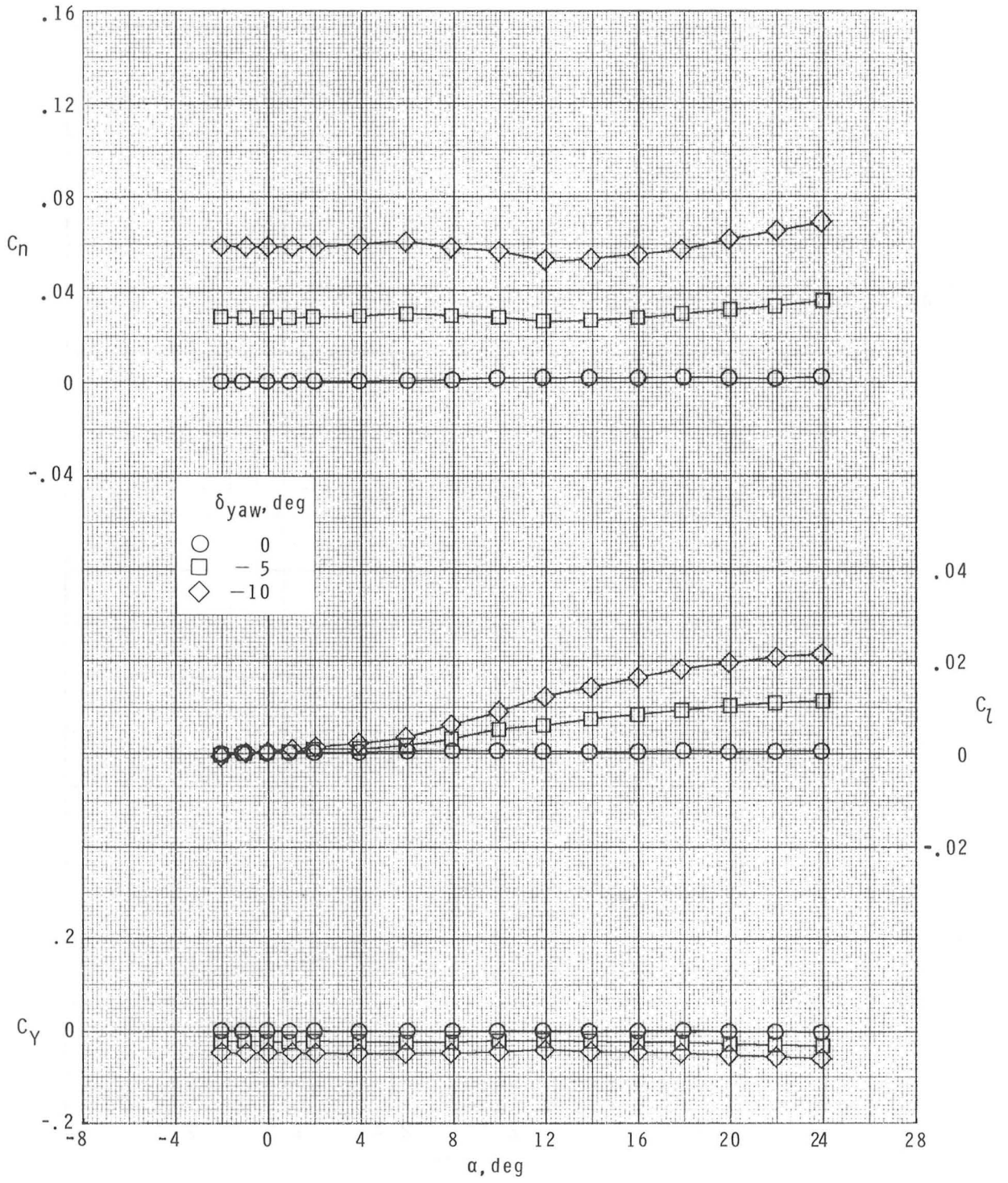

(d) M = 2.86.

Figure 26.- Concluded.

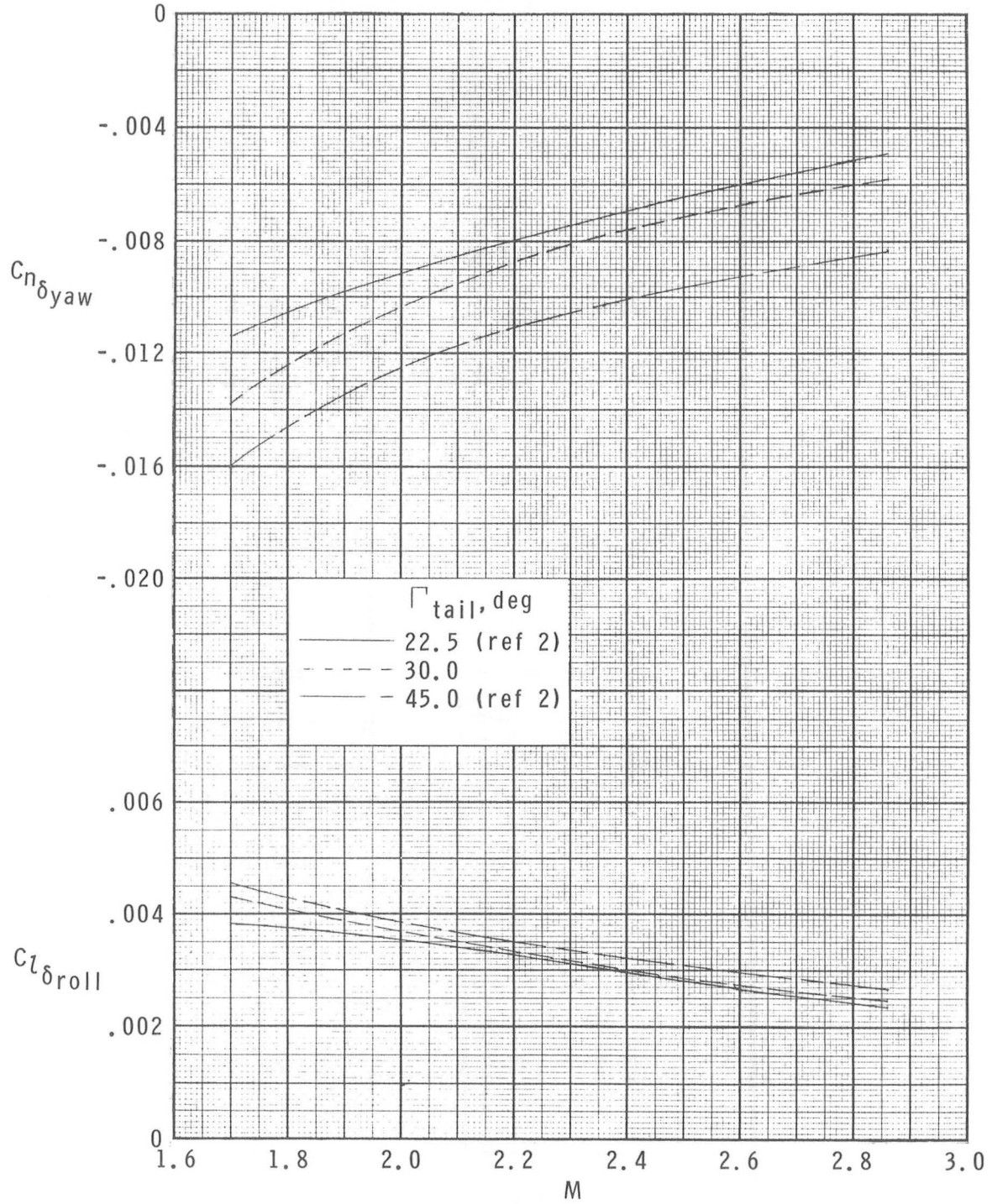

Figure 27.- Summary of tail-fin dihedral effect on roll- and yaw-control effectiveness of the centerline-aft-wing configuration. $\alpha \approx 0^{o}$.

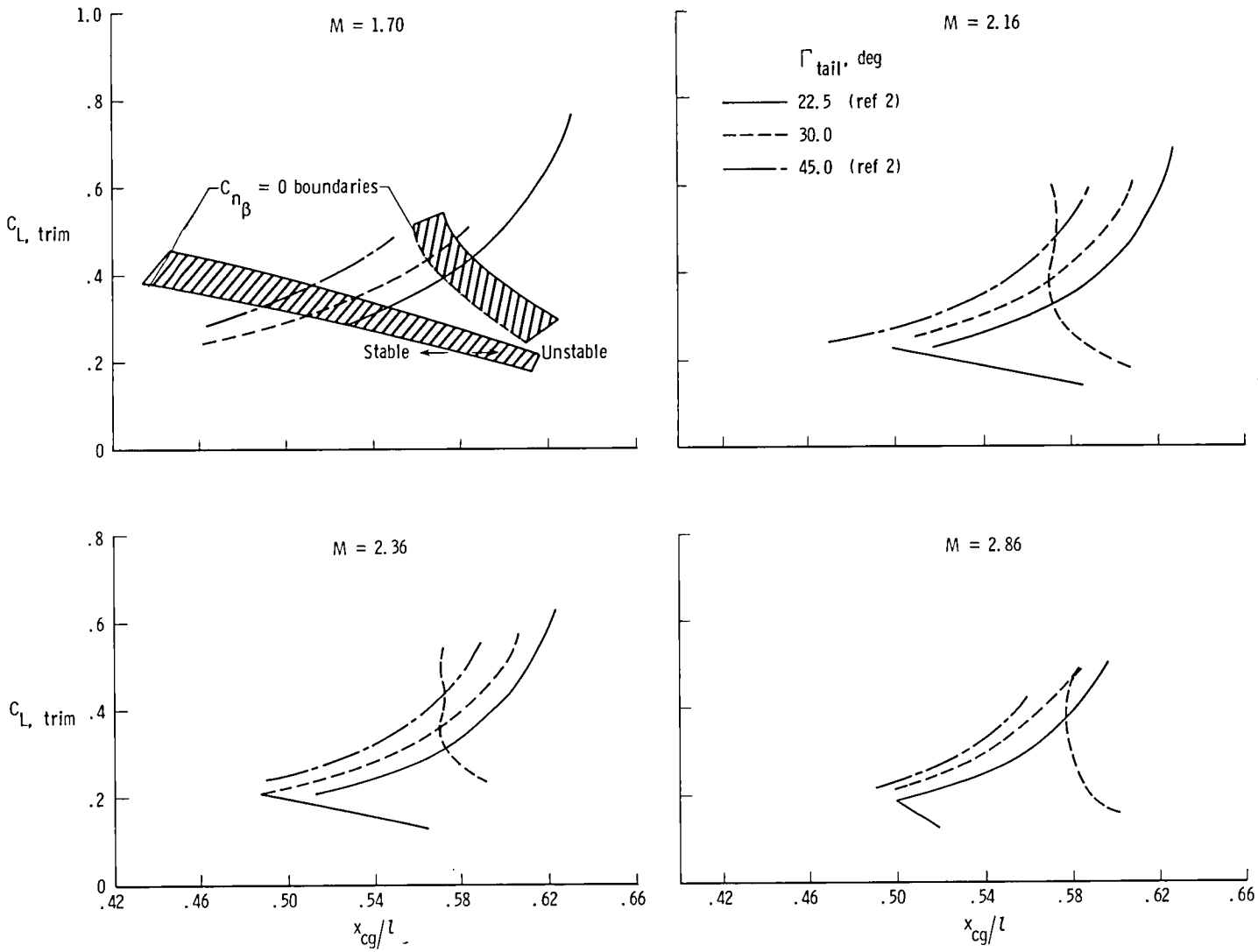

(a) Effect of tail-fin dihedral angle; centerline-aft-wing configuration.

Figure 28.- Variation of trimmed-lift coefficient with center-of-gravity location. $\delta_{pitch} = -20^{o}$.

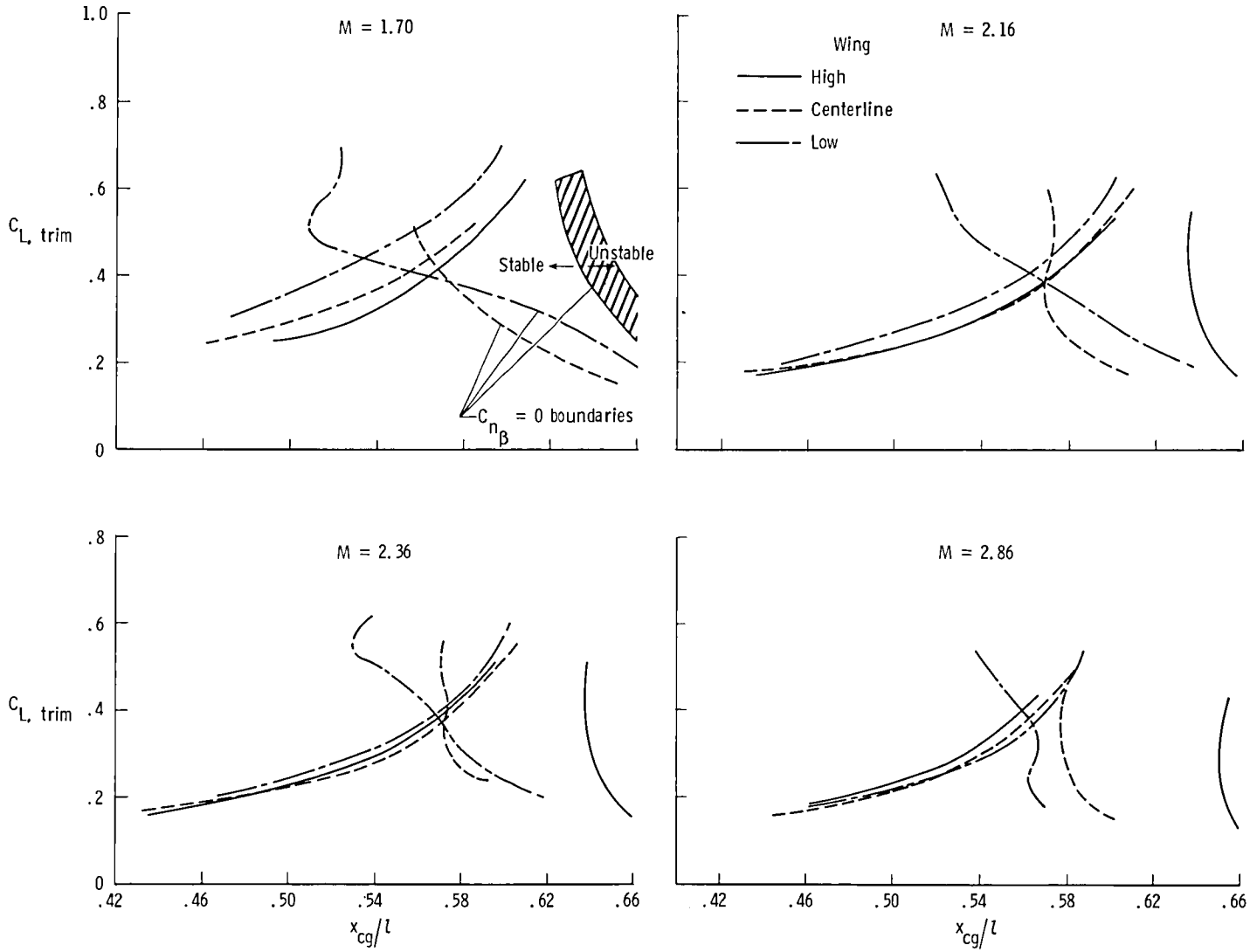

(b) Effect of wing vertical location; aft-wing configuration.

Figure 28.- Continued.

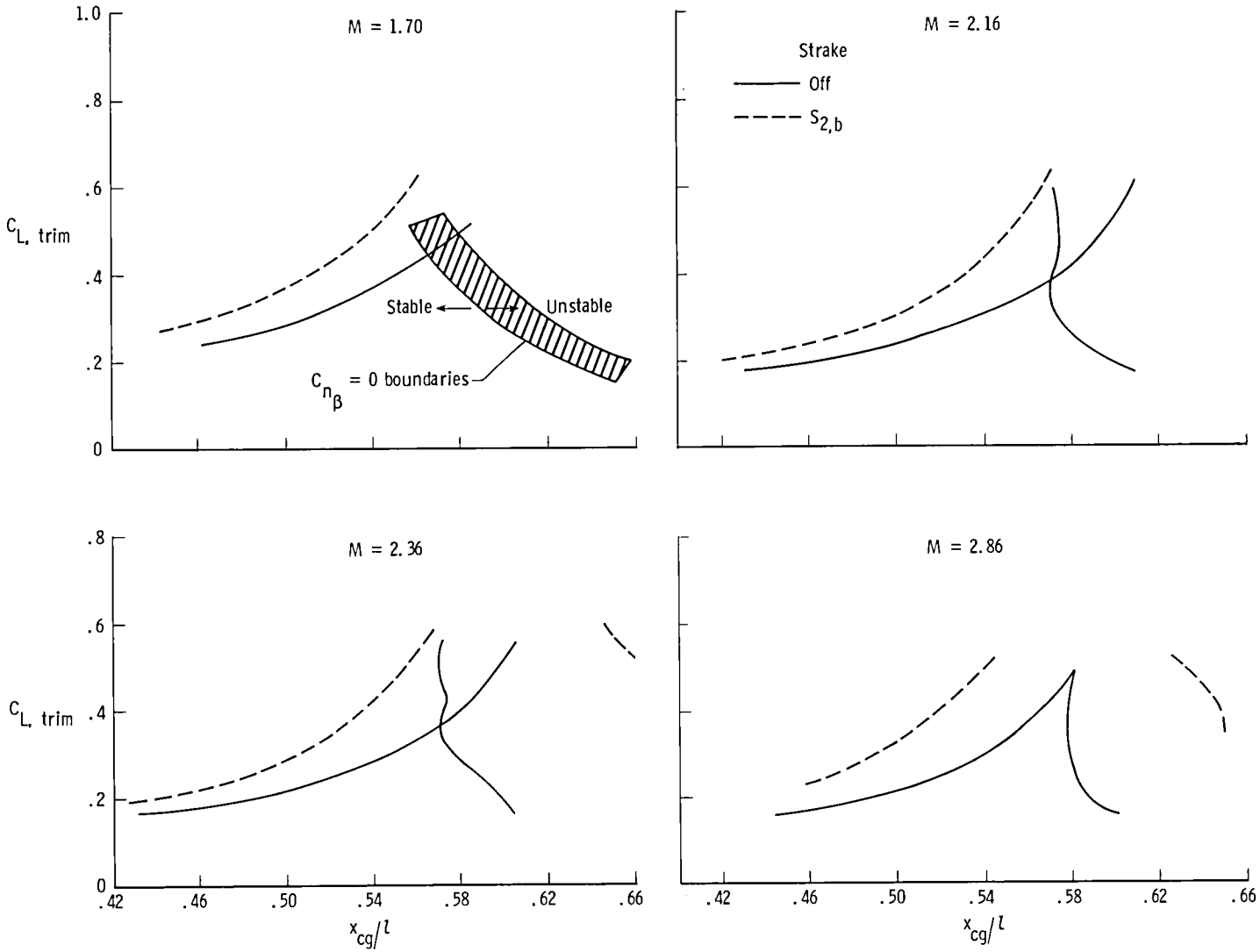

(c) Effect of nose-body strake; centerline-aft-wing configuration.

Figure 28.- Concluded.

1. Report No.	2. Government Accession No.	3. Recipient's Catalog No.
NASA TM-81878		

4. Title and Subtitle	5. Report Date
EFFECT OF WING LOCATION AND STRAKES ON STABILITY AND CONTROL CHARACTERISTICS OF A MONOPLANAR CIRCULAR MISSILE WITH LOW-PROFILE TAIL FINS AT SUPERSONIC SPEEDS	December 1980
	6. Performing Organization Code: 505-43-23-02
7. Author(s): A. B. Blair, Jr.	8. Performing Organization Report No.: L-13852
9. Performing Organization Name and Address: NASA Langley Research Center, Hampton, VA 23665	10. Work Unit No.
	11. Contract or Grant No.
12. Sponsoring Agency Name and Address: National Aeronautics and Space Administration, Washington, DC 20546	13. Type of Report and Period Covered: Technical Memorandum
	14. Sponsoring Agency Code

15. Supplementary Notes

16. Abstract

An experimental wind-tunnel investigation has been conducted at Mach numbers from 1.70 to 2.86 to extend the aerodynamic data base for wing-tail effects on stability and control characteristics of monoplanar circular missiles. The results are summarized to show the effects of tail-fin dihedral angle, wing location, and nose-body strakes.

The results indicate that an increase in tail-fin dihedral angle produces positive increments in directional stability that allow greater trimmed-lift-coefficient values (maneuver potential) to be obtained. An increase in wing-tail gap for the Mach number range reduces the aerodynamic-center travel and produces reductions in directional stability at the lower angles of attack. A change in wing height (vertical location) strongly influences the angle of attack at which pitch-up and the most directional stability occur. The addition of strakes to the baseline configuration increases directional stability, which allows a significant increase in stable-trimmed maneuver capability. The tail fins of the baseline configuration are effective in producing roll and yaw control that are accompanied by favorable yaw and roll, respectively.

17. Key Words (Suggested by Author(s))	18. Distribution Statement
Missile aerodynamics Monoplanar missiles Low-profile tails Strake effects Supersonic aerodynamics	Unclassified - Unlimited Subject Category 02

19. Security Classif. (of this report)	20. Security Classif. (of this page)	21. No. of Pages	22. Price
Unclassified	Unclassified	197	A09

For sale by the National Technical Information Service, Springfield, Virginia 22161

NASA-Langley, 1980